



HAL
open science

Identification of the mechanism of mixotrophy in *Phaeodactylum tricornutum*

Valeria Villanova

► **To cite this version:**

Valeria Villanova. Identification of the mechanism of mixotrophy in *Phaeodactylum tricornutum*. Cellular Biology. Université Grenoble Alpes, 2016. English. NNT : 2016GREAV053 . tel-01685787

HAL Id: tel-01685787

<https://theses.hal.science/tel-01685787>

Submitted on 16 Jan 2018

HAL is a multi-disciplinary open access archive for the deposit and dissemination of scientific research documents, whether they are published or not. The documents may come from teaching and research institutions in France or abroad, or from public or private research centers.

L'archive ouverte pluridisciplinaire **HAL**, est destinée au dépôt et à la diffusion de documents scientifiques de niveau recherche, publiés ou non, émanant des établissements d'enseignement et de recherche français ou étrangers, des laboratoires publics ou privés.

THÈSE

Pour obtenir le grade de

**DOCTEUR DE LA COMMUNAUTE UNIVERSITE
GRENOBLE ALPES**

Spécialité : **Biologie Végétale**

Arrêté ministériel : 7 août 2006

Présentée par

Valeria VILLANOVA

Thèse dirigée par **Giovanni FINAZZI** et
codirigée par **Julien PAGLIARDINI**

préparée au sein du **Laboratoire de Physiologie Cellulaire et
Végétale**
dans l'**École Doctorale Chimie et Science du Vivant**

Identification du mécanisme de la mixotrophie chez *Phaeodactylum tricornutum*

Thèse soutenue publiquement le **12/09/2016**,
devant le jury composé de :

M, Thomas, PFANNSCHMIDT

Professeur, Université de Grenoble (Président)

M, Michel, GOLDSCHMIDT-CLERMONT

Professeur, Université de Genève (Examinateur)

Mme, Fayza, DABOUSSI

Directrice de Recherche, INSA Toulouse (Rapporteur)

M, Tomas, MOROSINOTTO

Professeur, Università di Padova (Rapporteur)

M, Giovanni, FINAZZI

Directeur de Recherche, CNRS-iRTSV Grenoble (Directeur de thèse)

M, Julien, PAGLIARDINI

Chef du Département, Fermentalg (Co-Directeur de thèse)



Contents

Résumé.....	5
Abstract.....	6
Preface	7
1. General introduction.....	9
1.1 Diatoms.....	9
1.2. Photosynthesis and primary metabolism in diatoms.....	13
1.2.1 Oxygenic Photosynthesis	13
1.2.2 Photoprotection	16
1.2.3 Carbon fixation	17
1.2.4 Photorespiration	17
1.2.5 Central Carbon metabolism	19
1.3 Trophic variability in diatoms	22
1.3.1 Phototrophy	22
1.3.2 Heterotrophy.....	22
1.3.3 Mixotrophy.....	23
1.4 Lipid metabolism in microalgae.....	24
1.4.1 PUFAs biosynthetic pathway.....	25
1.4.2 TAGs biosynthetic pathways	27
1.4.3 Strategies for enhancing lipid production.....	29
2. Cross-talk chloroplast-mitochondria in diatoms	30
2.1 Preface	30
2.2 Electron flow pathways that produce extra ATP.....	31
2.3 AOX pathway	32
2.4 Biophysical analysis of photosynthesis.....	33
2.5 Energetic coupling between plastids and mitochondria drives CO ₂ assimilation in diatoms.....	36
2.6 Conclusions and remarks.....	67
3. Characterisation and optimisation of mixotrophy in <i>Phaeodactylum tricornutum</i>	69
3.1 Preface	69

3.2	Characterisation of mixotrophic metabolism in <i>Phaeodactylum tricornutum</i>	70
3.2.1	Previous investigations of glycerol metabolism in <i>Phaeodactylum tricornutum</i>	70
3.2.2	Omics analysis	71
3.3	Optimisation of mixotrophic metabolism by improving culture conditions.....	73
3.3.1	Culture medium/ nutrients	73
3.3.2	Light and NaHCO ₃ effect	74
3.3.3	Scale-up in fermentor	75
3.4	Boosting biomass quantity and quality by improved mixotrophic cultivation of the diatom <i>Phaeodactylum tricornutum</i>	76
3.5	Conclusions and remarks.....	129
4.	Effect of nitrogen and phosphorus starvation in <i>Phaeodactylum tricornutum</i>	131
4.1	Preface	131
4.2	Nitrogen and Phosphorous starvation in <i>Phaeodactylum</i>	132
4.3	Lipidomic analysis	133
4.4	Biodiversity on the ecotypes of <i>Phaeodactylum</i>	135
4.5	Membrane Glycerolipid Remodeling Triggered by Nitrogen and Phosphorus Starvation in <i>Phaeodactylum tricornutum</i> ¹	136
4.6	Conclusion and remarks	190
5.	Final Conclusions and remarks	192
	References	197

Résumé

Les diatomées jouent un rôle primordial dans l'écologie de la planète, car elles sont responsables du 20-40% de la productivité mondiale d'oxygène. Elles figurent parmi les organismes à fort potentiel biotechnologique pour des applications biocarburant. Les diatomées sont des organismes symbiotiques issus de la fusion d'un ancêtre hétérotrophe avec une ou plusieurs micro-algues photosynthétiques. Grâce à cette histoire évolutive complexe, les diatomées ont un métabolisme très flexible. Comme la plus part des microalgues elles peuvent utiliser la photosynthèse pour leur croissance, mais aussi la mixotrophie, *i.e.* la capacité de croître en présence de lumière et d'une source de carbone réduit. L'utilisation simultanée de la photosynthèse et de la respiration peut augmenter la productivité de la biomasse des microalgues et réduire ainsi le coût de leur exploitation industrielle. Dans cette thèse j'ai étudié le mécanisme et les conséquences du métabolisme mixotrophique chez la diatomée modèle *Phaeodactylum tricornutum*. J'ai contribué à étudier le mécanisme moléculaire à la base des interactions énergétiques entre chloroplaste et mitochondrie. Dans ce travail, nous avons démontré que le NADPH généré dans le chloroplaste est exporté vers la mitochondrie pour générer de l'ATP requis pour la fixation du CO₂ dans le chloroplaste. Cette interaction entre les deux organites cellulaires augmente la croissance de diatomées, et suggère que l'utilisation simultanée d'une source de carbone et de l'énergie lumineuse (mixotrophie) devrait augmenter la productivité de la biomasse chez les diatomées. Cette hypothèse a été testée dans la deuxième partie de ma thèse, où j'ai étudié les conséquences de la mixotrophie sur le métabolisme de *Phaeodactylum*. Grâce à une approche métabolomique, transcriptomique, lipidomique et de physiologie j'ai contribué à éclaircir les principales voies métaboliques (métabolisme centrale, métabolisme des lipides, métabolisme des polymères de réserve) concerné la mixotrophie. Dans la dernière partie de ce travail j'ai optimisé les conditions de culture et la composition du milieu afin d'améliorer la productivité en croissance mixotrophe chez *Phaeodactylum*. Ce résultat a été validé dans des photobioréacteurs à l'échelle labo pour tester le potentiel de l'exploitation industrielle de cet organisme.

Abstract

Diatoms are photosynthetic organisms with a strong influence on the global biogeochemistry. Moreover, they are extremely interesting as potential feedstocks for the production of high-value molecules and biofuel. They are endosymbiotic organisms originated by the fusion of a heterotrophic ancestor with one or more photosynthetic microalgae. This has led to an extremely flexible cell metabolism. Like other microalgae, diatoms are able to grow in the presence of both light and of a reduced carbon source. The simultaneous use of photosynthesis and respiration can increase biomass productivity and reduce the energy cost of the industrial exploitation of diatoms.

In this project, the mechanism and the consequences of mixotrophic metabolism have been studied in the model diatom *Phaeodactylum tricornutum*. In the first part, I have studied the molecular mechanism governing the interactions between chloroplast and mitochondrion. We have demonstrated that the NADPH generated in the plastid is exported to the mitochondrion to generate additional ATP, which, once back to the plastid, is used for carbon fixation. Overall, this work shows that the interaction between these two organelles increases carbon fixation and growth in diatoms. We hence suggest that the simultaneous use of carbon and light energy sources (*i.e.* mixotrophy) should enhance biomass productivity in diatoms. This hypothesis has been tested in the second part of my thesis, where I focused on the consequences of mixotrophy on metabolism. By combining metabolomic, transcriptomic, lipidomic and physiology approaches, I have contributed to elucidate the main pathways targeted by mixotrophy (central carbon, lipid and storage carbon metabolism). In the last part of this work, I have worked on improving the culture conditions and medium composition to boost microalgal productivity by mixotrophy. These conditions have been scaled-up in lab scale photobioreactors, revealing the industrial exploitation potential of *Phaeodactylum*.

Preface

This work was funded by a European grant (Marie Curie ITN "Accliphot") for a period of three years. The project involved the collaboration of 13 different partners between theoretical and experimental researchers from both academia and industry. The overall aim of Accliphot consortium is to study the acclimation process of photosynthetic organisms (*i.e. Arabidopsis thaliana, Chlamydomonas reinhardtii, Phaeodactylum tricornutum*) in order to optimise their exploitation for the production of biofuels and high-value molecules.

In particular, my project involved working in between basic research and industrial R&D.

The first part of my PhD thesis took place at LPCV laboratory (CEA, Grenoble) under the direction of Dr. Giovanni Finazzi and Dr. Dimitris Petroutsos. The second part was done in Fermentalg, a start-up committed to the development of fermentation processes in microalgae, under the direction of Dr. Julien Pagliardini and Adeline Le Monnier. The aim of this research was to characterise and optimise the mixotrophic growth of *Phaeodactylum tricornutum* considered a potential source of triacylglycerols (*i.e.* TAGs) for the production of biofuel.

To achieve this aim different objectives were pursued:

- Characterisation of the mechanism and the consequences of mixotrophic growth in *Phaeodactylum tricornutum* combining omics analyses and biophysical approach.
- Characterisation and comparison of the mechanism of TAG accumulation under nutrient starvation and in presence of a carbon source (mixotrophic growth) in *Phaeodactylum tricornutum*;
- Increase of mixotrophic performances (biomass and lipid productivity) by the optimisation of medium composition and culture conditions;
- Test the potential of the industrial exploitation of *Phaeodactylum*: Up-scale in lab scale photobioreactors and optimisation of fermentation processes.

This PhD thesis is organized in 5 chapters. The first chapter is a general introduction, followed from 3 experimental chapter, which contain three scientific manuscripts, and a final conclusion.

The aims of the three experimental chapters are:

Chapter 2: Chloroplast-mitochondria cross-talk in diatoms.

The aim of this work (Bailleul *et al.*, 2015) was to evaluate the interplay between the chloroplast (where the photosynthesis take place) and the mitochondria (site of respiration metabolism) using a biophysical approach in wild type and respiratory mutants in *Phaeodactylum*. The elucidation of the energetic exchanges between these key organelles in diatoms is a crucial step for the characterisation of the mechanism of mixotrophic growth in these organisms.

Chapter 3: Characterisation and optimisation of mixotrophy in *Phaeodactylum tricornutum*.

This research (Villanova *et al.*, paper in preparation) is divided in two main subjects: *i*) characterization of glycerol metabolism in *Phaeodactylum* and *ii*) optimisation of mixotrophic metabolism by improving culture conditions. In the first part of this research, several omics analyses (*i.e.* metabolomic, transcriptomic and lipidomic) have been used to identify the change in the metabolism during the mixotrophic growth of *Phaeodactylum*. The main purpose of the second part of this work was to enhance the performance of mixotrophy by improving medium composition and culture conditions. The optimised conditions have been then scaled-up in photobioreactors to test the potential of the industrial exploitation of *Phaeodactylum*.

Chapter 4: Effects of Nitrogen and Phosphate starvation on lipid content of *Phaeodactylum tricornutum*.

The aim of this work (Abida *et al.*, 2015) was to evaluate the effect of Nitrogen and Phosphate starvation on lipid content of the different ecotypes of *Phaeodactylum*. It represents the first reference of the glycerolipidomic of *Phaeodactylum* that allowed to characterize and dissect the lipid metabolic routes under various levels of nitrogen or phosphorus supplies.

Chapter 1

General introduction

1.1 Diatoms

Diatoms are unicellular eukaryotes responsible for about 20-25% of the global carbon dioxide fixation via photosynthesis (photoautotrophy). They are the most heterogeneous group of phytoplankton in seawater, counting about 200,000 different species that range in diameter from 5 μm to few millimetres. They can exist either as single cells or as colonies of connected cells (fig. 1.1a).

They are surrounded by a silica shell, *i.e.* the frustule (Round *et al.*, 1990). Based on the structure of the frustule, diatoms are distinguished into two main groups: centric with a radial symmetry and pennate with a bilateral symmetry (fig. 1.1b-1c).

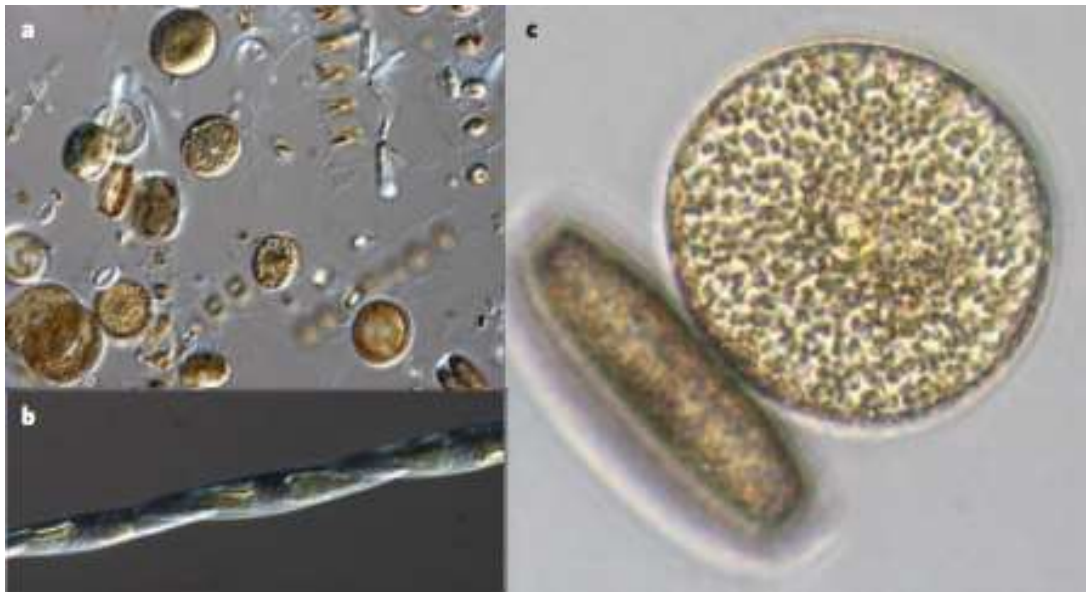


Fig. 1.1 Biodiversity of diatoms. (a)Diatoms can exist either as single cells or as colonies of connected cells. They are distinguished based on the structure of their frustule in pennate (b, *Pseudo-nitzschia*) and in centric (c, *Thalassiosira*). Image from Armbrust, Nature 2009.

A possible explanation of the high diatom variability can be found in their complex evolutionary history. Unlike plant, green and red algae, which derive from a primary endosymbiosis involving the fusion of a heterotrophic ancestor with a cyanobacterium (fig. 1.2a), diatoms are issued from a secondary endosymbiosis that involves a second fusion event between a green algae and/or red algae with an heterotrophic eukaryotic (fig. 1.2b). As a consequence, diatoms are characterized by a chimeric combination of genes and pathways acquired from endosymbiotic events and horizontal transfer with bacteria and virus (Armbrust *et al.*, 2009). Furthermore, the secondary endosymbiosis led them to have four plastid membranes: two more than land plant and others photosynthetic microalgae (Delwiche & Palmer 1997).

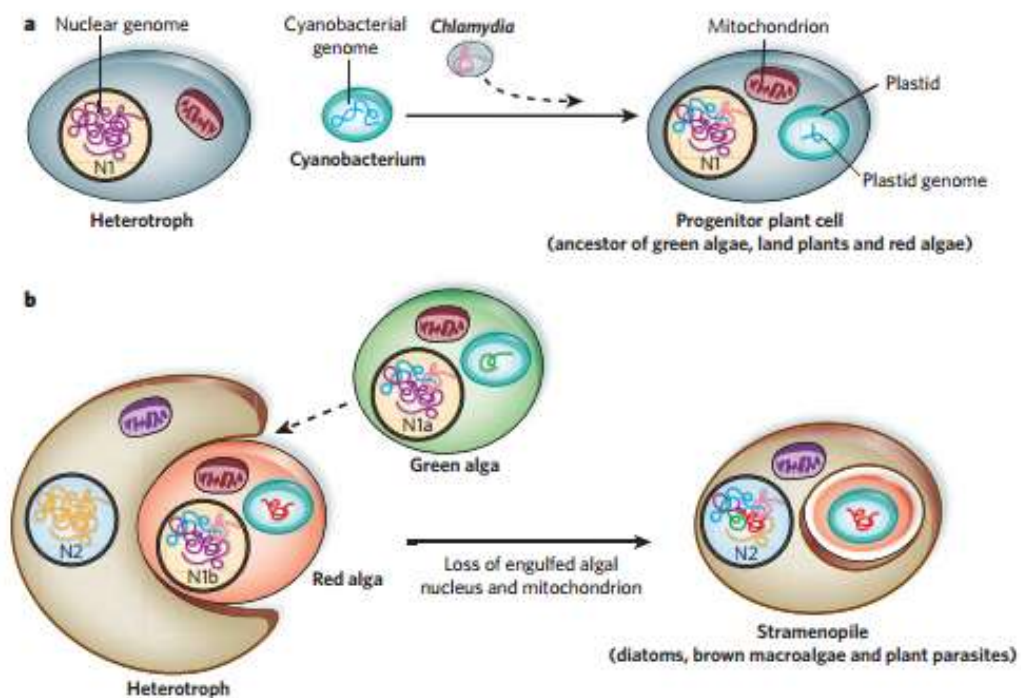


Fig. 1.2 Endosymbiosis events in photosynthetic organisms: (a) land plant, green and red algae were originated by the fusion of an heterotrophic ancestor and a cyanobacterium (primary endosymbiosis); (b) diatoms were originated by the fusion with a Green or/and Red alga with a different heterotroph (secondary endosymbiosis). Image from Armbrust, Nature 2009.

Another peculiarity of diatoms is their pigment profile that is quite different from that found in land plants and green algae. In fact, while green algae and land plant possess chlorophyll a and b, chlorophyll a and c are found in diatoms (Delwiche, 1999; Green, 2011). They also have

a large amount of the carotenoid fucoxanthin that give them their golden-brown colour. These pigments are involved in the light harvesting, being embedded in pigment containing protein complexes called fucoxanthin-chlorophyll-proteins (FCPs) (Green, 1996). Diatoms also possess accessory pigments such as diadinoxanthin (Ddx), diatoxanthin (Dtx), violaxanthin (Vx), antheraxanthin (Ax), and zeaxanthin (Zx) with the main function of protecting the cells from oxidative stress via photoprotection (see paragraph 1.2.2) (reviewed in Kuczynska *et al.*, 2015).

Diatoms are considered an emerging model for the study of photosynthesis and photoprotection mechanisms in the sea (see paragraphs 1.2.1-1.2.2). Furthermore, their ability to accumulate lipid as storage energy (*i.e.* 20%–30% of dry weight) makes them industrially attractive for the production of biofuels and high value products (see paragraph 1.4). In this project, almost all the experiments have been performed using the pennate *Phaeodactylum tricornutum* (see paragraph 1.1.1).

1.1.1 *Phaeodactylum tricornutum*

Bohlin described this microalga for the first time in 1897 as the unique specie of the genus *Phaeodactylum*. It was wrongly assigned first to the classes Chrysophyceae (Hendey 1954) and then to Chrysococcalian (Bourrelly & Dragesco 1955) as consequence of its unusual characteristics. In fact, *Phaeodactylum* possesses an atypical frustule structure that is only poorly silicified, and at variance with other diatoms, it does not require silicic acid to grow (Lewin *et al.*, 1958). Various ecotypes have been collected around the world and more than ten different accessions of *P. tricornutum* have been characterised (De Martino *et al.*, 2007, Abida *et al.*, 2015). They exist in three different morphotypes: fusiform, triradiate and oval (fig. 1. 3). Only the fusiform and triradiate forms have been isolated from natural environment while the oval form has been found only in cell culture. The change from one to the others forms can be stimulated by environmental change, however little information is available about their process of interconversion (Borowitzka & Volcani 1978, reviewed by Tesson *et al.*, 2009).

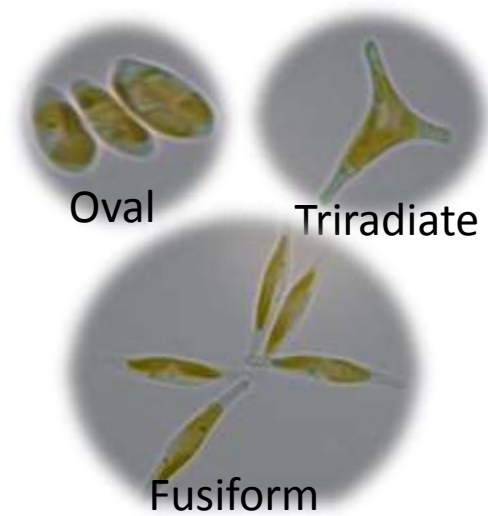


Fig. 1.3 The three morphotypes of *Phaeodactylum*.

Furthermore, *Phaeodactylum* is the second diatom (after the centric diatom *Thalassiosira pseudonana*) in which the genome was sequenced (Bowler *et al.*, 2008). This genome sequencing revealed interesting information such as the presence of hundreds of genes from bacteria as well as of animal-derived pathways, *i.e.* the ornithine-urea cycle. This pathway, absent in land plant and green algae, seems to be essential for diatom growth and carbon fixation (Allen *et al.*, 2011).

The availability of genome sequence and of molecular tools makes *P. tricornutum* a model organism for biotech purposes. It is possible to transform its genome by biolistic method (Apt *et al.*, 1996; Falciatore *et al.*, 1999) or by electroporation (Zhang & Hu 2014). More recently a high-throughput genetic transfer from *E. coli* to *P. tricornutum* via conjugation has been reported (Karas *et al.*, 2015). These methods allow to generate mutant lines, *i.e.* introducing either exogenous or endogenous genes controlled, *e.g.* by the strong light-induced promoters of the FCP proteins (Falciatore *et al.*, 1999). Moreover, different diatom expression vectors based on Invitrogen Gateway™ technology are available in *P. tricornutum*. This technology has been used for either functional analyses of overexpressed genes or subcellular localization by fusion to fluorescent proteins (Siaut *et al.*, 2007). Instead, knock-down (KD) mutants can be generated in *Phaeodactylum* via antisense RNA (asRNA) or RNA interference (RNAi) technology (De Riso *et al.*, 2009). These technologies are based on the expression of small complementary RNA that interacts with target mRNAs. This interaction leads to the downregulation of the gene of interest

either via mRNAs degradation or translation inhibition. Both RNAi and asRNA do not change the genetic code and are only able to reduce (not to eliminate) the gene function. However, recent advances in genome editing technologies (*i.e.* TALEN or CRISPR-Cas) in *Phaeodactylum* allow to the permanent elimination of gene function, *i.e.* generation of Knock-out (KO) mutant lines (Daboussi *et al.*, 2014).

Thanks to the development of these molecular tools in *Phaeodactylum*, now is possible to modify specific pathways leading to more efficient use of this organism for the production of high-value metabolites, *e.g.* triacylglycerols (TAGs) and polyunsaturated fatty acids (PUFAs) (see paragraph 1.4.3).

1.2. Photosynthesis and primary metabolism in diatoms

1.2.1 Oxygenic Photosynthesis

Photosynthesis is the process carried out by plant, algae, and some bacteria that involves the conversion of light energy into chemical energy. During this process, water and CO₂ are converted in carbohydrates and O₂. It comprises two different phases: the light and the dark reactions. The light reactions produce *i.e.* ATP and NADPH, which are consumed in the dark reactions to convert CO₂ to carbohydrates.

In plants, the light reaction begins with the absorption of light at the level of the antenna complex, *i.e.* FCPs (see paragraph 1.1.1), and the transfer of this energy to a reaction centre. Here, light energy is used for charge separation and electron flow through the photosynthetic electron transport chain constituted by: Photosynthems II (PSII), plastoquinone (PQ), Cytochrome b₆f (Cytb₆ f), plastocyanin (PC), Photosynthems I (PSI), ferredoxin (Fd), Fd-NADP⁺-oxidoreductase (FNR) and ATP synthase. The basis of this process are explained in the Z-scheme (Hill & Bendall 1960).

In this scheme, the photons captured by the antenna complex are transferred to the reaction centres of PSII, *i.e.* P₆₈₀. Here, the excited form of P₆₈₀, P₆₈₀^{*}, transfers the electron to the primary electron acceptor molecule, pheophytin and subsequently to a primary and secondary quinone acceptor (Q_A and Q_B). The double reduced Q_B is protonated, and released in the PQ pool. PQH₂ transfers its electrons to the Cyt b₆f complex, and PC. The PC reduces P₇₀₀⁺,

the oxidised chlorophyll donor of PSI. P_{700}^+ is generated by excitation of P_{700} upon reduction of the A_0 and A_1 acceptors by P_{700}^* . A_1 is in turn oxidised by the soluble electron carrier Fd, which ultimately reduces $NADP^+$ to NADPH via the ferredoxin NADP reductase, FNR, protein (fig. 1.4).

The process is similar in diatoms, however, they contain the cytochrome c_6 instead of PC (Bohme & Kunert 1980).

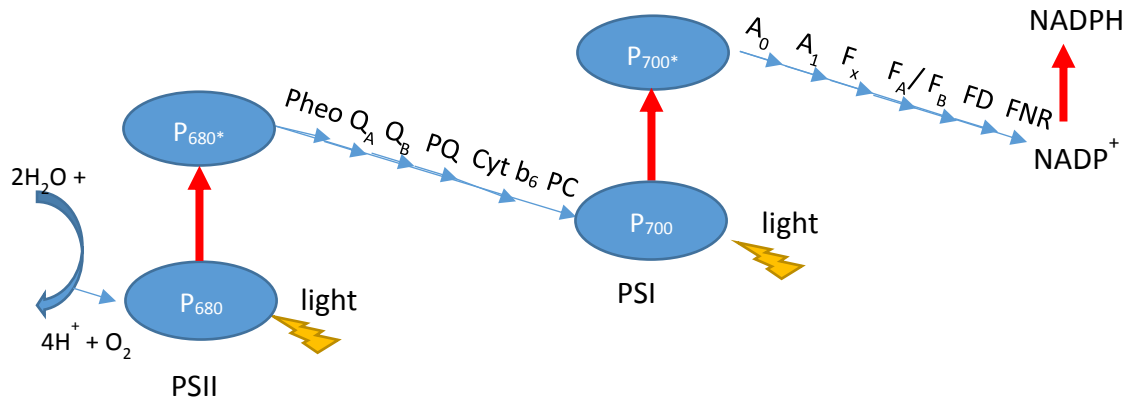


Fig. 1.4 The Z-scheme of photosynthetic electron transfer chain. It shows how electrons generated by light are transported from water to $NADP^+$ through the photosynthetic electron transport chain.

The electron transfer reactions resulting in the generation of a protons gradient across thylakoid membranes, which is used to produce ATP through the proton pump ATP-synthase. Finally, the ATP and NADPH generated by photosynthesis are used for CO_2 fixation and other cellular processes, as discussed in paragraphs 1.2.3-1.2.5.

The process described above is called linear electron flow (LEF), but photosynthetic electron transport can also occurs in a cyclic mode, *i.e.* cyclic electron flow (CEF)(Allen 2003). CEF involves the electron transfer from the ferredoxin back to the Cyt b_6f complex and then again to the PSI via cyt c or PC (Arnon *et al.*, 1954) (fig. 1.5). LEF is probably not sufficient to generate a proper ATP/NADPH ratio for carbon assimilation by Calvin cycle (Allen, 2002). In some photosynthetic organisms belonging to *viridiplantae* (plants and green algae), CEF can contribute to solve this problem (Shikanai *et al.*, 2007). However, recently Bailleul *et al.*, 2015 reported that in diatoms the CEF is not the main process involved in regulating ATP/NADPH level. The

alternative pathways for producing extra ATP in photosynthetic organisms will be discussed in paragraph 2.1.

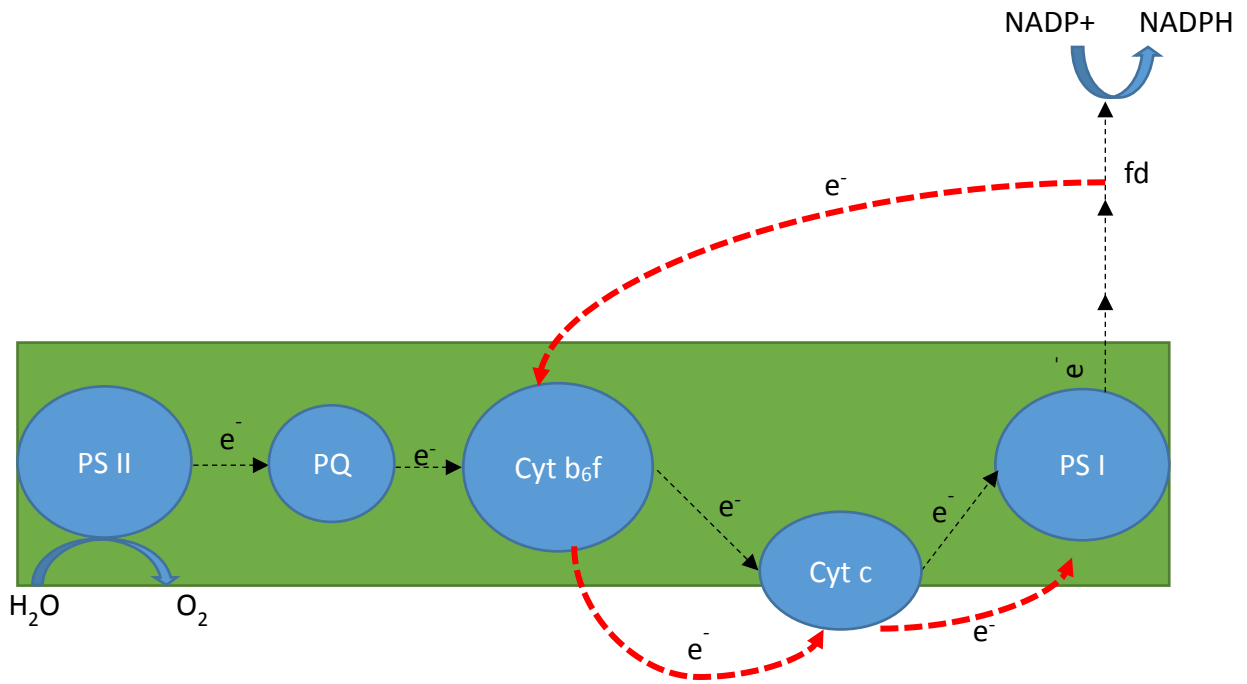


Fig. 1.5 Schematic representation of the linear (LEF) and cyclic electron transfer (CEF) in diatoms. The LEF goes from PSII to the NADP⁺ (black dotted lines); The CEF represents the electron transfer around the PSI (dotted red lines).

1.2.2 Photoprotection

As discussed above light is needed to produce ATP and NADPH via photosynthesis. However, excess of light can be harmful for the photosynthetic machinery, resulting in photodamage and the formation of reactive oxygen species (ROS). To avoid this problem, photoautotroph organisms have developed the capacity to dissipate the excess of photons as heat (Reviewed by Niyogi 1999). NPQ relies on the presence of specific protein effectors and on changes in the pigment composition of the antennae. In particular, diatoms can convert Ddx to Dtx and Vx to Zx (fig. 1.6) via a xanthophyll cycle to trigger NPQ. This process can be estimated through a non-invasive biophysical technique, *i.e.* Pulse Amplitude Modulated fluorescence (see paragraph 2.3).

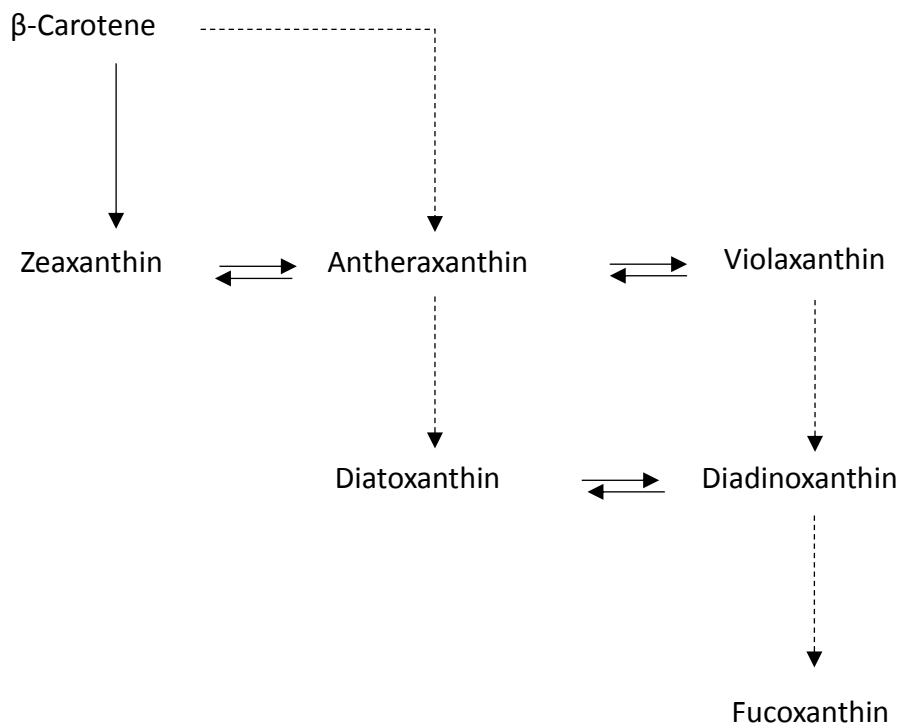


Fig. 1.6 Xanthophyll cycle in diatoms.

1.2.3 Carbon fixation

As mentioned above, the NADPH and ATP generated during the first part of photosynthesis are then used for carbon fixation within the dark phase. In phototrophs, two types of photosynthesis are possible: C₃ photosynthesis, with the formation of the 3 carbon compound phosphoglyceric acid (PGA) and C₄ with the formation of the 4 carbon compound oxaloacetic acid (OAA). Both types of products were found in diatoms, suggesting that probably both pathways are present (Roberts *et al.*, 2007).

The key enzyme for carbon fixation (C₃) is the ribulose-1,5-bisphosphate carboxylase/oxygenase (Rubisco). This enzyme catalyses the carboxylation of D-ribulose-1,5-bisphosphate (RuBP) via Calvin-Benson-Bassham cycle. However, Rubisco it is also capable of performing an oxygenation of RuBP. This process is known as photorespiration. The two reactions are competitive (oxygenation and carboxylation) but at high CO₂ concentration (and low O₂ concentration) the Rubisco preferentially performs the Calvin-Benson-Bassham cycle instead of the photorespiration and vice versa. To increase the relative CO₂ concentration and reduce photorespiration, some algae (including diatoms) have developed CO₂ concentrating mechanisms (CCM) based on the transport of bicarbonate (HCO₃⁻) into the chloroplast and the activity of the enzyme carbonic anhydrase (CA). This enzyme catalyses the conversion of the HCO₃⁻ in CO₂ increasing the concentration of the latter near the catalytic site of Rubisco (Reinfelder *et al.*, 2000).

1.2.4 Photorespiration

As mentioned in the previous paragraph, in high concentration of O₂ the Rubisco catalyse the oxygenation of RuBP via photorespiration. This process leads to the production of one molecule of 3-phospho-D-glycerate (3-PGA) and one of 2- phosphoglycolate (glycolate-2P). The latter can then recycles for further metabolism within peroxisomes and mitochondria or alternatively can be excreted into the medium (fig. 1.7) (Parker *et al.*, 2004) and the 3-PGA can enter the Calvin cycle.

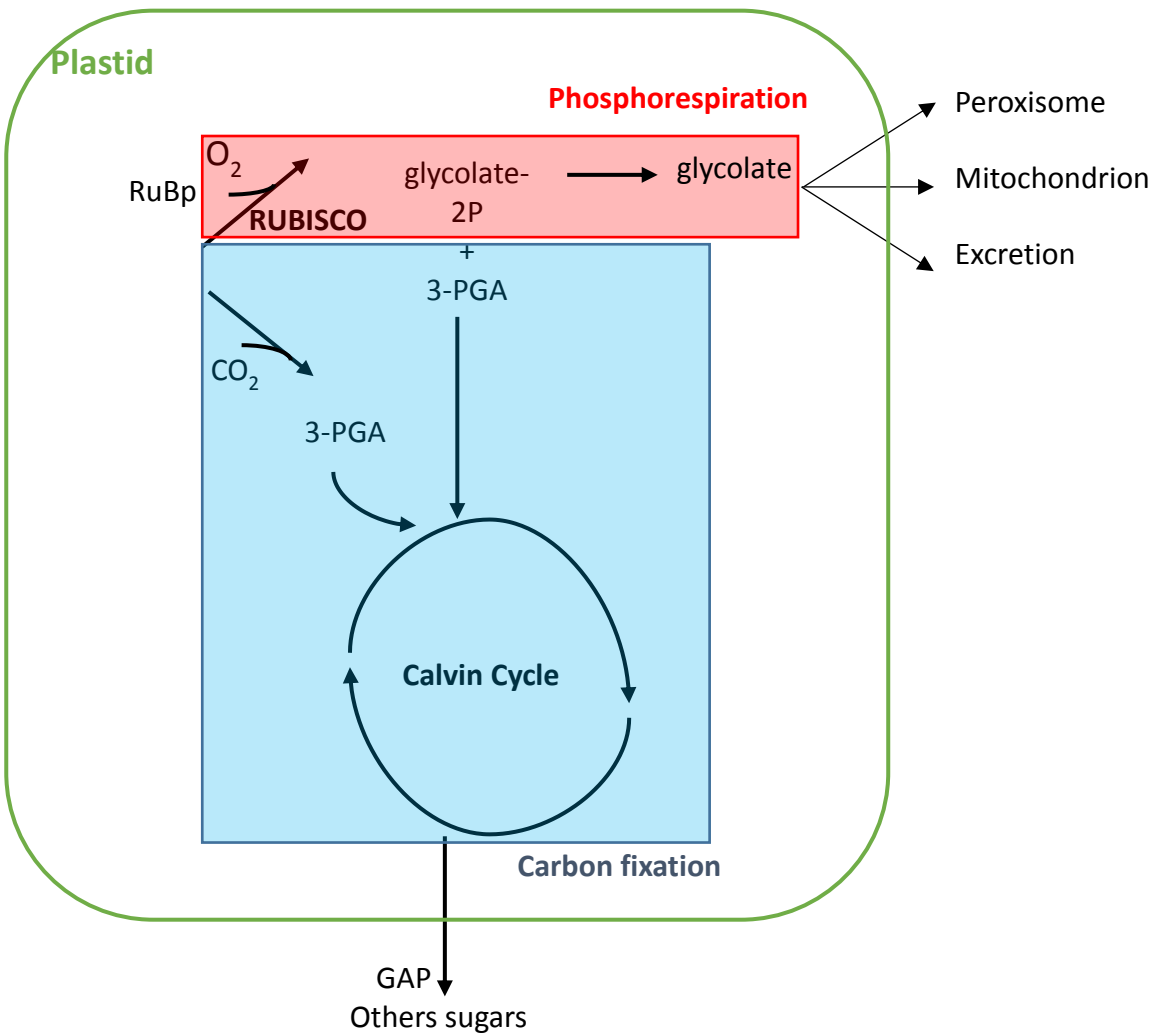


Fig. 1.7 Schematic representation of Photorespiration and Carbon fixation. The RUBISCO can catalyse both the carboxylation (carbon fixation) and the oxidation (Phosphorespiration) of the Rubilose-1-5-biphosphate (RuBp). The photorespiration pathway (Red box) forms the glycolate that can be directed in others cellular districts or excreted outside the cell. The Carbon fixation (Blue box) brings to the formation of 3-phospho-D-glycerate (3-PGA) that enters the Calvin cycle and forms the glyceraldeyde-3-phosphate (GAP). The latter can take part to different metabolic pathway leading to the formation of others carbohydrates.

1.2.5 Central Carbon metabolism

The central carbon metabolism includes all the pathways involve in the transport and oxidation of main carbon sources within the cells. In all photoautotrophic organisms, the principal pathways involved in the regulation of the carbon flux are glycolysis, gluconeogenesis, pyruvate metabolism and tricarboxylic acid (TCA) cycle.

The glycolysis is the degradation of glucose to produce ATP and pyruvate that can enter different metabolic pathways. In diatoms, several isoenzymes involved in glycolysis occur in different cellular compartment, *i.e.* chloroplast, mitochondrion, cytosol. Kroth *et al.*, 2008 showed that in these organisms a complete glycolysis pathway could occur in the chloroplast. However, diatoms possess also an atypical glycolytic pathway, *i.e.* the Embden–Meyerhof-Parnas pathway (EMP) (Fabris *et al.*, 2012). Bioinformatics and experimental evidences showed that in *Phaeodactylum*, the upper phase of EMP pathway is located in the cytosol while the lower phase is located in the mitochondria (Liaud *et al.*, 2000; Kroth *et al.*, 2008). The presence of the glycolysis pathway in the mitochondrion could provide intermediates for the TCA cycle. Indeed, the glycolytic end-product, *i.e.* pyruvate, can enter either the TCA cycle (mitochondria) or the fatty acids synthesis metabolism (chloroplast) (fig. 1. 8). The fatty acid synthesis will be described in the paragraph 1.4.1. The pyruvate can enter the TCA cycle trough conversion either to *i)* acetyl-CoA by pyruvate dehydrogenase, or *ii)* oxaloacetate by pyruvate carboxylase.

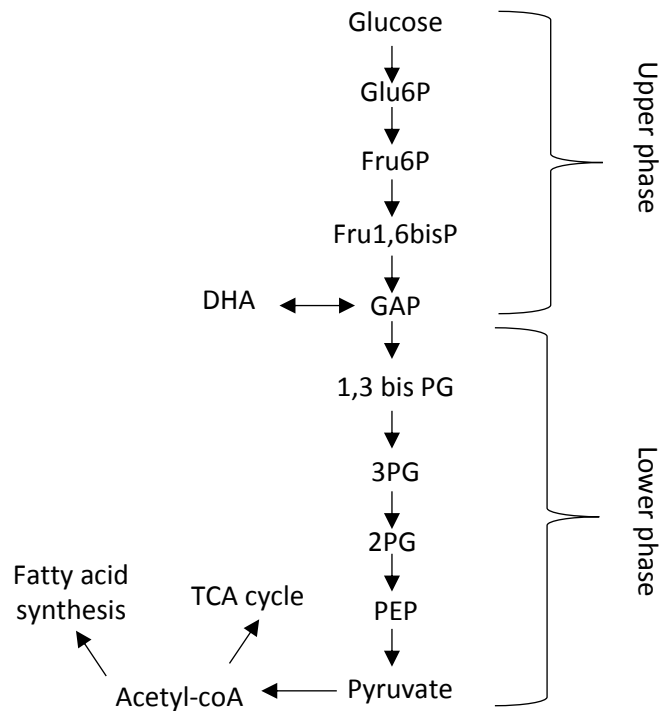


Fig. 1.8 Embden-Meyerhof-Parnas pathway in diatoms. The EMP pathway is divided in two phases upper (cytosol) and lower phases (mitochondria). The end-product pyruvate is then converted to the Acetyl-coA that can enter either in the TCA cycle or in the fatty acid synthesis.

TCA cycle takes place in the mitochondria and involves the oxidation of Acetyl-coA to produce CO₂, ATP and NADH (fig. 1. 9). However, in plant and yeast, some isoenzymes of TCA cycle are localised in cytoplasm (Millar *et al.*, 2011; Catoni *et al.*, 2003; Pallotta *et al.*, 1999) and this may be possible also in diatoms (Kroth *et al.*, 2008; Smith *et al.*, 2012). This pathway plays a key role in the cellular metabolism, *i*) providing intermediates important for biosynthetic reactions (*e.g.* lipids and carbohydrates); *ii*) supplying ATP and NADPH for cytoplasm and chloroplast and *iii*) regulating the redox state of the cell. The latter is regulated by specific metabolites shuttle in both chloroplasts and mitochondria that allows the exchanging of reducing equivalents between these organelles (Weber and Linka, 2010; Hempel *et al.*, 2010). This mechanism is only poorly understood in diatoms, the identification and subcellular localisation of transporters and enzymes involved in this process should be addressed (Prihoda *et al.*, 2012; Bailleul *et al.*, 2015).

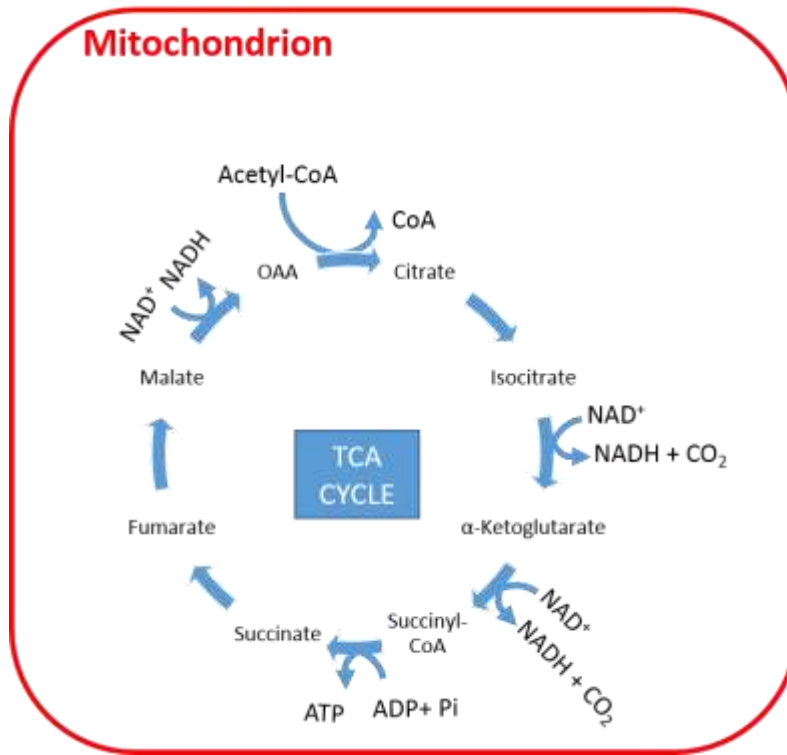


Fig. 1.9 TCA cycle. The TCA cycle take place in the mitochondria where the oxidation of the Acetyl-CoA leads to the formation of CO_2 , NADH and ATP.

The gluconeogenesis is the reverse of glycolysis and converts the pyruvate to glucose. The glucose produced can be used to synthesize storage carbohydrates. In diatoms, the principal storage carbohydrates is the chrysolaminarin, a water-soluble polysaccharide constituted by unit of β -glucans linked with 1-3 β -glycosidic bonds (Beattie *et al.*, 1961). It is accumulated in vacuoles under N-replete conditions. By contrast, diatoms accumulate lipids under N-deplete condition, *i.e.* the two pathways are competitive. The study of the central carbon metabolism is important for understanding the partition of fixed carbon into carbohydrates storage and lipids.

1.3 Trophic variability in diatoms

Diatoms exhibit trophic flexibility. The larger group of diatoms are photoautotrophs. However, some of them are also able to use organic carbon via respiration either in the dark (heterotrophs) or in presence of light (mixotrophs).

1.3.1 Phototrophy

Almost all diatoms are photosynthetic organisms, capable of fixing CO₂ via photosynthesis as described in the paragraph 1.2.1 and 1.2.3. Diatoms are considered amongst the most productive organisms in the ocean thanks to their capacity to adapt to environmental changes. (see paragraph 1.2.2). Moreover, it is possible to increase biomass productivity by increasing the CO₂ concentration in different algal species, including *Phaeodactylum* (Yongmanitchai & Ward 1991, Wu *et al.*, 2015). Similar results were obtained by Gardner *et al.*, 2012. The authors demonstrated that the addition of NaHCO₃ can stimulate the accumulation of TAG_s in both *Scenedesmus* and *Phaeodactylum*. The use of NaHCO₃ as inorganic carbon source results to be a cheaper and more suitable alternative to the CO₂ (Chi *et al.*, 2011). The use of organic carbon source for diatoms cultivation will be discuss in the next paragraphs (1.3.2 and 1.3.3).

1.3.2 Heterotrophy

A few species of diatoms can grow in heterotrophy by utilizing organic carbon substrates in the dark (Lewin & Lewin, 1960).

Two different categories of heterotrophs can be distinguished: *i*) obligate heterotrophs (*e.g.* *Nitzschia alba*) that lack photosynthetic pigments and are not able to perform photosynthesis and *ii*) facultative heterotrophs (*e.g.* *Cyclotella cryptica*) that can perform separately photosynthesis and respiration metabolism.

Three different species of *Nitzschia* belong to the first group. They are colourless pennate diatoms that are probably originated from a mutation of a photosynthetic progenitor that lost its chloroplast (Lewin *et al.*, 1967). It was reported that some of them are capable of heterotrophic growth on both simple (*i.e.* lactate, acetate and glucose) and complex carbohydrates with high productivity (Lewin *et al.*, 1960; Armstrong *et al.*, 2000).

Amongst facultative heterotrophs, the centric diatom *Cyclotella cryptica* is able to grow in presence of glucose in the dark, but it shows a lower productivity than in photoautotrophic conditions (Hellebust *et al.*, 1971). Some microalgae are obligate photoautotrophs because they possess an inefficient uptake of carbon sources (reviewed in Chen and Chen 2006). Therefore, metabolic engineering is a potential solution for a biotechnological utilization of these organisms. For example, the introduction of the gene encoding for the human glucose transporter (GLUT1) in *Phaeodactylum tricornutum* allowed the uptake of glucose in the dark (Zaslavskaja *et al.*, 2001) and consequent heterotrophic growth.

In some case, the use of the heterotrophic metabolism is economically more convenient than the phototrophic metabolism, resulting in higher lipids and biomass productivity. However, another economic aspect that has to be taken into account is the additional cost of organic carbon supplementation. To solve this problem wastewater and biodiesel waste (*i.e.* glycerol) are often used for the industrial exploitation of microalgae.

1.3.3 Mixotrophy

As described in the previous paragraph 1.3.2, only few species of diatoms are able to grow in heterotrophy and this process is not always convenient. For this reason, the mixotrophic metabolism is of major interest for biofuel production in diatoms (Wang *et al.*, 2012). Mixotrophy is the growth in presence of both light and organic carbon when both respiration and photosynthesis are simultaneously active. Different diatoms such as *Phaeodactylum tricornutum* (Cerón-García *et al.*, 2000; 2005; 2006), *Navicula saprophila*, and some species of *Nitzschia* species (Kitano *et al.*, 1997) can grow in mixotrophy. However, these diatoms show some differences in their mixotrophic growth.

Navicula saprophila is able to growth in acetic acid in presence and absence of light as well as in phototrophic mode. However, *N. saprophila* shows the highest growth capacity in mixotrophy, where its growth rate corresponds to the sum of the heterotrophic plus phototrophy growth. In addition, the growth in mixotrophy allowed obtaining the highest eicosapentaenoic acid (EPA, see paragraph 1.4.1) productivity comparing with the use of others trophic modes (Kitano *et al.*, 1997). On the other hand, the diatom *Nitzschia* showed higher EPA production in heterotrophy than in mixotrophy.

Finally, *P. tricornutum* is a facultative mixotroph that is not able to grow in absence of light. Previous works have shown that it is capable to grow in mixotrophy in presence of different carbon sources such as glycerol, acetate, glucose and fructose (Cerón-García *et al.*, 2000; 2005; Liu *et al.*, 2008; Wang *et al.*, 2012). So far, the glycerol is the best candidate for biomass and lipids productivity (Cerón-García *et al.*, 2005; 2006; 2013). However, information is still scarce on how glycerol is involved in central carbon and lipid metabolism. This has been one of the main objective of this PhD work.

1.4 Lipid metabolism in microalgae

As described above, phototrophic organisms are able to convert light energy to different cellular metabolites, including high-value products. In particular, microalgae, *i.e.* diatoms, are considered a promising source of lipids for the production of triacylglycerols (TAG_s) and polyunsaturated fatty acids (PUFA_s). The Fatty acid and lipid biosynthetic pathways in these organisms are similar to the ones present in higher plant and consisting of both a eukaryotic and a prokaryotic pathways (Hu *et al.*, 2008). These pathways are present in different compartments of algal cells: chloroplast, cytosol and endoplasmic reticulum and will discuss in paragraphs 1.4.1. and 1.4.2. However, we still do not know how these organisms prioritize carbon toward the production of these molecules. Usually, phototrophs use almost all the energy derived from the carbon fixation for growth and for the biosynthesis of carbohydrates under optimum growth condition (Melis 2013). By contrast, under adverse conditions, they stop growing and start accumulating storage molecules (*i.e.* lipids) (Cheng & He 2014). Because growth is arrested the biomass productivity of microalgae is highly reduced. The different strategies to overcome this problem will be discussed in paragraph 1.4.3.

1.4.1 PUFAs biosynthetic pathway

PUFAs are fatty acids with high number of carbons atoms (>16) with two or more double bonds. Among these, Docosahexaenoic acid (DHA) and Eicosapentaenoic acid (EPA) are important for human health and nutrition.

They are essential fatty acids that humans are not able to produce and hence have to be supplied in their diet. The primary sources of these PUFAs are fish and/or algae (natural producers). Indeed, different species of microalgae, including diatoms, have been found to produce large amount of these lipids. Therefore the demand of microalgae industrial cultivation for PUFA production is increasing. The first step of fatty acid biosynthesis is the conversion of the acetyl-CoA to malonyl-CoA.

This step is catalysed by the Acetyl-CoA carboxylase (ACCase) in the chloroplast (reviewed by Huerlimann & Heimann 2013). There, the fatty acid chains are extended up to a maximum length of 18 carbon by enzymes called fatty acids synthases. The fatty acids are then further extended by cytoplasmic fatty acids elongases, which can form very long (C20 — C24) saturated or monounsaturated fatty acids.

The PUFAs biosynthesis is completed by the action of a series of desaturases, which introduce several double bounds in the fatty acids. Specifically, PUFAs of the C16 and C18 variety are synthesised in the chloroplast, while the synthesis of longer chain of PUFA (LC-PUFAs) occurs between the endoplasmic reticulum and the cytosol (fig. 1.10).

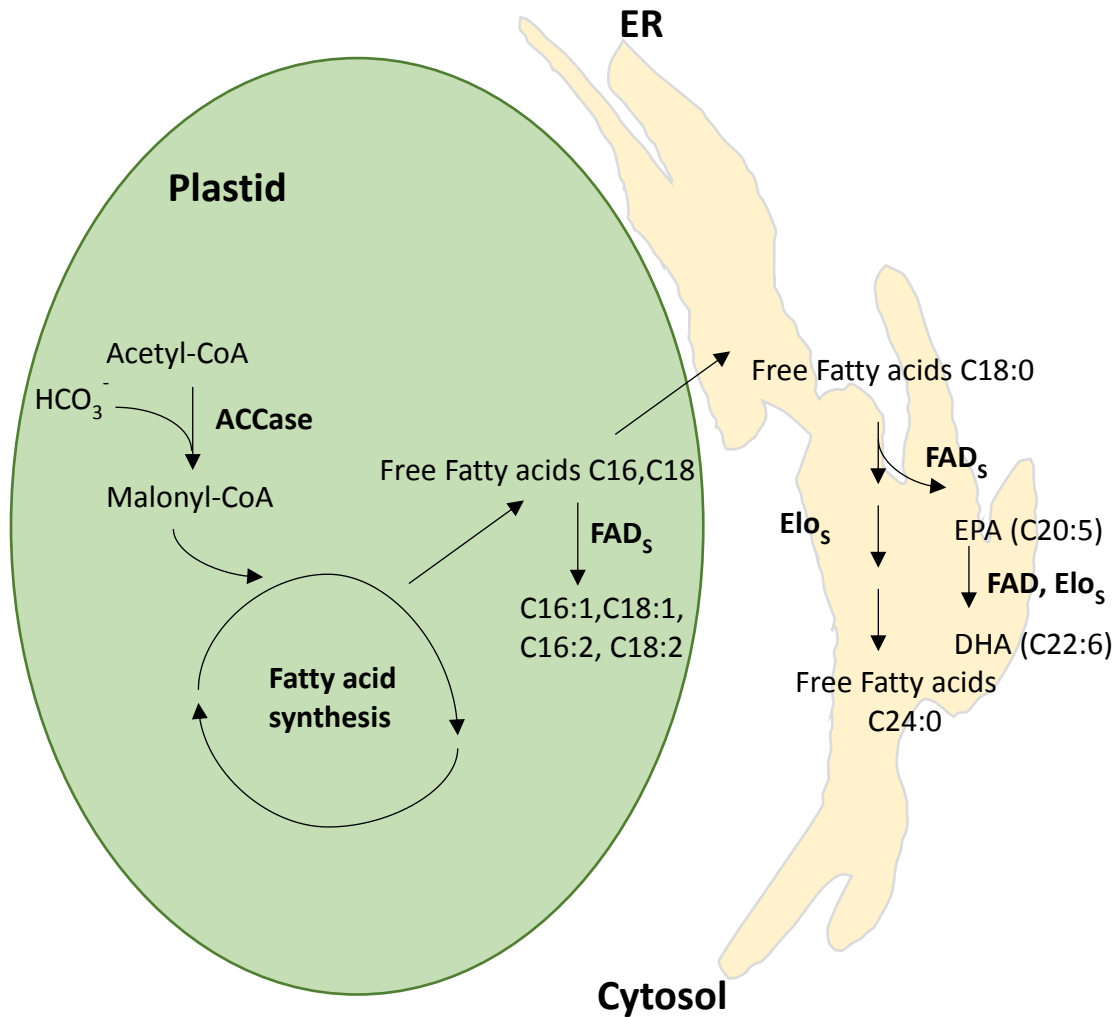


Fig. 1.10 Fatty acid and PUFAs synthesis. The fatty acid synthesis starts with the conversion of the Acetyl-CoA in Malonyl-CoA in the chloroplast. Here, are synthesized short fatty acids chain (i.e. C16-C18) by a serial of fatty acid synthases. The fatty acids are then extended by the fatty acids elongases (Elo_s) in the cytosol. The short PUFA are then formed by the action of fatty acid desaturases (FAD_s) in the chloroplast and the LC-PUFA (i.e. EPA, DHA) between the cytosol and the endoplasmic reticulum (ER).

1.4.2 TAGs biosynthetic pathways

TAGs, also known as oil, are esters of glycerol and fatty acids (FA), which can be converted to biofuel upon esterification. Microalgal-derived oil is a potential alternative to petroleum for the production of fuel. In fact, these organisms possess higher productivity and lower land area needed comparing with vegetable crops (Yusuf 2007).

The TAG biosynthesis in phototrophs occurs through different pathways: *i)* de novo synthesis, via the so called Kennedy pathway; *ii)* remodelling and degradation of existing membrane lipids (Breuer *et al.*, 2013; Roleda *et al.*, 2014; Dodson *et al.*, 2014). The Kennedy pathway involves the transfers of acyl groups to the glycerol-3-phosphate by endoplasmic reticulum acyltransferases (Hu *et al.*, 2008). This reaction leads to the formation of phosphatidic acid, which is dephosphorylated by a phosphatase to form diacylglycerol. The diacylglycerol represents the starting point for the biogenesis of membrane lipids (phosphatidylcholine, monogalatosyldiacylglycerol, etc.) and TAGs. The biosynthesis of photosynthetic membrane occurs in the chloroplast and the non-photosynthetic membrane synthesis occurs in the cytosol and endoplasmic reticulum. The last reaction for the TAG biosynthesis is catalysed by the diacylglycerol acyltransferase (DGAT), which represents the key rate-limiting enzyme of this reaction (Niy *et al.*, 2013; Yen *et al.*, 2008) (fig. 1.11A). Alternatively, DAG can also produced by the degradation of glycerophospholipids via phospholipases, *i.e.* recycling pre-existent membrane lipids (fig. 1.11B). Finally, TAGs can be produced via an acetyl-coA independent mechanism. This path involves the direct incorporation of fatty acids into phosphatidylcholine (PC) and the conversion to TAG by the action of a phospholipid: diacylglycerol acyltransferase (PDAT) (Bates *et al.*, 2012) (fig. 1.11C). The accumulation of TAGs generally occurs in specific structures called lipid bodies, which are visible on the microscope.

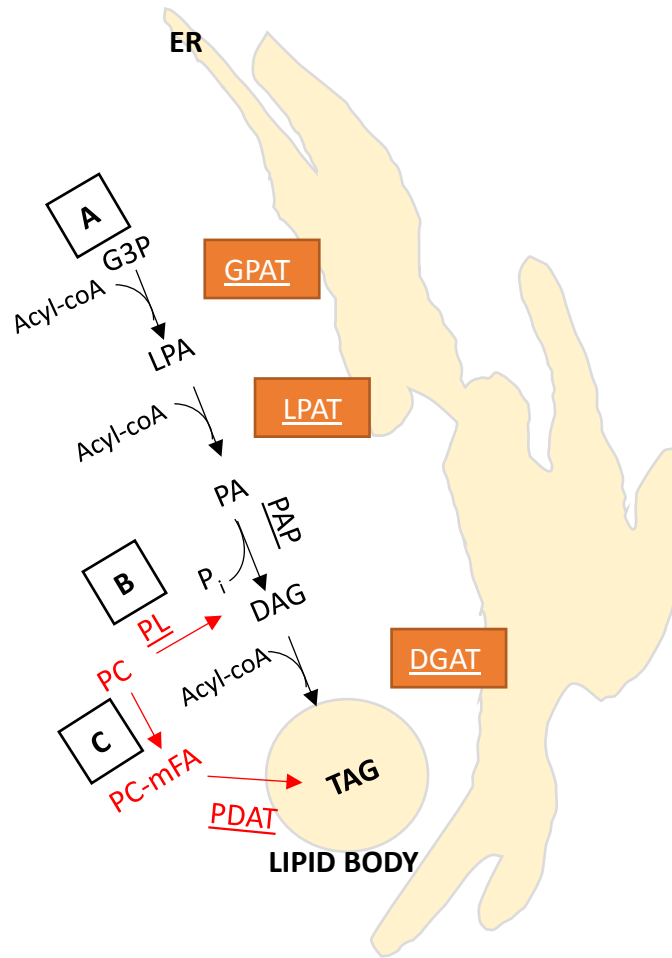


Fig. 1.11 Triacylglycerol biosynthesis pathways. Black and red indicate *de novo* and PC-derived TAG synthesis respectively A) Kennedy pathway catalysed by a serial of membrane acetyl transferases (GPAT, LPAT, DAGAT) and one phosphatase (PAP) between the cytosol and the endoplasmic reticulum; B) PC degradation via PL; C) Directly incorporation of PC in FA and TAG The TAGs are accumulated in lipid body. DAG, diacylglycerol; G3P, glycerol-3-phosphate; LPA, lyso-phosphatidic acid; PA, phosphatidic acid; PC, phosphatidylcholine; TAG, triacylglycerol. Enzymatic reactions are underlined: DGAT, acyl-CoA:DAG acyltransferase; GPAT, acyl-CoA:G3P acyltransferase; LPAT, acyl-CoA:LPA acyltransferase; PAP, PA phosphatase; PL, phospholipase; PDAT, phospholipid: diacylglycerol acyltransferase.

1.4.3 Strategies for enhancing lipid production

Different strategies exist to enhance lipid productivity in microalgae. The most diffused one is the exposure of target organisms to environmental or nutrient stress. However, in these conditions the biomass productivity is very low.

One possibility to solve this problem is metabolic engineering. In fact, thanks to the development of genomic and molecular tools, it is now possible to transform the genome of some microalgae and direct their metabolism towards the lipid biosynthesis. Different approaches are possible to achieve this goal such as: *i)* the overexpression of fatty acids or lipids biosynthesis genes, *ii)* the inhibition of competitive pathways of lipid biosynthesis, *i.e.* lipid catabolism and synthesis of storage carbohydrates. The characterization of these pathways is an essential step to target the right genes for the metabolic engineering and to increase the lipids productivity. For instance, the insertion of the $\Delta 5$ -elongase gene from the green alga *Ostreococcus tauri* in *Phaeodactylum tricornutum* enhanced the production of omega-3 fatty acid (Hamilton *et al.*, 2014). The metabolic engineering has been used also for increasing the triacylglycerols in *Phaeodactylum*. For example, the overexpression of glycerol-3-phosphate dehydrogenase (involved in the Kennedy pathway, see paragraph 1.4.2) enhanced the neutral fatty acid production (Yao *et al.*, 2014). Finally, it has been possible to induce the TAG production in *Phaeodactylum* inhibiting the carbon storage pathway via TALENs technology (Daboussi *et al.*, 2014).

An alternative possibility is the addition of carbon sources that in some microalgae can result in the increase of both lipids and biomass productivity, as discussed in paragraphs 1.3.1-1.3.3. In this study the effect on lipid production of both nutrient starvation (*i.e.* phosphorus and nitrogen) and carbonic organic and inorganic supplies have been investigated in *P. tricornutum*, see chapter 4 and 3 respectively.

Chapter 2

Cross-talk chloroplast-mitochondria in diatoms

2.1 Preface

This chapter describes the article “Energetic coupling between plastids and mitochondria drives CO₂ assimilation in diatoms” (Bailleul *et al.*, 2015). The first paragraphs present the electron flow pathways that produce extra ATP (2.2-2.3), the alternative oxidase pathway (AOX) and the biophysical analysis of photosynthesis. The paragraph 2.4 contains the published paper and finally, the paragraph 2.5 represents the conclusions and remarks of this work.

The aim of this study was to elucidate the molecular mechanisms of photosynthesis and respiration in diatoms. This is a fundamental prerequisite to understand the basis of mixotrophy. In photosynthesis, efficient carbon fixation requires a balanced input of energy (ATP) and reducing power (NADPH), *i.e.* ATP/NADPH ratio (Allen 2002). As already discussed in paragraph 1.2.1, some photosynthetic organisms (mostly belonging to *Viridiplantae*), regulate the NADP/ATP ratio by processes occurring within the chloroplast (*e.g.* CEF). However, our work suggests that diatoms modulate this ratio by constitutive energetic interactions between mitochondria and plastids. We demonstrated that the NADPH generated in the plastid is exported to the mitochondria to generate additional ATP. The produced ATP is then imported into the chloroplast, where it is used for carbon fixation. Consistent with this conclusion, respiratory mutants of *P. tricornutum* show a reduced photosynthetic capacity and phototrophic growth, demonstrating the crucial role of mitochondria for carbon fixation and growth in diatoms. Electron micrograph suggests that these energetic exchanges are likely mediated by physical contacts between plastidic and mitochondrial membranes. Overall, this work shows that the interaction between these two organelles increases the photosynthesis efficiency, likely explaining the ecological success of diatoms worldwide. As a corollary, this study also provides an indication that the simultaneous use of carbon and light energy sources (*i.e.* mixotrophic metabolism) should enhance biomass productivity in diatoms, making them more attractive and

competitive for biotech application. This is the working hypothesis that I have tested during my PhD.

2.2 Electron flow pathways that produce extra ATP

As described in the paragraph 1.2.1, oxygenic photosynthesis converts light into ATP and NADPH, by linear electron flow (LEF). However, the ATP/NADPH ratio produced by this process is not sufficient to support the energetic requirements of the carbon fixation. Different mechanisms exist in photosynthetic organism to provide extra ATP. They include the cyclic electron flow (as described in paragraph 1.2.1), the Mehler reaction, the plastoquinol terminal oxidase reaction (PTOX) and mitochondrial respiration (Ort 2002; Asada 1999; Laisk *et al.*, 2006; Zehr and Kudela 2009).

The Mehler reaction is the reduction of molecular oxygen by photosynthetic electrons to produce superoxide (O_2^-) at PSI level, which is converted by the superoxide dismutase (SOD) into H_2O_2 and O_2 . The H_2O_2 is then reconverted to H_2O by the ascorbate peroxidase (APX) (Asada 1999). This reaction not only protect the cells from the ROS (*i.e.* H_2O_2 and O_2^-) but also produces a monodehydroascorbate radical (MDA) (Miyake and Asada 1992), which can accept electrons from PSI and is coupled to an ATP synthase (Forti and Ehrenheim 1993). At the PSII level, an analogue reaction can occur, where molecular oxygen is reduced by the plastid terminal oxidase, PTOX, enzyme (Kuntz 2004). This process generates a proton gradient that can be used for by the ATP-synthase to produce ATP independently to the NADPH. In plant and green algae, the CEF results to be the most important pathway to regulate the ATP/NADPH ratio, while in cyanobacteria and the prasinophyte *Ostreococcus*, the PTOX pathway prevails. Instead, in diatoms these pathways seems to be only poorly active (Wilhelm *et al.*, 2006; Lepetit *et al.*, 2011).

Besides chloroplast localized processes, oxidative respiration can also affect carbon fixation (Curien *et al.*, 2016). In plants, this effect is mostly indirect (Raghavendra and Padmasree, 2003), and involves exchange of metabolites but does not affect photosynthesis under normal physiological steady state conditions (Dutilleul *et al.*, 2003; Cardol *et al.*, 2010). In *Phaeodactylum*, the presence of several transporters in both chloroplast and mitochondria, as well as the physical connection of the two organelles, suggests an intense exchange, which could

provide the mitochondrial ATP to the chloroplast. Moreover, the overexpression of the alternative oxidase (AOX) (*i.e.* alternative pathway of cytochrome) in iron-depleted diatoms cells suggests that mitochondrion plays an important role in dissipate excess reductants produced by photosynthesis (Allen *et al.*, 2008).

2.3 AOX pathway

The mitochondrial electron transport chain (ETC) contains 5 different complexes: *i)* the NADH dehydrogenase (complex I), *ii)* the succinate dehydrogenase (complex II) *iii)* the cytochrome bc_1 (CYTC, complex III) *iv)* the cytochrome oxidase (COX, complex IV) *and v)* the ATP synthase (complex V). The transfer of electrons within the ETC, coupled with proton translocation, generates a proton motive force (PMF) that is used by complex V to form ATP. In addition to these complexes, a cytochrome-independent alternative oxidase (AOX) is present in the mitochondrial membrane, to transfer electrons from the ubiquinol to O_2 , producing H_2O . (Millar 2011). In principle, the AOX shunts electrons between the complex III and IV, therefore reducing the proton motive force and, hence, the production of ATP. However, this enzyme is also involved in the regulation of excess reductants derived from photosynthesis during conditions of stress. In fact, it was reported that the AOX is overexpressed in iron-depleted cells in *Phaeodactylum* (Allen *et al.*, 2008).

The AOX activity can be measured by using an oxygen isotope discrimination technique. It is able to discriminate the respiration rate in cytochrome oxidase and alternative oxidase based on their differential use of oxygen isotopes ($^{18}O^{16}O$) (Guy *et al.*, 1989). In particular, the two enzymes possess a different mechanism for breaking the oxygen-oxygen bond and, hence, they produce different products that can be discriminate by mass spectroscopy analysis. Alternately, the generation of mutant with reduced AOX capacity can be used to examine the role of this complex in photosynthesis and growth (Florez-Carbo *et al.*, 2011; Yoshida *et al.*, 2011; Gandin *et al.*, 2012). Finally, the effect of AOX activity can be studied by using the salicylhydroxamic acid (SHAM), a competitive inhibitor of ubiquinol and therefore of AOX.

In this study, the activity of AOX was evaluated by measuring the effect of different respiratory inhibitors, such as antimycin A (*i.e.* inhibitor of Complex III) and SHAM (*i.e.* inhibitor of AOX) on wt and Knock-Down AOX mutants.

2.4 Biophysical analysis of photosynthesis

The development of non-invasive biophysical techniques have led to relevant progresses in photosynthesis research. The main techniques used in this field are: *i)* polarographic approach for oxygen detection (Joliot 1956, 1968) *ii)* Pulse Amplitude Modulated (PAM) fluorescence (Joliot *et al.*, 1980, 2004), *iii)* time resolved spectroscopy and in particular, measurements of the electrochromic shift (ECS) *in vivo* (Bailleul *et al.*, 2010; Klughammer *et al.*, 2013).

The polarographic approach is used to monitor the consumption/ production of O₂ *in vivo* experiment. This instrument is composed of a semi-hermetic chamber where a golden or platinum cathode and an Ag/AgCl anode are separated from the sample by O₂-permeable membrane. At the cathode, the O₂ is reduced to water. At the anode, the oxidation generates a potential difference between the two electrodes that can be measured. Constant stirring of the sample allows to equilibrate the oxygen consumed at the cathode so that the change on O₂ concentration is restricted to the sample. The potential difference is proportional to the oxygen tension in the sample after calibration with air-saturated solution.

The PAM fluorescence allows to monitor photosynthetic activity in algae and plants through the evaluation of photosynthetic parameters such as F_v/F_m, electron transfer rate (ETR) and non-photochemical quenching (NPQ). Furthermore, it allows to determine the physiological status of photosynthetic organism, CO₂ assimilation *in vivo*, etc.

The instrument is based on the use of three different types of light: *i)* measuring beam *ii)* saturation pulse and *iii)* actinic light. The first is a low intensity light that is not able to stimulate photosynthesis. The saturating light is a high-intensity light that saturates all reaction centres. Finally, the actinic light is a light of variable intensity that drives photosynthetic activity.

In the darkness, the plastoquinone molecules Q_a are maximally oxidized and the PSII reaction centres are “opened” (*i.e.* they are able to utilize the light energy for photosynthesis). When dark-adapted photosynthetic organisms are exposed to measuring beam light, a minimal

level of fluorescence is observed, F_0 . The further exposition to short pulse of saturating light leads to the reduction of Qa (*i.e.* reaction centres are “closed”) and the maximum fluorescence is reached, F_m .

The difference between F_m and F_0 is defined as fluorescence F_v . The ratio of F_v / F_m determines the maximum efficiency of PSII photochemistry (if all the reaction centres were opened) and gives an estimation of the physiological status of the studied organism. Different photosynthetic organisms display specific F_v / F_m values. For instance, non-stressed diatoms possess a F_v / F_m of about 0.6 but this value can drop dramatically under stress conditions. Thus, F_v / F_m can be used as a non-invasive probe to monitor stress response in photosynthetic organisms. Others photosynthetic parameters can be measured using different exposure times and intensities of the actinic light. ETR is calculated as $(F_m' - F) / F_m' \times \text{PAR} \times 0.5$ where F_m' and F represent the maximum and the minimum fluorescence upon saturating light during illumination with actinic light; PAR (photosynthetically active radiation) is the intensity of actinic light used to stimulate the photosynthesis and the term 0.5 represents the 50% of probability that one electron goes to the PSII (instead to the PSI). $(F_m' - F) / F_m'$ is similar to the F_v / F_m value but in this case is an indicator of the real amount of energy that can be used by PS II during the photosynthesis.

The non-photochemical quenching, NPQ is calculated as $(F_m - F_m') / F_m'$. This method allows to estimate the amount of energy that is dissipated by heat in presence of excess of light by subtracting the amount of energy that is used for photochemistry.

The measurement of Electro Chromic Shift (ECS) can provide a wide range of information in photosynthetic study (reviewed in Bailleul *et al.*, 2010).

During the photosynthesis, the movement of electrons and protons within the thylakoid membrane generates a PMF that is constituted by a gradient of proton concentration (ΔpH) and of electric potential ($\Delta\Psi$). The generation of the PMF allows to activate the ATP synthase and to produce ATP. The formation of $\Delta\Psi$ leads to the shift on pigments absorption, *i.e.* electrochromism. The analysis of this phenomenon is the basis of ECS measurement. The ECS signal can provide information on the function of photosynthetic complexes, and on alternative electron flow process. For instance, the analysis of ECS signal can be used to distinguish the

contribution of CEF and LEF (measured in light) or, of oxidative respiration (measured in dark) on the generation of $\Delta\Psi$ and hence on ATP production. The analysis of ECS in dark can use to elucidate the mechanism of respiration and photosynthesis interactions.

2.5 Energetic coupling between plastids and mitochondria drives CO₂ assimilation in diatoms

Benjamin Bailleul^{1,2,3,4}, Nicolas Berne¹, Omer Murik⁴, Dimitris Petroustos⁵, Judit Prihoda⁴, Atsuko Tanaka⁴, Valeria Villanova⁶, Richard Bligny⁵, Serena Flori⁵, Denis Falconet⁵, Anja Krieger-Liszkay⁷, Stefano Santabarbara⁸, Fabrice Rappaport³, Pierre Joliot³, Leila Tirichine⁴, Paul G. Falkowski², Pierre Cardol¹, Chris Bowler⁴ & Giovanni Finazzi⁵

¹Genetique et Physiologie des Microalgues, Département des Sciences de la vie and PhytoSYSTEMS, Université de Liège, B-4000 Liège, Belgium.

²Environmental Biophysics and Molecular Ecology Program, Departments of Marine and Coastal Sciences and of Earth and Planetary Sciences, Rutgers University, New Brunswick, New Jersey 08901, USA.

³Institut de Biologie Physico-Chimique (IBPC), UMR 7141, Centre National de la Recherche Scientifique (CNRS), Université Pierre et Marie Curie, 13 Rue Pierre et Marie Curie, F-75005 Paris, France.

⁴Ecology and Evolutionary Biology Section, Institut de Biologie de l'Ecole Normale Supérieure (IBENS), Centre National de la Recherche Scientifique (CNRS), UMR 8197, INSERM U1024, 46 Rue d'Ulm, F-75005 Paris, France.

⁵Laboratoire de Physiologie Cellulaire et Végétale, UMR 5168, Centre National de la Recherche Scientifique (CNRS), Commissariat à l'Énergie Atomique et aux Énergies Alternatives (CEA), Université Grenoble Alpes, Institut National Recherche Agronomique (INRA), Institut de Recherche en Sciences et Technologies pour le Vivant (iRTSV), CEA Grenoble, F-38054 Grenoble cedex 9, France.

⁶Fermental SA, F-33500 Libourne, France.

⁷Institute for Integrative Biology of the Cell (I2BC), Commissariat à l'Énergie Atomique et aux Énergies Alternatives (CEA), Centre National de la Recherche Scientifique (CNRS), Université Paris-Sud, Institut de Biologie et de Technologie de Saclay, F-91191 Gif-sur-Yvette cedex, France.

⁸Istituto di Biofisica, Consiglio Nazionale delle Ricerche, Via Celoria 26, I-20133 Milan, Italy.

ABSTRACT

Diatoms are one of the most ecologically successful classes of photosynthetic marine eukaryotes in the contemporary oceans. Over the past 30 million years, they have helped to moderate Earth's climate by absorbing carbon dioxide from the atmosphere, sequestering it via the biological carbon pump and ultimately burying organic carbon in the lithosphere¹. The proportion of planetary primary production by diatoms in the modern oceans is roughly equivalent to that of terrestrial rainforests². In photosynthesis, the efficient conversion of carbon dioxide into organic matter requires a tight control of the ATP/NADPH ratio which, in other photosynthetic organisms, relies principally on a range of plastid-localized ATP generating processes^{3–6}. Here we show that diatoms regulate ATP/NADPH through extensive energetic exchanges between plastids and mitochondria. This interaction comprises the re-routing of reducing power generated in the plastid towards mitochondria and the import of mitochondrial ATP into the plastid, and is mandatory for optimised carbon fixation and growth. We propose that the process may have contributed to the ecological success of diatoms in the ocean.

In oxygenic photosynthesis, light drives a linear electron flow from water to NADPH by the two photosystems (PS I and PS II), and the generation of an electrochemical proton gradient (or proton motive force, PMF) across the thylakoid membranes, which fuels ATP synthesis by an ATP synthase. Although the ratio of ATP/NADPH generated by linear electron flow is not entirely resolved^{7,8}, it is considered to be insufficient to fuel CO₂ import into the plastid and assimilation by the Calvin cycle^{8,9}. Therefore, to make up the shortfall, additional ATP must be produced by alternative pathways that do not generate NADPH. In *Viridiplantae* (including green algae and higher plants) these alternative electron pathways have been found in the chloroplast and mostly comprise cyclic electron flow (CEF) around PS I (ref. 3) and/or the water-to-water cycles¹⁰; that is, flows of electrons resulting from the oxidation of water at PS II that are re-routed to an oxidase activity. This last group of oxidases include the Mehler reaction at the PS I acceptor side^{4,11,12}, the activity of the plastoquinone terminal oxidase downstream of PS II (ref. 5) and the oxygenase activity of ribulose 1,5-bisphosphate carboxylase–oxygenase (Rubisco) (photorespiration⁶). Although genes encoding most components for these processes appear to be present in diatoms^{13–15}, it is currently unknown what mechanisms are used to balance the ATP/NADPH ratio.

We therefore investigated this question using the model species *Phaeodactylum tricornutum*. The PMF generated across thylakoid membranes comprises an electric field ($\Delta\Psi$) and a proton gradient (ΔpH). The $\Delta\Psi$ can be probed in vivo by measuring the electrochromic shift (ECS), that is the Stark effect, a modification of the absorption spectrum of specific pigments caused by changes in the transmembrane electric field in the plastid¹⁶. An ECS signal is present in *P. tricornutum* (Fig. 2.1a), and an analysis of the ECS signal relaxation after light exposure (Extended Data Fig. 2.1) reveals that it comprises two components displaying different spectra (Fig. 2.1a). One follows a linear dependence on the amplitude of $\Delta\Psi$ whereas the other follows a quadratic relationship (Fig. 2.1b). The existence of a 'quadratic ECS' is predicted by theory¹⁶ but has only been observed so far in mutants of green algae with altered pigment composition¹⁷. The peculiar existence of two different ECS probes in wild-type *P. tricornutum* cells allows an absolute quantification of the electric field, providing a valuable tool to analyse the PMF in a living cell (see Methods).

We plotted the amplitude of the quadratic versus linear ECS signals during the relaxation of a light-induced PMF and obtained a parabolic function (Fig. 2.1c, d and Extended Data Fig. 2.2). However, the ECS signals did not reach the minimum of the parabola in the dark, but rather remained positive. This indicates that a PMF is maintained across the thylakoid membrane of diatoms in the dark ($\Delta\Psi_d$, Fig. 2.1c). The field $\Delta\Psi_d$ can not only be dissipated by addition of an uncoupler (carbonyl cyanide-4-(trifluoromethoxy)phenylhydrazone (FCCP)), but also by blocking mitochondrial electron transport by anaerobiosis or addition of antimycin A (AA) plus salicylhydroxamic acid (SHAM). The combination of these two inhibitors blocks both the cyanide-sensitive (complex III) and the cyanide-insensitive (alternative oxidase, AOX) respiratory pathways (Fig. 2.1d). These results suggest that the residual PMF in the dark is generated in plastids by the chloroplast ATPase by hydrolysis of ATP derived from mitochondria (Fig. 2.1e)¹⁸. Furthermore, the extent of $\Delta\Psi_d$ observed in *P. tricornutum* is larger than that previously reported in green algae¹⁹, suggesting that the ATP exchange could be more efficient in diatoms.

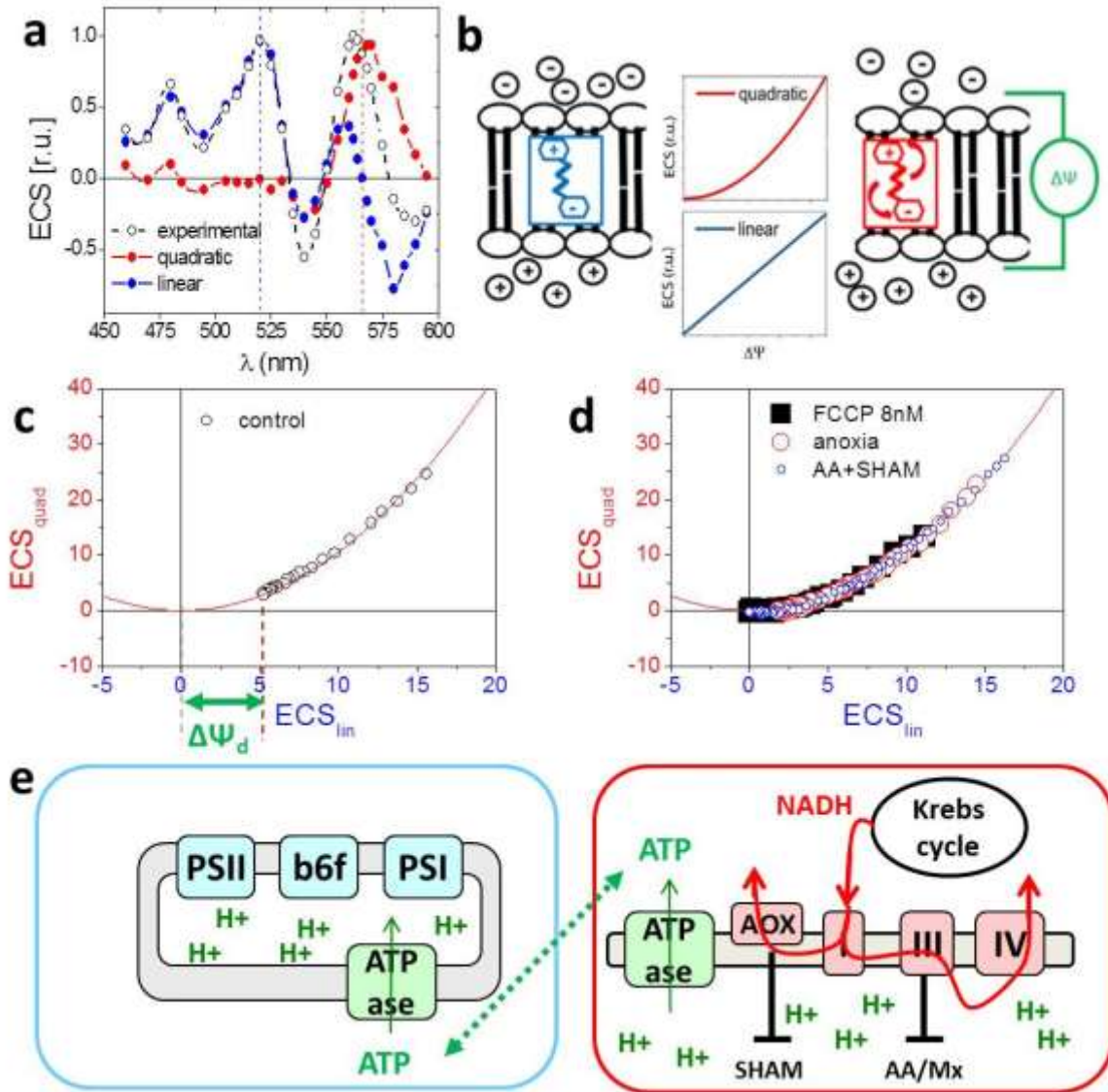


Fig. 2.1 ECS measures the PMF in *P. tricornutum*. **a**, Deconvolution of the experimental ECS spectrum (black) into linear (blue) and quadratic (red) spectral components (see Methods); r.u., relative units. **b**, Schematic representation of polar (blue) and polarizable (red) pigments, and their associated linear (blue) and quadratic (red) ECS responses to the electric field. Black: thylakoid lipid bilayer. Green '1' and '2' symbols: $\Delta\Psi$. Red arrows: pigment polarization induced by $\Delta\Psi$. **c**, **d**, Relationship between quadratic and linear ECS in control (**c**) and in cells treated with uncoupler (8nM FCCP, black squares), anaerobiosis (red circles) and respiratory inhibitors (AA, 5mM, and SHAM, 1 mM; blue circles) (**d**). Green arrow: extent of the dark electric field ($\Delta\Psi_d$). Representative of five (**c**) and three (**d**) independent biological samples. **e**, Schematic representation of the energetic interactions between plastid (left) and mitochondria (right) in the dark. Red arrows: respiratory electron flows. Green dashed line: putative ATP/ADP exchange pathway between the organelles. ATPase, ATPase/ synthase; b₆f, cytochrome b₆f; I/III/IV, respiratory complexes I, III and IV.

To evaluate what mechanism regulates ATP/NADPH in the light in *P. tricornutum*, we first used the linear ECS to probe the CEF capacity (see Methods). CEF turned out to represent only a very low fraction of the maximum electron flow capacity (Fig. 2.2a and Extended Data Fig. 2.3a, c) and was insensitive to changes in the photosynthetic flux (Fig. 2.2a). Thus, it appears very unlikely that CEF could regulate ATP/ NADPH fluxes. Next, we explored the water-to-water cycle using membrane-inlet mass spectrometry on cells incubated with $^{18}\text{O}_2$. O_2 consumption increased with light, being ~ 2.5 -fold higher at saturating light intensities than in the dark (Extended Data Fig. 2.3b, d). We also found that the light-stimulated O_2 consumption was blocked by 3-(3,4-dichlorophenyl)-1,1-dimethyl-urea (DCMU), which inhibits O_2 production by PS II (Extended Data Fig. 2.3b, d), indicating that this process is fed by electrons generated by PS II. O_2 consumption increased linearly with O_2 production, in agreement with earlier findings in another diatom species ²⁰, indicating that a constant proportion ($\sim 10\%$) of the electron flow from photosynthesis is re-routed to an O_2 -consuming pathway, regardless of light intensity (Fig. 2.2b). To test whether the O_2 -consuming pathway occurs in the plastid or relies on mitochondrial activity, we used increasing concentrations of inhibitors to titrate respiration and tested possible consequences on photosynthesis. We reasoned that if respiration consumes reducing equivalents generated in the plastid to generate additional ATP, any mitochondrial dysfunction should negatively impact photosynthesis.

We found that this was indeed the case, as photosynthetic electron transfer rate (ETR PS II) linearly followed changes in respiration (Fig. 2.2c and Extended Data Fig. 2.4). We conclude that a partial re-routing of the photosynthetic flow towards mitochondrial respiration rather than CEF optimises photosynthesis in diatoms, providing commensurate ATP per NADPH at all irradiances (Fig. 2.2d).

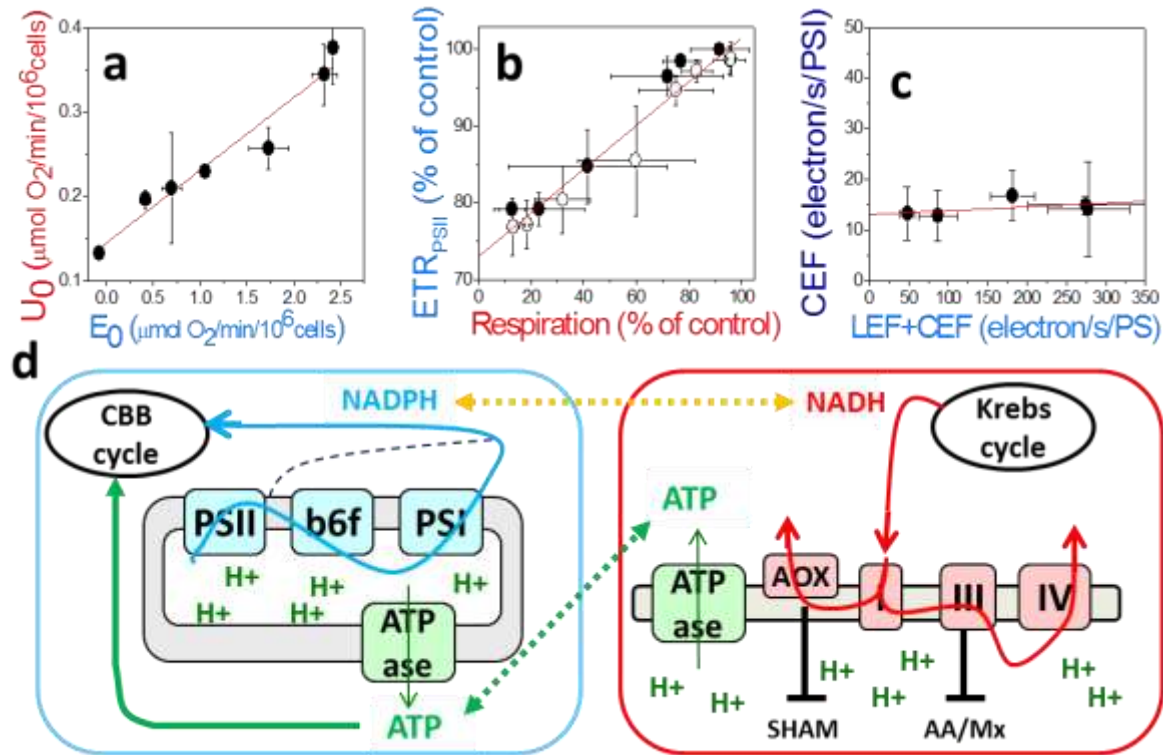


Fig. 2.2 Energetic interactions between mitochondria and plastid in *P. tricornutum*. **a**, Relationship between CEF capacity and total electron flow (TEF, \pm s.d. from data in Extended Data Fig. 3a, c). **b**, Relationship between oxygen uptake (U_0) and gross photosynthesis (E_0) as measured by membrane-inlet mass spectrometry (\pm s.e.m. from data in Extended Data Fig. 3b, d). **c**, Dependency of photosynthetic activity (ETR_{PSII}) on respiration rates (as the percentage of control, \pm s.d. from data in Extended Data Fig. 4). Closed circles: SHAM+AA; open circles: SHAM + myxothiazol treatments (see Methods). **d**, Schematic representation of possible plastid-mitochondria metabolic interactions in the light. Continuous and dashed blue arrows: photosynthetic linear and cyclic flows, respectively. Yellow arrow: exchange of reducing equivalents. For other symbols, see text and Fig. 1e.

Photosynthetic activity displayed increasing sensitivity to AOX inhibition with light, suggesting that cyanide-insensitive respiration becomes prominent in high light (Fig. 2.3a). This prompted us to generate AOX knockdown cell lines of *P. tricornutum*. Two independent clones were selected on the basis of reduced AOX protein accumulation (Fig. 2.3b) and decreased activity (measured as the SHAM-sensitive, AA-insensitive component of respiration; Extended Data Fig. 2.5a). The AOX contribution, representing, 50% of dark respiration in wild-type cells (Extended Data Fig. 2.4e), was decreased two-fold in the two knockdown lines (Extended Data Fig. 2.5a). Confocal microscopy confirmed the mitochondrial localization of the targeted gene product (Extended Data Fig. 2.6a). The reduced AOX activity in the knockdown lines paralleled a

diminished PMF in the dark ($\Delta\Psi_d$, Extended Data Fig. 2.5b), despite the fact that overall dark respiration was slightly higher (Extended Data Fig. 2.5a). This effect was strongly enhanced by addition of AA (Extended Data Fig. 2.5b). The decreased AOX activity also correlated with a decreased photosynthetic capacity, especially under high light intensities (similar to SHAM-treated wild-type cells; Fig. 2.3a), and a diminished growth rate (Fig. 2.3c), which was exacerbated further by inhibiting complex III using AA (Extended Data Fig. 2.5c). The growth and photosynthetic phenotypes were not due to changes in the accumulation of the photosynthetic complexes, for which we detected comparable levels of representative proteins in all cell lines (Fig. 2.3b). The only exception was a small decrease in the cytochrome b_6f content in the knockdown cell lines, which nonetheless did not decrease its overall catalytic turnover (Extended Data Fig. 2.7).

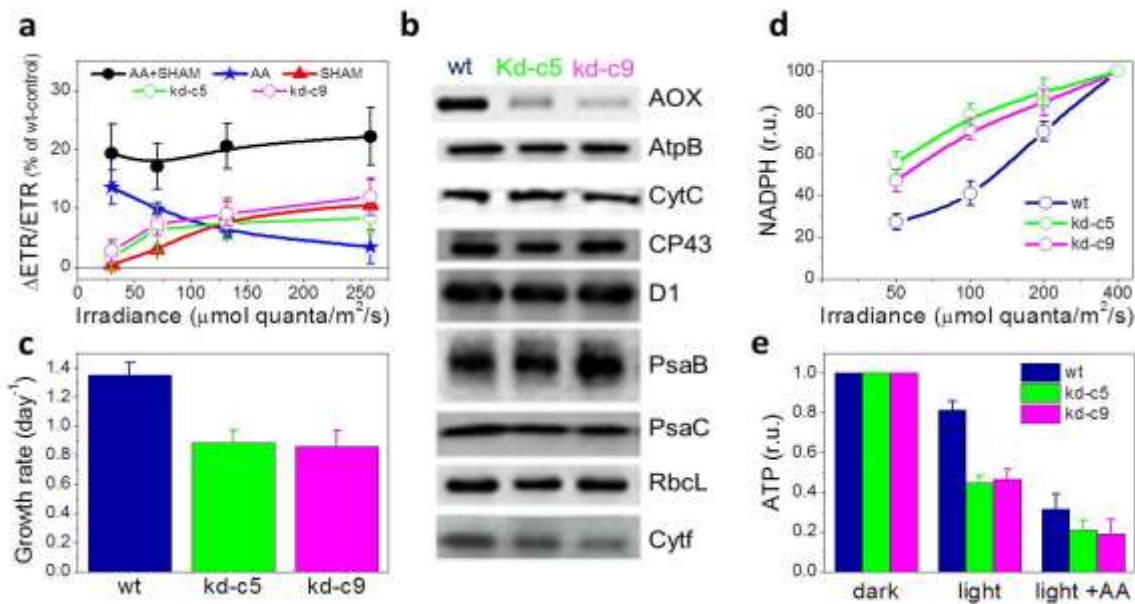


Fig. 2.3 Phenotypic traits of AOX knockdown lines of *P. tricornutum*. **a**, Relative sensitivity of photosynthesis ($ETR_{PS II}$) to addition of respiratory inhibitors: AA (blue), SHAM (red) and AA + SHAM (black) ($n = 3 \pm \text{s.D.}$), or to knockdown of AOX ($n = 5 \pm \text{s.d.}$). Green and pink: kd-c5 and kd-c9, respectively. **b**, Western blot analysis of photosynthetic and respiratory complexes. **c**, Growth rates of the wild-type and AOX lines ($n = 7 \pm \text{s.d.}$). **d**, In vivo light dependency of NADPH redox state in wild-type and AOX lines. Data are normalized to the maximum value in the light. **e**, In vivo ^{31}P -NMR evaluation of the NTP content in wild-type and AOX knockdown lines, in the dark or in low light, with or without AA (data normalized to the dark values). **d, e**, Three independent biological samples

Our working model presented in Fig. 2.2d predicts that disruption of the plastid–mitochondria interaction in the knockdown cell lines should lead to the accumulation of NADPH and a decreased cellular content of ATP in the light. Indeed, *in vivo* assessments of the pools of NADPH and ATP in wild-type and knockdown cell lines confirmed an increase in the NADPH/NADP⁺ ratio with light intensity (Fig. 2.3d and Extended Data Fig. 2.8a), accompanied by a net decrease of cellular ATP levels (Fig. 2.3e and Extended Data Fig. 2.8b), both of which were more drastic in AOX knockdown cells than wild-type cells. These observations confirm that mitochondrial respiration is directly involved in the adjustment of the ATP to NADPH ratio in the plastid.

We then examined the generality of our findings in other diatom species. The similar ECS features (linear and quadratic components) in *Thalassiosira pseudonana*, *Thalassiosira weissflogii*, *Fragilaria pinnata* and *Ditylum brightwellii* (Fig. 2.4a) were used to confirm the presence of a PMF in the plastids in the dark at the expense of hydrolysis of ATP supplied by the mitochondria in all cases (Fig. 2.4b). Moreover, a negligible contribution of CEF (Extended Data Fig. 2.9) and a significant involvement of mitochondrial respiration to photosynthesis (Extended Data Fig. 2.10) were found in all these species. The involvement of mitochondrial respiration in the *optimisation* of photosynthesis therefore appears to be a general and conserved feature in diatoms.

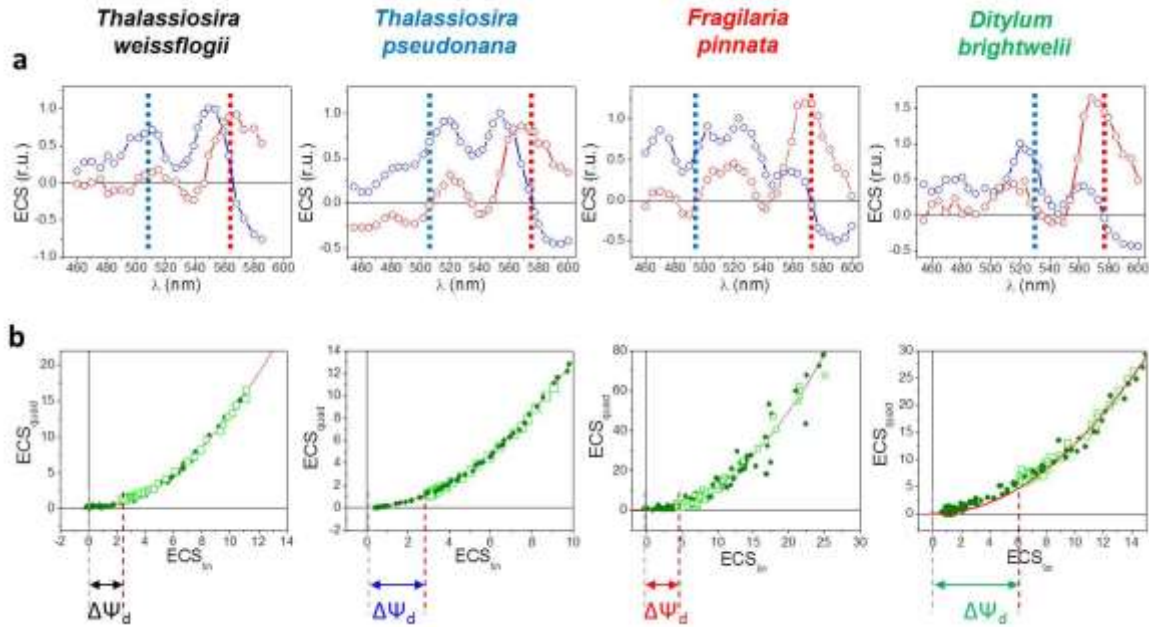


Fig. 2.4 ATP transfer from mitochondria to plastid in representative diatoms. **a**, Spectra of the linear (blue) and quadratic (red) ECS probes in four diatoms. Blue and red vertical dashed lines represent the wavelengths used for linear and quadratic ECS, respectively. Spectra are normalized to 1 at the maximum value of the linear ECS. **b**, Relationship between the quadratic and the linear ECS in control conditions (open symbols) and in AA+SHAM conditions (filled symbols). $\Delta\Psi_d$ is represented as a horizontal arrow. Data are representative of three independent biological samples.

We conclude that ATP generation sets the rate of photosynthetic carbon assimilation in diatoms, as suggested in other photosynthetic organisms⁸, but that in contrast with the *Viridiplantae*, *optimisation* of diatom photosynthesis does not rely on plastid-localized processes. Instead, constitutive energetic interactions between diatom mitochondria and plastids ensure the sharing of reducing equivalents and ATP to fuel CO₂ assimilation in the light (Fig. 2.2d). While the process we have uncovered has some similarities to the export of reducing equivalents from the plastids towards mitochondria in plants and green algae, the fundamental difference is that in plants and green algae the process serves as a valve to dissipate excess of reducing power²¹, and can only participate in the regulation of the ATP/NADPH ratio when the chloroplast capacity to make extra ATP is genetically disrupted^{22–24}. We propose that the presence of trans-porters such as the malate shuttle²¹, which are encoded in diatom genomes¹³, as well as the very tight physical interactions observed in diatoms between plastids and mitochondria (Extended Data Fig. 2.6b), may make these energetic interactions possible between the two organelles. Because

diatom plastids are surrounded by four membranes rather than two as in *Viridiplantae*¹³, it will be of interest to elucidate the configuration of such transporters, as well as the rationale for the diminished CEF efficiency in diatoms. More generally, the coupling of respiratory and photosynthetic activities in diatoms should be explored in the context of resource utilization in the ocean and as a means to boost the production of useful metabolites for biotechnology.

METHODS

No statistical methods were used to predetermine sample size. The experiments were not randomized. The investigators were not blinded to allocation during experiments and outcome assessment.

Growth conditions. Wild-type and AOX transformant lines of *P. tricornutum* Pt1 8.6 (CCMP 2561) were grown in artificial sea water (ASW25). *T. pseudonana* (CCMP 1335), *T. weissflogii* (CCMP 1336), *F. pinnata* (CCAP 1029/2) and *D. brightwellii* (CCMP 359) were grown in F/2 medium, supplemented with silicate²⁶. All strains were grown at $19 \pm 1^\circ\text{C}$ in semi-continuous batch culture (with moderate shaking for *P. tricornutum*, *T. pseudonana* and *T. weissflogii*). The photoperiod was 12 h light/12 h dark, and light irradiance was $70 \mu\text{mol quanta m}^{-2} \text{s}^{-1}$. Cell concentration was determined daily with a Z2 Coulter Counter analyser (Beckman Coulter) to ensure all the experiments were performed with cells in exponential phase. For biophysical measurements, cells were concentrated by centrifugation and resuspended in their growth medium (supplemented with 10% w/v Ficoll to prevent cell sedimentation) and kept in the dark at least 30 min before measurements.

Inhibitors. DCMU, 2,5-dibromo-3-methyl-6-isopropyl-p-benzoquinone (DBMIB), FCCP, AA, myxothiazol and SHAM (Sigma-Aldrich) were dissolved in ethanol, whereas hydroxylamine, glucose, glucose oxidase and catalase (Sigma-Aldrich) were dissolved in deionized water. FCCP was used at a very low concentration ($8 \mu\text{M}$, Fig. 2.1d) to allow the disruption of the dark PMF without preventing the light-induced generation of PMF needed to quantify $\Delta\Psi_d$. AA and myxothiazol were used at $5 \mu\text{M}$, unless otherwise stated. DCMU was used at a concentration of $15 \mu\text{M}$. In every measurement involving hydroxylamine or SHAM, the lowest inhibitor

concentration to induce a full inhibition of PS II activity or maximum inhibition of respiration, respectively, was used. The range of concentrations used was 30–100 μM and 0.5–1 mM for hydroxylamine and SHAM, respectively. Anaerobic conditions were obtained through incubation with catalase (1,000 U ml^{-1}), glucose (10 mM) and glucose oxidase (20,000 U ml^{-1}). AA has been previously described as an inhibitor of cyclic electron flow, affecting the NDH-independent pathway²⁷. This potential effect was ruled out in diatoms because no change in cyclic electron flow was noticed upon addition of AA. Consistent with the fact that genes encoding some members of the NDH complex are absent in diatom genomes, this indicates that AA does not affect the NDH-independent CEF pathway in diatoms. AA and myxothiazol were preferred to potassium cyanide to block the cyanide sensitive pathway of respiration because potassium cyanide also affects Rubisco activity²⁸, ascorbate peroxidase²⁹ and Cu/ Zn superoxide dismutase³⁰.

Deconvolution of linear and quadratic ECS components. To deconvolute the linear and quadratic contributions to the ECS signals, cells were left for an hour in the cuvette to reach complete anaerobiosis. In these conditions, the ATP synthase activity is slowed down³¹, and long-living ECS signals are no longer contaminated with other light-induced absorption changes (principally associated with c-type cytochromes). Light stimulation of cells was achieved with a series of six laser single-turnover (duration ,7 ns) saturating flashes, provided by a laser dye (LDS 698) pumped by a frequency doubled Nd-YAG laser (Quatel). We considered that the relaxation of the electric field generated by the light stimulus is described by the exponential function $\Delta\Psi = \Delta\Psi_0 \exp(-t/\tau)$, where t is time, $\Delta\Psi_0$ is the initial electric field generated by the light, and τ is the electric-field decay lifetime. The linear and quadratic components of the ECS are theoretically proportional to $\Delta\Psi$ and $\Delta\Psi^2$, respectively. Therefore, the $\Delta I/I$ spectro-temporal matrices (from 460 to 600 nm) can be described by a sum of two exponentials: $\gamma(\lambda, \tau) = A(\lambda) \exp(-t/\tau) + B(\lambda) \exp(-2t/\tau) + C(\lambda)$. The kinetics of ECS relaxation were fitted by a global routine, which considers the lifetime t as a global (wavelength-independent) variable, and the amplitudes of linear and quadratic components (A and B , respectively) as local (wavelength-dependent) variables. A non-decaying component (C) was also included in the fit to account for a small fraction of residual

signal at long delay times. The plot of the A and B amplitudes as a function of the wavelength provides the decay associated spectra of the linear and quadratic contributions to the ECS signal, respectively, which are shown in Fig. 2.1a. The fit was performed with homemade software, which used the MINUIT package, developed and distributed by CERN (Geneva, Switzerland) and implemented in FORTRAN77. It minimizes the reduced sum of squared residues between the model function and the experimental data, employing a two-step protocol involving an initial search that utilizes the Simplex method (Nelder–Mead algorithm) and a refined search using the Levenberg–Marquardt algorithm as described in ref. 32. The quality of the fit description was judged on the basis of reduced sum of squared residues statistics, visual inspection of the fit residuals, residuals autocorrelation and stability of the solutions upon random perturbation of the best-fit. The deconvolution was performed on two independent biological samples, giving similar results.

Measurements of c-type cytochromes and linear and quadratic ECS. Absorption difference signals were measured at different wavelengths with a Joliot-type spectrophotometer (JTS-10, Biologic), equipped with a white probing LED and the appropriate interference filters (3–8 nm bandwidth). For $\Delta\Psi_d$ measurements, the PMF was increased using an ~ 10 ms pulse of saturating ($4,500 \mu\text{mol quanta m}^{-2} \text{s}^{-1}$) red light (see Extended Data Fig. 2.3 for representative ECS kinetics). For *P. tricornutum*, ECS signals were evaluated using three wavelengths, to eliminate contribution from c-type cytochromes (see Extended Data Fig. 2.2). The latter was calculated as $\text{cyt } c = [554] - 0.4[520] - 0.4[566]$, where [554], [520] and [566] are the absorption difference signals at 554 nm, 520 nm and 566 nm, respectively. The very similar relaxation of c-type cytochromes in aerobic and anaerobic conditions, despite very different ECS relaxations (Extended Data Fig. 2.2b), demonstrates the validity of the cyt c deconvolution procedure. Then, ecs_{lin} and ecs_{quad} (ECS signals before correction for $\Delta\Psi_d$) were estimated from the following relationships: $\text{ecs}_{\text{lin}} = [520] - 0.25 \text{ cyt } c$ and $\text{ecs}_{\text{quad}} = [566] + 0.15 \text{ cyt } c$. For the other diatoms, appropriate wavelengths were chosen for calculating ecs_{lin} and ecs_{quad} (red and blue lines in Fig. 2.4) to minimize the cytochrome c contributions. The relationships between ecs_{quad} and ecs_{lin} were fitted with the parabolic equation $\text{ecs}_{\text{quad}} + \alpha \Delta\Psi_d^2 = \alpha (\text{ecs}_{\text{lin}} + \Delta\Psi_d)^2$, where $\Delta\Psi_d$ is the electrical component of the PMF in the dark and α is constant for all the conditions in a diatom species (see Extended Data Fig. 2.2c).

The ecs_{lin} and ecs_{quad} values represent ECS changes relative to dark values. Therefore, we corrected them for the dark electric field. This leads to $ECS_{lin} = ecs_{lin} + \Delta\Psi_d$, and $ECS_{quad} = ecs_{quad} + \alpha\Delta\Psi_d^2$, namely absolute values of the ECS signals. This simply corresponds to a shift of the x- and y-axes to allow the minimum of the parabola to coincide with the origin of the axes (see Extended Data Fig. 2.2d), and gives $ECS_{quad} = \alpha ECS_{lin}^2$. This leads to the evaluation of $\Delta\Psi_d$ as the minimal ECS_{lin} value of the experimental data. In Fig. 2.1c, d, and Extended Data Fig. 2.2c, d, ECS data were normalized to the ecs_{lin} increase upon a saturating laser flash (that is, one charge separation per photosystem, see ref. 33). This allows the estimation of $\Delta\Psi_d$ in *P. tricornutum* as approximately five charge separations by PS, namely, 100 mV (ref. 12) (Fig. 2.1c). The presence of linear and quadratic ECS components allows measurement of the absolute value of $\Delta\Psi$ in the dark ($\Delta\Psi_d$). Indeed the amplitude of the linear ECS response (ecs_{lin}) observed upon a light stimulus increasing $\Delta\Psi$ is constant, namely independent of the value of the field pre-existing the illumination ($\Delta\Psi_d$). Conversely, the amplitude of the quadratic ECS response (ecs_{quad}) is a function of the value of $\Delta\Psi_d$. Therefore, plotting the amplitude of the ecs_{quad} versus ecs_{lin} allows quantification of the absolute value of the electric field in the dark ($\Delta\Psi_d$).

Cyt b_6f turnover was measured through the slow phase (phase b^{31}) of the linear ECS, which reflects b_6f -catalysed charge transfer across the membranes, and through the reduction rate of the c-type cytochromes (c_6/f), using the three-wave-lengths deconvolution procedure described above. Measurements were performed after a saturating laser flash.

Measurements of photosynthetic flows. For calculation of the TEF (the sum of linear and cyclic electron flows) and CEF capacities, we measured the photochemical rates in the absence and presence, respectively, of DCMU. In brief, under steady-state illumination conditions, the ECS signal results from concomitant transmembrane potential generation by PS II, the cytochrome b_6f complex and PS I, and from transmembrane potential dissipation by the plastid ATP synthase. When light is switched off, PS activities stop immediately, while ATP synthase and cytochrome b_6f complex activities remain (transiently) unchanged. Therefore, the difference between the slopes of the linear ECS signal (ECS_{lin}) measured in the light and after the light is switched off (SD - SL) is proportional to the rate of PS I and PS II photochemistry (that is, to the rate of 'total' electron flow, Extended Data Fig. 2.3a). Because the linear ECS has been normalized to the

amplitude of the linear ECS signal induced by a saturating laser flash³⁴ (see above), the difference of slopes evaluates the number of charge separations per photosystem and per second. The rate of CEF can be evaluated using the same approach under conditions where PS II activity is inhibited by DCMU, and dividing this slope by the linear ECS signal induced by a saturating laser flash in the presence of PS II inhibitors (one charge separation per PS I (ref. 34)). This was done using saturating concentrations of DCMU, which block PS II oxidation, and of hydroxylamine, to avoid charge recombination within PS II.

Fluorescence-based measurements. Fluorescence-based photosynthetic parameters were measured with a fluorescence imaging setup described in ref. 35. Photosynthetic electron transfer rate ETR PS II and NPQ were calculated, respectively, as $I(F_{m'} - F)/F_{m'}$ and $(F_m - F_{m'})/F_{m'}$, where F and $F_{m'}$ are the steady-state and maximum fluorescence intensities in light-acclimated cells (respectively), F_m is the maximal fluorescence intensity in dark-adapted cells, and I is the light irradiance in $\mu\text{mol quanta m}^{-2} \text{s}^{-1}$ (refs 36, 37). In Fig. 2.2c and Extended Data Fig. 2.4a, d, the light irradiance is $30 \mu\text{mol quanta m}^{-2} \text{s}^{-1}$. The light saturation curves of ETR PS II were fitted with the exponential rise function.

$P = P_{\text{max}}(1 - \exp(-E/E_k))$, where P_{max} is the maximal photosynthetic electron transport rate and E_k is the optimal light. $\Delta\text{ETR}/\text{ETR}$ (Fig. 2.3a) was calculated as $(\text{ETR}_{\text{ref}} - \text{ETR}) \times 100/\text{ETR}_{\text{ref}}$, the reference being the value measured in wild-type cells in untreated conditions.

Membrane-inlet mass spectrometry measurements. Samples were introduced in a 3 ml thermostated cuvette, which was connected to a Quadrupole Mass Spectrometer (QMS 200, Pfeiffer Vacuum Prisma) by a stainless steel vacuum tube (0.125 inches) passing through a water trap filled with ethanol and dry ice. The sample was separated from the tube via a gas-permeable inlet system (poly-tetrafluoroethylene (PTFE) membrane). $^{18}\text{O}_2$ was added as a bubble to the algal suspension, and the bubble was removed before the experiment. The measurements of the partial pressures of $^{16}\text{O}_2$ ($p^{16}\text{O}_2$, $m/z = 32$), $^{18}\text{O}_2$ ($p^{18}\text{O}_2$, $m/z = 36$) and argon ($m/z = 40$) were performed after the cuvette was sealed. A blue light-emitting diode (LED) source was connected to the cuvette, and the light irradiance was manually adjustable in the 0 to $\sim 800 \mu\text{mol quanta m}^{-2} \text{s}^{-1}$ range. The temperature was kept at $19 \pm 1 \text{ }^\circ\text{C}$ in the cuvette during the experiment.

To calculate gross O₂ production (E₀) and uptake (U₀), respectively production and consumption by the cells, we adapted the equations from ref. 38:

$$U_0 = (\Delta[^{18}\text{O}]/\Delta t + k[^{18}\text{O}])(([^{18}\text{O}] + [^{16}\text{O}]/[^{18}\text{O}])$$
$$E_0 = (\Delta[^{16}\text{O}]/\Delta t + k[^{16}\text{O}]) + U_0([^{18}\text{O}] + [^{16}\text{O}]/[^{16}\text{O}])$$

where k is the rate constant of O₂ decrease measured in the absence of algae. We normalized O₂ to Argon (a biologically inert gas with very similar solubility properties), which decreases the sensitivity of O₂ measurements to fluctuations by ~80% (ref. 39). The gas concentrations were calibrated by measuring the air-equilibrated O₂ concentration (stirring deionized water in the open cuvette for at least 5 h) and background O₂ (bubbling with N₂).

Respiration rates. Respiration rates were measured as O₂ exchange rates using a Clark-type oxygen electrode at 19 °C (Hansatech Instruments). AOX capacity was measured as SHAM-sensitive respiration in conditions where the cyanide-sensitive pathway was inhibited beforehand (AA, 5 μM).

ATP/NADPH in vivo measurements. NADP⁺/NADPH redox changes were followed in living cells using a Dual-PAM (Walz). NADPH fluorescence was measured at 460 nm, upon excitation in the near ultraviolet. Chlorophyll a concentration was ~5 μg ml⁻¹. ATP content was measured using an in vivo ³¹P-AMX 400 NMR spectrometer equipped with a 25-mm multinuclear probe tuned at 161.9 MHz, and a homemade lighting system, as described in ref. 40. The relative ATP content was estimated in vivo from the surface of α-, β- and γ-phosphorus resonance peaks corresponding to the three phosphates of NTPs, which dominate the NMR spectra with inorganic phosphate and polyphosphates⁴¹.

Western blots and immunolocalization. Protein samples (5–10 μg) were loaded on 13% SDS–polyacrylamide gel electrophoresis (PAGE) gels and blotted to nitro-cellulose. Primary AOX antibody was custom designed (Sdix, 1:4,000 dilution). All other antisera used were obtained from Agrisera (<http://www.agrisera.com/en/info/catalog.html>). The blots were developed with ECL detection reagent and images of the blots were obtained using a CCD (charge-coupled device) imager (Chemidock MP Imaging, Bio-Rad). The results presented in Fig. 2.3b are

representative of a total of five western blots on independent biological samples. Immunolocalization of AOX was generally done as described in ref. 34. Briefly, cells were fixed with 2% formaldehyde in culture media for 20 min, washed three times with marine phosphate buffer (mPBS, see ref. 42) and permeabilized by 1% Triton X-100 in mPBS for 10 min. The cells were washed again, blocked for 30 min in 1% BSA in mPBS, and incubated overnight at room temperature (25 °C) with anti-AOX antibody from rabbit (custom design, Sdix, 1:200 dilution in mPBS). The cells were then rinsed with mPBS and incubated with donkey Alexa 488-conjugated anti-rabbit IgG antibody (Life Technologies, at 1:100 dilution in mPBS) for 2 h at room temperature. Cells were then stained with 0.5 µg ml⁻¹ DAPI (49,69-diamidino-2-phenylindole, Life Technologies) for 10 min and mounted with Vectashield (Vector Laboratories) after a rinse. Finally the cells were observed using a Leica SP5 confocal microscope (Leica Microsystems).

Electron microscopy. For transmission electron microscopy, *P. tricornutum* cells were fixed in 0.1 M cacodylate buffer (Sigma-Aldrich), pH 7.4, containing 2.5% glutaraldehyde (TAAB), 2% formaldehyde (Polysciences) for 1 h at room temperature and then prepared according to a modified protocol from T. J. Deerinck *et al.*, (<http://ncmir.ucsd.edu/sbfsem-protocol.pdf>). After the dehyd-ration steps, the cells were infiltrated with ethanol/Epon resin mixture (2/3–1/3 for 1 h and 1/3–2/3 for 1 h) and finally embedded in Epon in a 60 °C oven for 48 h or longer. Ultrathin sections (60 nm) were prepared with a diamond knife on an UC6 Leica ultramicrotome and collected on 200 µM mesh nickel grids before examining on a JEOL 1200 EX electron microscope.

AOX knockdown lines. Partial coding sequence of AOX (identity Phatr2_bd1075) was amplified using primers AOXcFwd (TGCTCCGGAGGACAAT GAATTCGC) and AOXcRev (TGGTCTAGACGTCGCGATGTTC), cut by EcoRI/XbaI (Fermentas) and cloned into an EcoRI/XbaI-digested antisense construct⁴³, under control of the FcpB promoter. The AOX antisense construct was introduced into wild-type *P. tricornutum* cells using the standard microparticle bombardment procedure with a PDS-1000/He Particle Delivery System (Bio-Rad)^{43,44}. After 2 days, cells were transferred to F/2-supplemented–filtered seawater plates containing 100 µg ml⁻¹ phleomycin, a selective antibiotic for the Sh ble gene (InvivoGen, 09K30-MM). Putative antisense lines were verified for the presence of the transformed DNA by PCR screening using

the primers ShbleFwd (ACCAAGTGCCGTTCCGGTG) and ShbleRev (TCGGTCAGTCCTGCTCCTC), and the most strongly silenced lines were chosen on the basis of reduction of AOX protein levels as measured by SDS-PAGE western blot with an anti-AOX antibody (see section on western blots and immunolocalization).

REFERENCES

Falkowski, P. G. The evolution of modern eukaryotic phytoplankton. *Science* 305, 354–360 (2004).

Field, C. B., Behrenfeld, M. J., Randerson, J. T. & Falkowski, P. G. Primary production of the biosphere: integrating terrestrial and oceanic components. *Science* 281, 237–240 (1998).

Shikanai, T. Cyclic electron transport around photosystem I: genetic approaches. *Annu. Rev. Plant Biol.* 58, 199–217 (2007).

Asada, K. The water–water cycle as alternative photon and electron sinks. *Phil. Trans. R. Soc. Lond. B* 355, 1419–1431 (2000).

Cardol, P. et al. An original adaptation of photosynthesis in the marine green alga *Ostreococcus*. *Proc. Natl Acad. Sci. USA* 105, 7881–7886 (2008).

Ort, D. R. & Baker, N. R. A photoprotective role of O₂ as an alternative electron sink in photosynthesis? *Curr. Opin. Plant Biol.* 5, 193–198 (2002).

Petersen, J., Förster, K., Turina, P. & Graßber, P. Comparison of the H₁/ATP ratios of the H₁-ATP synthases from yeast and from chloroplast. *Proc. Natl Acad. Sci. USA* 109, 11150–11155 (2012).

Allen, J. F. Photosynthesis of ATP-electrons, proton pumps, rotors, and poise. *Cell* 110, 273–276 (2002).

Lucker, B. & Kramer, D. M. Regulation of cyclic electron flow in *Chlamydomonas reinhardtii* under fluctuating carbon availability. *Photosynth. Res.* 117, 449–459 (2013).

Allen, J. F. Oxygen reduction and optimum production of ATP in photosynthesis. *Nature* 256, 599–600 (1975).

Radmer, R. J. & Kok, B. Photoreduction of O₂ primes and replaces CO₂ assimilation. *Plant Physiol.* 58, 336–340 (1976).

Badger, M. R. Photosynthetic oxygen exchange. *Annu. Rev. Plant Physiol.* 36, 27–53 (1985).

Prihoda, J. et al. Chloroplast-mitochondria cross-talk in diatoms. *J. Exp. Bot.* 63, 1543–1557 (2012).

Bowler, C. et al. The *Phaeodactylum* genome reveals the evolutionary history of diatom genomes. *Nature* 456, 239–244 (2008).

Grouneva, I., Rokka, A. & Aro, E.-M. The thylakoid membrane proteome of two marine diatoms outlines both diatom-specific and species-specific features of the photosynthetic machinery. *J. Proteome Res.* 10, 5338–5353 (2011).

Witt, H. T. Energy conversion in the functional membrane of photosynthesis. Analysis by light pulse and electric pulse methods. The central role of the electric field. *Biochim. Biophys. Acta* 505, 355–427 (1979).

Joliot, P. & Joliot, A. Characterization of linear and quadratic electrochromic probes in *Chlorella sorokiniana* and *Chlamydomonas reinhardtii*. *Biochim. Biophys. Acta* 975, 355–360 (1989).

Diner, B. & Joliot, P. Effect of the transmembrane electric field on the photochemical and quenching properties of photosystem II in vivo. *Biochim. Biophys. Acta* 423, 479–498 (1976).

Finazzi, G. & Rappaport, F. In vivo characterization of the electrochemical proton gradient generated in darkness in green algae and its kinetics effects on cytochrome b_6f turnover. *Biochemistry* 37, 9999–10005 (1998).

Waring, J., Klenell, M., Bechtold, U., Underwood, G. J. C. & Baker, N. R. Light-induced responses of oxygen photo-reduction, reactive oxygen species production and scavenging in two diatom species. *J. Phycol.* 46, 1206–1217 (2010).

Kinoshita, H. et al. The chloroplastic 2-oxoglutarate/malate transporter has dual function as the malate valve and in carbon/nitrogen metabolism. *Plant J.* 65, 15–26 (2011).

Lemaire, C., Wollman, F. A. & Bennoun, P. Restoration of phototrophic growth in a mutant of *Chlamydomonas reinhardtii* in which the chloroplast *atpB* gene of the ATP synthase has a deletion: an example of mitochondria-dependent photosynthesis. *Proc. Natl Acad. Sci. USA* 85, 1344–1348 (1988).

Cardol, P. *et al.* Impaired respiration discloses the physiological significance of state transitions in *Chlamydomonas*. *Proc. Natl Acad. Sci. USA* 106, 15979–15984 (2009).

Dang, K. V. *et al.* Combined increases in mitochondrial cooperation and oxygen photoreduction compensate for deficiency in cyclic electron flow in *Chlamydomonas reinhardtii*. *Plant Cell* 26, 3036–3050 (2014).

Vartanian, M., Descler's, J., Quinet, M., Douady, S. & Lopez, P. J. Plasticity and robustness of pattern formation in the model diatom *Phaeodactylum tricornutum*. *New Phytol.* 182, 429–442 (2009).

Guillard, R. R. L. in *Culture of Marine Invertebrate Animals* (eds Smith W. L. & Chanley H.) 26–60 (Plenum, 1975).

Joe't, T., Cournac, L., Horvath, E. M., Medgyesy, P. & Peltier, G. Increased sensitivity of photosynthesis to antimycin A induced by inactivation of the chloroplast *ndhB* gene. Evidence

for a participation of the NADH-dehydrogenase complex to cyclic electron flow around photosystem I. *Plant Physiol.* 125, 1919–1929 (2001).

Wishnick, M. & Lane, M. D. Inhibition of ribulose diphosphate carboxylase by cyanide. Inactive ternary complex of enzyme, ribulose diphosphate, and cyanide. *J. Biol. Chem.* 244, 55–59 (1969).

Nakano, Y. & Asada, K. Purification of ascorbate peroxidase in spinach chloroplasts; its inactivation in ascorbate-depleted medium and reactivation by monodehydroascorbate radical. *Plant Cell Physiol.* 28, 131–140 (1987).

Asada, K., Takahashi, M. A. & Nagate, M. Assay and inhibitors of spinach superoxide dismutase. *Agric. Biol. Chem.* 38, 471–473 (1974).

Joliot, P. & Delosme, R. Flash induced 529 nm absorption change in green algae. *Biochim. Biophys. Acta* 357, 267–284 (1974).

Santabarbara, S., Redding, K. E. & Rappaport, F. Temperature dependence of the reduction of p-7001 by tightly bound plastocyanin in vivo. *Biochemistry* 48, 10457–10466 (2009).

Melis, A. Kinetic analysis of P-700 photoconversion: effect of secondary electron donation and plastocyanin inhibition. *Arch. Biochem. Biophys.* 217, 536–545 (1982).

Bailleul, B., Cardol, P., Breyton, C. & Finazzi, G. Electrochromism: a useful probe to study algal photosynthesis. *Photosynth. Res.* 106, 179–189 (2010).

Johnson, X. et al. A new setup for in vivo fluorescence imaging of photosynthetic activity. *Photosynth. Res.* 102, 85–93 (2009).

Genty, B., Briantais, J. M. & Baker, N. R. The relationship between the quantum yield of photosynthetic electron transport and quenching of chlorophyll fluorescence. *Biochim. Biophys. Acta* 990, 87–92 (1989).

Bilger, W. & Björkman, O. Role of the xanthophyll cycle in photoprotection elucidated by measurements of light-induced absorbance changes, fluorescence and photosynthesis in leaves of *Hedera canariensis*. *Photosynth. Res.* 25, 173–186 (1990).

Peltier, G. & Thibault, P. O₂ uptake in the light in *Chlamydomonas*. *Plant Physiol.* 79, 225–230 (1985).

Kana, T. M. et al. A membrane inlet mass spectrometer for rapid and high-precision determination of N₂, O₂, and Ar in environmental water samples. *Anal. Chem.* 66, 4166–4170 (1994).

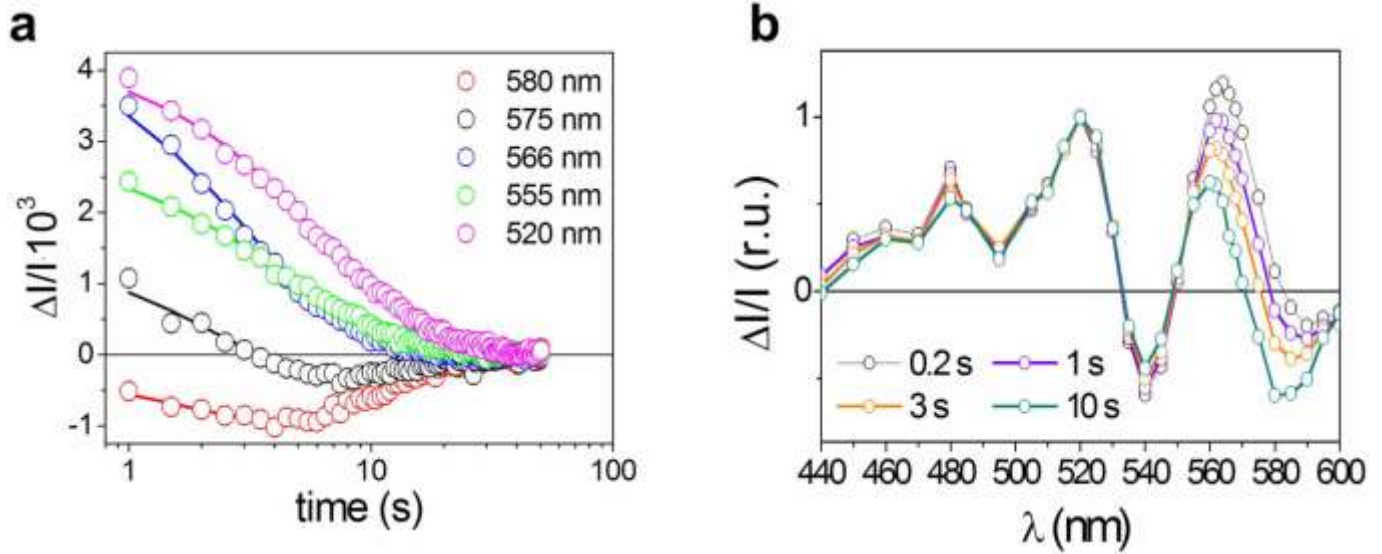
Rivasseau, C. et al. Accumulation of 2-C-methyl-D-erythritol 2,4-cyclodiphosphate in illuminated plant leaves at supraoptimal temperatures reveals a bottleneck of the prokaryotic methylerythritol 4-phosphate pathway of isoprenoid biosynthesis. *Plant Cell Environ.* 32, 82–92 (2009).

Bligny, R. & Douce, R. NMR and plant metabolism. *Curr. Opin. Plant Biol.* 4, 191–196 (2001).

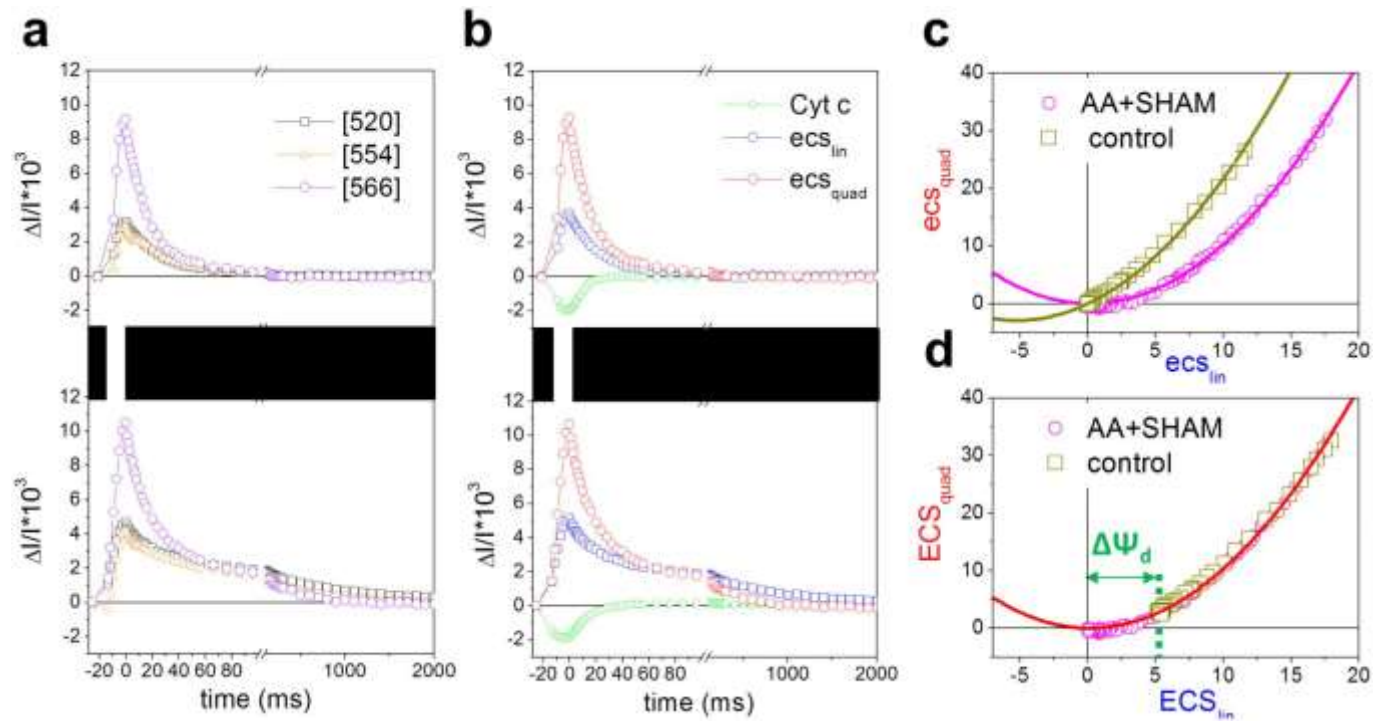
Van de Meene, A. M. L. & Pickett-Heaps, J. D. Valve morphogenesis in the centric diatom *Rhizosolenia setigera* (Bacillariophyceae, Centrales) and its taxonomic implications. *Eur. J. Phycol.* 39, 93–104 (2004).

De Riso, V. et al. Gene silencing in the marine diatom *Phaeodactylum tricornutum*. *Nucleic Acids Res.* 37, e96 (2009).

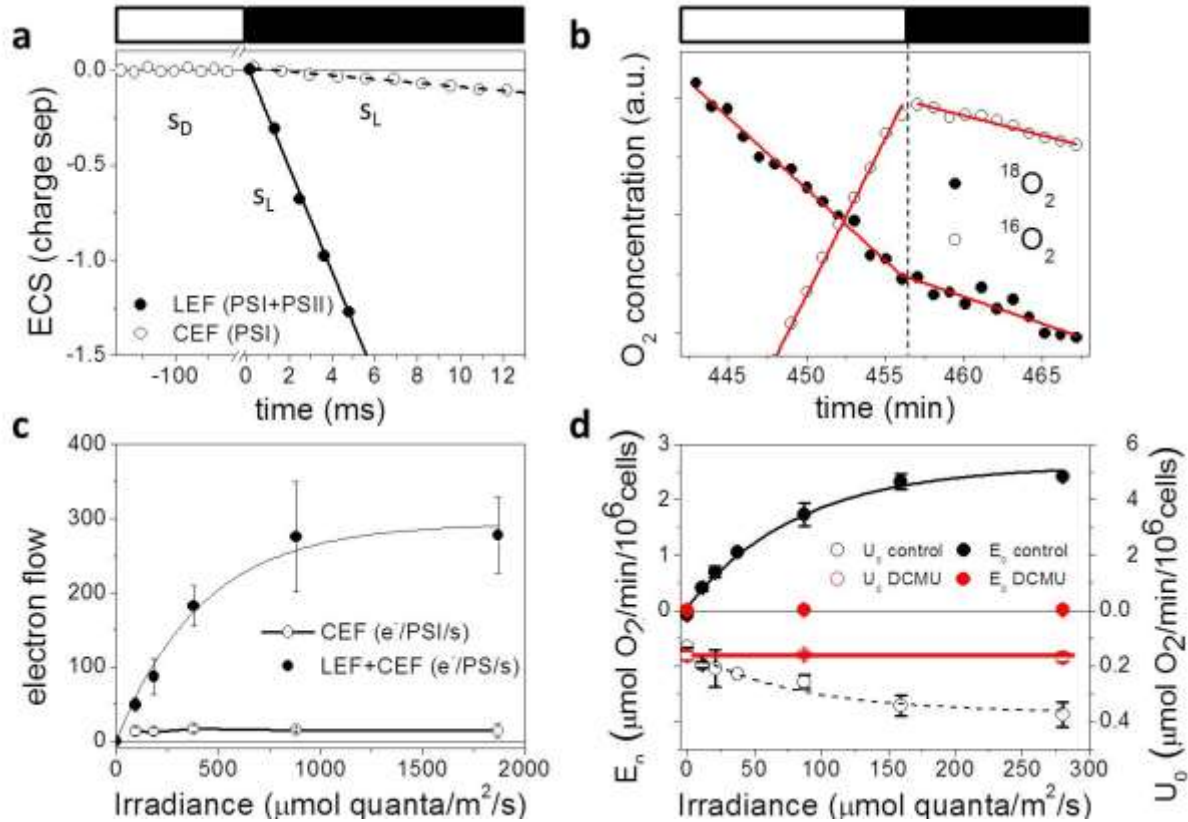
Falciatore, A., Casotti, R., Leblanc, C., Abrescia, C. & Bowler, C. Transformation of nonselectable reporter genes in marine diatoms. *Mar. Biotechnol. (NY)* 1, 239–251 (1999).



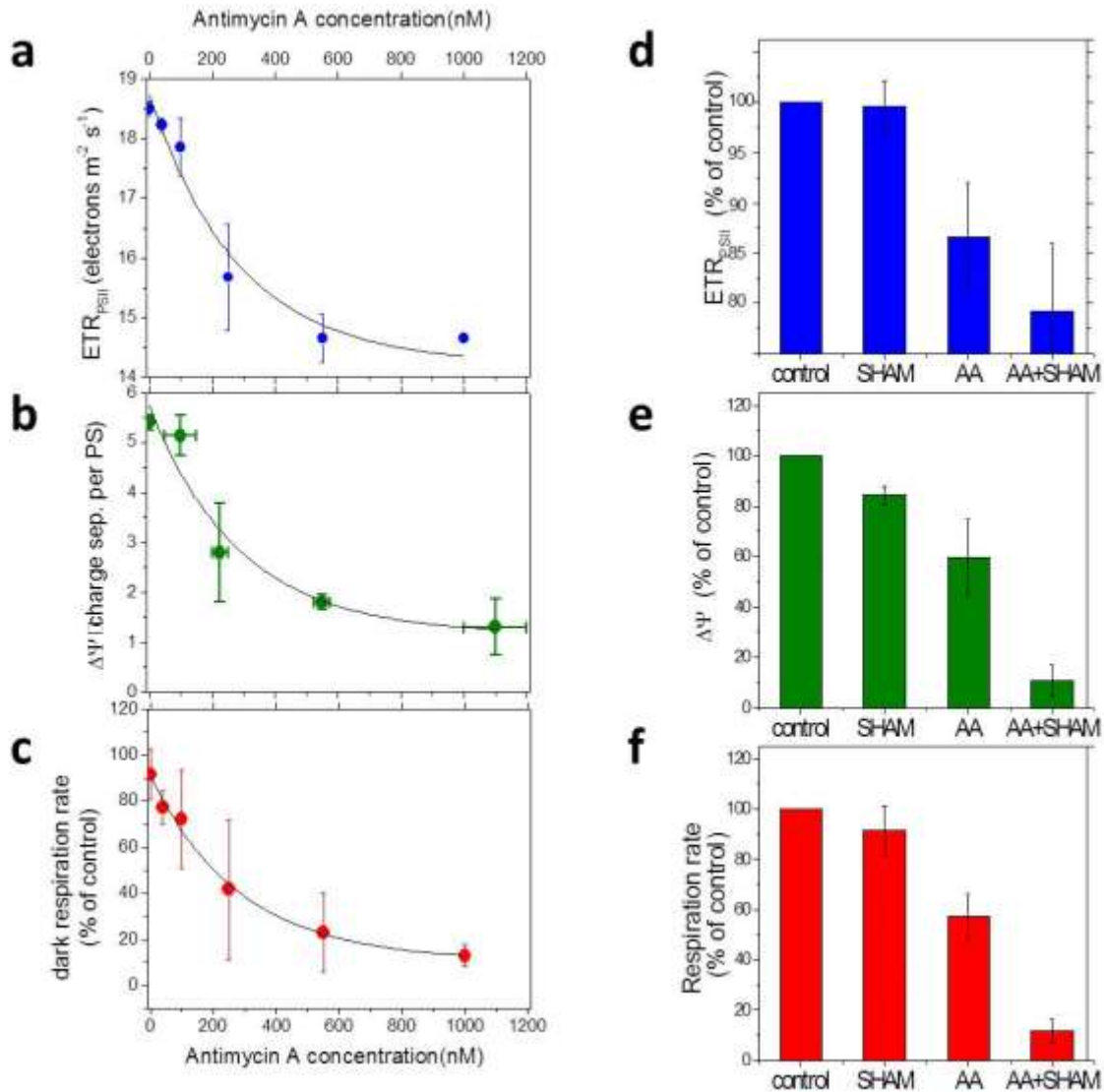
Extended Data Figure 2.1 Deconvolution of the quadratic and linear ECS in *P. tricornutum*. **a**, Absorption difference ($\Delta I/I$) kinetics followed at different wavelengths in *P. tricornutum*, after a series of six saturating laser flashes, in anaerobic conditions. Solid lines correspond to the global fit of the experimental data with a sum of two exponential decays, with time constants t and $2t$, respectively, as expected for linear and quadratic dependencies (see Methods). **b**, $\Delta I/I$ spectra are shown at different times during ECS relaxation. All spectra were normalized to 1 at 520 nm for better comparison. The observation that the blue and green parts of the spectrum are homothetic during relaxation, while changes are seen in the red most part of it, reflects the presence of the two ECS components, having different relaxation kinetics.



Extended Data Figure 2.2. Separation of c-type cytochrome signals from linear and quadratic ECS signals in *P. tricornutum*. **a**, Kinetics of $\Delta I/I$ changes at 520, 554 and 566 nm during an ~ 10 ms pulse of saturating red light ($4,500 \mu\text{mol quanta m}^{-2} \text{s}^{-1}$) and the subsequent dark relaxation (top: control conditions; bottom: AA + SHAM). **b**, Kinetics of ecs_{lin} , ecs_{quad} changes and c-type cytochrome redox state, from kinetics in **a**, after deconvolution as explained in Methods. **c**, **d**, Relationship between the quadratic and the linear ECS, before (ecs_{lin} , ecs_{quad} , **c**) and after (ECS_{lin} , ECS_{quad} , **d**) correction for the dark electric field (see Methods). Dark yellow and magenta symbols correspond to control and AA + SHAM conditions, respectively. The green arrow indicates the value of $\Delta\Psi_d$ in control conditions. Data are representative of five independent biological samples. The black boxes in **a** and **b** indicate periods of darkness.

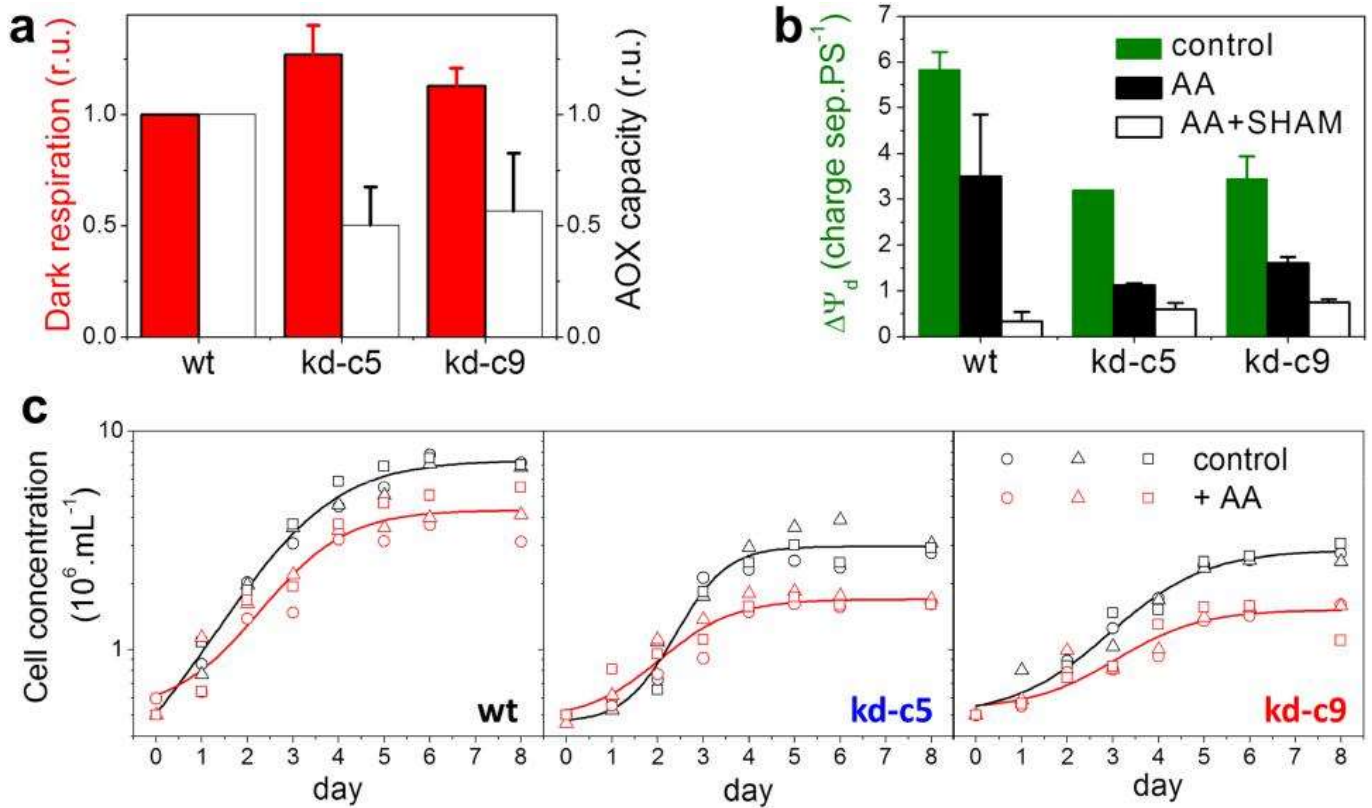


Extended Data Figure 2.3 Cyclic electron flow and water-to-water cycles in *P. tricornutum*. **a**, Representative traces of changes in ECS_{lin} (normalized as explained in Methods, namely expressed in charge separation per PS) to evaluate linear and cyclic electron flow. Cells were illuminated with 1,870 μmol quanta m⁻² s⁻¹ of red light, in absence (filled circles) and presence (open circles) of DCMU and then transferred to the dark; r.u., relative units. **b**, Representative traces of the ¹⁸O₂ and ¹⁶O₂ concentrations at the offset of a 280 μmol quanta m⁻² s⁻¹ blue light; a.u., arbitrary units. In **a** and **b**, light and dark periods are represented by white and black boxes, respectively. **c**, Photochemical rate corresponding to total electron flow (TEF, dark symbols, data from four independent biological samples) and CEF (red symbols, n = 8 ± s.d.) at different irradiances. TEF and CEF were estimated from the initial slope of the ECS decay, as (S_D - S_L control) and (S_D - S_L DCMU), respectively (see Methods). **d**, Light-dependencies of oxygen uptake (U_O, half-filled symbols) and gross photosynthesis (E_O, open symbols) in control conditions (dark) and in the presence of DCMU (red). Data from two independent biological samples (squares and circles).

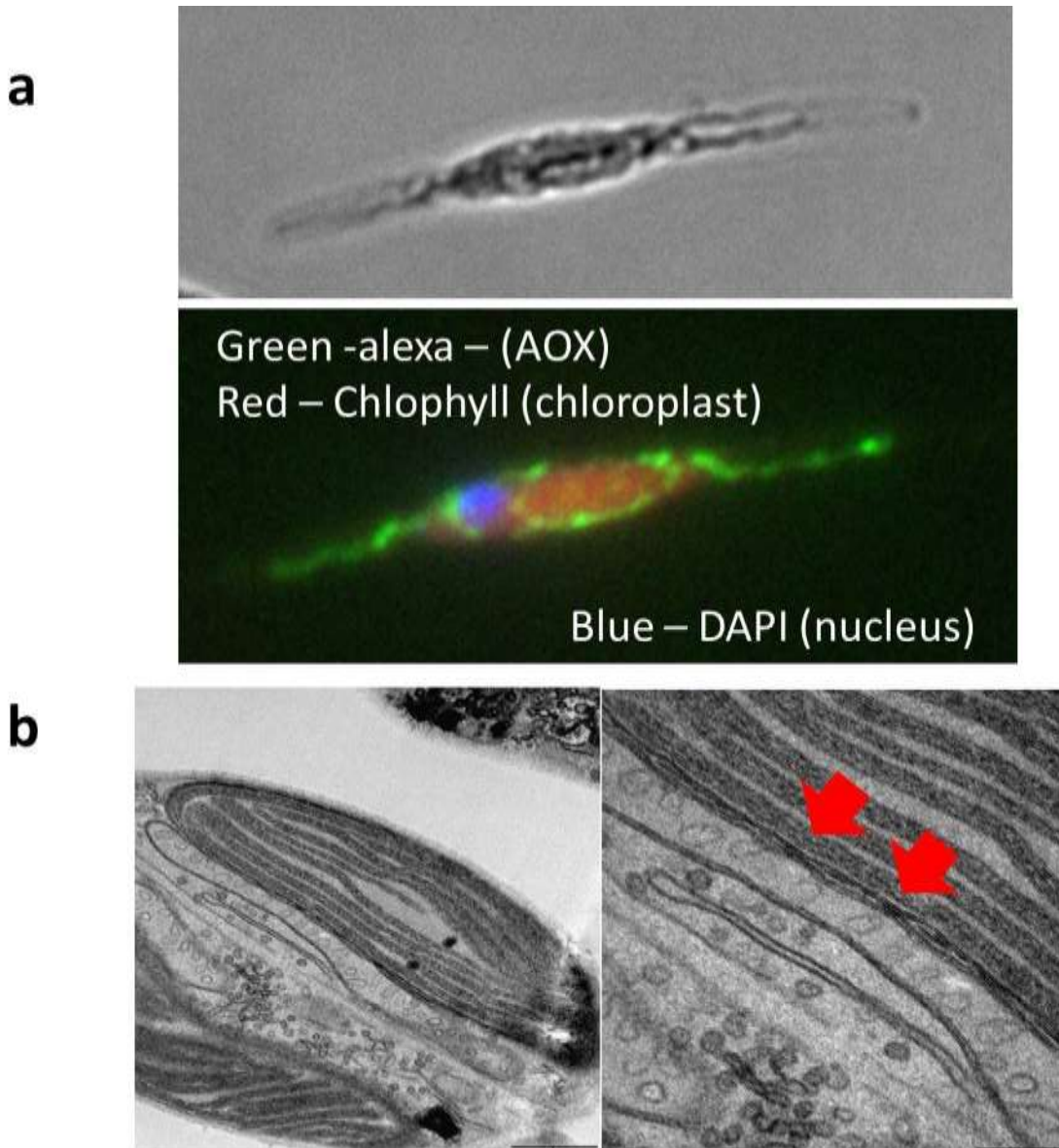


Extended Data Figure 2.4 $\Delta\Psi_d$ and photosynthesis under respiratory inhibition in *P. tricornutum*.

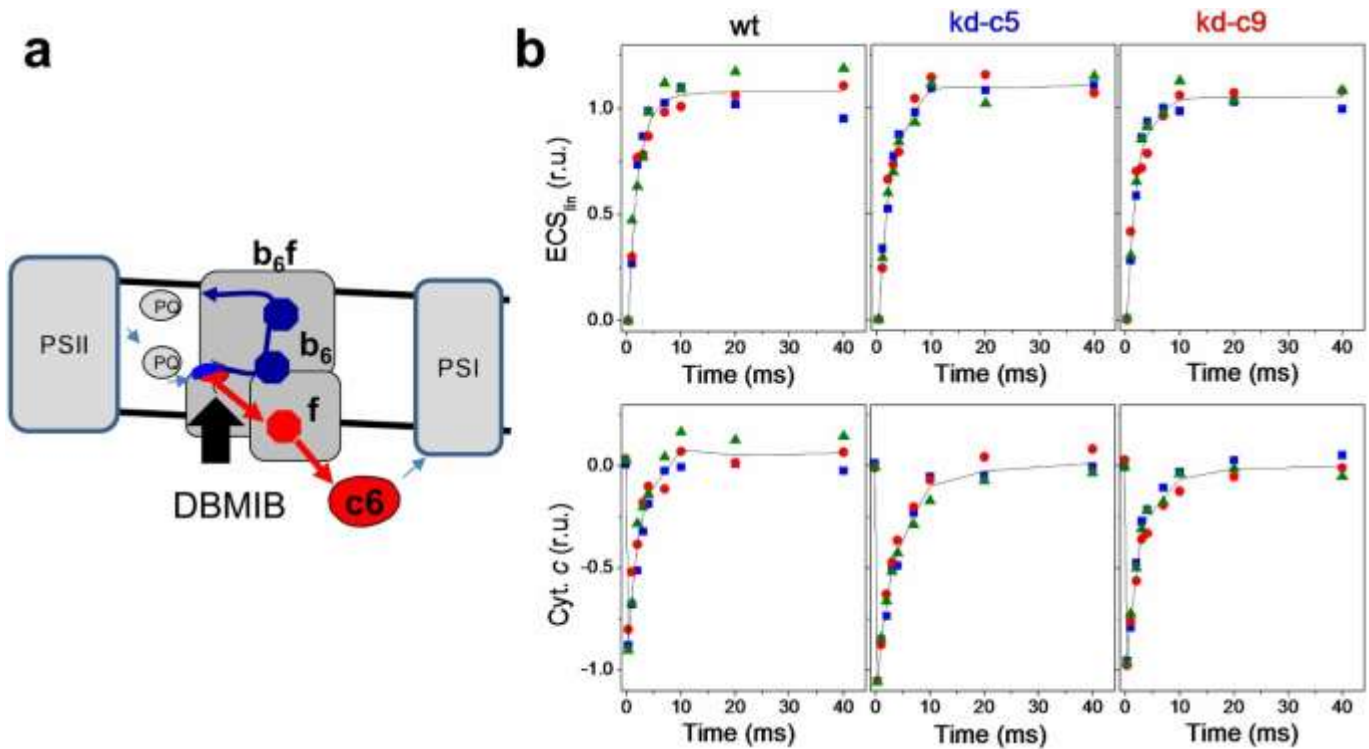
a–c, Dependency of the ETR_{PSII} (**a**), $\Delta\Psi_d$ (**b**) and dark respiration (**c**) upon inhibition of the cyanide-sensitive respiratory pathway with different concentrations of antimycin A, in the presence of saturating SHAM (1 mM). Data from two independent biological samples. Experimental data were fitted with a mono-exponential decay function. **d, e**, ETR_{PSII} (**d**), $\Delta\Psi_d$ and dark respiration (**e**), expressed as percentage of control, in the presence of saturating AA (5 μ M), SHAM (1 mM) or AA + SHAM (four independent experiments \pm s.d.). **f**, Relationship between $\Delta\Psi_d$ and mitochondrial respiration in samples treated with increasing concentrations of AA in the presence of 1 mM SHAM (mean value \pm s.e.m. from b and c).



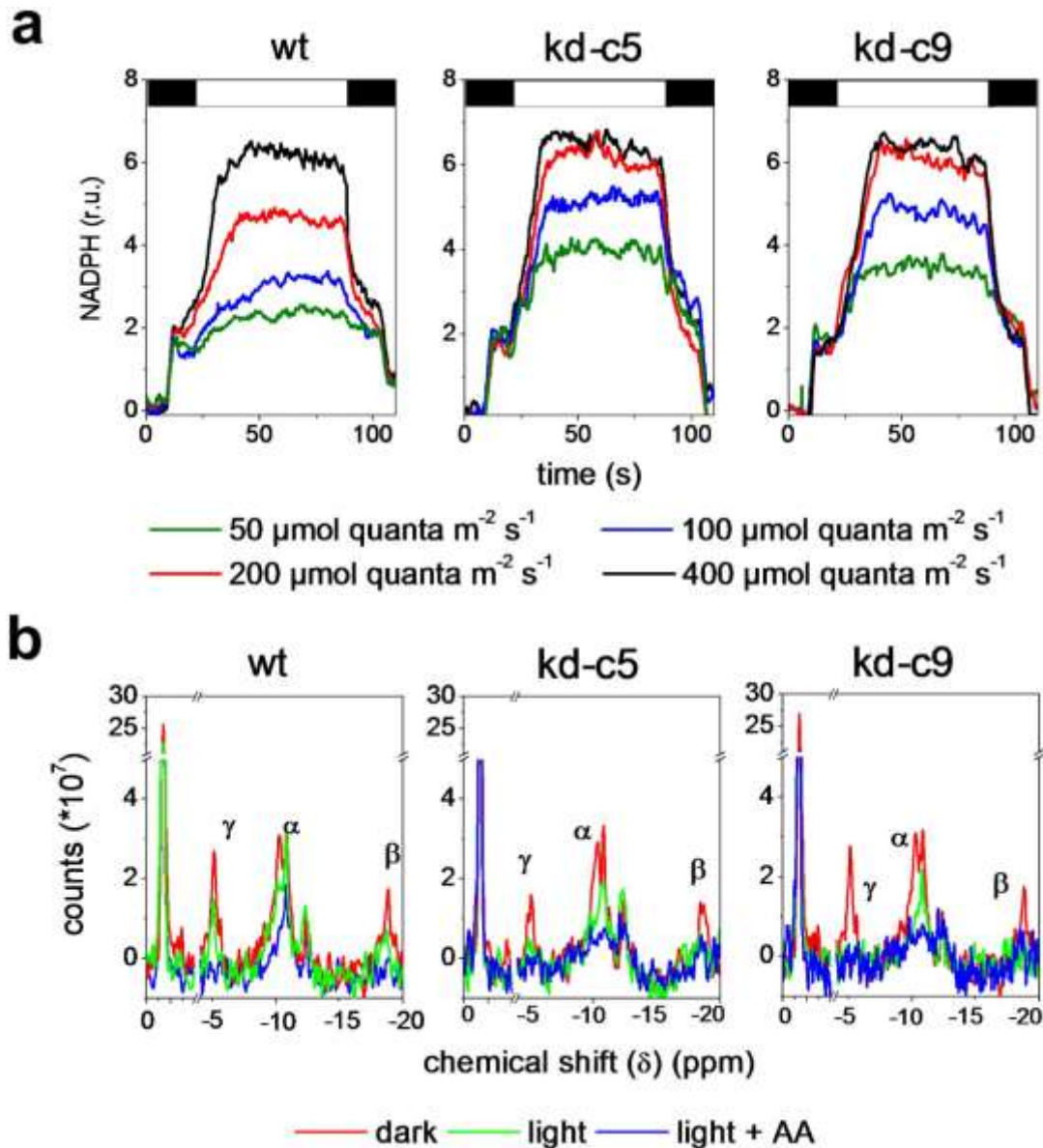
Extended Data Figure 2.5 Dark respiration, PMF and growth in AOX knockdown lines of *P. tricornutum*. **a**, Respiratory activity of wild-type and AOX knockdown lines. Total respiration rate (red bars) and the contribution of the AOX capacity (white bars, see Methods) were normalized to wild-type values ($n = 5 \pm \text{s.d.}$). **b**, ECS-based measurements of $\Delta\Psi_d$ in wild-type ($n = 3 \pm \text{s.d.}$) and AOX knockdown lines ($n = 2 \pm \text{s.e.m.}$), in control conditions (green), in the presence of AA (dark green) and in the presence of AA + SHAM (white). **c**, Growth curves of wild-type and AOX knockdown lines in the presence/absence of AA ($2 \mu\text{M}$). Three independent growth curves are shown for each strain/condition. AA was added every day and cells were grown in continuous light to prevent them from dying in the dark because of lack of respiration.



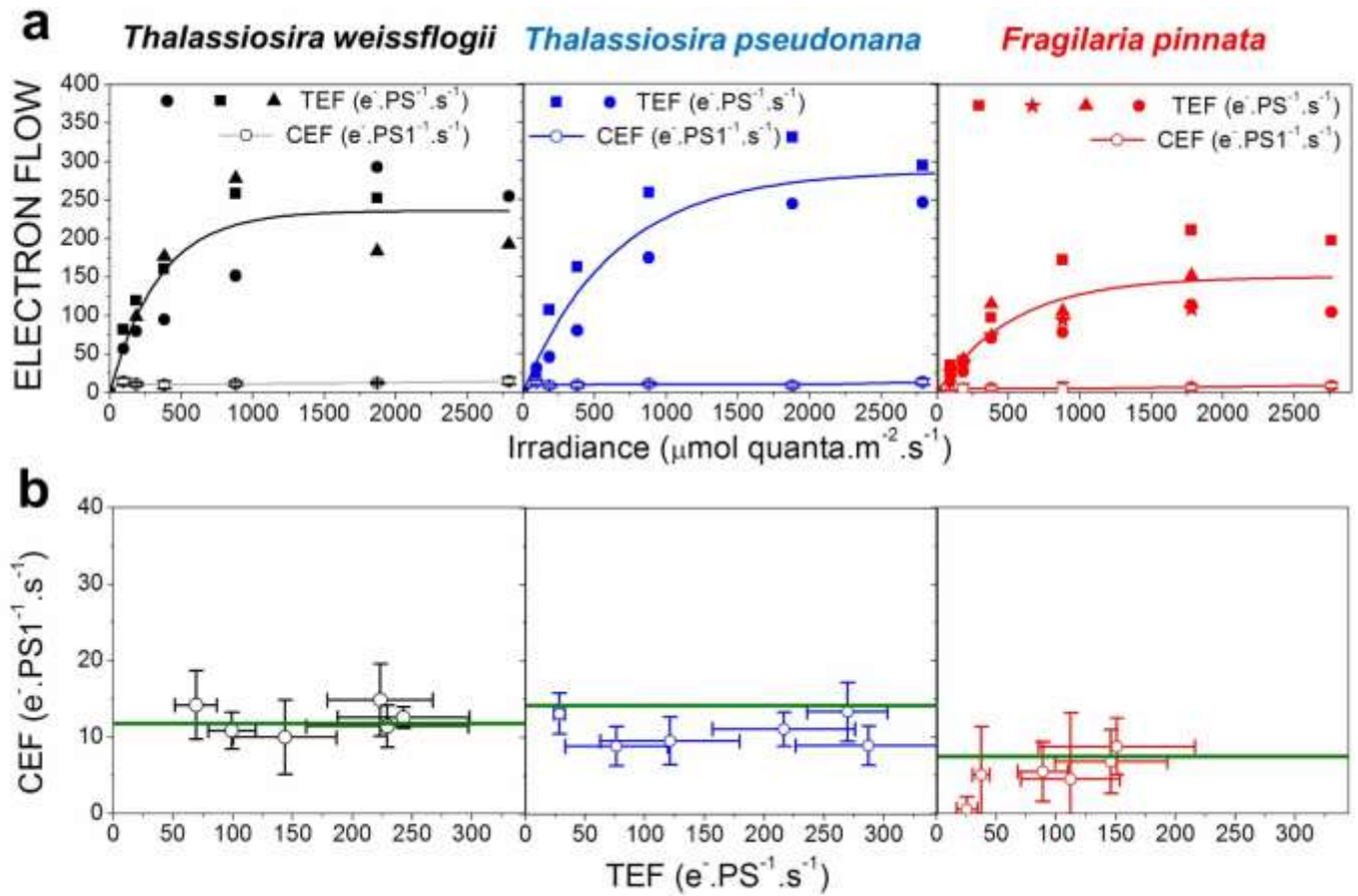
Extended Data Figure 2.6 Subcellular localization of AOX in *P. tricornutum* and plastid–mitochondria interaction in *P. tricornutum* wild-type cells. **a**, Subcellular localization of AOX. Cells were treated with an anti-AOX antibody and then with a secondary Alexa Fluor 488 antibody (see Methods). Positions of plastid and nuclei are indicated by chlorophyll a autofluorescence (red) and DAPI staining (blue), respectively. The pattern of AOX localization is highly similar to that observed with the mitochondria-specific mito-tracker probe (data not shown). Images are representative of 60 cells from three independent biological samples. **b**, Electron micrographs of the plastid–mitochondria juxtaposition in *P. tricornutum*. Arrows indicate possible physical contacts between the plastid and mitochondrial membranes. Image is representative of 51 images from seven independent biological samples.



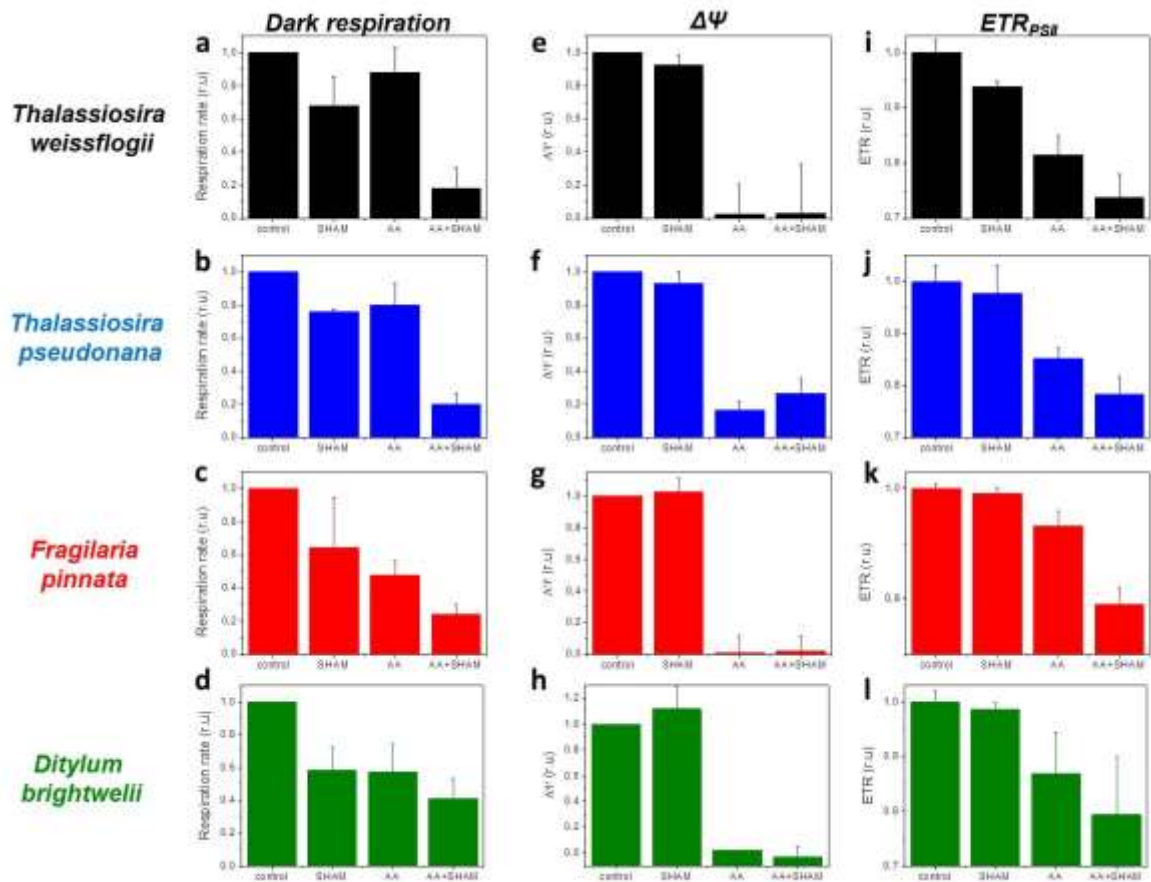
Extended Data Figure 2.7 Cytochrome b_6f turnover in *P. tricornutum* wild-type and AOX knockdown lines. **a**, Schematic representation of the electron-flow reaction steps in the cytochrome b_6f complex, which can be evaluated by spectroscopic measurements. **b**, Slow phase of ECS_{lin} indicating cytochrome b_6 activity (top) and time-resolved redox changes of cytochromes c_6/f (bottom) in wild-type and AOX knockdown lines (kd-c5 and kd-c9). *P. tricornutum* cells were exposed to saturating single-turnover laser flashes given 10 s apart. Data were normalized to the amplitude of the fast phase of the ECS_{lin} signal. Cytochrome c and ECS_{lin} were deconvoluted as explained in Methods. Three independent biological samples are shown in red, blue and green colours. Cell concentration was 2×10^7 cells per millilitre. Note that both the slow phase of the ECS_{lin} and the reduction of cytochromes c_6/f were completely abolished by the plastoquinone competitive inhibitor DBMIB (10 μ M; black arrow).



Extended Data Figure 2.8 *In vivo* changes in the NADPH redox state and ATP in wild-type and AOX knockdown lines. **a**, Changes in NADPH at different light intensities. Light and dark periods are represented by white and black boxes, respectively. Light intensities were 50, 100, 200 and 400 $\mu\text{mol quanta m}^{-2} \text{s}^{-1}$ (green, blue, red, and black traces, respectively). Chlorophyll concentration was $\sim 5 \mu\text{g ml}^{-1}$. **b**, Spectra from cells of wild-type (left) and AOX knockdown lines c5 (middle) and c9 (right) in the dark (red), light (green) and light + AA (blue) conditions are shown, with normalization to the internal standard (methylenediphosphonate; pH 8.9). The positions of the α -, β - and γ -phosphates of NTPs are shown. **a**, **b**, Representative of three independent biological samples.



Extended Data Figure 2.9 Cyclic electron flow in representative diatoms. a, Total electron flow (filled symbols) was measured at different light irradiances, as illustrated in Extended Data Fig. 2.3, in *T. weissflogii* (black, n = 3 independent biological samples), *T. pseudonana* (blue, n = 2) and *F. pinnata* (red, n = 4). Cyclic electron flow capacity was also measured for every species (open circles, five independent biological samples \pm s.d.). **b**, CEF capacity was plotted against TEF. CEF and TEF are presented as mean values \pm s.d. from a. The green line corresponds to CEF = 5% of the maximal total electron flow.



Extended Data Figure 2.10 $\Delta\Psi_d$ and photosynthesis under conditions of respiratory inhibition in representative diatoms. Dark respiration (a–d), $\Delta\Psi_d$ (e–h) and ETR_{psII} (i–l) in untreated cells and after treatment with inhibitors of respiration antimycin A, and/or SHAM at saturating concentrations. **a, e, i, T. weissflogii** (black). **b, f, j, T. pseudonana** (blue). **c, g, k, F. pinnata** (red). **d, h, l, D. brightwellii** (green). The data represent the mean value \pm s.d. of three (l), four (d), five (f, h, k), six (a, c, e, j), seven (b, i) or eight (g) independent experiments. All data were normalized to the control value.

2.6 Conclusions and remarks

In this study a wide range of biophysical tools has been used to evaluate the interplay between the chloroplast and the mitochondria in diatoms. The possibility to measure the ECS in *Phaeodactylum* allows to follow the dynamics of the PFM in different conditions and to reveal mitochondrial-chloroplast interactions. The presence of ECS signal in dark indicates that the PMF is maintained across the thylakoid membranes, also when the photosynthetic machinery is not active. By contrast, the PFM was dissipated in anaerobiosis, or in presence of the respiratory inhibitors AA and SHAM. These findings suggest that the presence of PMF in the dark was due to communication between mitochondria and chloroplast (*i.e.* the exportation of ATP from mitochondria to chloroplast).

Similar results were obtained in green algae (Finazzi and Rappaport 1988), however in these organisms, CEF plays the most important role in the regulation of ATP/NADPH ratio (Finazzi *et al.*, 2005). This was not the case for *Phaeodactylum*, in which the CEF showed to have a very low contribution on the total electron flow (TEF). The contribution of chloroplast-mitochondria interaction, instead, is much more relevant on the production of extra ATP for the carbon fixation, as demonstrated by several evidences. The determination of oxygen consumption by a polarographic approach, which was confirmed by a membrane inlet mass spectrometry (MIMS) approach, revealed that dialog between photosynthesis and respiration is bidirectional, as shown from a reduced respiration activity in presence of the inhibitor of PSII (*i.e.* DCMU). In addition, knock-down AOX mutants have showed reduced growth rate, photosynthetic capacity (*i.e.* ETR) and cellular ATP level as well as increased cellular NADPH level comparing with wt. These results support the hypothesis that the reducing power (*i.e.* NADPH) generated during the photosynthesis is exported to the mitochondria, and the ATP produced during the oxidative respiration is redirected towards to the chloroplast to provide the extra energy needed for the carbon fixation. Hence, the correct function of both mitochondria and chloroplast, as well as the exchanges of molecules between the two organelles are crucial for carbon fixation and growth in *Phaeodactylum*. In addition, we found similar results in other diatoms (*Thalassiosira pseudonana*, *T. weissflogii*, *Fragilaria pinnata* and *Ditylum brightwellii*). Therefore, the involvement of mitochondrial respiration in the optimisation of photosynthesis is a process

conserved on this group and could explain their ecological success in the oceans. Future works should entail the analysis of plastid and mitochondrial transporters in order to understand the real actors involved in these communications. Furthermore, the analysis of ECS can be also used to detect changes in the mechanism of photosynthesis and respiration under nutrient deficiencies or in presence of a carbon source. These analyses could help to further elucidate the mechanism of lipids accumulation and of mixotrophy (addressed in the chapter 4).

To conclude, we have studied the interactions between the photosynthetic and respiratory electron chains in *Phaeodactylum*, and this allowed to elucidate the mechanism of mixotrophy. Our findings showed that only the optimisation of both respiration and photosynthesis can boost the growth and productivity in this organism. These hypotheses have been tested in the second work of my PhD (chapter 3) where the consequences of the mixotrophic growth (using the glycerol as carbon source) were analysed by combining different omics analyses.

Chapter 3

Characterisation and optimisation of mixotrophy in *Phaeodactylum tricornutum*

3.1 Preface

This chapter contains the main project of my PhD work and it is divided in three sections. The first section is an introduction of this work and it is further divided in two main paragraphs: *i)* Characterisation of mixotrophic metabolism in *Phaeodactylum tricornutum* and *ii)* Optimisation of mixotrophic metabolism by improving culture conditions. The second section contains the manuscript (Villanova *et al.*,) that is in preparation for submission. The third part contains the conclusions of this work and other remarks.

In the article presented in this chapter (“Boosting biomass quantity and quality by improved mixotrophic culture of the diatom *Phaeodactylum tricornutum*), we first studied the mechanism and consequences of mixotrophic growth in the diatom *Phaeodactylum tricornutum* by combining omics analyses and physiological approaches. In the second part of this work, we exploited these knowledges to improve algal biomass productivity. This was done by optimising the medium composition to increase the efficiency of the mixotrophic metabolism and consequently enhance the biomass. Eventually, the optimised conditions were scaled-up to 2L-photobioreactors, where a better system control (temperature, pH, light, aeration/mixing) allowed a further improvement of the biomass capacity of *Phaeodactylum tricornutum*.

3.2 Characterisation of mixotrophic metabolism in *Phaeodactylum tricornutum*

As discussed in paragraph 1.3.3, *P. tricornutum* is a facultative mixotroph that is able to grow in presence of both light and different carbon sources (Cerón-García *et al.*, 2000; 2005; 2013; Liu *et al.*, 2008; Wang *et al.*, 2012). Amongst them, the glycerol is the most attractive carbon source for biotechnological applications because it is abundant and cheap (being a by-product of biodiesel production) and it has already been reported to enhance biomass and lipid productivity in *P. tricornutum* (Cerón-García *et al.*, 2005; 2006; 2013). However, information on how glycerol addition leads to increase growth and lipid productivity is still scarce. Indeed, its consequences on central carbon and lipid metabolism in the diatom are not precisely known. This question has been addressed by the present work, by combining various omics analyses.

3.2.1 Previous investigations of glycerol metabolism in *Phaeodactylum tricornutum*

Previous work on glycerol metabolism has been done growing *Phaeodactylum* on ¹³C-labeled glycerol (Zheng *et al.*, 2013, Huang *et al.*, 2015). The idea behind these experiments is that, upon uptake and metabolism, the carbon backbone of the glycerol will be distributed between different metabolites, where it will become detectable through nuclear magnetic resonance (NMR) or gas chromatography mass spectrometry (GC-MS). In particular, Zheng *et al.*, 2013 used this technique to investigate both glucose and glycerol metabolic fluxes. This work revealed that under mixotrophic growth *Phaeodactylum* converted the carbon source mostly in glycine and serine (two amino acids involved in photorespiratory reactions). Similar results were found in Huang *et al.*, 2015, where it was confirmed that the glycerol is metabolized by *Phaeodactylum* and converted in glycine and serine, and this reaction is active mostly in N-deplete conditions. Isotope labelling experiment allowed to detect the distribution of ¹³C enrichments in all the amino acids but not in all the others metabolites. Moreover, the change in the gene expression level was not investigated. To have a global view of mixotrophic metabolism in *Phaeodactylum*, further investigations are needed.

3.2.2 Omics analysis

The omics technologies are any large-scale analysis, which are available to quantify the absolute content of differences in the DNA (genomics), RNA (transcriptomics), proteins (proteomics) and metabolites (metabolomics) levels, within an organism, tissue, cell or organelle. These analyses are needed to provide a global view of pathways, processes and metabolic changes in biological systems. In general, only an integrated analysis of different omics technologies allows having a complete scenario of the cellular behaviour in the studied process (*i.e.* from gene to metabolite regulation).

In this paragraph, I will present the transcriptomic and metabolic analyses that have been used in this study. The lipidomic analysis (a subset of metabolomics) performed on *P. tricornutum* cells will be illustrated in the next chapter.

Transcriptomic analysis is commonly used to detect differential gene expression profiles under different culture conditions. For instance, this analysis has been performed in *Phaeodactylum tricornutum* in order to understand its response to different external factors such as nutrient starvation, silicic acid and stressors contaminants (Allen *et al.*, 2008; Yang *et al.*, 2014; Levitan *et al.*, 2015; Alipanah *et al.*, 2015, Sapriel *et al.*, 2009; Osborn *et al.*, 2013). Alternately, the transcriptomic analysis can be used to pinpoint genes for the metabolic engineering (Levitano *et al.*, 2015).

Two different approaches can be used to do transcriptomic analysis: RNA-sequencing and microarray analysis. The first one is based on the complete sequencing of the RNA present in a biological sample by next-generation sequencing (NGS) (Wang *et al.*, 2009). It is able to detect small differences in expression gene levels and/or in gene sequences. However, the large amount of data produced by this analysis requires specific facilities to be analysed. Here, we decide instead to use a microarray analysis, thanks to an ongoing collaboration with another member of the ITN “AccliPhot”, UPMC in the Angela Falciatore’s laboratory. The microarray, similarly to RNA sequencing, is able to detect expression profiling within cells. This approach is based on the hybridisation of fluorescent-labelled RNA (or cDNA after retro transcription) extracted by cells with a pre-arrayed chip containing the partial or the entire genome of the target organism (Shalon *et al.*, 1996). This technique allows comparing the gene expression level of samples

treated in different ways. A very common approach for this purpose is the two-channel microarray. In this case, the RNA extracted from cells growth in the two conditions are labelled with different fluorescent dyes (*i.e.* Cy3 and Cy5) mixed and let hybridised with the chip. The changes in the expression levels of genes are usually expressed as \log_2 of the Cy5/Cy3 ratios in biological replicates. The data are then tested for statistical significance in gene expression changes. This technology has been used in this study to analyse the change in expression level of *Phaeodactylum* cells grown in presence/absence of glycerol. Only when these dataset were integrated with the others analyses, it was possible to clarify the mixotrophic metabolism in *Phaeodactylum*.

The metabolomics approach allows the simultaneous analysis of different type of molecules, *i.e.* amino acids, sugars, organic compounds, fatty acids etc. However, due to the huge number of targeted molecules and the complexity of their chemical structures, it is still impossible to map the entire metabolome of a given organism simultaneously. The principal tools available to detect a large number of metabolites are: *i)* nuclear magnetic resonance (NMR) and *ii)* mass spectrometry coupled to a gas or a liquid chromatography (*i.e.* GC-MS, and LC-MS). NMR has been used to analyse the metabolism of both plant tissue and microalgae (Bligny and Douce 2001). This technique allows the detection of metabolites in an organism and has the advantage of allowing both *in vitro* and *in vivo* analysis. The NMR experiments provide specific fingerprints for different molecules, which can then be analysed thanks to online databases (*i.e.* biological magnetic resonance data bank, BMRB and spectral database for organic compounds, SDBS). However, the disadvantage of NMR is that this technique has a low sensitivity, and thus requires highly concentrated samples (Shulaev, 2006). Therefore we did not use it for our study, which targets cells in the early exponential phase. In this case, extremely large volumes would have been needed to reach the cell concentration required for NMR analysis.

MS technology, instead, shows higher resolution and it allow to identify a large number of metabolites even at low cell concentration. Of course, this technique can only be used on extracts. Normally, the metabolites are first separated by chromatography (*i.e.* LC or GC) and then analysed by MS. In our case the metabolomics analysis was performed using a GC-MS

platform. This technique has already been used in different species of cyanobacteria (Huege *et al.*, 2011) and microalgae (Fernie *et al.*, 2012; Allen *et al.*, 2008; Obata *et al.*, 2013; Sue *et al.*, 2014).

To conclude, by combining transcriptomic, metabolomics and lipidomic approaches, we have provided a rather complete scenario of the metabolic changes associated with the mixotrophic metabolism in *Phaeodactylum tricornutum*.

3.3 Optimisation of mixotrophic metabolism by improving culture conditions

In principle, the metabolism information obtained from the omics approach can be used to modify, and hence enhance, the specific pathways by metabolic engineering, as described in paragraph 1.4.3. However, other limiting factors such as nutrients, light, pH, aeration/mixing, temperature, etc have to be taken into account for the efficient industrial exploitation of microalgae and will be discussed in the next paragraphs.

3.3.1 Culture medium/ nutrients

The cultivation of microalgae in industrial scale requests higher cell density than those found in nature to make the process suitable with the market. To obtain higher biomass concentration, the microalgae need to be grown in media that contains higher concentrations of specific elements that are limiting growth in seawater. The nutrients that have to be supplied to microalgal cultures are divided into two main categories based on their final concentration: macronutrients (*i.e.* nitrogen, phosphorus and carbon) and micronutrients (*i.e.* iron, copper, manganese, zinc etc.). Nitrogen and phosphorus (after carbon) are often the most important macronutrients required for the growth of microalgae (Wijffels and Barbosa, 2010) and the deprivation of these elements triggers TAG accumulation in *Phaeodactylum* as will be discussed in the next chapter (Abida *et al.*, 2015). Also the micronutrients are essential for algal growth because of their role as cofactors of key enzymes (Morel *et al.*, 2014). For

instance, iron is a redox active metal present in several metalloproteins involved in photosynthesis, respiration and nitrogen assimilation and hence is very important in phototrophs (Moore *et al.*, 2013). Manganese also plays a very important role in the growth of the diatom *Thalassiosira pseudonana* (Sunda and Huntsman 1996). Indeed, the manganese is involved in vital process of phototrophic organism such as the oxidation of water done by PSII complex, and the conversion of superoxide (O_2^-) radical into molecular oxygen (O_2) and hydrogen peroxide (H_2O_2) (Sunda and Huntsman, 1998).

Zinc is also essential, as shown by the examples of the green alga *Chlamydomonas reinhardtii*, where it impacts CO_2 assimilation and Cu homeostasis (Malasarn *et al.*, 2013), and of the diatom *T. weissflogii*, where it seems to be associated with carbonic anhydrase (CA) regulating the rate of carbon uptake and fixation (Morel *et al.*, 1994).

Finally, the copper is an essential component of the photosynthetic chain of *viridiplantae*, being the redox cofactor of the electron carrier plastocyanin (Merchant *et al.*, 2012). However, too elevated concentrations of these elements may result in oxidative damage or in decrease of growth rate of cells (Choudhary *et al.*, 2007).

For all these reasons, the optimisation of medium composition is a crucial step for enhancing the biomass concentration of the selected microalgae. This has been done in this work by balancing the elemental composition of *Phaeodactylum tricornutum* with that of ESAW medium (as reported in others microalgae by Mandalam and Palsson 1998; Danquah *et al.*, 2010).

3.3.2 Light and $NaHCO_3$ effect

Light is another important parameter to consider for the optimisation of phototrophic and mixotrophic algal cultivation. Indeed, the light not only affects photosynthesis activity but it can also changes the biomass composition of microalgae, due to acclimation phenomena (*i.e.* pigments and lipids content) (Falkowski and Owens, 1980; Rashid *et al.*, 2015). Increasing the light intensity usually tends to increment the algal growth rate up to the light saturation level. However, when light becomes oversaturating, it can lead to the formation of harmful

products (*i.e.* ROS) and, hence, decrease algal biomass productivity (Richmond *et al.*, 2000). To avoid this phenomenon (*i.e.* photoinhibition, described in paragraph 1.2.2) light intensity has to be optimised in relation to cell density, so that the culture does not become light limited or photodamaged (Hu *et al.*, 1998). Following this rationale, in experiments performed in photobioreactors, the light intensity was gradually increased along cell density enhancement.

Moreover, a carbon source is also needed for growth; depending on phototrophic vs mixotrophic conditions (see paragraphs 1.3.1-1.3.3) the carbon source can be inorganic (*i.e.* CO₂ or NaHCO₃) or organic (*i.e.* glycerol). In both cases, an increase of biomass concentration is observed (Mus *et al.*, 2013). In the experiments presented below, we tested the role of both inorganic and organic carbon source in *Phaeodactylum* in order to enhance both photosynthesis and respiration processes, and hence the mixotrophic metabolism.

3.3.3 Scale-up in fermentor

The last step of the optimisation processes for microalgal cultivation is the up-scaling in fermentors. Two main alternatives exist for the cultivation of microalgae in larger scale: open ponds (*e.g.* natural lakes, lagoons, ponds or artificial ponds/ containers) and photo-bioreactors (PBRs). Open pond systems are more sensible to contaminations of microorganisms and hardly allow a control of external parameters such as temperature, pH and light. However, this system has much lower maintenance costs comparing to PBRs (Darzins *et al.*, 2010). For all these reasons, the fermentation in open pond is usually the best way to cultivate microalgae under unusual growth conditions (*i.e.* high temperature, low pH), in which the probability of contaminations is reduced. Instead, the cultivation in PBRs, thanks to a better control of the systems (pH, temperature, light etc...), allows to obtain higher biomass productivity and to maintain axenic cultures (Sheehan *et al.*, 1998). In this study, *Phaeodactylum* was grown in 2L-photobioreactor (Applikon schiedam the Netherlands) monitoring and controlling pH, temperature, aeration-mixing and pO₂. Finally, the light was supplied continuously with external light panels ranging from 40 to 300 $\mu\text{E m}^{-2} \text{s}^{-1}$. This allows growing axenic cultures for about 50 days.

3.4 Boosting biomass quantity and quality by improved mixotrophic cultivation of the diatom *Phaeodactylum tricornutum*.

Valeria Villanova^{1,2}, Antonio Emidio Fortunato³, Dipali Singh⁵, Melissa Conte², Toshihiro Obata⁴, Juliette Johuet², Alisdair R. Fernie⁴, Mark Poolman⁵, Eric Marechal², Angela Falciatore³, Adeline Le Monnier¹, Julien Pagliardini¹, Dimitris Petroutsos^{2*}, Giovanni Finazzi^{2*}

¹Fermentalg SA, F-33500 Libourne, France,

²Laboratoire de Physiologie Cellulaire et Vegetale, UMR5168, Centre National de la Recherche Scientifique (CNRS), Commissariat à l'Energie Atomique et aux Energies Alternatives (CEA), Université Grenoble Alpes, Institut National Recherche Agronomique (INRA), Institut de Recherche en Sciences et Technologies pour le Vivant (IRTSV), CEA Grenoble, F-38054 Grenoble cedex 9, France;

³Université Pierre et Marie Curie, UMR7238, CNRS-Université Pierre et Marie Curie (UMPC), 75006 Paris, France.

⁴Max-Planck Institut für Molekulare Pflanzenphysiologie, Am Mühlenberg 1, 14476 Golm-Potsdam, Germany,

⁵Department of Biological and Medical Sciences, Oxford Brookes University, Oxford, OX3 0BP, U.K.

*To whom correspondence should be addressed: Dimitris.Petroutsos@cea.fr; Giovanni.Finazzi@cea.fr

ABSTRACT

Diatoms are prominent marine microalgae, attracting attention not only from an ecological point of view, but also for their possible use for biotech applications. They can be cultivated in phototrophic conditions, using sunlight as the only energy source, or in mixotrophic mode, where both light and external reduced carbon contribute to biomass accumulation. In this study, we investigated the consequences of mixotrophy on the growth and metabolism of the pennate diatom *Phaeodactylum tricornutum*, using glycerol as a source of reduced carbon. Transcriptomic, metabolomic and physiological data indicate that glycerol affects the central-carbon, the carbon-storage and the lipid metabolisms of the diatom. In particular, glycerol addition mimics some typical responses of nitrogen limitation on lipid metabolism at the level of TAG accumulation and fatty acids composition. However, glycerol did not diminish photosynthetic activity and cell growth, at variance with nutrient limitation, revealing clear advantages for biotechnological applications. Finally, we show that the benefits of glycerol on biomass and lipid productivity can be largely enhanced by optimising the micronutrient content of the growth medium, in both flask and photobioreactor driven cultures.

INTRODUCTION

Diatoms are unicellular eukaryotes responsible for about 20-25% of the global carbon dioxide fixation via photosynthesis (photoautotrophy). Issued from a complex endosymbiotic events in which a red alga (but possibly also a green alga) was engulfed by heterotrophic eukaryotic host, diatoms display a complex combination of genes and pathways acquired from endosymbiotic events and horizontal transfer with bacteria and virus (Armbrust *et al.*, 2009). Ultimately, this metabolic chimeric structure is believed to be one essential component of the great evolutionary success (Thomas and Dieckmann, 2002; Hutchins *et al.*, 1998) and of the high biotechnological potential of these algae (Chisti 2007). Diatoms silica shells can be directly incorporated into nanostructures or used as vectors for drug delivery (Lechner *et al.*, 2015). Diatoms are also targeted organisms for pharmaceutical, cosmetic and food applications as a natural source of polyunsaturated fatty acids, pigments and antioxidants (Vinayak *et al.*, 2015). Finally, diatoms are considered as promising organisms for the production of biofuels, because of their capacity to accumulate up to 30-40% triacylglycerols (TAG) under stress conditions (Chisti 2007). TAGs can be synthesised by conversion of membrane phospholipids that, following hydrolysis of the polar head produces diacylglycerol (DAG) which is then acylated into TAG. Alternatively, they can be synthesised *ex novo* under nitrogen starvation via a route called the Kennedy pathway, involving a diacylglycerol acyltransferase and *de novo* DAG and acetyl-CoA synthesis (*e.g.* Simionato *et al.*, 2013; Abida *et al.*, 2015). TAG can be readily converted into biodiesel after trans-esterification (Balat and Balat 2008).

One major drawback related to biofuel production from nutrient starved algae is that growth is rapidly arrested upon nutrient limitation, because most of the cellular building blocks (membranes, proteins) are degraded to mobilize nutrients for housekeeping functions. This difficulty is often circumvented through a temporal segregation of biomass production (replete conditions) and TAG production (stress conditions) (Kumar *et al.*, 2010; Jia *et al.*, 2015). Alternatively, molecular engineering of metabolism can be employed to enhance lipid productivity in unstarved algae for biofuel application. Fox

example, diverting metabolism from the generation of other storage molecules, like sugars, has led to high TAG accumulation in diatoms even in nutrient replete conditions (Daboussi *et al.*, 2014). Another approach to boost algal productivity consists in implementing biomass generation during the replete phase, to increase the final yield (San Pedro *et al.*, 2014; Xiao *et al.*, 2015). This approach is not specifically targeted to a given metabolite, because the increased biomass can be used for different purposes, depending on the treatment performed during the starvation phase. Moreover, the same approach can be applied to metabolic engineered algae, to improve their growth.

Because of their metabolic flexibility, different growth modes can be applied to microalgae and diatoms in particular. The first one is photoautotrophy, where light energy directly fuels CO₂ assimilation into reduced carbon via photosynthesis. This requires a photochemical conversion by the two photosystems (PSs), PSI and PSII, electron flow to generated reducing power (NADPH) and ATP, which are consumed for CO₂ uptake by Rubisco and the Calvin Benson Bassham cycle (CBB cycle).

Earlier experiments have shown that it is possible to increase both lipids and biomass productivity by increasing the CO₂ concentration in various algal species, including *Phaeodactylum* (Yongmanitchai and Ward 1991, Wu *et al.*, 2015, Gardner *et al.*, 2012). In particular, Gardner and colleagues showed that NaHCO₃ can actively stimulate TAG accumulation in both *Scenedesmus* and *Phaeodactylum*. The use of NaHCO₃ as inorganic carbon source for growth, can be explained by the existence of carbon concentrating mechanisms in diatoms (Curien *et al.*, 2016) and represents cheaper alternative to CO₂ bubbling (Chi *et al.*, 2011).

The second mode is heterotrophy, in which algae grow without light by fermenting or respiring exogenous sugars (Lewin and Lewin, 1960). Amongst the heterotrophs, two different categories can be recognized: *i.* obligate heterotrophs (*i.e.* *Nitzschia alba*) that lacks photosynthetic pigments and are not able to perform photosynthesis and *ii.* facultative heterotrophs (*i.e.* *Cyclotella cryptica*) that can perform separately photosynthesis and respiration. *C. cryptica* is able to grow in presence of glucose in the dark, but show lower productivity than using the photoautotrophic metabolism

(Hellebust *et al.*, 1971). In fact, some microalgae are obligate photoautotrophs because they possess an inefficient uptake of carbon source (reviewed in Chen and Chen 2006). Consequently, it was shown that the introduction of the gene encoding for the human glucose transporter (GLUT1) in *Phaeodactylum tricornutum* allows the uptake of glucose in the dark (Zaslavskaja *et al.*, 2001), thereby improving biomass production.

A third mode of cultivation is mixotrophy, *i.e.* the growth in presence of both light and organic carbon. This mode, which involves the utilization of respiration and photosynthesis simultaneously, is of major interest for biofuel production in diatoms (Wang *et al.*, 2012). Various diatoms such as *Phaeodactylum tricornutum* (Cerón-García *et al.*, 2000; 2005; 2006), *Navicula saprophila*, and some species of *Nitzschia* (Kitano *et al.*, 1997) have been reported to grow mixotrophically, although with different efficiencies and substrate specificity. *Navicula saprophila* is able to grow in phototrophic mode as well as in presence of acetic acid, both in the absence or presence of light. However, the highest growth rate is observed when reduced carbon is added in the light (mixotrophy), roughly corresponding to the sum of the growth rates obtained in heterotrophy and phototrophy. In mixotrophic conditions, *N. saprophila* also showed the highest EPA productivity when compared to the other trophic modes (Kitano *et al.*, 1997).

Despite the potential of mixotrophic growth, the metabolic consequences and the mechanism behind this process are still poorly understood. Model diatoms like *P. tricornutum* are also facultative mixotrophs, able to use glycerol, acetate, glucose and fructose for growth (Cerón-García *et al.*, 2000; 2005; Liu *et al.*, 2009; Wang *et al.*, 2012). This possibility is extremely interesting as it opens the possibility to investigate the molecular mechanism of mixotrophy, which is still largely unknown to date. Results showing that diatoms optimise their photosynthetic efficiency via constitutive energetic interactions between mitochondria and plastids (Bailleul *et al.*, 2015) have suggested a molecular interpretation for mixotrophic growth. Indeed, coupling of respiratory and photosynthetic activities via exchanges of NADPH and ATP provides a tight coordination of these two processes. This coordination likely allows an efficient utilization of light and

reduced carbon by mixotrophy. On the other hand, the consequences of mixotrophy on cell metabolism are still poorly studied. By combining several omics approaches (lipidomics, transcriptomics and metabolomics) with physiological measurements, our data provide a comprehensive picture of the metabolic changes induced by this growth mode. Moreover, we show that mixotrophic growth in both flask and photobioreactor scales can be further improved by customizing the oligoelement content of standard media, as required for possible biotech applications.

METHODS

Algal culture.

Strains and growth media. Axenic cultures of *Phaeodactylum tricornutum* (Pt1, CCAP 1055/3, De Martino *et al.*, 2007) were grown in 250 ml flask either in artificial seawater ESAW (Berges *et al.*, 2001) supplemented with extra NaNO₃ and NaH₂PO₄ to reach a final concentration of 0.47 g/L N and 0.03 g/L P (this medium will be referred as E10 from now on). These increased concentrations avoid N or P depletion during growth (Abida *et al.*, 2015). For N-depletion experiments, cells were shifted to a N-free medium (called here E0). Cells were grown in a chamber at 20°C, 40 μE m⁻² s⁻¹ irradiance with a 12-h-light / 12-h-dark photoperiod and shaking at 100 rpm. For mixotrophic growth experiments, filter sterilized glycerol was added at a final concentration of 4,6 g/L to N repleted and N depleted (E10+GLY, E0+GLY).

Alternatively, the E10 medium was further optimised by comparing the elemental composition of *P. tricornutum* (Reboloso-Fuentes *et al.*, 2001) with that of E10 medium following an approach previously established in other microalgae (Mandalam and Palsson, 1998 and Danquah *et al.*, 2010). This revealed that the E10 medium is deficient in nitrogen, phosphorus, iron, manganese, zinc, and copper at high biomass concentrations. Thus, a new medium (called ESAW enriched, or EE) was redesigned by increasing the concentration of NaNO₃, NaH₂PO₄.H₂O, FeEDTA, ZnSO₄.7H₂O, MnSO₄

.4H₂O and CuSO₄. 5H₂O to 2.5 g/L, 0.20 g/L, 0.0216 g/L, 0.589 mg/L, 2.55 mg/L and 0.66 mg/L respectively. The amount of others elements was maintained the same as in E10 medium. In some experiments, the EE medium was supplemented with NaHCO₃ (1.26 g/L) to test the algal growth capacity in absence and presence of glycerol (*i.e.* EE+BIC, EE+BIC+GLY).

To monitor algal growth, samples were taken daily (in the end of the light period) and growth was estimated by *i.* cell counting using a LUNA™ instrument (Logos Biosystems, Inc. USA) or *ii.* measuring the optical density at 750 nm using a double beam UV/ visible spectrophotometer. In the latter case, cell concentration was evaluated from a previously established calibration curve. The initial inoculum was 0.5 and 2x10⁶ cells/mL for N-replete and N-deplete condition respectively. Cells were collected after 5 days for metabolomic and transcriptomic analyses.

Biolog™ plates assessment of growth and respiration. The consequences of 192 different carbon sources on algal growth was screened to pinpoint possible candidates for mixotrophic cultivation of *P. tricornutum* using Phenotype Biolog MicroArrays™. This microplate assay is based on the use of 96 well plate containing pre-arrayed substrates such as carbohydrates, amino acids and carboxylic compounds. In this study, 2 x10⁶ cells/mL were resuspended in the E10 medium and 200 µL were deposited into each well. Growth was followed daily and substrates that improve growth were selected from a duplicate experiment. The best metabolites were scaled up to 250 mL flask. A phototrophic control was grown in parallel.

To verify if these substrates were respired by *P. tricornutum*, different cell concentrations (2, 4 and 8 x 10⁶ cells/ mL) were dark-grown in a 24-well microplate with 50 mM of the selected molecules in presence of Biolog redox dye mix A. The intensity of color produced by the reduction of a tetrazolium compound during cell respiration (Bochner 2003) was determined by estimated with a cell plate reader (infinite, Tecan, Switzerland) to quantify respiration. Phototrophic control culture was used as negative control.

Nitrogen and phosphate concentration. Nitrogen and phosphate concentration in supernatant were determined using a Merck RQflex reflectometer (E. Merck, 64271 Domsstadt, Germany) with test strips (Reflectoquant nitrate and phosphate).

Scale-up in 2-L photobioreactor. The optimised conditions were carried out in duplicate in 2-L photo-bioreactors (Applikon Schiedam, The Netherlands). All cultures were sparged continuously with air at flow rate of 0.5 L/m. The pH was controlled at 8 by automatic on-demand injection of 0.25 N of HNO₃. Temperature was controlled at 20 °C by circulating water. Light was supplied continuously with external light panels ranging from 40 to 300 μE m⁻² s⁻¹.

Dry Cell Weight protocol. Millipore membrane filter (diameter 47 mm, μ = 0.45 μm) placed in an aluminium cup (ø x h = 70 x 6 mm) were dried 24h in an oven at 105 °C and weighted. From 2 to 10 mL of culture was filtered through dried filter. The filter was rinsed with sea water (2 x filtered volume). Finally, the filter + biomass was dried for 24h and weighted again. The dry cell weight (dcw) was calculated as: [weight of (filter+aluminium cup+biomass)] - [weight of (filter+ aluminium cup)]/ L of filtered culture and expressed as g/L.

Spectroscopy.

Chlorophyll Fluorescence Measurements. All the photosynthetic parameters were determined using a Speedzen MX fluorescence imaging setup (JBeamBio, France) as described in (Johnson *et al.*, 2009). For each sample, 3 x 200 μl of algal culture were transferred in a 24 well plate. Maximum quantum yield of PSII ($F_v/F_m = (F_m - F_0)/F_m$) was determined after 15 min of dark incubation, where F_m and F_0 are the maximum and minimum fluorescence of dark-adapted cells, respectively. Non-photochemical quenching (NPQ) was calculated as $(F_m - F_m')/F_m'$, where F_m' and F_m are maximum fluorescence of light-adapted and dark-adapted cells respectively. Photosynthetic electron transfer rate (ETR) was calculated as $0.5 \times I \times Y(II)$, where 0.5 represents the fraction of light absorbed by PSII (half of the total incident light), I is the incident light intensity and $Y(II)$ is the quantum yield of PSII in the light. The latter is defined as $(F_m' -$

$F_{ss})/F_{m'}$, where F_{ss} is the fluorescence emission measured in the presence of the light (Maxwell and Johnson 2000).

Nile Red analysis. Accumulation of triacylglycerols was monitored by Nile Red (Sigma-Aldrich) fluorescent staining as detailed in (Abida *et al.*, 2015). Shortly, 40 μ L of Nile Red dye (2.5 μ g/mL stock concentration, in 100% DMSO) were added to 160 μ L cell suspension (1-5 million cells/mL) in 96-well white microplate and mixed. After 20 minutes of incubation at room temperature into the dark the Nile Red fluorescence was measured (530/580 nm: excitation/emission). The data were then normalised per millions of cells.

Metabolite analysis

Glycerol concentration. The glycerol concentration of 2 mL of filtered supernatant was done on Shimadzu HPLC with a Hi-plex H+ (7.7 X 300 mm) Agilent column. The analysis was performed using the mobile phase 5 mM H_2SO_4 . The detection wavelength was set at 880 nm using a RI RID-10A Detector with a flow rate of 0.6 mL/min and a temperature of 60°C. The peaks quantification was performed by comparison of a range of 6 standards.

Total lipids extraction. Total lipids are extracted according to Folch *et al.*, 1957. About 20 mg of dried cells were homogenized with 1 mL of Chloroform/Methanol 2:1. The cells are then lysed using a TissueLyser II (Qiagen) with an agitation of 1 minute and a frequency of 300 s^{-1} . The lysate is washed with 200 μ L of NaCl 0.9 % and vortex for some seconds in order to form the emulsion. The solution is centrifuged 5 min at 13000 rpm to separate the two phases and the lower phase is placed in fresh pre-weighed glass tubes. The upper phase is washed with chloroform; lysis and centrifugation steps are repeated in order to recovery more lipids. The wash with chloroform is repeated at least twice. The lower phases (containing lipids) collected in glass tubes are evaporated under a nitrogen stream at 65°C. The glass tubes are weighed to determine the percentage of lipids extracted per dry cell weight.

Separation by TLC, and Analyses by GC-FID and MS. Glycerolipids were extracted from lipid extract of *P. tricornutum* cells as described in (Abida *et al.*, 2015). To quantify the various classes of nonpolar and polar glycerolipids, lipids were separated by TLC onto glass-backed silica gel plates (Merck) using two distinct resolving systems (Simionato *et al.*, 2013). To isolate nonpolar lipids including TAG and free FA, lipids were resolved by TLC run in one dimension with hexane:diethylether:acetic acid (70:30:1, v/v). Lipids were recovered from the silica powder after the addition of chloroform:methanol (1:2, v/v) thorough mixing and collection of the chloroform phase (Bligh and Dyer, 1959). Lipids were then dried under argon and either quantified by methanolysis and GC-FID.

Metabolites extraction and GC-MS Based Metabolite Profiling. Metabolites were extracted with some modifications of the protocol described in Obata *et al* 2013. Ten-millions of cells were harvested on a Durapore-HV membrane filter disk with 2.5 cm diameter and 0.45 μm pores (Millipore, Billerica, MA) by vacuum filtration. The filter with the cells was then transferred into a 1.5 ml tube and frozen in liquid nitrogen. Frozen samples were stored at $-80\text{ }^{\circ}\text{C}$ till metabolite extraction. Metabolites were extracted immersing the filter in 1 ml of 90% (v/v) methanol containing $0.1\ \mu\text{g mL}^{-1}$. The tubes were sonicated in a water bath type sonicator for 1 min in the ice cold water and then incubated at 4 degree for 1 h with shake. The remaining solution was centrifuged at $22,000 \times g$ for 5 min at $4\text{ }^{\circ}\text{C}$. A 50 μL aliquot of the supernatant was used for Chla determination and 900 μL was dried by a vacuum concentrator (SpeedVac concentrator, Thermo, Waltham, MA). Dried samples were stored at $-80\text{ }^{\circ}\text{C}$ after filling the tubes with argon gas. The metabolite profile was determined as described in Obata *et al* 2013.

Quantification of intracellular pyruvate. The concentration of pyruvate was evaluated by fluorescence-based method using the pyruvate assay kit (Cayman chemical).

Microarray analysis and statistics.

RNA extraction and gene expression analysis. The RNA was extracted and gene expression was analysed as described in Fortunato *et al.*, 2016. Total RNA was extracted as described in Huysman *et al.*, 2013. For RT-qPCR, 500 ng of total RNA were reverse-

transcribed using the QuantiTect Reverse Transcription Kit (Qiagen, USA) and the reaction accomplished with 12.5 ng cDNA as template, following the SsoAdvanced Universal SYBR Green Supermix instructions (Bio-Rad, USA), in a CFX 96 Real-Time Detection System (Bio-Rad). Primer efficiencies were determined as described in Pfaffl, 2001. RPS (ribosome binding site) and/or TBP (TATAA-box binding protein) were used as reference genes and normalization performed as described in Saut *et al.*, 2007.

For microarray analyses, total RNA was processed with the RNA clean-up protocol of the RNeasy Mini Kit (Qiagen, USA). 200 ng of total RNA were labeled with fluorescent Cy3 and Cy5 dyes using the Low Input Quick Amp Labeling Kit, Two-Color (Agilent, USA). Three biologically independent experiments were tested for each condition, using dye switch, and hybridized on 8x60K *P. tricornutum* whole-genome 60-mer oligonucleotide microarrays (Agilent Technologies) following the Agilent protocol. The microarray chip (Platform GPL21013) was designed based on the *P. tricornutum* genome, version Phatr2 (<http://genome.jgi.doe.gov/Phatr2/Phatr2.home.html>). Slides were scanned using a 2-micron Agilent microarray scanner and the resulting images analyzed using the Agilent Feature Extraction 11.5 software. Microarray normalization was performed by global lowess using Goulphar (Lemoine *et al.*, 2006). For each gene, the Cy5/Cy3 ratios corresponding to the different probes were averaged and mean of the biological replicates was calculated.

Statistical analysis. Data from three different experiments were tested for statistical significance of the variations in gene expression. This was determined using the t-test implemented in MeV 4.9. The three independent replicates were used to perform a one-class analysis using a p Value of 0.01. A threshold of expression of absolute Log₂ (fold change) value > 0.8 has been used to select genes differentially expressed between the test and the control conditions.

RESULTS

Consequences of mixotrophic growth on biomass production in *P. tricornutum* cells.

As a first step to optimise the biomass productivity of *P. tricornutum*, we analyzed the effect of external reduced carbon sources on the growth and physiological properties of cells in Erlenmeyer flasks. These culture experiments were performed in artificial seawater (ESAW) supplemented with 10 X concentration of N and P (E10 medium), to avoid nitrogen and phosphorous starvation during growth (Abida *et al.*, 2015). To identify the best respiratory substrate, we first grew *P. tricornutum* cells in Biolog™ plates supplemented with different carbon sources for 6 days. This allowed monitoring biomass productivity (via OD changes) and respiration, using a specific dye (see methods). We found that only few compounds enhanced growth of *P. tricornutum* cells by increasing their respiration (Fig. 3.S1). They include acetate, serine, fumarate and glycerol. Among them, glycerol was chosen as the final substrate, as its availability on large scale and low cost makes it compatible with industrial cultivation (Cerón-García *et al.*, 2005; 2006; 2013). When tested in 50 mL erlenmeyers, glycerol increased biomass production by a factor of 2 (Fig. 3.1A). Its effect was gradual, because of the progressive consumption of this compound by the algae (Fig. 3.1B), and became clearly visible after 5 days of growth.

The enhanced growth capacity observed in glycerol supplemented cells resulted in a much faster consumption of nitrogen (Fig. 3.1C) and phosphate (Fig. 3.1D), leading to a complete depletion by the end of the growth phase.

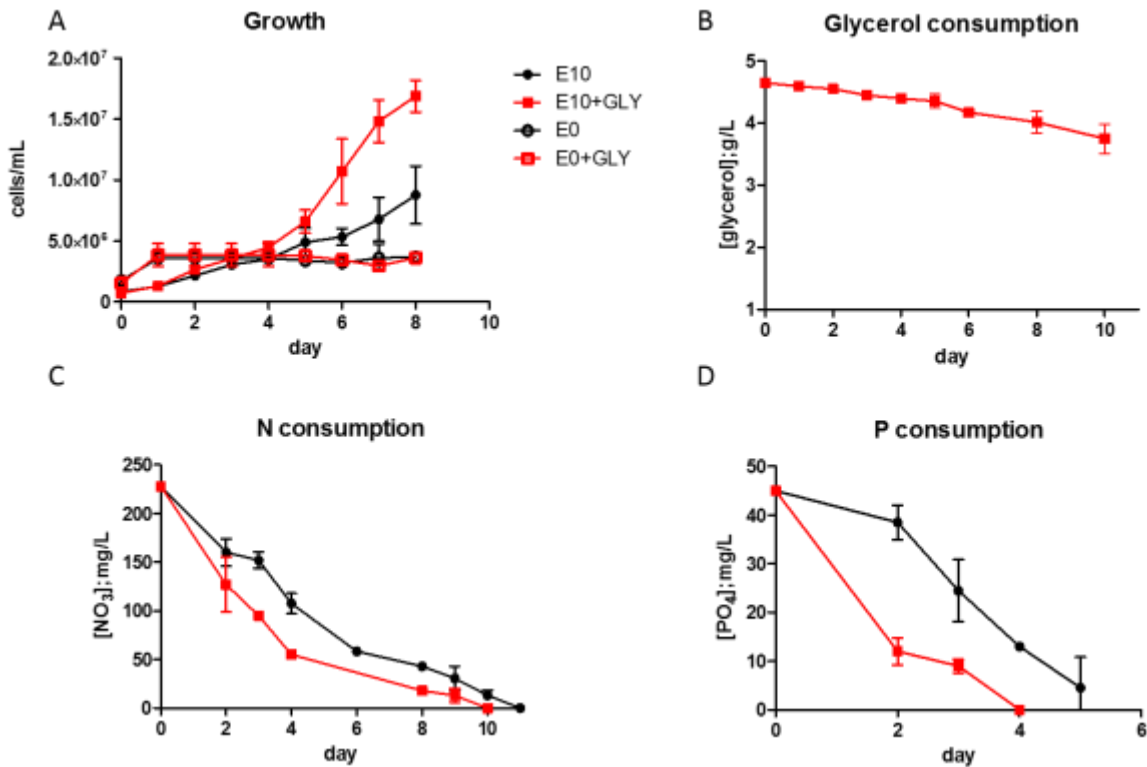


Fig. 3.1 Growth curves and nutrients consumption of *P. tricornutum*. A. Growth curves of *Phaeodactylum tricornutum* cells in N-replete and N-deplete condition in the presence/absence of glycerol. Two different starting cell densities were used in N-replete and N-deplete condition: 10^6 cells/mL and 2×10^6 cells/mL respectively. B. Glycerol consumption of *P. tricornutum* cells in N-replete conditions. C. Nitrate and D. phosphate consumption kinetics in *P. tricornutum* cultures in N-replete condition in the presence/absence of glycerol; Each result is the average of two biological replicates \pm SD. E10:N-replete condition; E0: N-deplete condition; GLY: glycerol.

Because nutrient starvation (and nitrogen in particular) affects photosynthesis (Saha *et al.*, 2003; Li *et al.*, 2008), we looked for possible effects of glycerol on photosynthetic parameters, measuring the quantum yield of PSII (F_v/F_m), the linear electron flow between PSII and PSI (ETR), and the photoprotective responses of the cells via NPQ. We found (Fig. 3.2), that glycerol addition had only minor effects on these parameters not only at the beginning of the experiment (day one), but also at day five, where the

consequences of this compound on growth become evident, as well as at the end of the growth experiment (day 10). Thus, we conclude that glycerol has no effects on photosynthesis. As a corollary of this experiment, we confirmed the large decrease in photosynthesis in *P. tricornutum* cells upon transfer to -N, which was related to a diminished cell content of the photosynthetic membranes (Fig. 3.S2).

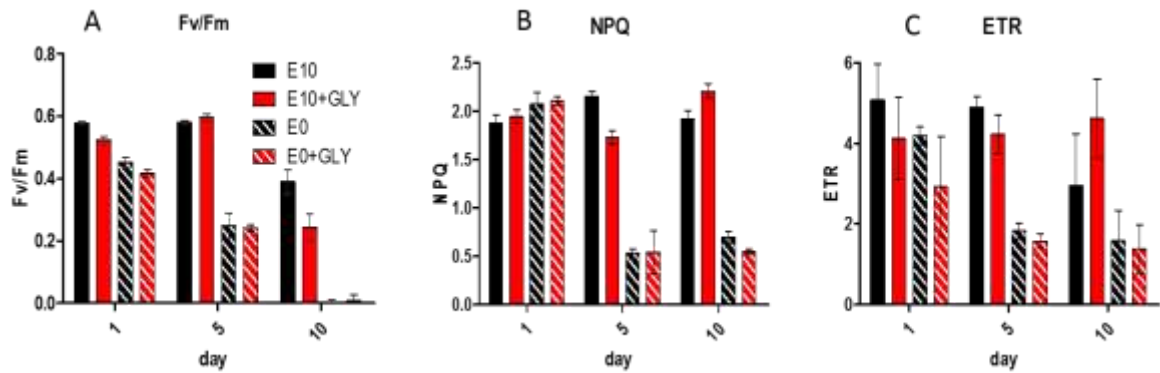


Fig. 3.2. Photosynthetic activity in *P. tricornutum*. A. Photosynthetic efficiency represented as F_v/F_m ratio; B. Non-photochemical quenching (NPQ) and C. Electron transport rate (ETR) of cells cultivated for 1, 5 and 10 days in N- replete or N- deplete conditions (full in both phototrophic and mixotrophic mode (black and red respectively). Each result is the average of two biological replicates \pm SD. E10:N-replete condition; E0: N-deplete condition; GLY: glycerol.

Metabolic and transcriptomic assessment of glycerol-mediated changes in P. tricornutum cells. The data presented above allow concluding that the glycerol-mediated improvement of biomass productivity in *P. tricornutum* is not due to a direct effect on photosynthesis. We explored therefore the possibility that this compound could affect the cell metabolism. Indeed, previous results suggest that glycerol affects the cellular lipid content (Cerón-García *et al.*, 2005; 2006; 2013). To assess possible metabolic changes, we therefore focused first on TAG accumulation using Nile Red fluorescence as a non-invasive cellular quantification tool (Fig. 3.3A). We found (Fig. 3.3B) that Nile Red fluorescence was enhanced by glycerol even in N replete cells at day 5. The choice of day 5 as the reference for all the metabolic analyses is justified by the need to measure changes at the earliest stage of the glycerol response, to avoid artefacts related to cell ageing and/or consumption of other nutrients. Thus, day 5 turned out to be the obvious choice, as it represents the first data point in which a significant effect of this compound is detected (Fig. 3.1).

The finding that glycerol increases Nile Red fluorescence even in N supplemented cells suggests that this compound affects the lipid metabolism even in unstarved conditions. This conclusion was further substantiated by the quantification of total lipid content (Fig. 3.3C), and of the DAG and TAG fractions (Fig. 3.3D-E) by mass spectrometry. We found, that the TAG content was specifically increased by glycerol (Fig. 3.3D), in agreement with the Nile Red observations. We also observed, as expected, that the total lipid content was largely enhanced by nitrogen starvation. Conversely, glycerol addition did not modify this parameter significantly (Fig. 3.3C). In parallel to the changes in the TAG content, we also observed that the TAG fatty acids (FA) composition was modified by glycerol. In particular C16:0 and C16:1 FA were higher in glycerol grown cells (Fig. 3.S3), suggesting that this compound induces FA neosynthesis (Simionato *et al.*, 2013; Abida *et al.*, 2015). Glycerol also leads to a higher amount of C20:5, as already reported in case of N limitation in *P. tricornutum*. Overall, glycerol addition seems to mimic nitrogen limitation on lipid metabolism (Abida *et al.*, 2015), although to a lower extent.

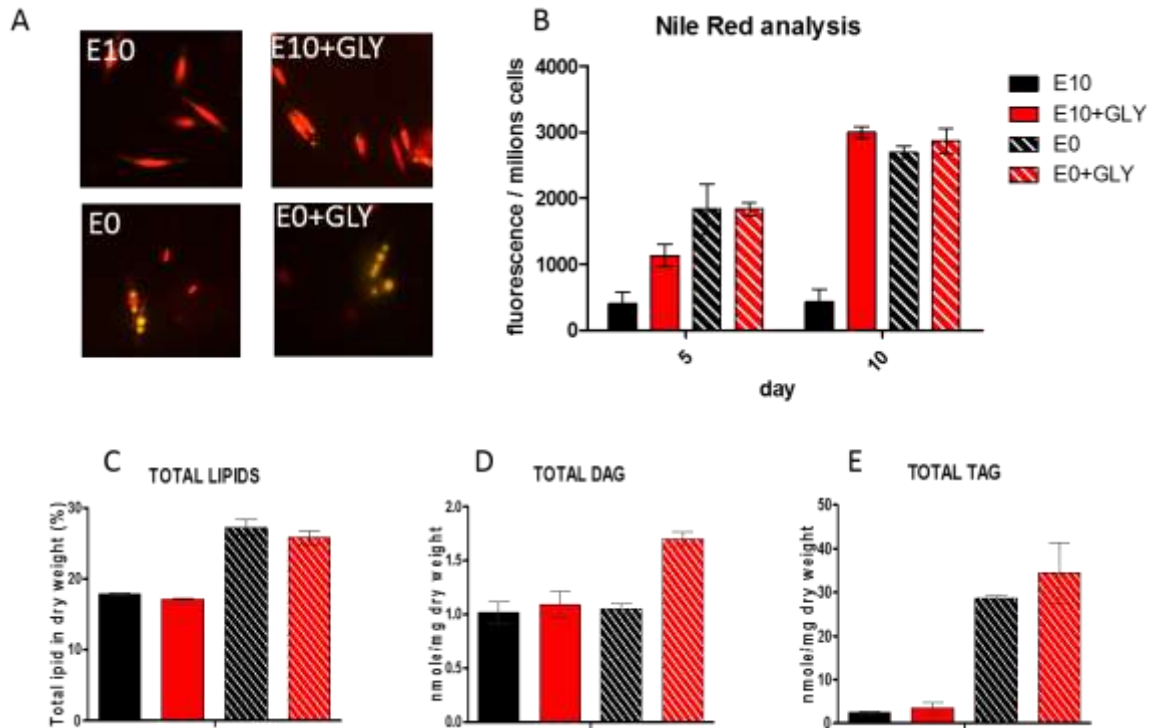


Fig. 3.3 Lipid and acylglycerols production in *P. tricornutum*. A. Epifluorescence images of cells stained at day 5 with Nile Red dye. B. Neutral lipid content normalized per millions of cells determined by Nile Red staining at day 5 and 10. C. Total lipids accumulation at day 5 in *P. tricornutum* expressed as percentage of dry weight. D. DAG and E. TAG accumulation at day 5 in *P. tricornutum* normalized per mg of dry cells. Each result is the average of two biological replicates \pm SD. E10: N-replete condition; E0: N-deplete condition; GLY: glycerol.

However, glycerol has an obvious advantage over N limitation for lipid accumulation, as its addition has a positive effect on growth at variance with N limitation (STable I).

To better understand the effect of glycerol on the cell metabolism, we compared the metabolic profile of cells grown in the absence and presence of glycerol for 5 days. We found that most of the metabolites analyzed by Gas-Chromatography Mass-Spectroscopy in our extracts were not significantly affected by glycerol addition (Fig. 3.S4). However, a few of them displayed significant changes. In particular, five metabolites (lactate, xylose, trehalose, DHA and mannitol) were upregulated in presence of glycerol while five others (fructose, valine, alanine, guanidine and leucine) were repressed by this compound. Overall, the symmetric changes of lactate, valine, serine

and leucine suggest that the pyruvate hub could be affected by glycerol (Fig. 3.4). To test this possibility, we directly quantify the pyruvate content in the same cell extracts using a commercial kit (Fig. 3.S5) because this metabolite could not be measured with the GC-MS approach. We found that glycerol addition increased the pyruvate content, suggesting a higher flux from the sources (aminocids and glycerol) to the sinks (*i.e.* pyruvate fermentation to produce lactate). On the other hand, the complementary changes in fructose, trehalose and mannitol also points to a change in carbon storage metabolism (Fig. 3.4). Finally, the change in DHA is compatible with the modification of the lipid metabolism suggested by the lipidomic analysis. To corroborate the hypothesis that glycerol affects primary, storage carbon and lipid metabolisms, we performed a comparative transcriptomic analysis, using cells grown for 5 days in the absence and presence of glycerol as the starting material for RNA extraction and hybridization on a microarray containing the entire nuclear genome of *P. tricornutum* (Agilent Technologies). We found that several genes were differentially expressed in presence of glycerol (Fig 3.4, STable II). After gene annotation and refined statistical analysis, we restricted this pool to 10 genes (STable III). Most of them were involved in lipid, amino acid metabolism, glycolysis pathway, consistent with the conclusions about central carbon metabolism, lipid and storage biosynthesis derived from metabolic analyses (Fig. 3.4). In particular, the finding that the pyruvate carboxylase gene was induced by glycerol likely provides a rationale for the increased respiratory activity measured upon glycerol addition using the colorimetric assay coupled to the BiologTM experiment (Fig 3.S1). Consistent with this conclusion, direct assessment of oxygen consumption by a polarographic approach (Fig 3.S6) revealed enhanced respiration activity by glycerol addition.

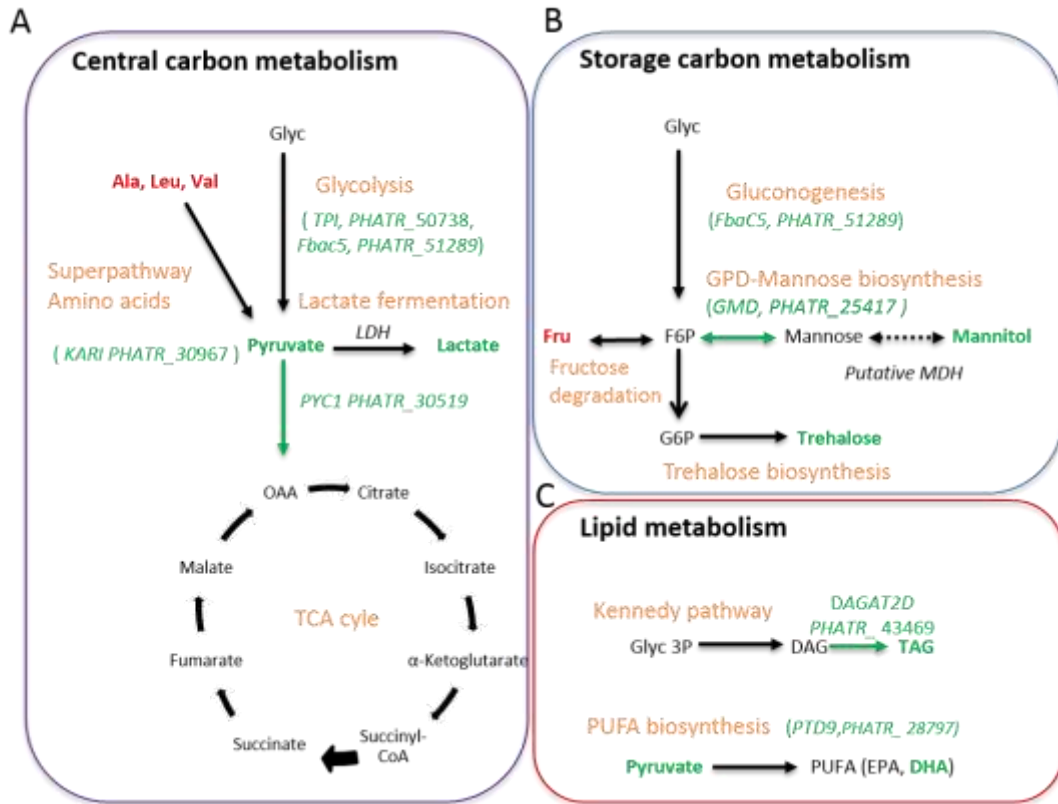


Fig. 3.4 Hypothetical cellular pathways involved in the mixotrophic growth of *P. tricornutum*. Hypothetical pathways involved in **A.** central carbon, **B.** storage carbon and **C.** lipid metabolism during the mixotrophic growth of *P. tricornutum* are shown. Italic green type represents gene transcripts found to be up-regulated in presence of glycerol in microarray analysis, gene numbers are also indicated. Bold green or red type represents metabolites that were detected in the current study by GC-MS analysis in cells grown in mixotrophy or phototrophy respectively. Changes for pyruvate are provided by direct estimates with a “Pyruvate Assay Kit” (see methods) and TAG in lipidomics analysis. Glyc= Glycerol; Glyc3P= glycerol 3 phosphate; TPI=Triphosphateisomerase; Fbac5= fructose biphosphate aldolase; PYC1= pyruvatecarboxylase; OAA= Oxaloacetic acid; Fru= fructose; F6P=fructose-6-phosphate; G6P=glucose-6 phosphate; AG3P=Acyl Glycerol 3phosphate; DAGAT2D=Diacyl Glycerol acyltransferase 3 phosphate.

Mixotrophic growth can be further improved upon optimisation of the element composition of the ESAW medium. In order to further improving the utilization of light and carbon sources for biomass production in mixotrophic cultures of *Phaeodactylum*, we optimised the composition of the artificial seawater employed for cell growth. In particular, we focused on elemental balance approach between growth medium (*i.e.* E10) and biomass composition of *Phaeodactylum* (Reboloso-Fuentes *et al.*, 2001) to obtain high biomass concentration (see methods).

Following the same rationale of Mandalam and Palsson 1998 and Danquah *et al.*, 2010, we re-evaluated the medium composition for *P. tricornutum*, and we increased the concentration of specific elements (*i.e.* nitrate, phosphate, iron, zinc, manganese and copper). This allowed defining a new artificial seawater medium (EE), which increased growth in mixotrophic conditions, likely because of the higher glycerol utilization (Fig. 3.5A-B). By testing separately, the effect of macro and micronutrients

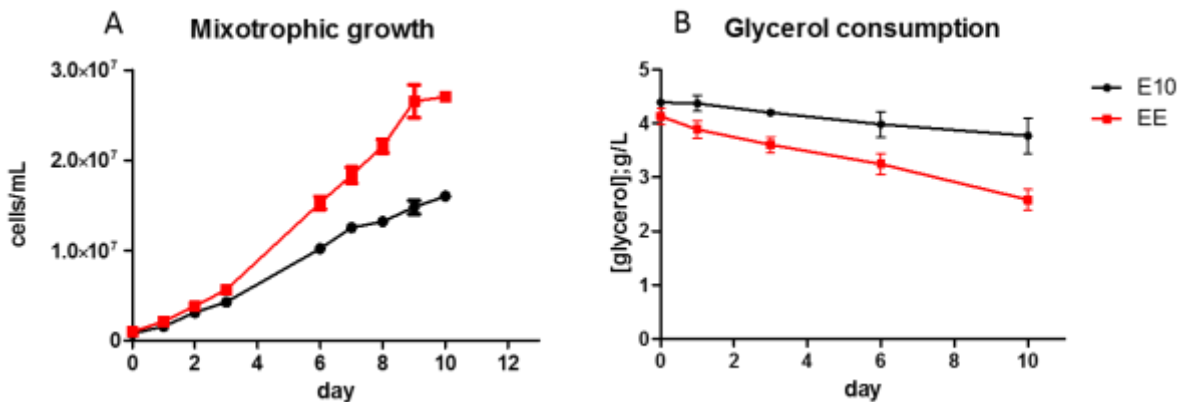


Fig. 3.5 Optimisation of growth medium in *Phaeodactylum*. A. Mixotrophic growth of *P. tricornutum* and B. glycerol consumption in the initial (black line) and in the optimised medium (red line). Each result is the average of two biological replicates \pm SD. E10=ESAW 10XN; EE= ESAW enriched.

present in the EE medium on algal growth when cultivated in the E10 medium (Fig. 3.S7), we reached the conclusion that the enhanced mixotrophic growth was caused by the modified trace elements. This suggests that when trace elements are customized to an organism of interest in terms of composition and /or concentration, growth can be enhanced without affecting the algal physiological responses, and the production of biotech relevant molecules, as TAGs, in line with previous conclusions in the green alga *Chlamydomonas reinhardtii* (Kropat *et al.*, 2011).

The EE medium not only promoted a higher biomass productivity, but also increased the cellular pigment (Fig. 3.6A and B) and lipid content (Fig. 3.6C).

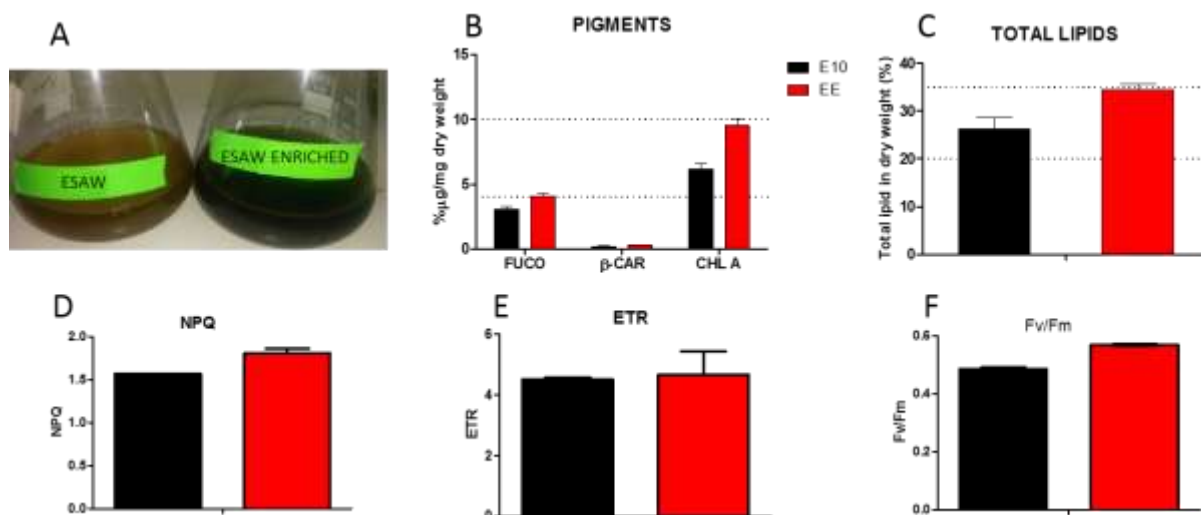


Fig. 3.6 Impact of improved medium on biomass composition and on photosynthetic parameters. A. Pictures of 10 days-cultured cells in the E10 (left) and EE medium (right). **B.** Pigments and **C.** total lipids content in cells grown 10 days in E10 (black bar) and EE (red bar) cultured cell extracts. **D.** Photosynthetic efficiency represented as F_v/F_m ratio; **E.** Electron transport rate (ETR) and **F.** Non-photochemical quenching (NPQ) of cells cultivated for 10 days in E10 (black bar) and EE (red bar) medium. Each result is the average of two biological replicates \pm SD. E10=ESAW 10XN; EE= ESaw enriched.

The positive effect of the EE medium on mixotrophic growth became even larger upon addition of bicarbonate in the medium (Fig. 3.7), indicating a possible limitation of CO₂ supply in our shake-flask cultures. This possibility was confirmed by results

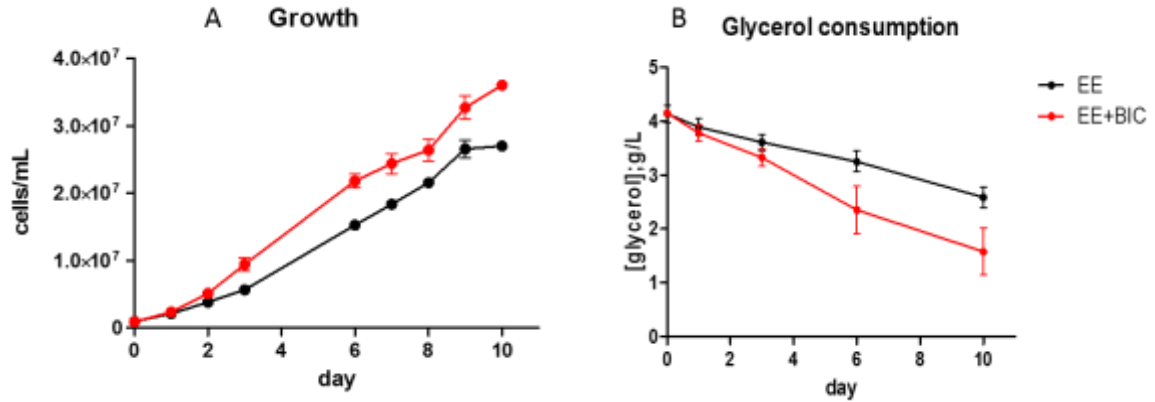


Fig. 3.7 Effect of bicarbonate on mixotrophic growth. A. Mixotrophic growth of *P. tricornutum* grown and B. glycerol consumption in ESAW enriched (black line) and in ESAW enriched + bicarbonate (red line). Each result is the average of two biological replicates ± SD. EE= ESAW enriched; EE+BIC= ESAW enriched + bicarbonate

obtained in small scale photobioreactors, where HCO₃, light and glycerol supply were optimised (Fig. 3.8). In these conditions, biomass productivity was largely increased (STable I), when compared to initial conditions. Overall, we found a biomass concentration and productivity (STable I) similar to those previously reported in *P. tricornutum* cultures exposed to a much higher light intensity (*i.e.* 750 μE m⁻² s⁻¹) (Cèron-García *et al.*, 2013).

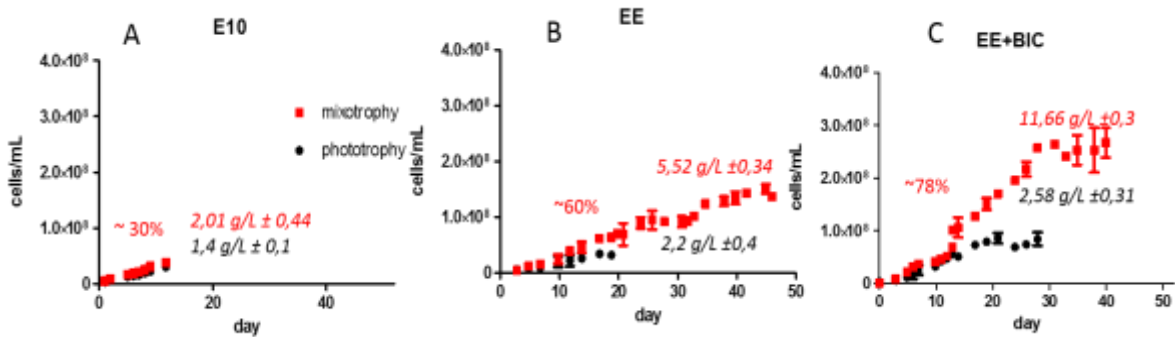


Fig. 3.8 Scale-up to photobioreactors. Growth profile of *P. tricornutum* grown in 2L-fermentor in **A.** E10 **B.** EE and **C.** EE+ BIC in both phototrophic (black circles) and mixotrophic (red squares) mode. The maximum biomass are also indicated in each condition. The *optimisation* of medium composition and culture conditions allows to increase the efficiency of mixotrophy from 30% up to 78 %. Each result is the average of two biological replicates ± SD.

DISCUSSION

Improving biomass productivity in P. tricornutum by optimising mixotrophic growth.

Diatoms are photosynthetic unicellular microalgae that dominate the oceans. They are extremely interesting for ecological purposes but also as potential feedstocks for sustainable biofuels, because of their biomass yield and capacity to accumulate lipids, and the possibility to engineer their metabolism. Thanks to their metabolic flexibility, diatoms can produce biomass via different modes of growth. Diatoms can be cultivated phototrophically, simply converting the sunlight energy into reduced carbon via photosynthesis. This can be a cheap way to produce biomass because they only use sunlight as an energy source, but it is often limited by the difficulties in optimising light penetration, gas diffusion and temperature control in outdoor photobioreactors and race ponds (Chisti *et al.*, 2007; 2008). While some microalgae can grow heterotrophically via sugar fermentation in the dark, this is not possible in *Phaeodactylum*, which can use sugars in the dark only upon metabolic engineering (Zaslavskaja *et al.*, 2001). On the other hand, *P. tricornutum* can grow mixotrophically, *i.e.* using simultaneously light and reduced carbon (Cèron-García *et al.*, 2000; 2005; 2013). This mode of cultivation

represents an interesting alternative to phototrophic growth, because algae grown mixotrophically have, in principle, a lower requirement for optimum light penetration, and can make use of cheap and easily available carbon sources, like glycerol, leading to a high biomass productivity (Cèron-García *et al.*, 2000; 2005; 2013).

Starting from these general considerations, the first goal of this work was to optimise the simultaneous use of light, CO₂ and reduced carbon in mixotrophically grown *Phaeodactylum* cells. For this purpose we optimise an artificial seawater based growth medium (ESAW) by implementing both the macronutrient (phosphate and nitrogen) and the micronutrient (trace metal elements) components. Eventually, we generated the EE medium, where biomass productivity was enhanced by a factor of 2 when compared to the E10 medium (Fig. 3.6). This medium contains 10 times higher concentrations of phosphate and nitrogen (0.467 g/L of NaNO₃ and 0.03 g/L of NaH₂PO₄·H₂O) to avoid N or P depletion during growth. By assessing the consequences of the different fractions of the EE medium on growth, we demonstrated that changes in the trace metal components are mostly responsible for the positive effects of the EE on *Phaeodactylum*, in agreement with earlier results obtained in different groups of microalgae (Kropat *et al.*, 2011; Danquod *et al.*, 2010).

When *Phaeodactylum* cells are grown in the EE medium, not only the cell number is increased, but also the quality of the biomass is improved, as indicated by the increased pigment and lipid content per dry weight. This likely reflects the better physiological state of the cells in the EE cultures, as suggested by their higher content of triradiate cells, when compared to ESAW 10X driven cultures (fig. 3.S8). *P. tricornutum* is a pleiomorphic alga that displays three major morphotypes: the fusiform, the oval, and the triradiate one. The first two represent the “normal” and the “stress” morphotype, as deduced by studies on the responses to temperature or salinity stress (De Martino *et al.*, 2007). Conversely, the latter form is very rarely observed in laboratory cultures, but is the most abundant one in the ocean. Therefore, it likely represents the truly physiological state of the alga.

In the EE medium we also observed that HCO_3^- largely increased mixotrophic growth. This observation can be explained based on our previous observation that photosynthesis and respiration are tightly linked in diatoms via the active exchange of reducing power and ATP to optimise carbon assimilation (Bailleul *et al.*, 2015). In the frame of this hypothesis, one may expect that when photosynthesis is no longer limited by CO_2 availability (*i.e.* in the presence of external bicarbonate in our case) a higher amount of ATP is generated by mitochondria. This would be needed for CO_2 assimilation, thus leading to a high respiratory activity and consumption of reduced carbon. In line with this idea, recent modelling of mixotrophic metabolism $\pm \text{CO}_2$ based on flux balance analysis of *P. tricornutum* (Kim *et al.*, 2015) has suggested that the ATP flux through mitochondria is around 1.2 times higher than the flux in the plastid. This “extra capacity” could fulfill the need for “extra” ATP for carbon assimilation, which we estimated in the range of 10-15% (Bailleul *et al.*, 2015) in *P. tricornutum*.

On the other hand, another possibility was considered by the authors, namely that the transport of reductants from the chloroplast to the mitochondria could not only provide a benefit for the cell energy balance, but also provide carbon skeletons for anabolic activity. Some of our observation support this conclusion. We found that while oxygen uptake is stimulated in all conditions by addition of glycerol, indicating enhanced respiration, photosynthesis is only enhanced when bicarbonate is added. This indicates that external reduced carbon can be used in different modes depending on limitation of the photosynthetic performances of the alga and in particular for anabolic purposes.

Metabolic consequences of glycerol mediated mixotrophic growth. Our characterization of mixotrophy in diatoms also includes the investigation of the metabolic consequences of glycerol addition on the cells, via metabolomic and transcriptomic analysis. The glycerol metabolism of *P. tricornutum* was previously investigated by isotope labelling experiments using ^{13}C -glycerol as carbon source (Zheng *et al.*, 2013; Huang *et al.*, 2015). These studies conclude that under mixotrophic conditions *P. tricornutum* cells mostly convert this compound into glycine and serine.

This stems from enhanced conversion of glyoxylate via the photorespiratory alanine/glyoxylate aminotransferase and serine hydroxymethyltransferase enzymes (Zhen *et al.*, 2013; Kim *et al.*, 2015). In our analysis no significant changes in the serine and glycine cellular content were seen, while other amino acids show significant modifications upon glycerol addition. A possible explanation for this apparent contradiction is that the authors of these studies specifically focused on mixotrophic growth cells, where serine and glycine are synthesised from glycerol. Conversely, we compared phototrophically and mixotrophically grown cells. Therefore, it appears that while both phototrophy and mixotrophy lead to production of glycine and serine via photorespiration, the efficiency rate of this metabolic path is not specifically enhanced by glycerol addition.

On the other hand, the combination of omics analyses (lipidomics, transcriptomics and metabolomics) employed here pinpoint several metabolic changes, which are specifically induced by glycerol driven mixotrophy. They include changes in central-carbon, carbon-storage and lipid metabolisms in *Phaeodactylum* (Fig. 3.4). Overall, we propose a model in which glycerol is firstly degraded to the dihydroxyacetone phosphate (DHAP) via glycerol-3-phosphate (gly 3P) by a glycerol kinase and a glycerol-3-P dehydrogenase. Then, the DHAP enters into glycolysis pathway, consistent with the overexpression of two enzymes in the microarray analysis (*i.e.* *TPI*, *PHATR_50738* and *Fbac5*, *PHATR_51289*). At the same time, the level of pyruvate (*i.e.* end-product of glycolysis) increases, likely because of the enhanced flux from the amino acids alanine, leucine, and valine (Fig. 3.4). The changes in the pyruvate metabolic hub affect several metabolic pathways. First, we see that glycerol enhances pyruvate fermentation to lactate via lactic dehydrogenase (*i.e.* *LDH*). However, pyruvate can also be converted by the pyruvate carboxylase to oxaloacetic acid and enter the TCA cycle, as shown by the increased respiratory rate, and by the upregulation of the pyruvate carboxylase enzyme (*i.e.* *PYC1*, *PHATR_30519*). According to our data, glycerol can also be converted to fructose-6-phosphate (F6P) and glucose-6-phosphate (G6P) via gluconeogenesis. These sugars can be transformed into carbon storage carbohydrates, as observed here in the

case of trehalose and mannitol. This finding is particularly interesting because it suggests that besides chrysolaminarin (1,3- β -D-glucan), which are the most abundant storage form of sugars in diatoms (Kroth *et al.*, 2008), *P. tricornutum* can accumulate other storage sugars. Consistent with this, *P. tricornutum* possesses a complete set of enzymes for synthesis of trehalose and mannose and we observe in our analysis that one of them was up-regulated by glycerol (*i.e.* GDP-mannose 4,6-dehydratase, *PHATR_25417*). Moreover, we identified a putative mannitol dehydrogenase in the genome of *Phaeodactylum* (*i.e.* *PHATH_30246*) that is involved in the conversion of the mannose into mannitol. This gene showed some homologies (c. 37, 2%) with the mannose dehydrogenase enzyme M1PDH from the brown algae *Ectocarpus siliculosus*. Both the trehalose and mannitol pathway have been already identified in brown algae, where they seem to be inherited by red algal progenitor and lateral gene transfer from *Actinobacteria* respectively (Michel *et al.* 2010). Thus, it is reasonable to assume that a similar situation may be present in *P. tricornutum*.

Finally, glycerol addition also affects the lipid metabolism, consistent with previous reports (Cèron-García *et al.*, 2006). In particular, our analysis indicates that its addition enhances both the PUFA (*i.e.* DHA) and TAG production, as evidenced by the metabolomics and lipidomics analysis, respectively. These conclusions are also corroborated by our microarray analysis, which reveals an up-regulation of the fatty acids desaturases *PTD9* (*PHATR_28797*) as well as the acetyl-transferase *DAGAT2D* (*PHATR_43469*) involved in the PUFA and TAG biosynthesis respectively. Moreover, our analysis of the fatty acids composition of TAGs in glycerol treated cells also suggests that their accumulation is due to neosynthesis but also to some degradation of pre-existing membrane lipids. In general, TAGs can be produced by two main routes in a cell: *i. de novo* synthesis of fresh fatty acids directly incorporated into TAGs via the Kennedy pathway or *ii.* conversion of preexisting polar glycerolipids (Li-Beisson *et al.*, 2013). TAGs generated by the first route contain newly generated fatty acids, *i.e.*, high levels of C16:0 and C16:1 fatty acids. Conversely, TAGs obtained from recycling of membrane lipids contain fatty acids with a substantial proportion of elongated and polyunsaturated

molecular species such as C20:5 fatty acids. Our data indicate that glycerol-grown cells contain a higher amount of 16:0 and 16:1 fatty acids, consistent with the occurrence of neosynthesis. However, this compound also leads to an increased accumulation of C20:5 fatty acids, consistent with the occurrence of some membrane lipids turnover. This behavior is very similar to the one observed in *P. tricornutum* cells upon exposure to nutrient (nitrogen) starvation.

However, at variance with N limited cells, glycerol, supplemented do not display any *i.* significant degradation of the most abundant thylakoids lipids, *i.e.* MGDG and DGDG (fig. 3.S9), and *ii.* any loss of photosynthetic activity. Thus, although the consequences of glycerol addition of lipids are reminding of those of nitrogen starvation (Abida *et al.*, 2015) in terms of TAG accumulation and changes in the fatty acids profile, this compound seems to act mainly at the level of lipid biosynthesis than degradation.

CONCLUSIONS

This work highlights the potential of mixotrophic growth for biotechnology applications. Indeed this growth mode can largely enhances biomass productivity, using available carbon sources. This mode of growth also has advantages in terms of lipid accumulation, as glycerol reproduces some typical response of nitrogen limited cells, in terms of TAG accumulation and fatty acids composition. Moreover, it does not diminish (and in some cases increase) photosynthetic activity (at variance with nitrogen limitation). However, another economic aspect that has to be taken into account is the additional cost of organic carbon supplementation. To solve this problem wastewater and biodiesel waste (*i.e.* glycerol) can be used for the industrial exploitation of microalgae. Interestingly we show that the optimised medium (*i.e.* by implementing micronutrients/HCO₃ supply) largely enhances mixotrophy and allows to reach state of the art productivity levels also in the presence of relatively low light intensities, when compared to previous experiments ($\leq 300\mu\text{E}$, this work vs $750\mu\text{E}$, Cèron-García *et al.*,

2013). This also shows the potential of this approach in terms of the reduction of the energy input required for high biomass productivity.

Finally, our deep characterization of mixotrophic metabolism reveals the main metabolic pathways targeted by glycerol. This information indicates possible targets for metabolic engineering, to enhance the efficiency of this phenomenon. Typically, inhibition of the biosynthesis of storage carbohydrates (*i.e.* trehalose and mannitol) could potentially direct the carbon (derived from glycerol) towards TAG production (as already reported in the case of the main sugar storage polymer, chrysolaminarin in Daboussi *et al.*, 2014). Ongoing integration of our data into a mathematical model will reveal other possible target to further increase the algal production capabilities.

REFERENCES

Abida, H. *et al.*, Membrane Glycerolipid Remodeling Triggered by Nitrogen and Phosphorus Starvation in *Phaeodactylum tricornutum*. *Plant Physiol.* **167**, 118–36 (2015).

Balat, M. & Balat, H. A critical review of bio-based diesel as a vehicular fuel. *Energy Convers. Manag.* **49**, 2727–2741 (2008).

Berges, J. A., Franklin, D. J. & Harrison, P. J. Evolution of an artificial seawater medium: Improvements in enriched seawater, artificial water over the last two decades. *J. Phycol.* **37**, 1138–1145 (2001).

Bligh, E. G. & Dyer, W. J. A rapid method of total lipid extraction and purification. *Can. J. Biochem. Physiol.* **37**, 911–917 (1959).

Cèron-García C M, Fernández Sevilla, J., Acién Fernández, F., Molina Grima, E. & García Camacho, F. Mixotrophic growth of *Phaeodactylum tricornutum* on glycerol: growth rate and fatty acid profile. *J. Appl. Phycol.* **12**, 239–248 (2000).

Cèron-García C M, Fernández-Sevilla J, Sánchez-Mirón A, García-Camacho F, Contreras-Gómez A, Molina-Grima E. Mixotrophic production of marine microalga *Phaeodactylum tricornutum* on various carbon sources. *J. Microbiol. Biotechnol.* **16**, 689–694 (2006).

Cèron-García C M, Fernández-Sevilla J, Sánchez-Mirón A, García-Camacho F, Contreras-Gómez A, Molina-Grima E. Mixotrophic growth of *Phaeodactylum tricornutum* on fructose and glycerol in fed-batch and semi-continuous modes. *Bioresource Technology* **147**, 569–576 (2013).

Cèron-García C M, Sánchez Mirón, A., Fernández Sevilla, J. M., Molina Grima, E. & García Camacho, F. Mixotrophic growth of the microalga *Phaeodactylum tricornutum*: Influence

of different nitrogen and organic carbon sources on productivity and biomass composition. *Process Biochem.* 40, 297- 305 (2005).

Chen, G.-Q. & Chen, F. Growing phototrophic cells without light. *Biotechnol. Lett.* 28, 607–616 (2006).

Chi, Z., O'Fallon, J. V. & Chen, S. Bicarbonate produced from carbon capture for algae culture. *Trends in Biotechnology* 29, 537–541 (2011).

Chisti, Y. Biodiesel from microalgae beats bioethanol. *Trends Biotechnol.* 26, 126–131 (2008).

Chisti, Y. Biodiesel from microalgae. *Biotechnology Advances* 25(3), 294-306 (2007).

Daboussi F., Leduc S, Maréchal A, Dubois G, Guyot V, Perez-Michaut C, Amato A, Falciatore A, Juillerat A, Beurdeley M, Voytas D, Cavarec L, Duchateau P. Genome engineering empowers the diatom *Phaeodactylum tricornutum* for biotechnology. *Nat. Commun.* 5, 3831 (2014).

Danquah, M. K., R. Harun, R. H. Cultivation Medium Design Via Elemental Balancing for *Tetraselmis suecica*. *Chem. Biochem. Eng.* 24, 361–369 (2010).

De Martino, A. , Meichenin, A., Shi, J., Pan, K. & Bowler, C. Genetic and phenotypic characterization of *Phaeodactylum tricornutum* (Bacillariophyceae) accessions. *J. Phycol.* (2007). doi:10.1111/j.1529-8817.2007.00384.x

Folch, J., Less, M. & Sloane Stanley, G. H. A simple method for the isolation and purification of total lipides from animal tissues. *J. Biol. Chem.* 226, 497–509 (1957).

Gardner, R. D. et al., Use of sodium bicarbonate to stimulate triacylglycerol accumulation in the chlorophyte *Scenedesmus* sp. and the diatom *Phaeodactylum tricornutum*. *J. Appl. Phycol.* 24, 1311–1320 (2012).

Hellebust, J. A. Glucose uptake by *Cyclotella cryptica*: dark induction and light inactivation of transport system. *J. Phycol.* 7, 345–349 (1971).

Hutchins, D. a., DiTullio, G. R., Zhang, Y. & Bruland, K. W. An iron limitation mosaic in the California upwelling regime. *Limnol. Oceanogr.* 43, 1037–1054 (1998).

Huysman, M. J. J. et al., AUREOCHROME1a-Mediated Induction of the Diatom-Specific Cyclin dsCYC2 Controls the Onset of Cell Division in Diatoms (*Phaeodactylum tricornutum*). *Plant Cell Online* 25, 215–228 (2013).

Huysman, M.J., et al., (2013). AUREOCHROME1a-mediated induction of the diatom-specific cyclin dsCYC2 controls the onset of cell division in diatoms (*Phaeodactylum tricornutum*). *Plant Cell* 25, 215–228 (2013).

Jia, J. et al., Molecular mechanisms for photosynthetic carbon partitioning into storage neutral lipids in *Nannochloropsis oceanica* under nitrogen-depletion conditions. *Algal Res.* 7, 66–77 (2015).

Johnson, X. et al., A new setup for in vivo fluorescence imaging of photosynthetic activity.

Kim, J. et al., Flux balance analysis of primary metabolism in the diatom *Phaeodactylum tricornutum*. *Plant J.* (2015). doi:10.1111/tpj.13081

Kitano, M., Matsukawa, R. & Karube, I. Changes in eicosapentaenoic acid content of *Navicula saprophila*, *Rhodomonas salina* and *Nitzschia* sp. under mixotrophic conditions. *J. Appl. Phycol.* (1997). doi:10.1023/A:1007908618017

Kropat, J. et al., A revised mineral nutrient supplement increases biomass and growth rate in *Chlamydomonas reinhardtii*. *Plant J.* 66, 770–780 (2011).

Kroth, P. G. et al., A model for carbohydrate metabolism in the diatom *Phaeodactylum tricornutum* deduced from comparative whole genome analysis. *PLoS One* 3, e1426 (2008).

Kumar, A. et al., Enhanced CO₂ fixation and biofuel production via microalgae: Recent developments and future directions. *Trends in Biotechnology* 28, 371–380 (2010).

Lechner, C. C. & Becker, C. F. W. Silaffins in silica biomineralization and biomimetic silica precipitation. *Marine Drugs* 13, 5297–5333 (2015).

Lemoine, S., Combes, F., Servant, N., and Le Crom, S.. Goulphar: rapid access and expertise for standard two-color microarray normalization methods. *BMC Bioinformatics* 7, 467 (2006).

Lewin, J. C. & Lewin, R. A. Auxotrophy and heterotrophy in marine littoral diatoms. *Can. J. Microbiol* 6, 127–134 (1960).

Li, Y., Horsman, M., Wang, B., Wu, N., and Lan, C. Q.. Effects of nitrogen sources on cell growth and lipid accumulation of green alga *Neochloris oleoabundans*. *Appl. Microbiol. Biotechnol* 81, 629–636 (2008). doi:10.1007/s00253-008-1681-1

Li-Beisson, Y. et al., Acyl-lipid metabolism. *Arabidopsis Book* 11, e0133 (2013).

Liu X, Duan S, Li A, Xu N, Cai Z, Hu Z. Effects of organic carbon sources on growth, photosynthesis, and respiration of *Phaeodactylum tricornutum*. *Journal of Applied Phycology* 21, 239-246 (2009).

Mandalam, R. K. & Palsson, B. Ø. Elemental balancing of biomass and medium composition enhances growth capacity in high-density *Chlorella vulgaris* cultures. *Biotechnol. Bioeng* 59, 605–611 (1998).

Maxwell, K. & Johnson, G. N. Chlorophyll fluorescence--a practical guide. *J. Exp. Bot.* 51, 659–668 (2000).

Michel, G., Tonon, T., Scornet, D., Cock, J. M. & Kloareg, B. Central and storage carbon metabolism of the brown alga *Ectocarpus siliculosus*: Insights into the origin and evolution of storage carbohydrates in Eukaryotes. *New Phytol.* (2010). doi:10.1111/j.1469-8137.2010.03345.x

Parkinson, J. & Gordon, R. Beyond micromachining: The potential of diatoms. *Trends in Biotechnology* 17, 190–196 (1999).

Pfaffl, M. W. A new mathematical model for relative quantification in real-time RT-PCR. *Nucleic Acids Res.* 29, e45 (2001).

Pfaffl, M.W.. A new mathematical model for relative quantification in real-time RT-PCR. *Nucleic Acids Res.* 29: e45.(2001).

Reboloso-Fuentes, M. M., Navarro-Pérez, A., García-Camacho, F., Ramos-Miras, J. J. & Guil-Guerrero, J. L. Biomass nutrient profiles of the microalga *Phaeodactylum tricornutum*. *J. Agric. Food Chem.* (2001). doi:10.1021/jf0010376

Saha, S. K., Uma, L., and Subramanian, G.. Nitrogen stress induced changes in the marine cyanobacterium *Oscillatoria willei* BDU 130511. *FEMS Microbiol. Ecol.* 45, 263–272 (2003). doi:10.1016/S0168-6496(03)00162-4

San Pedro, A., Gonzalez-Lopez, C. V., Acien, F. G. & Molina-Grima, E. Outdoor pilot-scale production of *Nannochloropsis gaditana*: Influence of culture parameters and lipid production rates in tubular photobioreactors. *Bioresour. Technol.* 169, 667–676 (2014).

Siaut, M., Heijde, M., Mangogna, M., Montsant, A., Coesel, S., Allen, A., Manfredonia, A., Falciatore, A., and Bowler, C. Molecular toolbox for studying diatom biology in *Phaeodactylum tricornutum*. *Gene* 406: 23–35(2007).

Simionato, D., Basso, S., Giacometti, G. M. & Morosinotto, T. Optimisation of light use efficiency for biofuel production in algae. *Biophys. Chem.* 182, 71–78 (2013).

Thomas, D. N. & Dieckmann, G. S. Antarctic Sea ice--a habitat for extremophiles. *Science*. 295, 641–644 (2002).

Vinayak, V. et al., Diatom milking? A review and new approaches. *Marine Drugs* 13, 2629–2665 (2015).

Wang H. A study on lipid production of the mixotrophic microalgae *Phaeodactylum tricornutum* on various carbon sources. *African Journal of Microbiology Research* 6, 1041-1047 (2012).

Wu, S. et al., Enzyme activity highlights the importance of the oxidative pentose phosphate pathway in lipid accumulation and growth of *Phaeodactylum tricornutum* under CO₂ concentration. *Biotechnol. Biofuels* 8, 78 (2015).

Xiao, Y. et al., Simultaneous accumulation of neutral lipids and biomass in *Nannochloropsis oceanica* IMET1 under high light intensity and nitrogen replete conditions. *Algal Res.* 11, 55–62 (2015).

Yongmanitchai, W. & Ward, O. P. Growth of and omega-3 fatty acid production by *Phaeodactylum tricornutum* under different culture conditions. *Appl. Environ. Microbiol.* 57, 419–425 (1991).

Zaslavskaja, L. A. et al., Trophic Conversion of an Obligate Photoautotrophic Organism Through Metabolic Engineering. *Science*. 292, 2073–2075 (2001).

Zheng, Y., Quinn, A. H. & Sriram, G. Experimental evidence and isotopomer analysis of mixotrophic glucose metabolism in the marine diatom *Phaeodactylum tricornutum*. *Microbial cell factories* 12, (2013).

Figure Legends

Fig. 3.1 Growth curves and nutrients consumption of *Phaeodactylum tricornutum*.

A. Growth curves of *Phaeodactylum tricornutum* cells in N-replete and N-deplete condition in the presence/absence of glycerol. Two different starting cell density were used in N-replete and N-deplete condition: 10^6 cells/mL and 2×10^6 cells/mL respectively. **B.** Glycerol consumption of *P. tricornutum* cells in N-replete conditions. **C.** Nitrate and **D.** phosphate consumption kinetics in *P. tricornutum* cultures in N-replete condition in the presence/absence of glycerol; Each result is the average of two biological replicates \pm SD. E10: N-replete condition; E0: N-deplete condition; GLY: glycerol.

Fig. 3.2. Photosynthetic activity in *P. tricornutum*. **A.** Photosynthetic efficiency represented as F_v/F_m ratio; **B.** Non-photochemical quenching (NPQ) and **C.** Electron transport rate (ETR) of cells cultivated for 5 and 10 days in N- replete or N- deplete conditions in both phototrophic and mixotrophic mode. Each result is the average of two biological replicates \pm SD. E10: N-replete condition; E0: N-deplete condition; GLY: glycerol.

Fig. 3.3 Lipid and acylglycerols production in *P. tricornutum*. **A.** Epifluorescence images of cells stained 5 days with Nile Red dye. **B.** Neutral lipid content normalized per millions of cells determined by Nile Red staining at day 5 and 10. **C.** Total lipids accumulation at day 5 in *P. tricornutum* expressed as percentage of dry weight. **D.** DAG and **E.** TAG accumulation at day 5 in *P. tricornutum* normalized per mg of dry cells. Each result is the average of two biological replicates \pm SD. E10: N-replete condition; E0: N-deplete condition; GLY: glycerol.

Fig. 3.4 Hypothetical cellular pathways involved in the mixotrophic growth of *P. tricornutum*. Hypothetical pathways involved in **A.** central carbon, **B.** storage carbon and **C.** lipid metabolism during the mixotrophic growth of *P. tricornutum* are shown. Italic green type represents gene transcripts found to be up-regulated in presence of glycerol in microarray analysis, gene numbers are also indicated. Bold green or red type

represents metabolites that were detected in the current study by GC-MS analysis in cells grown in mixotrophy or phototrophy respectively. Changes for pyruvate are provided by direct estimates with a “Pyruvate Assay Kit” (see methods) and TAG in lipidomics analysis. Glyc= Glycerol; Glyc3P= glycerol 3 phosphate; TPI=Triphosphateisomerase; Fbac5= fructose biphosphate aldolase; PYC1= pyruvatecarboxylase; OAA= Oxaloacetic acid; Fru= fructose; F6P=fructose-6-phosphate; G6P=glucose-6 phosphate; AG3P=Acyl Glycerol 3phosphate; DAGAT2D=Diacyl Glycerol acyltransferase 3 phosphate.

Fig. 3.5 Optimisation of growth medium in *Phaeodactylum*. **A.** Mixotrophic growth of *P. tricornutum* and **B.** glycerol consumption in the initial (black line) and in the optimised medium (red line). Each result is the average of two biological replicates \pm SD. E10=ESAW 10XN; EE= ESAW enriched.

Fig. 3.6 Impact of improved medium on biomass composition and on photosynthetic parameters. **A.** Pictures of 10 days-cultured cells in the E10 (left) and EE medium (right). **B.** Pigment and **C.** total lipids content in cells grown 10 days in E10 (black bar) and EE (red bar) cultured cell extracts. **D.** Photosynthetic efficiency represented as F_v/F_m ratio; **E.** Non-photochemical quenching (NPQ) and **F.** Electron transport rate (ETR) of cells cultivated 10 days in E10 (black bar) and EE (red bar) medium. Each result is the average of two biological replicates \pm SD. E10=ESAW 10XN; EE= ESAW enriched.

Fig. 3.7 Effect of bicarbonate on mixotrophic growth. **A.** Mixotrophic growth of *P. tricornutum* grown and **B.** glycerol consumption in ESAW enriched (black line) and in ESAW enriched + bicarbonate (red line). Each result is the average of two biological replicates \pm SD. EE= ESAW enriched; EE+BIC= ESAW enriched + bicarbonate.

Fig. 3.8 Scale-up to photobioreactors. Growth profile of *P. tricornutum* grown in 2L-fermentor in **A.** E10 **B.** EE and **C.** EE+ BIC in both phototrophic (black circles) and

mixotrophic (red squares) mode. The maximum biomass are also indicated in each condition. The optimisation of medium composition and culture conditions allows to increase the efficiency of mixotrophy from 30% up to 78 %. Each result is the average of two biological replicates \pm SD.

Fig. 3.S1 Screening of mixotrophic efficiency by biolog and redox dye assay in *Phaeodactylum tricornutum*. **A.** OD changes of *P. tricornutum* cells grown for 6 days in Biolog™ plates that contains about 200 different compounds (see methods). Blue and red dots represent compounds that show a decrease or an increase on growth comparing with the phototrophic control. Black dots represent the compounds that does not affect the growth of *Phaeodactylum*. **B.** Fluorescent based-assay to monitoring the changes in respiration using the *Redox Dye A* in presence of the selected compounds (see methods). **C.** Growth profile of *P. tricornutum* on some selected compounds and a phototrophic control in 250 mL flask; *gly*= *glycerol*, *Ser*=*serine*, *NaAc*= *Sodium Acetate*, *Fum*= *fumarate*.

Fig. 3.S2 EM pictures of *P. tricornutum* cells under starved (A) and replete (B) conditions. The degradation of the photosynthetic membranes, and the appearance of lipid bodies in -N condition is shown by a red arrow.

Fig. 3.S3 Quantitative analysis of *P. tricornutum* glycerolipids. TAG profile in a total lipid extract from cells grown in replete conditions (A) and deplete conditions (B) in both mixotrophic and phototrophic mode. Glycerolipids are expressed in nmol / mg of dry cells. Each result is the average of two biological replicates \pm SD. E10:N-replete condition; E0: N-deplete condition; GLY: glycerol.

Fig. 3.S4 Metabolomic analysis of *P. tricornutum* grown in N-replete condition. The ratio \log_2 mixo/photo > 0 represents all the metabolites that were over-expressed in

mixotrophy in replete condition, while the ratio $\log_2 \text{mixo/photo} < 0$ the metabolites down-regulate in this condition. Each result is the average of six biological replicates.

Fig. 3.S5 Quantification of intracellular pyruvate by fluorescence-based method. A. Pyruvate standard curve. **B.** Quantification of intracellular pyruvate in cells grown in phototrophy (E10) and mixotrophy (E10+GLY).

Fig. 3.S6 Respiration and photosynthesis analysis in *P. tricornutum*. Direct assessment of oxygen consumption by a polarographic approach in **A.** E10, **B.** EE, **C.** EE + BIC in both phototrophy (black bar) and mixotrophy (red bar).

Fig. 3.S7 Optimisation of growth medium in *Phaeodactylum tricornutum*. Growth profiles of cells grown in E10 (black); EE (red); E10 supplemented with 2.50 g/L of NaNO_3 and 0.20 g/L of $\text{NaH}_2\text{PO}_4 \cdot \text{H}_2\text{O}$ (green); E10 supplemented with 0.0216 g/L of Fe-EDTA (yellow) and E10 supplemented with 0.589 mg/L of $\text{ZnSO}_4 \cdot 7\text{H}_2\text{O}$, 2.55 mg/L of $\text{MnSO}_4 \cdot 4\text{H}_2\text{O}$ and 0.66 mg/L of $\text{CuSO}_4 \cdot 5\text{H}_2\text{O}$ (blue).

Fig. 3.S8 Morphotypes in *Phaeodactylum* cells. Transmission Microscope pictures of cells grown in **A.** E10 and **B.** EE. Red arrows indicate triradiate morphotype detected.

Fig. 3.S9 Membrane lipid composition in *Phaeodactylum*. Lipid analysis of cells grow in N-replete conditions and N-deplete conditions in both mixotrophic and phototrophic mode. Each result is the average of two biological replicates \pm SD. SQDG, sulfoquinovosyldiacylglycerol; DGDG, digalactosyldiacylglycerol; MGDG, monogalactosyldiacylglycerol; PC, phosphatidylcholine; E10:N-replete condition; E0: N-deplete condition; GLY: glycerol.

Supplemental data

Supplemental Figure 3.S1

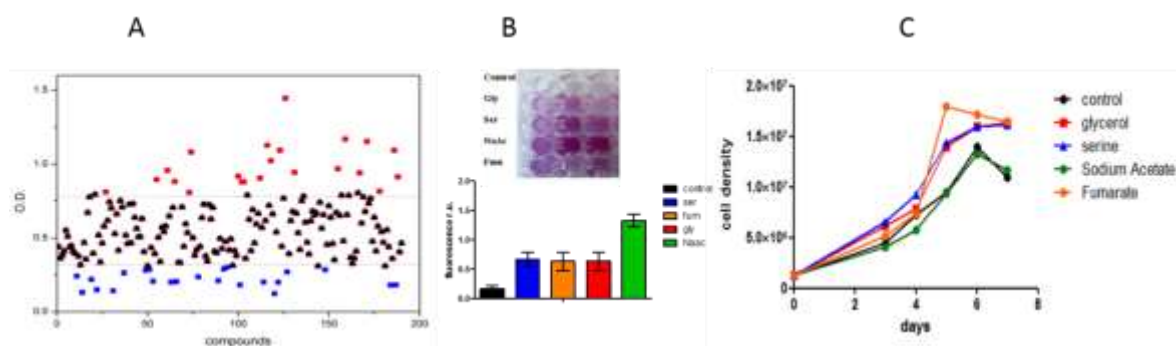


Fig. 3.S1 Screening of mixotrophic efficiency by biolug and redox dye assay in *P. tricornutum*.

A. OD changes of *P. tricornutum* cells grown for 6 days in Biolug™ plates that contains about 200 different compounds (see methods). Blue and red dots represent compounds that show a decrease or an increase on growth comparing with the phototrophic control. Black dots represent the compounds that does not affect the growth of *P. tricornutum*. **B.** Fluorescent based-assay to monitoring the changes in respiration using the *Redox Dye A* in presence of the selected compounds (see methods). **C.** Growth profile of *P. tricornutum* on some selected compounds and a phototrophic control in 250 mL flask; *gly*= glycerol, *Ser*=serine, *NaAc*= Sodium Acetate, *Fum*= fumarate.

Supplemental Figure 3.S2

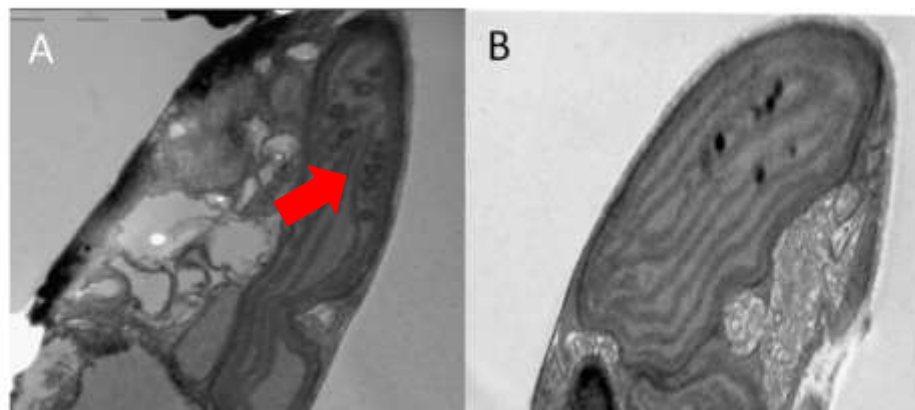


Fig. 3.S2 EM pictures of *P. tricornutum* cells under starved (A) and replete (B) conditions. The degradation of the photosynthetic membranes and the appearance of lipid bodies in -N condition is shown by a red arrow

Supplemental Figure 3.S3

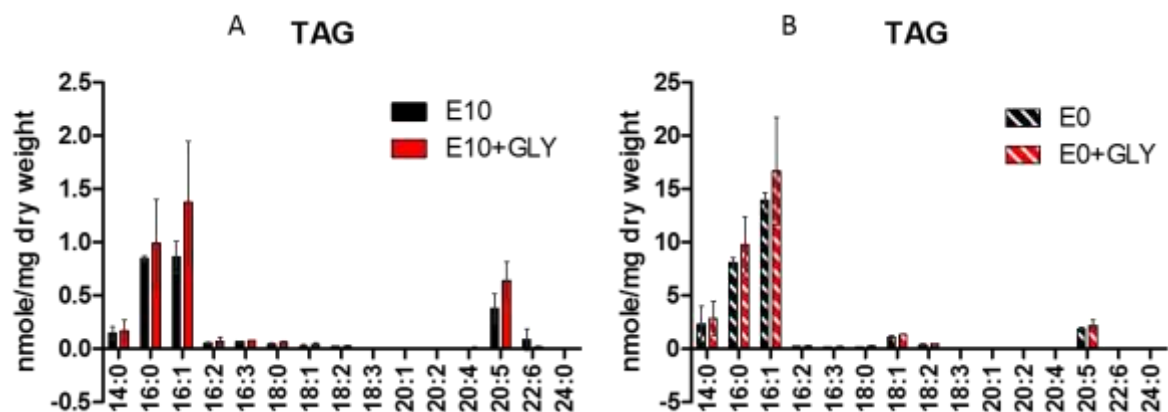


Fig. 3.S3 Quantitative analysis of *P. tricornutum* glycerolipids. TAG profile in a total lipid extract from cells grown in N replete conditions (A) and deplete conditions (B) in both mixotrophic and phototrophic mode. Glycerolipids are expressed in nmol / mg of dry cells. Each result is the average of two biological replicates \pm SD. E10:N-replete condition; E0: N-deplete condition; GLY: glycerol.

Supplemental Figure 3.S4

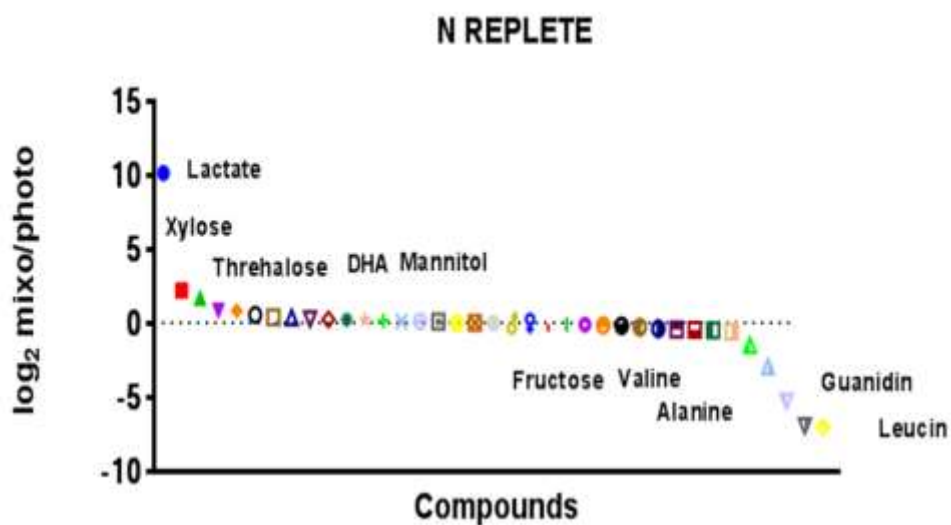


Fig. 3.S4 Metabolomic analysis of *P. tricornutum* grown in N-replete condition. The ratio $\log_2 \text{mixo/photo} > 0$ represents all the metabolites that were over-expressed in mixotrophy in replete condition, while the ratio $\log_2 \text{mixo/photo} < 0$ the metabolites down-regulate in this condition. Each result is the average of six biological replicates

Supplemental Figure 3.S5

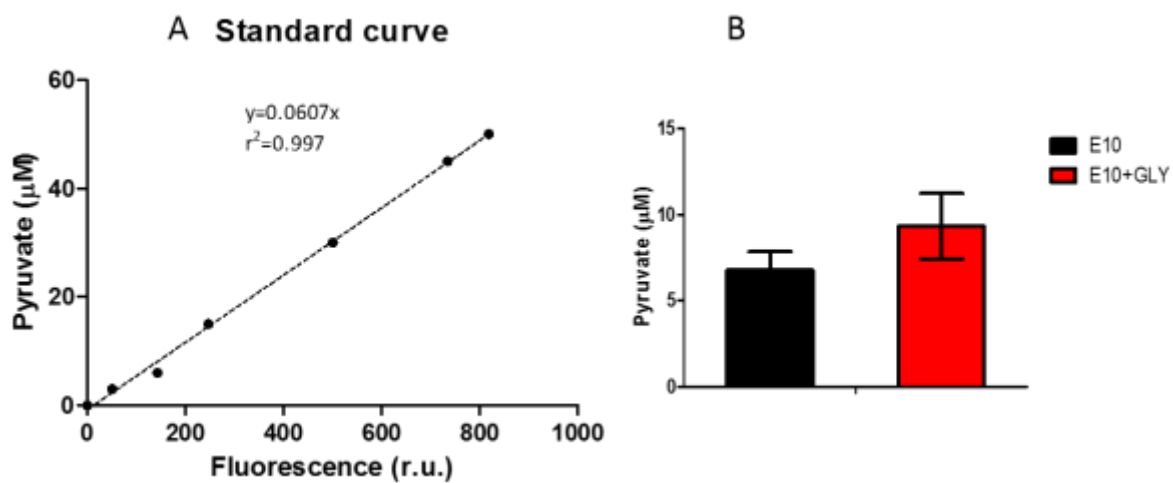


Fig. 3.S5 Quantification of intracellular pyruvate by fluorescence-based method. A. Pyruvate standard curve. **B.** Quantification of intracellular pyruvate in cells grown in phototrophy (E10) and mixotrophy (E10+GLY).

Supplemental Figure 3.S6

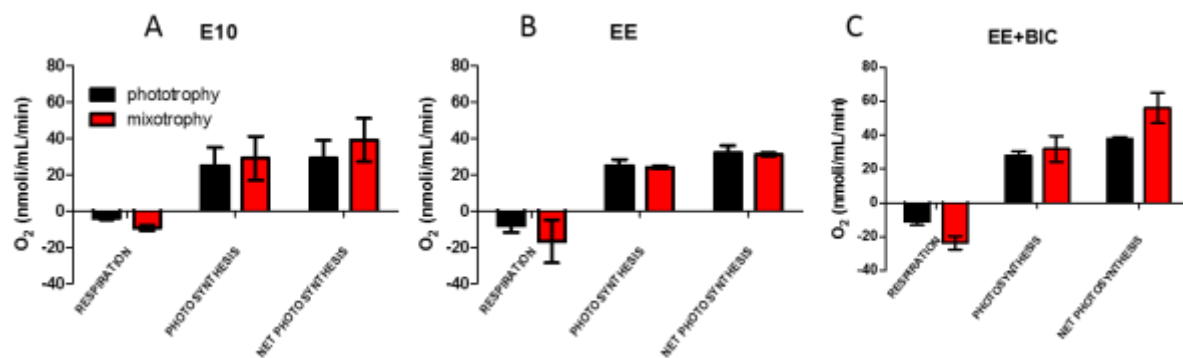


Fig. 3.S6 Respiration and photosynthesis analysis in *P. tricornutum*. Direct assessment of oxygen consumption by a polarographic approach in **A.** E10, **B.** EE, **C.** EE + BIC in both phototrophy (black bar) and mixotrophy (red bar).

Supplemental Figure 3.S7

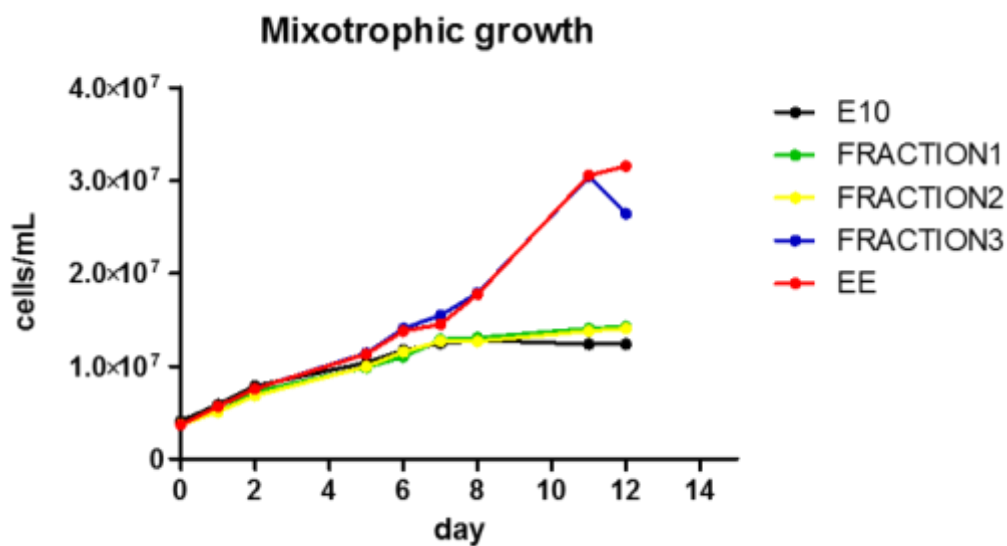


Fig. 3.S7 Optimisation of growth medium in *P. tricornutum*. Growth profiles of cells grown in E10 (black); EE (red); E10 supplemented with 2.50 g/L of NaNO_3 and 0.20 g/L of $\text{NaH}_2\text{PO}_4 \cdot \text{H}_2\text{O}$ (green); E10 supplemented with 0.0216 g/L of Fe-EDTA (yellow) and E10 supplemented with 0.589 mg/L of $\text{ZnSO}_4 \cdot 7\text{H}_2\text{O}$, 2.55 mg/L of $\text{MnSO}_4 \cdot 4\text{H}_2\text{O}$ and 0.66 mg/L of $\text{CuSO}_4 \cdot 5\text{H}_2\text{O}$ (blue).

Supplemental Figure 3.S8

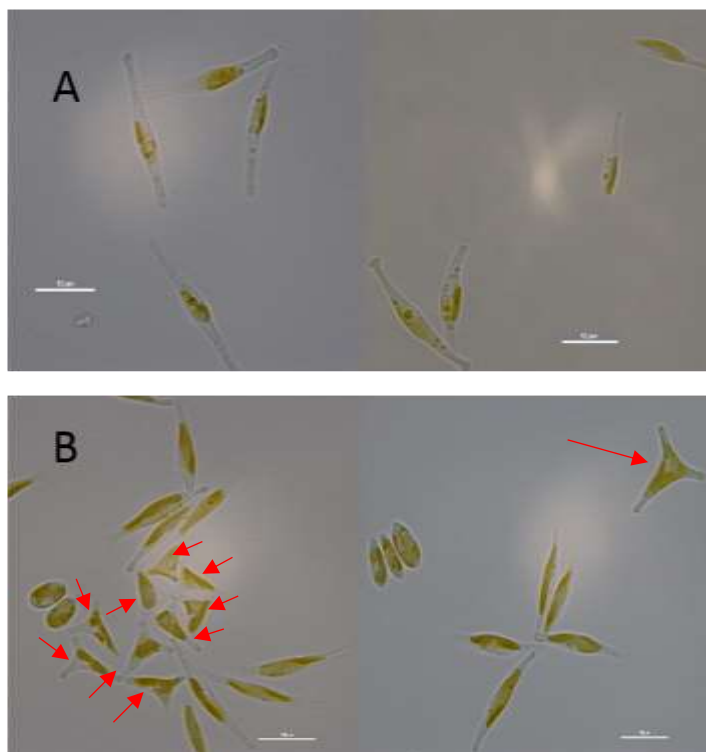


Fig. 3.S8 Morphotypes in *P. tricornutum* cells. Transmission Microscope pictures of cells grown in **A.** E10 and **B.** EE. Red arrows indicated triradiate morphotype detected.

Supplemental Figure 3.S9

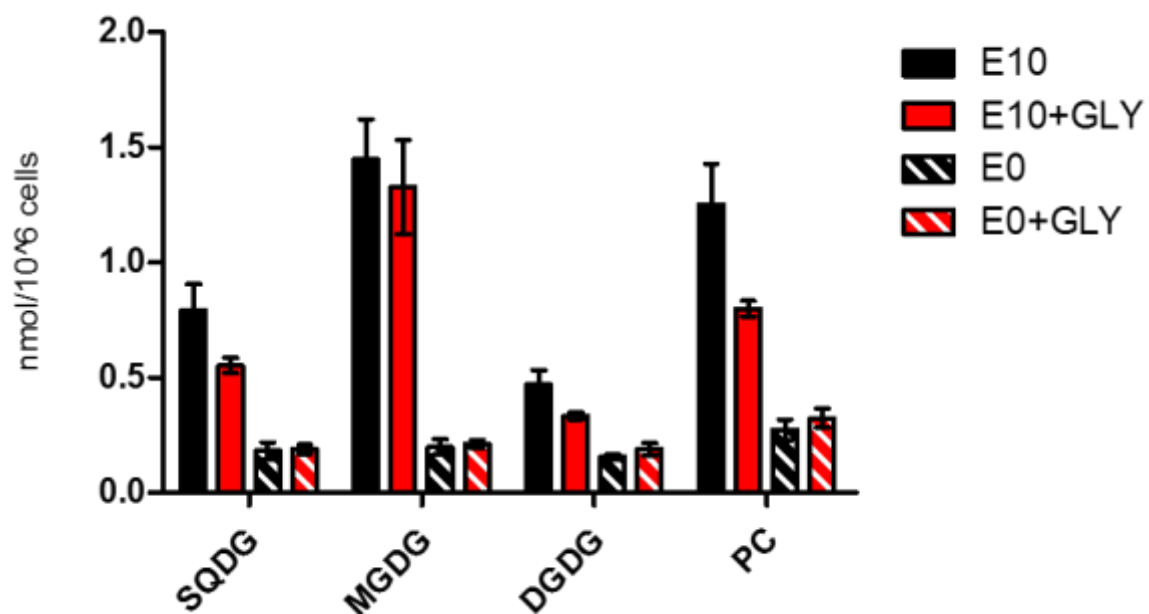


Fig. 3.S9 Membrane lipid composition in *P. tricornutum*. Lipid analysis of cells grow in N-replete conditions and N-deplete conditions in both mixotrophic and phototrophic mode. Each result is the average of two biological replicates \pm SD. SQDG, sulfoquinovosyldiacylglycerol; DGDG, digalactosyldiacylglycerol; MGDG, monogalactosyldiacylglycerol; PC, phosphatidylcholine; E10: N-replete condition; E0: N-deplete condition; GLY: glycerol.

Table I. Biomass productivity of *Phaeodactylum* grown in 2L-fermentors in different culture medium. E10=ESAW 10XN; EE= ESAW ENRICHED; EE+BIC= ESAW ENRICHED + BICARBONATE; GLY=glycerol

Productivity	E10	E10+GLY	EE	EE+GLY	EE+BIC	EE+BIC+GLY
max mg/h/L	5.3	5.6	5.5	16.4	8.5	21.5

Table II. Genes selected in microarray analysis. The table shows the genes selected in microarray analysis that significantly changed (Log_2 fold change $> \pm 0.8$ and p value < 0.01) in transcript abundance between mixotrophic and phototrophic conditions. A full description of the genes, fold-change values, standard deviation, t value and sub-cellular localitation prediction using ChloroP, targetP and ASAFind are reported. Each result is the average of three biological replicates \pm SD.

Phath_3	Phath_2	Annotation	Log ₂ fold change	Standard deviation	t value	Pathway	ChloroP/target P predictor	Reliability in chloroP/targetP	ASAFind Prediction
Phatr3_128797	Phatr2_28797	Stearylidesaturase (delta9desaturase)	2,27	0,52	8,43	EPA biosynthesis	Others	3	Not plastid, SignalP negative
Phatr3_141423	Phatr2_51289	FbaC5 (fructose bisphosphate aldolase)	1,58	0,30	9,50	Glycolysis	Chloro	2	Plastid, low confidence
Phatr3_130967	Phatr2_30967	ketol acid reducto isomerase	1,50	0,24	10,80	Super pathway leucine, valine	Chloro	4	Plastid, high confidence
Phatr3_150738	Phatr2_50738	Triosephosphate isomerase	1,46	0,22	11,31	Glycolysis	Chloro	3	Plastid, low confidence
Phatr3_130519	Phatr2_30519	PYC1_pyruvate carboxylase	1,29	0,95	5,21	TCA cycle	Mito	2	Not plastid, SignalP negative
Phatr3_131718	Phatr2_31718	Inosine-5'-monophosphate dehydrogenase	1,26	0,16	13,57	Urate biosynthesis	Others	1	Not plastid, SignalP negative
Phatr3_125417	Phatr2_25417	Gdp-mannose 4,6-dehydratase	0,92	0,08	21,15	GDP-L-fucose biosynthesis I	Others	2	Not plastid, SignalP negative
Phatr3_143469	Phatr2_43469	DGAT2D - Diacylglycerol acyltransferase	0,83	0,14	10,17	Kennedy pathway	Secretory	1	Not plastid, SignalP negative
Phatr3_12164	Phatr2_2164	D-xylose:proton symporter	-1,12	0,27	10,20	Xylose degradation	Secretory	2	Not plastid, SignalP negative
Phatr3_146275	Phatr2_46275	HYP (FA desaturase type 1 domain)	-2,29	0,25	15,60	Unknown	others	2	Not plastid, SignalP negative

STable III. Full Microarray data set of STableII. Significance analysis of microarray revealed 282 genes differentially expressed in mixotrophy, with respect to phototrophy. Fold-change values, standard deviation, statistical values and annotation (when possible) are reported.

Gene number (Phatr2)	Log2 Fold,change	Gene std,dev,	t value	p value	Annotation
49283	3,08	0,44	12,19	0,01	Predicted protein
42882	2,34	0,52	20,16	0,00	Predicted protein
28797	2,27	0,20	10,01	0,01	stearoylidesaturase (delta9desaturase)
33087	1,61	0,26	10,70	0,01	Predicted protein
46822	1,58	0,14	19,32	0,00	Predicted protein
51289	1,58	0,30	10,02	0,01	FbaC5 (fructose-bisphosphate aldolase)
30967	1,50	0,24	10,80	0,01	ketol acid reducto isomerase
50738	1,46	0,22	11,31	0,01	Triosephosphate isomerase
48920	1,67	0,01	333,00	0,00	Predicted protein
43961	1,44	0,22	11,52	0,01	Predicted protein
31718	1,26	0,16	13,57	0,01	Inosine-5'-monophosph dehydrogenase
44522	1,10	0,13	14,40	0,00	Predicted protein
43703	1,04	0,14	12,64	0,01	Predicted protein
40998	1,03	0,06	30,35	0,00	Predicted protein
31878	1,02	0,16	10,73	0,01	Predicted protein
45855	1,00	0,10	16,82	0,00	Predicted protein
25417	0,92	0,08	21,15	0,00	Gdp-mannose 4,6-dehydratase
9983	0,87	0,13	11,59	0,01	Predicted protein
45509	0,84	0,05	32,39	0,00	Predicted protein
43469	0,83	0,14	10,17	0,01	DGAT2D - Diacylglycerol acyltransferase
43024	0,77	0,04	31,90	0,00	Predicted protein
19122	0,74	0,04	31,86	0,00	Predicted protein
12679	0,73	0,10	12,87	0,01	Predicted protein
45939	0,72	0,04	29,82	0,00	Predicted protein
54330	0,70	0,08	15,19	0,00	Predicted protein
43683	0,67	0,04	32,19	0,00	Predicted protein
34564	0,66	0,08	15,14	0,00	Predicted protein
44203	0,64	0,06	17,75	0,00	Predicted protein
47170	0,63	0,07	15,62	0,00	Predicted protein
31939	0,62	0,09	12,23	0,01	Predicted protein
35810	0,61	0,03	35,22	0,00	Tim23
40534	0,59	0,10	10,71	0,01	Predicted protein
35858	0,58	0,03	31,43	0,00	Predicted protein
51345	0,56	0,01	96,99	0,00	Predicted protein

Characterisation and optimisation of mixotrophy in *Phaeodactylum tricornutum*

Gene number (Phatr2)	Log2 Fold,change	Gene std,dev,	t value	p value	Annotation
24922	0,56	0,02	63,12	0,00	Predicted protein
41745	0,54	0,05	18,00	0,00	Predicted protein
46821	0,52	0,07	13,61	0,01	Predicted protein
7430	0,51	0,01	88,33	0,00	Predicted protein
36293	0,51	0,06	14,56	0,00	Predicted protein
39471	0,51	0,05	17,10	0,00	Predicted protein
48325	0,50	0,05	16,99	0,00	Predicted protein
49907	0,49	0,07	12,55	0,01	Predicted protein
18899	0,48	0,03	32,81	0,00	Predicted protein
43072	0,48	0,03	25,68	0,00	Predicted protein
9283	0,47	0,08	10,55	0,01	Predicted protein
45607	0,47	0,07	11,63	0,01	Predicted protein
14161	0,47	0,05	15,75	0,00	Predicted protein
27240	0,46	0,07	11,38	0,01	Predicted protein
43725	0,46	0,03	30,11	0,00	Predicted protein
54376	0,44	0,06	13,50	0,01	Predicted protein
28222	0,43	0,05	16,64	0,00	Predicted protein
9883	0,40	0,06	12,68	0,01	Predicted protein
36744	0,37	0,05	14,34	0,00	Predicted protein
50462	0,37	0,06	11,74	0,01	Predicted protein
45555	0,35	0,06	9,97	0,01	Predicted protein
28568	0,34	0,01	58,89	0,00	Predicted protein
12535	0,34	0,05	11,59	0,01	Predicted protein
16283	0,34	0,05	12,34	0,01	Predicted protein
9706	0,34	0,06	10,25	0,01	Predicted protein
44851	0,33	0,04	13,11	0,01	Predicted protein
35620	0,32	0,02	24,25	0,00	Predicted protein
45618	0,31	0,05	11,72	0,01	Predicted protein
47233	0,31	0,05	10,74	0,01	Predicted protein
19692	0,30	0,05	10,00	0,01	Predicted protein
31713	0,28	0,04	13,97	0,01	Predicted protein
47023	0,28	0,04	11,13	0,01	Predicted protein
22247	0,27	0,05	10,24	0,01	Predicted protein
45758	0,24	0,03	13,11	0,01	Predicted protein
43086	0,24	0,03	14,20	0,00	Predicted protein
32841	0,23	0,04	10,00	0,01	Predicted protein
1484	0,23	0,03	13,28	0,01	Predicted protein
15233	0,23	0,03	15,06	0,00	Predicted protein
40994	0,23	0,03	11,50	0,01	Predicted protein
22955	0,22	0,02	18,58	0,00	Predicted protein

Gene number (Phatr2)	Log2 Fold,change	Gene std,dev,	t value	p value	Annotation
46132	0,22	0,04	10,57	0,01	Predicted protein
47165	0,18	0,01	55,00	0,00	Predicted protein
38587	0,18	0,03	11,78	0,01	Predicted protein
11799	0,17	0,02	19,65	0,00	Predicted protein
31841	0,17	0,02	12,50	0,01	Predicted protein
50139	0,16	0,02	17,76	0,00	Predicted protein
46307	0,14	0,01	21,50	0,00	Predicted protein
20331	0,13	0,02	11,09	0,01	Predicted protein
38662	0,13	0,01	19,00	0,00	Predicted protein
43387	0,12	0,02	13,23	0,01	Predicted protein
48362	0,11	0,02	12,85	0,01	Predicted protein
6076	0,09	0,02	10,58	0,01	Predicted protein
37368	0,06	0,01	10,39	0,01	Predicted protein
43885	0,06	0,01	17,00	0,00	Predicted protein
47059	0,04	0,00	Infinity	0,00	Predicted protein
49943	-0,05	0,00	Infinity	0,00	Predicted protein
41386	-0,11	0,02	11,00	0,01	Predicted protein
15286	-0,11	0,02	12,85	0,01	Predicted protein
40610	-0,12	0,01	35,00	0,00	Predicted protein
39244	-0,18	0,00	Infinity	0,00	Predicted protein
46813	-0,12	0,02	10,39	0,01	Predicted protein
36531	-0,15	0,02	16,63	0,00	Predicted protein
36377	-0,15	0,02	15,00	0,00	Predicted protein
9157	-0,15	0,02	12,76	0,01	Predicted protein
44738	-0,16	0,01	27,71	0,00	Predicted protein
37232	-0,16	0,02	12,25	0,01	Predicted protein
46580	-0,16	0,01	49,00	0,00	Predicted protein
49457	-0,18	0,02	14,70	0,00	Predicted protein
40760	-0,18	0,02	15,59	0,00	Predicted protein
49481	-0,20	0,01	34,64	0,00	Predicted protein
32453	-0,23	0,02	23,00	0,00	Predicted protein
7181	-0,23	0,04	11,51	0,01	Predicted protein
49576	-0,24	0,01	35,50	0,00	Predicted protein
49529	-0,24	0,01	36,50	0,00	Predicted protein
15399	-0,25	0,02	20,52	0,00	Predicted protein
45393	-0,27	0,05	10,24	0,01	Predicted protein
39214	-0,27	0,04	11,69	0,01	Predicted protein
45438	-0,27	0,04	10,73	0,01	Predicted protein

Characterisation and optimisation of mixotrophy in *Phaeodactylum tricornutum*

Gene number (Phatr2)	Log2 Fold,change	Gene std,dev,	t value	p value	Annotation
50419	-0,28	0,04	11,13	0,01	Predicted protein
50052	-0,28	0,02	32,13	0,00	Predicted protein
45427	-0,29	0,04	12,29	0,01	Predicted protein
36444	-0,30	0,04	12,71	0,01	Predicted protein
38848	-0,30	0,03	15,98	0,00	Predicted protein
54879	-0,30	0,02	25,98	0,00	Predicted protein
28331	-0,31	0,03	16,88	0,00	Predicted protein
48790	-0,33	0,03	18,52	0,00	Predicted protein
50026	-0,33	0,04	14,00	0,01	Predicted protein
28374	-0,33	0,06	10,27	0,01	Predicted protein
37840	-0,33	0,05	11,00	0,01	Predicted protein
43867	-0,33	0,05	10,80	0,01	Predicted protein
44702	-0,33	0,06	10,27	0,01	Predicted protein
45815	-0,33	0,01	100,00	0,00	Predicted protein
47352	-0,34	0,03	23,63	0,00	Predicted protein
50130	-0,35	0,02	29,40	0,00	Predicted protein
43619	-0,37	0,04	17,77	0,00	Predicted protein
32759	-0,38	0,03	24,88	0,00	Predicted protein
25334	-0,38	0,06	12,06	0,01	Predicted protein
42518	-0,39	0,02	32,17	0,00	Predicted protein
49977	-0,40	0,06	11,39	0,01	Predicted protein
147576	-0,41	0,04	18,60	0,00	Predicted protein
42457	-0,42	0,06	12,69	0,01	Predicted protein
13922	-0,42	0,05	14,55	0,00	Predicted protein
50489	-0,44	0,06	13,50	0,01	Predicted protein
49620	-0,45	0,05	16,75	0,00	Predicted protein
43543	-0,45	0,06	12,81	0,01	Predicted protein
23646	-0,47	0,05	16,28	0,00	Predicted protein
35854	-0,47	0,06	13,57	0,01	Predicted protein
47865	-0,49	0,08	10,65	0,01	Predicted protein
43027	-0,51	0,06	14,98	0,00	Predicted protein
47680	-0,51	0,04	25,32	0,00	Predicted protein
44845	-0,53	0,08	12,05	0,01	Predicted protein
11235	-0,54	0,07	14,13	0,00	Predicted protein
44766	-0,54	0,05	20,87	0,00	Predicted protein
44656	-0,55	0,05	19,19	0,00	Predicted protein
46143	-0,56	0,04	23,44	0,00	Predicted protein
45055	-0,60	0,04	29,76	0,00	Predicted protein
12121	-0,42	0,01	83,00	0,01	Predicted protein
15224	-0,61	0,07	15,25	0,00	Predicted protein

Characterisation and optimisation of mixotrophy in *Phaeodactylum tricornutum*

Gene number (Phatr2)	Log2 Fold,change	Gene std,dev,	t value	p value	Annotation
48040	-0,61	0,03	39,93	0,00	Predicted protein
50213	-0,61	0,06	18,68	0,00	Predicted protein
13253	-0,62	0,06	18,78	0,00	Predicted protein
35721	-0,64	0,06	18,24	0,00	Predicted protein
39283	-0,65	0,10	11,08	0,01	Predicted protein
49022	-0,66	0,05	21,60	0,00	Predicted protein
43441	-0,70	0,12	9,97	0,01	Predicted protein
47966	-0,72	0,11	11,04	0,01	Predicted protein
50304	-0,73	0,09	14,93	0,00	Predicted protein
32629	-0,75	0,08	17,23	0,00	Predicted protein
46117	-0,77	0,10	13,79	0,01	Predicted protein
15806	-0,78	0,09	15,20	0,00	Predicted protein
47655	-0,79	0,06	22,30	0,00	Predicted protein
31876	-0,98	0,12	14,60	0,00	Predicted protein
48291	-1,02	0,10	17,94	0,00	Predicted protein
1199	-1,04	0,15	12,32	0,01	Predicted protein
48021	-1,04	0,15	11,99	0,01	Predicted protein
2164	-1,12	0,27	10,99	0,01	D-xylose:proton symporter
42568	-1,15	0,18	11,33	0,01	Predicted protein
44192	-1,23	0,19	11,13	0,01	Predicted protein
40368	-1,30	0,12	18,57	0,00	Predicted protein
38713	-1,70	0,26	11,23	0,01	Predicted protein
46275	-2,29	0,25	15,60	0,00	HYP (FA desaturase type 1 domain)

3.5 Conclusions and remarks

In this chapter, we performed an in depth characterization of mixotrophic growth in *P. tricornutum* using the glycerol as carbon source. We found that glycerol enhanced cell growth and lipid production without altering its photosynthesis capacity. Therefore, this study supports the idea that the glycerol can be used to boost lipids and biomass, and resulting in a good alternative to nitrogen starvation stress.

Furthermore, the combination of omics analyses revealed the main pathways used by the glycerol to support growth and lipid production. In this study, the glycerol is involved in carbon central, lipid and carbon storage metabolism. The latter results to be a competitive pathway of lipids metabolism and it was already showed that blocking the production of chrysolaminarin by metabolic engineering is possible to increase the TAG accumulation (Daboussi *et al.*, 2014). In the presented study, the metabolomics analysis showed that *Phaeodactylum* can accumulate others storage carbohydrates (*i.e.* trehalose and mannitol) in mixotrophy, suggesting that the inhibition of the biosynthesis of these compounds could direct the carbon (derived from glycerol) towards lipid production. Alternately, the overexpression of genes involved in glycerol degradation pathway (*i.e.* glycerol kinase, PHATR_50770) or codifying for glycerol receptors (*i.e.* glycerol-3-phosphate carrier, PHATR DRAFT_43611 and glycerol uptake protein PHATR DRAFT_4871) could enhance the glycerol metabolism and increase the biomass productivity of *Phaeodactylum*.

The second part of the presented work focused on the optimisation of mixotrophy by improving medium composition and culture conditions. By balancing the ESAW medium (previously used) with the elementary composition of *Phaeodactylum* it was possible to pinpoint those elements that were limited in the growth medium. This analysis showed that the microelements (*i.e.* Cu, Zn, Mn) were mostly limiting the growth of the diatom. Indeed, the increasing of their concentration in the growth medium (ESAW enriched) improved the performance of the mixotrophic growth in *Phaeodactylum*. Here, Cu, Zn and Mn showed to be essential for the algal growth most likely because they are involved in key reactions of photosynthesis, respiration, and carbon fixation (see paragraph 3.2.1).

In addition, the supplementation of bicarbonate together with the glycerol in the optimised medium further enhanced the mixotrophic metabolism most likely thanks to the simultaneous optimisation of both photosynthesis and respiration processes (as confirmed by the analysis done with the oxigraph). These findings confirmed the results obtained in the article presented in the previous chapter (Bailleul *et al.*, 2015) showing that there is an energetic coupling between chloroplast and mitochondria and the communication between the two organelles is crucial for optimising carbon fixation and growth. Finally, the up-scaling on photo-bioreactors allowed a better control of the algae culture and to obtain higher biomass concentration.

In conclusion, this work highlighted the potential of mixotrophic growth for the industrial exploitation of microalgae. Indeed, the pennate *Phaeodactylum* could be used as a model for better understand the processes behind this growth mode in others more competitive microalgae. Moreover, the combination of different optimisation processes, *i.e.* metabolic engineering, process design and mathematical model, can result in cumulative effect and further increase the algal production capabilities.

Chapter 4

Effect of nitrogen and phosphorus starvation in *Phaeodactylum tricornutum*.

4.1 Preface

This chapter describes the article “Membrane Glycerolipid Remodeling Triggered by Nitrogen and Phosphorus Starvation in *Phaeodactylum tricornutum*” (Abida *et al.*, 2015). The first paragraphs (4.2-4.3) introduce nitrogen and phosphorus starvation effects in *Phaeodactylum*, lipidomic analysis and biodiversity on the ecotypes of *Phaeodactylum*.

The paragraph 4.4 contains the published article and paragraph 4.5 presents the conclusions and remarks of this work.

The aim of this work was to evaluate the effect of nitrogen and phosphate starvation on lipid content in the different ecotypes of *Phaeodactylum*. However, the effect of nutrient starvation was investigated in depth only on the Pt1 strain (the fully sequenced reference strain for *P. tricornutum*). In this strain, lipidomic analysis was performed in order to characterize and dissect the lipid metabolic routes under various levels of nitrogen or phosphorus supplies. These analyses revealed that the nitrogen deprivation has a more severe effect on cell physiology (decrease of F_v/F_m and growth arrest) and leads to a faster TAG accumulation when comparing with phosphorus deprivation. Overall, this work defined for the first time a reference for the glycerolipidome in *Phaeodactylum*.

4.2 Nitrogen and Phosphorous starvation in *Phaeodactylum*

Nitrogen (N) and phosphorus (P) are main components of biological macromolecules such as proteins, nucleic acids and lipids and are involved in several metabolic processes within cells. Therefore, they are key nutrients for microalgae growth (Wijffels and Barbosa, 2010), and their limitation may cause morphological and physiological changes of cells (Litchman *et al.*, 2009). Due to the potential applications for biofuels production the mechanism of TAG triggered by the starvation of these nutrients has been investigated in detail combining different approaches in *Phaeodactylum tricornutum* (Alonso *et al.*, 2000; Yu *et al.*, 2009; Levitan *et al.*, 2014). Under these stress conditions, the cells try to obtain the limiting element by the degradation of N-or P-containing cellular components (*i.e.* protein, nucleic acid and membrane lipid) and consequently they alter their metabolism. However, some differences are present between the mechanism of response to N and P starvation in *Phaeodactylum* as it will be described below.

N starvation causes severe alteration on the physiology of *Phaeodactylum*. Nitrogen-depleted cells tend to degrade proteins in order to mobilize the nitrogen that is needed for basal metabolism. N deprivation affects also the photosynthetic apparatus (*i.e.* decrease of LHC proteins levels) and inhibits the synthesis of pigment leading to decreased photosynthetic efficiency (Geider *et al.*, 1993; Alipanah *et al.*, 2015). In addition, under this stress condition, *Phaeodactylum* cells stop to grow and the energy derived from the carbon fixation is redirected to lipid accumulation, mainly TAG. In particular, amino acids and nucleic acids metabolism are decreased in favor of glycolysis and TCA cycle (Yang *et al.*, 2013; Ge *et al.*, 2014; Alipanah *et al.*, 2015; Levitan *et al.*, 2015). These pathways lead to the production of some intermediates (*i.e.* NADPH, malate, pyruvate etc.) that are involved into the fatty acid biosynthesis (Falkowski *et al.*, 1985). As discussed on paragraph 1.4.2, TAG can be produced by different pathways: *i)* *de novo* synthesis using the glycerol-3 phosphate as a precursor (*i.e.* Kennedy pathways) or *ii)* via degradation of membrane lipids. In the second pathway, the TAG are synthesised by phospholipid:DAG acyltransferases that transfer a fatty acyl moiety from a phospholipid to the intermediate DAG (Yoon *et al.*, 2012).

Different results showed that under N starvation *Phaeodactylum* accumulates TAG either via *de novo* biosynthesis (Simionato *et al.*, 2013) or by recycling plastid membrane lipids (Levitan *et al.*, 2015), or using both pathways (Alipanah *et al.*, 2015).

P starvation has minor effect on the physiology of *Phaeodactylum*. Under this condition, the cells continue to grow and the photosynthetic efficiency is not affected (Venezuela *et al.*, 2012). Indeed, *Phaeodactylum* cells possess an internal reserve of phosphate (*i.e.* polyphosphate storage) and do not need to degrade others cellular components for recycling the nutrient (Leitao *et al.*, 1995). However, phosphate-depleted cells re-adapt their metabolism, *i.e.* up-regulation of TCA and glycolysis and down-regulation of transcription factors (Yang *et al.*, 2014). Moreover, transmission electron microscopy images reveals that the intracellular membrane are partially degraded while the structure of chloroplast remains unaltered in P-deprived cells (Yang *et al.*, 2014). This suggests that probably the TAG are produced by recycling extraplastic membrane lipids in this condition. The complete profile of lipid composition in *Phaeodactylum* can help to confirm and implement the previous knowledge on the mechanism of lipids accumulation under nutrients starvation. In the presented study, we investigated this process via lipidomic analysis.

4.3 Lipidomic analysis

In the previous chapter were described the main principles of the “omics” analyses, specially transcriptomic and metabolomic. Here, I will present the lipidomic analysis that is a branch of metabolomics based on the analysis of the complete lipid profile in biological systems (Han and Gross 2003). The lipids can be divided in neutral lipids (*i.e.* DAG and TAG), polar lipids (*i.e.* phosphoglycerolipids and glycolipids) and apolar lipids. The class of polar lipids includes glycolipids and phosphoglycerolipids. The first are the main constituent of photosynthetic membranes and are divided in galactoglycerolipids with one or two galactose residues, *i.e.* MGDG (monogalactosyldiacylglycerol) and DGDG (digalactosyldiacylglycerol) (Allen *et al.*, 1996) and sulfur-containing lipids, *i.e.* SQDG (sulfoquinovosyldiacylglycerol) (Benson *et al.*, 1966). Although in a smaller percentage, the

photosynthetic membranes (thylakoids) also contain one phospholipid, *i.e.* phosphatidyl glycerol (PG). Finally, phosphatidyl choline (PC) and phosphatidyl ethanolamine (PE) are the two most abundant phospholipid species found in in extraplastidic membranes of eukaryotic cells (Henneberry *et al.*, 2001). Due to the large variability on their physical-chemical properties, different types of analysis are needed to characterize the various classes. The TLC (thin layer chromatography) allows to separate lipid classes based on their hydrophobicity. In general, this technique separates a mixture of compounds that are dissolved in a hydrophobic solvent (mobile phase) according to their mobility on a thin surface usually made of silica or alumina (stationary phase). Hydrophilic compounds have high affinity for the stationary phase and will not move very far and hydrophobic compounds show opposite behavior. In lipidomic analysis, one-dimensional and two-dimensional TLC systems are used to separate neutrals lipids and free fatty acids (DAG, TAG, FFA) and polar glycerolipids (*i.e.* MGDG, DGDG, SQDG, PC, PG, PE etc.) respectively. These species can then be analyzed by mass spectrometry and/ or by gas chromatography to determine and quantify the corresponding fatty acids profiles. The detailed fatty acids profile is also very important to elucidate the lipid metabolism. For instance, an increase of short chain fatty acids (*i.e.* 16:0, 16:1) is usually the signature of a neo synthesis of lipids by an organism. Indeed, these are synthesised by a serial of enzymes (fatty acid synthases) into the chloroplast up to a maximum length of 18 carbon. The short chain fatty acids are then extended up to 24 carbon between the cytoplasm and endoplasmic reticulum. Here, specific desaturases can transform the long chain fatty acids in PUFA (*i.e.* 20:5), the main component of cellular membrane (see paragraph 1.4.1 for more details). Hence, the increase of long chain fatty acids (*i.e.* 20:5) corresponds to lipids obtained from recycling of membrane lipids (*i.e.* MGDG, DGDG, SQDG etc.).

Lipidomics analysis has been used in different microalgae such as *Nannochloropsis*, *Chlamydomonas*, *Nitzschia* (Simionato *et al.*, 2013; Yang *et al.*, 2015; Su *et al.*, 2013; Li *et al.*, 2015). In the following manuscript, we provided a reference for the glycerolipidome of *Phaeodactylum*.

4.4 Biodiversity on the ecotypes of *Phaeodactylum*

Different ecotypes of *Phaeodactylum tricornutum* (Pt1-Pt10) have been identified and characterized morphologically and genetically (De Martino *et al.*, 2007). Based on the genetic variability of the molecular marker ITS2 they were divided on 4 genetic classes (*i.e.* A-D). They are originated from different geographic area and show different shapes and physiological characteristics. *P. tricornutum* is a pleiomorphic alga that displays three major morphotypes depending on environmental conditions, *i.e.* fusiform, oval, and triradiate. The first two represent the “normal” and the “stress” morphotype in laboratory cultures, as deduced by studies on the responses to temperature or salinity stress (De Martino *et al.*, 2007). Conversely, the latter form is very rarely observed in laboratory cultures, but it has been found in different field samples (Bohlin 1897, Wilson 1946, Johansen 1991). Most of the ecotypes studied in laboratory so far are predominantly fusiform, while two of them are oval (Pt3 and Pt9) and one triradiate (Pt8). They also show differential cells size. Most of the ecotypes range from 19 to 24 μm , however the ecotype Pt 5 show bigger cells (25-30 μm) and the ecotypes Pt6 and Pt7 smaller (15-19 μm). So far, no significant correlation has been observed between geographic origin, morphology and genotype (De Martino *et al.*, 2007).

So far one ecotype (Pt1) was fully sequenced (*i.e.* Pt1.86) (Bowler *et al.*, 2008) and only two ecotypes (*i.e.* Pt1 and Pt4) were genetically transformed (Falciatore *et al.*, 1999; Siaux *et al.*, 2007; Apt *et al.*, 1996; Zaslavskaja *et al.*, 2000; Kilian and Kroth 2005). The latter (*i.e.* Pt4) has been clustered alone in genotype B (De Martino *et al.*, 2007), and is a natural mutant of LHCX1 and shows reduced NPQ capacity (Bailleul *et al.*, 2010). This genetic variation is probably due to the adaptation of the strain to the environment. More detailed characterization of these ecotypes could help to understand some important mechanisms of *Phaeodactylum* taking advantage of its natural biodiversity.

In this study the accumulation of TAG has been investigated in the different ecotypes of *Phaeodactylum*.

4.5 Membrane Glycerolipid Remodeling Triggered by Nitrogen and Phosphorus Starvation in *Phaeodactylum tricornutum*¹

Heni Abida², Lina-Juana Dolch ², Coline Meï², Valeria Villanova, Melissa Conte, Maryse A. Block, Giovanni Finazzi, Olivier Bastien, Leïla Tirichine, Chris Bowler, Fabrice Rébeillé, Dimitris Petroutsos *, Juliette Jouhet*, and Eric Maréchal*

Environmental and Evolutionary Genomics Section, Institut de Biologie de l'École Normale Supérieure, Centre National de la Recherche Scientifique Unité Mixte de Recherche 8197, Institut National de la Santé et de la Recherche Médicale, U1024, 75005 Paris, France (H.A., L.T., C.B.);

Laboratoire de Physiologie Cellulaire et Végétale, Unité Mixte de Recherche 5168 Centre National de la Recherche Scientifique-Commissariat à l'Énergie Atomique-Université Grenoble Alpes, Institut de Recherche en Sciences et Technologies pour le Vivant, Commissariat à l'Énergie Atomique Grenoble, 38054 Grenoble cedex 9, France (L.-J.D., C.M., M.C., M.A.B., G.F., O.B., F.R., D.P., J.J., E.M.);

Fermentalg SA, F-33500 Libourne, France (V.V.).

This work was supported by the Agence Nationale de la Recherche (grant no. ANR-12-BIME-0005 [DiaDomOil] to C.B., G.F., D.P., and E.M.), the Commissariat à l'Énergie Atomique Life Science Division (bioenergy grant EliciTAG to M.C. and E.M.), a European Research Council Advanced Grant (Diatomite; to C.B.), the Centre National de la Recherche Scientifique (Défi Transition Énergétique grant to L.T. and G.F.), the OCEANOMICS program from the French Ministry of Research (to E.M.), and the Institut Carnot Lipides pour la Santé et l'Industrie (to E.M.).

¹These authors contributed equally to the article.

²Address correspondence to dimitris.petroutsos@cea.fr, juliette.jouhet@cea.fr, and eric.marechal@cea.fr.

ABSTRACT

Diatoms constitute a major phylum of phytoplankton biodiversity in ocean water and freshwater ecosystems. They are known to respond to some chemical variations of the environment by the accumulation of triacylglycerol, but the relative changes occurring in membrane glycerolipids have not yet been studied. Our goal was first to define a reference for the glycerolipidome of the marine model diatom *Phaeodactylum tricornutum*, a necessary prerequisite to characterize and dissect the lipid metabolic routes that are orchestrated and regulated to build up each subcellular membrane compartment. By combining multiple analytical techniques, we determined the glycerolipid profile of *P. tricornutum* grown with various levels of nitrogen or phosphorus supplies. In different *P. tricornutum* accessions collected worldwide, a deprivation of either nutrient triggered an accumulation of triacylglycerol, but with different time scales and magnitudes. We investigated in depth the effect of nutrient starvation on the Pt1 strain (Culture Collection of Algae and Protozoa no. 1055/3). Nitrogen deprivation was the more severe stress, triggering thylakoid senescence and growth arrest. By contrast, phosphorus deprivation induced a stepwise adaptive response. The time scale of the glycerolipidome changes and the comparison with large-scale transcriptome studies were consistent with an exhaustion of unknown primary phosphorus-storage molecules (possibly polyphosphate) and a transcriptional control of some genes coding for specific lipid synthesis enzymes. We propose that phospholipids are secondary phosphorus-storage molecules broken down upon phosphorus deprivation, while nonphosphorus lipids are synthesised consistently with a phosphatidylglycerol-to-sulfolipid and a phosphatidylcholine-to-betaine lipid replacement followed by a late accumulation of triacylglycerol.

Diatoms are a major component of phytoplankton communities, believed to be responsible for up to one-fourth of global primary productivity (Scala and Bowler, 2001). They live in an environment where light, temperature, pH, oxygen, carbon dioxide, nutrients, and all kinds of physicochemical parameters can vary dramatically. Nitrogen (N), phosphorus (P), and iron are the most often limiting or colimiting nutrients (Mills *et al.*, 2004; Moore *et al.*, 2013), and N is more often limiting than P in marine systems, with the reverse in freshwaters (Hecky and Kilham, 1988). As a selection pressure, the relative fluctuations of N and P have been proposed to be responsible for the differences of size distributions of diatoms, freshwater species being smaller than marine ones due to the ambient scarcity of P (Litchman *et al.*, 2009). Nutrient scarcity is a criterion to define oligotrophic areas in oceans. A study by Van Mooy *et al.*, (2009) on phytoplanktonic communities in an oligotrophic marine region, where P is scarce (less than 10 nM), observed that diatoms reduced their P requirements by synthesizing less phosphoglycerolipids, in particular phosphatidyl-choline (PC) and phosphatidylglycerol (PG), and more nonphosphorus lipids, such as sulfoquinovosyldiacylglycerol (SQDG) and betaine lipids (BL), as compared with communities growing in a P-rich region (more than 100 nM). However, that study did not consider the levels of two other nonphosphorus lipid classes (*i.e.* the chloroplast galactoglycerolipids, in particular monogalactosyldiacyl-glycerol [MGDG]) and digalactosyldiacylglycerol (DGDG), and triacylglycerol (TAG). When Van Mooy *et al.*, (2009) examined planktonic membrane lipids at the two locations, their observations were consistent with a PG-to-SQDG and a PC-to-BL replacement triggered by P shortage. In a complementary set of experiments, they cultivated the di-atom *Thalassiosira pseudonana* in a P-depleted or P-replete artificial medium and found variations of the SQDG-PG and BL-PC ratios in line with their on-site observations (Van Mooy *et al.*, 2009), supporting that lipid remodeling could be one of the most essential mechanisms allowing a given species to acclimate and populate oligotrophic areas.

Phospholipid-to-nonphosphorus lipid replacement has been studied in depth in the plant *Arabidopsis* (*Arabidopsis thaliana*; Benning and Ohta, 2005; Shimojima and Ohta,

2011; Boudière *et al.*, 2012; Dubots *et al.*, 2012; Nakamura, 2013; Petroutsos *et al.*, 2014). In *Arabidopsis*, PC and PG contents decrease upon P starvation, and the synthesis of plastid glycolipids (*i.e.* MGDG, DGDG, and SQDG) increases coincidentally. Based on the acyl profiles of glycerolipids, it is possible to identify the metabolic routes that are mobilized in this remodeling. In *Arabidopsis*, MGDG can be synthesised using diacylglycerol (DAG) generated locally inside the plastid, via the so-called prokaryotic pathway, or using diacyl precursors diverted from nonplastid phospholipids, via the so-called eukaryotic pathway (Browse *et al.*, 1986). The prokaryotic structure is characterized by a 16-carbon (C16) fatty acid (FA) at position sn-2 of the glycerol backbone, like cyanobacterial lipids, whereas the eukaryotic structure contains an 18-carbon (C18) FA at position sn-2. Thus, in *Arabidopsis*, (1) 18:3/16:3-MGDG originates from the stepwise galactosylation of prokaryotic 18:1/16:0-DAG followed by a rapid desaturation into the trienoic form; and (2) 18:3/18:3-MGDG relies on the import and galactosylation of eukaryotic precursors derived from phospholipids, most notably having 18:2/18:2 structures (Maréchal *et al.*, 1994), also followed by a desaturation into the trienoic form. Upon P shortage, the eukaryotic pathway is activated; PC hydrolysis releases a diacyl intermediate, which is then transferred to the plastid to synthesize MGDG and DGDG (Jouhet *et al.*, 2003), creating a virtuous recycling of lipid intermediates between phospholipid breakdown and galactolipid increase. The *Arabidopsis* response to low P combines a rapid metabolic regulation, coupling MGDG synthesis to the phospholipid status (Dubots *et al.*, 2010, 2012), with a longer term genomic reprogramming (Misson *et al.*, 2005; Morcuende *et al.*, 2007) characterized by the up-regulation of phospholipases C and D (hydrolyzing phospholipids) and of monogalactosyldiacyl and digalactosyldiacyl isoforms (the galactosyltransferases synthesizing MGDG and DGDG, respectively). In P-starved conditions, a PG-to-SQDG re-placement is observed and is considered to be a ubiquitous phenomenon in photosynthetic organisms, enabling the preservation of an anionic lipid environment to the photosystems in the thylakoids (Boudière *et al.*, 2014). No intense trafficking is required for this replacement, as SQDG and PG are both chloroplast lipids. The most spectacular feature of *Arabidopsis* lipid remodeling consists in the replacement of PC in a variety of subcellular locations, such as the plasma

membrane, the tonoplast, and the mitochondria (but not observed in the endoplasmic reticulum [ER]), by DGDG synthesised in the chloroplast, using still uncharacterized lipid export systems (Andersson *et al.*, 2003, 2005; Jouhet *et al.*, 2003, 2004, 2007, 2010; Sandelius *et al.*, 2007; Tjellström *et al.*, 2008).

Lipid modifications triggered in *Arabidopsis* by a deprivation of N have not been studied as extensively. Upon N shortage, the quantity of N-containing lipids, in particular PC and phosphatidylethanolamine (PE), seems to be unaffected (Gaude *et al.*, 2007). On the other hand, the main response includes a relative decrease of MGDG and an increase of DGDG, concomitant with an up-regulation of the genes encoding both digalactosyldiacyl isoforms, and a small increase of TAG synthesis (Gaude *et al.*, 2007). It is not known whether any lipid trafficking can be triggered by N shortage, nor whether there are any changes in the lipid composition of cell compartments, like those documented in cells exposed to P shortage.

No such comprehensive study has been made in a diatom model. Acyl profiles of all glycerolipid classes and quantifications still have to be determined. The existence of redundant metabolic routes, similar to the prokaryotic and eukaryotic pathways dissected in *Arabidopsis*, also requires assessment. The conservation of some processes occurring in plants, such as a decrease of MGDG and an increase of DGDG in N-depleted conditions or an increase of MGDG and DGDG and a putative PC-to-DGDG replacement in P-depleted conditions, also should be investigated.

Studies in diatoms have benefited from developments in two model species, the centric diatom *T. pseudonana* (*Coscinodiscophyceae*) and the pennate diatom *Phaeodactylum tricornutum* (*Bacillariophyceae*), for which intense efforts have resulted in fully sequenced genomes (Armbrust *et al.*, 2004; Bowler *et al.*, 2008) and provided reference data for transcriptomic (Maheswari *et al.*, 2005, 2009; Allen *et al.*, 2008; Sapriel *et al.*, 2009; Shrestha *et al.*, 2012; Chauton *et al.*, 2013) and whole-cell proteomic (Montsant

et al., 2005; Nunn *et al.*, 2009) analyses. *P. tricornutum* is pleiomorphic, with three major morphotypes (fusiform, triradiate, and oval). A series of axenic strains have been collected in various marine environments worldwide, denoted Pt1 to Pt10 (De Martino *et al.*, 2007), allowing analyses of phenotypic variations and the adaptation to various habitats.

In photosynthetic organisms, it is usually considered that, in standard conditions, phospholipids are mostly present in the endomembrane system, whereas non-phosphorus glycolipids are in the plastid. However, this distinction might be more complex in diatoms due to the physical connection between some membranes limiting the plastid with the endomembrane system and/or mitochondria. Briefly, like all eukaryotes, diatoms contain a conventional endomembrane system comprising the ER, nuclear envelope, Golgi, trans-Golgi network, plasma membrane, etc., which are connected to each other by vesicular shuttles or tubular structures (Brighthouse *et al.*, 2010). In addition, two semiautonomous organelles of endosymbiotic origins are present, a mitochondrion limited by two membranes and a plastid bounded by four membranes, which originate from a secondary endosymbiosis (Dorrell and Smith, 2011; Petroutsos *et al.*, 2014). A continuum occurs between the ER and the outermost membrane of the plastid (Kroth *et al.*, 2008). The glycerolipid composition of each of the four membranes that surround the plastid is simply unknown. Therefore, it is difficult to speculate on the location of MGDG and DGDG synthesis and whether any export of DGDG to other locations of the cell could be plausible, like that observed in plants. Given the current state of membrane fractionation techniques, only global analyses can be performed. By contrast with other omics data, and although previous targeted studies have allowed the structural determination of some isolated glycerolipid classes (Arao *et al.*, 1987; Yongmanitchai and Ward, 1993; Naumann *et al.*, 2011), the complete membrane glycerolipidome of *P. tricornutum* has not been fully characterized. The analyses of membrane glycerolipid remodeling in diatoms should also consider the accumulation of TAG triggered by nutrient shortage, which has been scrutinized in much more detail due to the potential applications for biofuels and green

chemistry (Alonso *et al.*, 2000; Rezanka *et al.*, 2011; Zendejas *et al.*, 2012; Levitan *et al.*, 2014).

In this article, by combining multiple analytical techniques, we sought to characterize comprehensively the major membrane glycerolipid classes in *P. tricornutum*, together with TAG. FA profiles of each class have been determined, providing acyl signatures that can be used as markers for diacyl moiety origins and fluxes. With a fully characterized glycerolipidome in hand, we then analyzed changes triggered by N and/or P depletion and deduced from lipid class and acyl signature variations the dynamic processes driving the observed lipid remodeling.

RESULTS

Comparison of *P. tricornutum* Ecotypes in Nutrient-Replete and Nutrient-Limiting Batch Cultivation

We examined the responses of all available *P. tricornutum* accessions, collected originally in various geographical regions and covering all known morphotypes (*i.e.* the fusiform shape commonly observed in laboratory conditions, the triradiate shape thought to be more abundant in nature, and the oval shape, indicative of a temperature or salinity stress; De Martino *et al.*, 2007; Fig. 4.1A). In our growth conditions, most accessions were fusiform except Pt8, which is mainly triradiate, and Pt3 and Pt9, which are oval. Cells grown in nutrient-replete conditions (0.55 mM N and 0.0224 mM P, called here 1N1P) were shifted to 2N (0N1P) or 2P (1N0P) medium.

Nonpolar lipid accumulation (mainly TAG), known to be triggered by nutrient shortage in phytoplankton, was monitored using Nile Red fluorescence staining. N depletion triggered a faster TAG accumulation as compared with P depletion; therefore, the comparison of the response of the different ecotypes to 2N or 2P was made 3 d after N

depletion (Fig. 4.1B) and 8 d after P depletion (Fig. 4.1C). All accessions showed a marked accumulation of TAG shortly after N depletion, except Pt4, which exhibited a relatively modest increase (a representative experiment is shown in Figure 4.1B). The detection of nonpolar lipid accumulation in response to low P required a much longer cultivation time in P-depleted medium, and no significant TAG accumulation could be detected after 3 to 5 d. After 8 d of growth in a P-limited medium, a contrasting phenotype in the series of Pt accessions could be observed (a representative experiment is shown in Figure 4.1C), with a substantial accumulation of nonpolar lipid in all accessions except Pt4, Pt10, and PtHK, in which the Nile Red staining was lower than a 2-fold increase, as compared with cells grown in a replete medium.

We did not observe any correlation between the magnitude of response to N or P depletion and the corresponding morphotypes. Phenotypic variations might be related, rather, to the efficiency of N or P storage systems in the different accessions and/or to the signaling and metabolic processes activated by the lack of nutrients. In all cases, an increase of Nile Red fluorescence, even moderate, was always detected, thus demonstrating that TAG accumulation is a marker of nutrient shortage. We decided to pursue our experiments on Pt1, the most commonly used strain in laboratories, which responded significantly to both N and P deprivations.

Effect of nitrogen and phosphorus starvation in *Phaeodactylum tricornutum*.

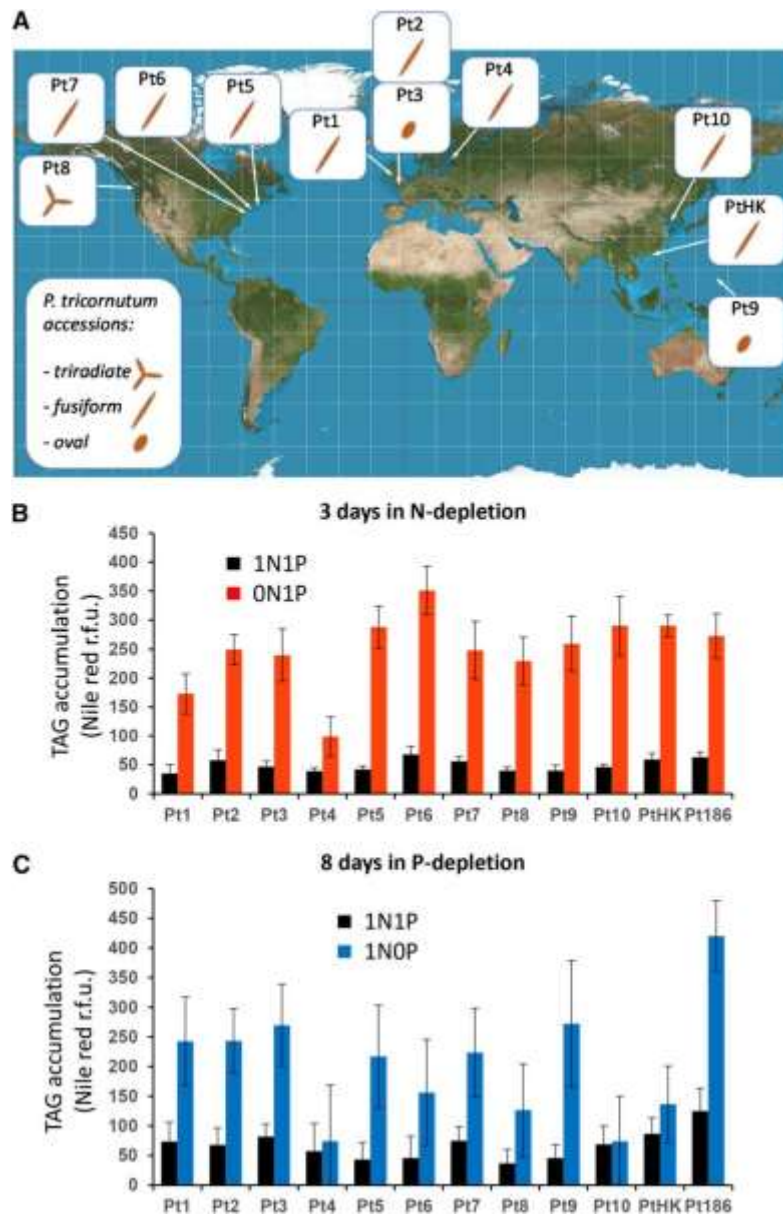


Fig. 4.1. Preliminary comparison of accessions of *P. tricornutum* grown in artificial medium depleted in N or P. **A** Massachusetts, Geographical origin and major morphotypes of Pt accessions. The origin areas of sampling of Pt accessions are shown: Pt1 off Blackpool, United Kingdom; Pt2 and Pt3 off Plymouth, United Kingdom; Pt4 near the island of Segelska; Pt5 in the Gulf of Maine; Pt6 off WoodsHole, Massachusetts; Pt7 off Long Island, New York; Pt8 near Vancouver, Canada; Pt9, Territory of Guam, Micronesia; PtHK, near Hong Kong; and Pt10, in the Yellow Sea. The genomic strain Pt1 8.6 derives from the Pt1 accession. Pt3 is a stress form deriving from Pt2. Major morphotypes observed for each accession in artificial seawater are indicated (i.e. the triradiate, fusiform, and oval morphotypes; from De Martino *et al.*, [2007]). **B**, Accumulation of nonpolar lipids in N-limiting conditions. Cells in the exponential phase of growth were harvested by centrifugation and transferred to a fresh replete (1N1P; black bars) or N-depleted (ON1P; red bars) ESAW medium. Nonpolar lipid accumulation was measured after 3 d by Nile Red staining and expressed as fluorescence intensity normalized by cell number. **C**, Accumulation of nonpolar lipids in P-limiting conditions. Cells in the exponential phase of growth were harvested by centrifugation and transferred to a fresh replete (1N1P; black bars) or P-depleted (1NOP; blue bars) ESAW medium. Nonpolar lipid accumulation was measured after 8 d by Nile Red staining and expressed as fluorescence intensity normalized by cell number. r.f.u., Relative fluorescence units.

Effects of N and P Depletion on the Growth and Photosynthesis of *P. tricornutum*

Since P depletion exerted an effect after a longer time period than N depletion, we had to be sure, when studying the effect of P shortage, that no exhaustion of N occurred during the time of observation and that control conditions were indeed kept replete. To avoid such issues, we adjusted the initial nutrient-replete conditions to concentrations 10 times higher than that applied in our comparative study of ecotypes (*i.e.* 5.5 mM N and 0.22 mM P [a medium called 10N10P]). We checked that the 10N10P medium supported the growth of *P. tricornutum* Pt1 at higher cell densities compared with the 1N1P medium (Supplemental Fig. 4.S1A). Most importantly, the photosynthetic capacity of cells, probed as photosynthetic capacity (F_v/F_m), remained unaltered for 10 d in the 10N10P medium, in stark contrast with cells grown in 1N1P medium, where F_v/F_m dropped quickly during the growth period (Supplemental Fig. 4.S1B). After 5 d of cultivation in 1N1P medium, a decrease of F_v/F_m and an increase of nonpolar lipid content were measured (Supplemental Fig. 4.S1C), reflecting a nutrient limitation in the 1N1P medium that did not occur in the 10N10P condition.

We then evaluated the time scale of the Pt1 response after transfer to nutrient-limiting conditions. For this, the diatoms were grown in 10N10P medium until they reached a cell density of 6 to 7 million cells mL⁻¹. Cells were centrifuged, washed with 0N0P medium, and resuspended in 10N10P, 0N10P, and 10N0P media at a starting cell density of 3 to 3.5 million cells mL⁻¹. N depletion resulted in growth arrest after 1 d (Supplemental Fig. 4.S2A) and led to an accumulation of nonpolar lipids after 4 d (based on Nile Red fluorescence; Supplemental Fig. 4.S2B). P depletion affected neither growth nor lipid accumulation between days 0 and 4 (Supplemental Fig. 4.S2, A and B), consistent with the delay observed for the different accessions grown in 0N1P or 1N0P medium, before any visible effect could be measured (Fig. 4.1, B and C).

We then cultivated Pt1 cells in sufficient amounts to analyze in parallel their cell phenotypes, photosynthetic properties, and lipidomic profiles. Based on previous experiments (Supplemental Fig. 4.S2B), F_v/F_m was selected as an indicator of nutrient limitation (Fig. 4.2A). At day 5, cells grown in 10N10P and 0N10P were harvested, whereas cells grown in 10N0P were kept in the culture medium until day 13. We should note that at days 5, 8, and 10, 30% of the 10N0P culture volume was replaced by fresh 10N0P medium to ensure that no other nutrient limitation besides P would occur. In parallel, a 10N10P culture was similarly complemented with fresh 10N10P medium and kept as a control condition during the same period. After 13 d of P limitation, the cells were clearly impacted in their photosynthetic activity (Fig. 4.2A) and showed a high nonpolar lipid content (Fig. 4.2B). At the same time point, the control cultures also showed a slightly diminished F_v/F_m , which was not attributed to N or P deprivation, since we did not observe any TAG accumulation (Fig. 4.2B). Since we did not detect any significant change in the TAG content and membrane glycerolipid profile of cells grown in 10N10P medium collected after 5 or 13 d of culture, we used cells collected after 5 d in 10N10P as a control to compare nutrient-starved and nutrient-replete cells.

Comprehensive Characterization of the Glycerolipid Content of *P. tricornutum*

Pt1 Grown in Nutrient-Replete Medium

We extracted the lipids from *P. tricornutum* cells with great caution to avoid lipid degradation. For this purpose, samples were freeze dried rapidly after harvest and lipids were extracted following a treatment in boiling ethanol to inactivate lipase activities. An aliquot fraction of the total extract of glycerolipids was transesterified in the presence of methanol, thus producing fatty acid methyl esters (FAMES) that were separated by gas chromatography and quantified by flame ionization detection (GC -FID), as described in “Materials and Methods.” We used thin-layer chromatography (TLC)

Effect of nitrogen and phosphorus starvation in *Phaeodactylum tricornutum*.

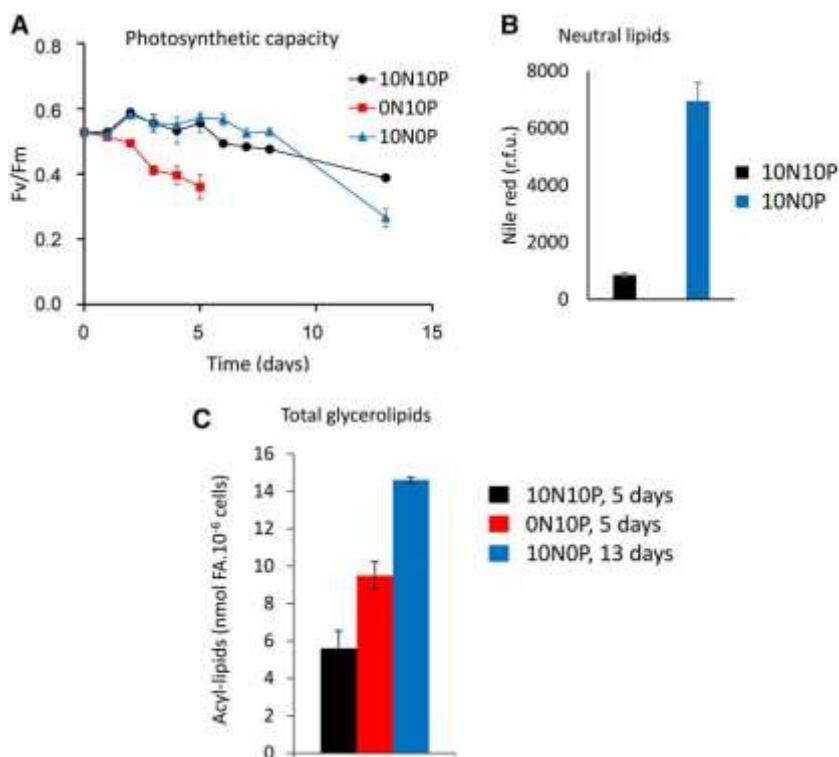


Fig. 4.2 Photosynthetic activity and lipid accumulation in the Pt1 ecotype of *P. tricornutum* cultivated in replete or N- or P-depleted conditions. **A**, Time-course evolution of photosynthetic efficiency. The F_v/F_m ratio, representative of the photosynthetic efficiency of the diatom, was measured for Pt1 cells grown either in a replete medium (10N10P; black) or in medium deprived of N (0N10P; blue) or P (10N0P; red). **B**, Non-polar lipid accumulation measured at day 13. Nonpolar lipid accumulation was estimated by Nile Red fluorescence normalized to cell number. In 10N10P, the fluorescence signal remained at background level, indicating that the F_v/F_m decrease was not due to N or P starvation. r.f.u., Relative fluorescence units. **C**, Total glycerolipid accumulation. The total level of glycerolipids (membrane lipids + TAG) was estimated by the total FA content after 5 d of cultivation in the replete condition (black bar) or following N starvation (red bar) or 13 d of P starvation (blue bar). To avoid any N deficiency in 10N10P or 10N0P culture, the media were replaced by fresh ESAW 10N10P medium every 3 d

to separate the different classes of glycerolipids, combining robust one-dimensional and two dimensional TLC systems to separate, on the one hand, nonpolar glycerolipids and free FA, and on the other hand, polar glycerolipids (phosphoglycerolipids and nonphosphorus glycerolipids; Fig. 4.3; Supplemental Fig. 4.S3). We analyzed the structure of lipids in each spot revealed on the TLC plate (see “Materials and Methods”) by mass spectrometry (MS; Tables I–III) and determined the corresponding FAME profiles by GC-FID.

The total glycerolipid extract from *P. tricornutum* grown in a 10N10P medium had a FA composition similar to those already reported in the literature for diatoms (Guschina and Harwood, 2006; Liang *et al.*, 2014) and eustigmatophytes such as *Nannochloropsis graditana* (Simionato *et al.*, 2013): that is, strikingly enriched in C16 molecular species (16:0, 16:1, 16:2, and 16:3) and eicosapentaenoic acid (20:5) and poor in C18 FAs (Fig. 4.4A).

We analyzed the different classes of glycerolipids in the extract (Fig. 4.4B), providing, to our knowledge, the first reference for a complete glycerolipidome of *P. tricornutum* in unstressed conditions. The profile is dominated by MGDG, SQDG, and PC, which together represent more than 75% of the total content. We also confirmed the presence of 20:5 acyl-SQDG, as reported previously (Naumann *et al.*, 2011; Supplemental Fig. 4.S4). We identified a spot corresponding to diacylglyceryl-hydroxy-methyl-N,N,N-trimethyl-b-alanine (DGTA; Figs. 4.3 and 4.4B; Supplemental Fig. 4.S3), a betaine glycerolipid that had not yet been reported for *P. tricornutum* but has been reported for other algae such as *Phaeocystis sp.* (*Haptophyceae*), *Ochromonas danica* (*Chrysophyceae*), and some brown algae such as *Fucus vesiculosus* (*Phaeophyceae*; Dembitsky, 1996). DGTA has the same mass as diacylglyceryl-N,N,N-trimethylhomoserine (DGTS) but could be discriminated by a different migration position on two-dimensional TLC (Vogel and Eichenberger, 1992) and, following tandem mass spectrometry (MS²) fragmentation, by the absence of a fragment

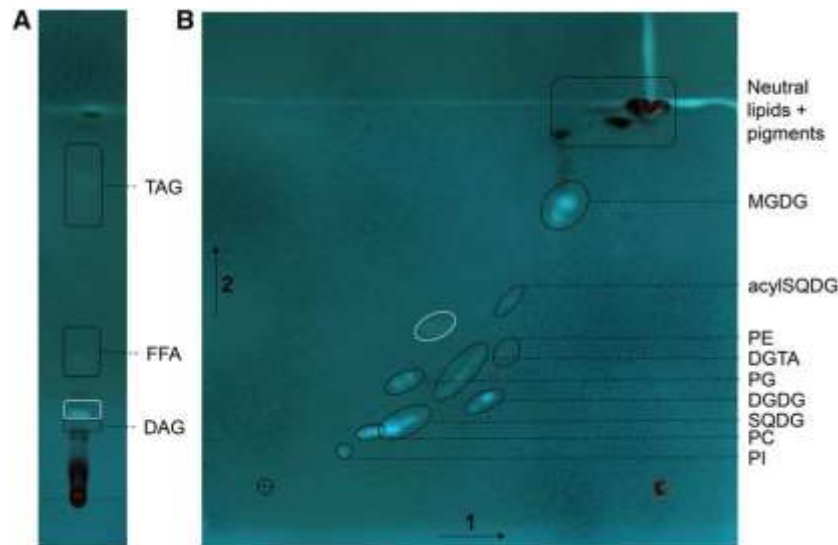


Fig. 4.3 Separation by TLC of the glycerolipids from *P. tricornutum*. Lipids from Pt1 cells grown in a replete medium (10N10P) were extracted and resolved following the procedures described in “Materials and Methods.” The cross indicates the initial deposit. A, One-dimensional separation of nonpolar lipids (DAG and TAG) and free FA (FFA). Migration was performed in hexane: diethylether:acetic acid (70:30:1, v/v). B, Two-dimensional separation of polar (membrane) lipids. Migration was performed in chloroform:methanol:water (65:25:4, v/v) for the first dimension (arrow 1) and chloroform:acetone:methanol:acetic acid:water (50:20:10:10:5, v/v) for the second migration (arrow 2). Lipids were visualized under UV light, after spraying with 2% 8-anilino-1-naphthalenesulfonic acid in methanol, and scraped off the plate for analyses. Identification of the lipid in each spot was performed by MS2 analyses. The spot circled in white is an unknown compound with a structure that differs from a glycerolipid.

corresponding to a loss of mass-to-charge ratio (m/z 87; Armada *et al.*, 2013). We did not detect the presence of DGTS in *P. tricornutum*.

Nonpolar lipids, DAG and TAG, are also present but in minor amounts (*e.g.* TAG represented only 1%– 3% of the total glycerolipids when cells were grown in the 10N10P medium; Fig. 4.4B). We were not able to identify in our TLC system any spot corresponding to phosphatidic acid, diphosphatidylglycerol, and phosphatidylSer. This does not mean that these phospholipids are absent in *P. tricornutum* but indicates that they each represent less than 1% of the total glycerolipid content. Overall, the main lipids are the four chloroplast lipids present in every photosynthetic membrane (*i.e.* MGDG, SQDG, DGDG, and PG) together with PC, which is usually the main glycerolipid in nonplastid membranes, although in diatoms its abundance in the four membranes surrounding the chloroplast cannot be excluded.

The positioning of FAs on each glycerolipid (summarized in Table III) was determined using MS and MS2 analyses, as described in Table II. The FA molar profiles (percentage) of the three main membrane lipids and the nonpolar glycerolipids are shown in Figure 4.5.

Several general features can be deduced from Table III. First, we confirmed previous analyses (Arao *et al.*, 1987; Yongmanitchai and Ward, 1993) reporting that 16:3 is always located at the sn -2 position and 20:5 at the sn-1 position, except when two 20:5s are present. Almost all glycolipids have a C16 FA at the sn-2 position, suggesting that the plastid lysophosphatidic acid acyltransferase (LPAAT), an enzyme called *Arabidopsis* seed gene2 (ATS2) in plants, has a very high selectivity for a C16-acyl carrier protein (C16-ACP), as in higher plants (Frentzen *et al.*, 1983), and that the plastid pathway (also known as the prokaryotic pathway) for the synthesis of the diacylglycerol backbone of glycolipids is largely dominant in diatoms (Mongrand *et al.*, 1998). Considering MGDG, for example, the most abundant species is 20:5/16:3, in agreement with our gas chromatography analyses (Fig. 4.5). Generally speaking, 16:3 and 16:4 are restricted to MGDG and only found at the sn-2 position. Considering DGDG, synthesised from MGDG, the sn-2 position is also esterified exclusively to a C16-FA, suggesting that these molecular species could originate from the same plastidic pathway. FAs in the sn-2 position are more saturated than those in MGDG (no 16:3 and 16:4 could be detected), suggesting that the desaturation of MGDG in 16:3 and 16:4 could be a way to lock an MGDG diacylglycerol backbone, preventing its utilization as a substrate for the synthesis of other glycerolipids, as shown previously in plants (Boudière *et al.*, 2012; Petroutsos *et al.*, 2014) and in *Chlamydomonas reinhardtii* (Li *et al.*, 2012). By contrast with plants, the sn-1 position of MGDG contains a very low proportion of C18 molecular species, with only about 8% of 18:0/16:3. The acyl profile of the different lipid classes, therefore,

Table 1. Identification of glycerolipids from *P. tricornutum*

Characteristic fragments generated by fragmentation of the parent ion (MS2) are shown, together with the associated references.

Analyzed Lipids	Polarity	Ion Analyzed	Specific Fragments in MS2 Scan	References
Phospholipids				
PC	+	[M + H] ⁺	Neutral loss of <i>m/z</i> 59	Domingues et al. (1998)
PE	+	[M + H] ⁺	Neutral loss of 141	Brügger et al. (1997)
Phosphatidylserine	+	[M + H] ⁺	Neutral loss of 185	Brügger et al. (1997)
PG	+	[M + NH ₄] ⁺	Neutral loss of 189	Taguchi et al. (2005)
PI	+	[M - H] ⁻	Precursors of <i>m/z</i> 241	Hsu and Turk (2000b)
Phosphatidic acid	+	[M + NH ₄] ⁺	Neutral loss of 115	Li-Beisson et al. (2010)
Nonphosphorus glycerolipids				
SQDG	-	[M - H] ⁻	Precursors of <i>m/z</i> 225	Gage et al. (1992); Welti et al. (2003)
ASQ	-	[M - H] ⁻	Precursors of <i>m/z</i> 509	Naumann et al. (2011)
MGDG	+	[M + NH ₄] ⁺	Neutral loss of 179	Li-Beisson et al. (2010)
DGDG	+	[M + NH ₄] ⁺	Neutral loss of 341	Moreau et al. (2008)
DGTA	+	[M + H] ⁺	Precursors of <i>m/z</i> 236; neutral loss of 59; no neutral loss of 87 as found for DGTS	Armada et al. (2013)
Neutral glycerolipids				
Free FA	-	[M - H] ⁻		
DAG	+	[M + NH ₄] ⁺	Scan of [M+NH ₄ -RCOONH ₄] ⁺	Camera et al. (2010)
TAG	+	[M + NH ₄] ⁺	Scan of [M+NH ₄ -RCOONH ₄] ⁺	Hsu and Turk (2010)

indicates (1) that the FA synthases of the chloroplast produce 14:0, 16:0, and 18:0 species, (2) that the acyl-ACP D9-desaturase is mainly active on 16:0 rather than on 18:0, and (3) that the plastid glycerol-3-phosphate acyl-transferase (an enzyme called ATS1 in plants) may have a lower affinity for C18 substrates than plant ATS1. The relative availability of acyl-ACP substrates (C16, C18, and C20 molecular species) also might be an important determinant, as it was recently reported that the level of C18 FA increased in MGDG when shifting the growth temperature from 20°C to 30°C, a condition known to lower 20:5 biosynthesis (Dodson *et al.*, 2014). PE, PC, and DGTA, which are likely synthesised in extraplastidic membranes, also contain C16 species at the sn-2 position, together with C18 and C20 FAs. The occurrence of a C16 FA at the sn-2 position in this lipid is consistent with two hypotheses: either an export of a prokaryotic diacylglycerol backbone or the fact that the microsomal LPAAT has no selectivity for FA molecular species, by contrast with the plastid LPAAT. Thus, in *P. tricornutum*, no specific signature could be determined for a potential eukaryotic pathway providing diacyl precursors to plastid lipids, as defined, respectively, in *Arabidopsis* and other microalgae such as *C. reinhardtii* (Fan *et al.*, 2011). A similar unbiased chain-length incorporation at the sn-2 position in *P. tricornutum* has also

been observed in some chlorophytes such as *Dunaliella bardawil* (Davidi *et al.*, 2014), despite their distant lineages. In addition, PE, PC, and DGTA retained most of the C18 present in the cells. It is also noteworthy that we found only one species of phosphatidylinositide (PI), with a 16:1/16:0 scaffold, suggesting a peculiar role for this phospholipid. PG showed two major species, 20:5/16:1 and 16:1/16:0, always with a C16 at position sn-2. It was reported previously that 16:1 at the sn-1 position was 16:1 (v-7) (cis-desaturation in v-7 or D-9 position) and 16:1 at the sn-2 position was 16:1(v-13)t (transdesaturation at position v-13; Arao *et al.*, 1987). Because the C16 transisomer is found only in chloroplast PG, it is likely that the 20:5/16:1 PG is located in plastids and that the 16:1/16:0 PG, similar to PI, is an extraplastidic PG species.

Table II. Conditions for the regiochemical assignment of FAs at sn-1, sn-2, and sn-3 positions in glycerolipids from *P. tricornutum*

Analyzed Lipids	Polarity	Ion Analyzed	MS2 Fragment Properties	References
Phospholipids				
PC	+	$[M + H]^+$	$[M+H-R_2CH = C = O]^+ > [M+H-R_1CH = C = O]^+$	Hsu and Turk (2003)
PE	-	$[M - H]^-$	$[R_2COO]^- > [R_1COO]^-$	Hsu and Turk (2000a)
PG	-	$[M - H]^-$	$[M-H-R_2COOH]^- > [M-H-R_1COOH]^-$	Hsu and Turk (2001)
PI	-	$[M - H]^-$	$M-H-R_2COOH]^- > [M-H-R_1COOH]^-$	Hsu and Turk (2000b)
Nonphosphorus glycerolipids				
SQDG	-	$[M - H]^-$	$[M-H-R_1COOH]^- > [M-H-R_2COOH]^-$	Zianni <i>et al.</i> (2013)
ASQ	-	$[M - H]^-$	$[M-H-R_1COOH]^- > [M-H-R_2COOH]^-$	Naumann <i>et al.</i> (2011)
MGDG	+	$[M + Na]^+$	$[M+Na-R_1COO]^+ > [M+Na-R_2COO]^+$	Guella <i>et al.</i> (2003)
DGDG	+	$[M + Na]^+$	$[M+Na-R_1COO]^+ > [M+Na-R_2COO]^+$	Guella <i>et al.</i> (2003)
DGTA	+	$[M + H]^+$	$[M+H-R_2COOH]^+ > [M+H-R_1COOH]^+$	By analogy with phospholipid diacylglycerol moiety
Nonpolar glycerolipids				
DAG	+	$[M + NH_4]^+$	$[M+NH_4-R_1COONH_4]^+ > [M+NH_4-R_2COONH_4]^+$	Camera <i>et al.</i> (2010)
TAG	+	$[M + NH_4]^+$	$[M+NH_4-R_{1/3}COO]^+ > [M+NH_4-R_2COO]^+$	Hsu and Turk (2010)

Table III. Positional distribution of FAs, and molecular species found in each glycerolipid class

Only molecules that represent more than 5% of all the species present in the class are indicated. The asterisk indicates where the *sn*-1 and *sn*-2 positions could not be discriminated. Major molecular species of a given lipid class are shown in bold characters.

<i>sn</i> -1/ <i>sn</i> -2	MGDG	DGDG	SQDG	ASQ	PG	PC	DGTA	PE	PI	DAG	TAG
14:0/16:0			6.9	6							
14:0/16:1			16.5	13.2						14.5	
16:0/16:0			4.6								
16:1/16:0	5.2	8.7	23.9	8.2	31.7				100	54.8*	
16:1/16:1	6.6	14.1			4.9	5.2	5.1			30.8	
16:1/16:2		5.4									
16:1/16:3	7.9										
16:1/18:1	5.4										
16:1/24:0			9.7								
16:2/16:0			9.6								
16:2/16:3	10.5										
18:0/16:3	7.7										
18:2/18:2						5.2					
20:5/14:0				12.7							
20:5/16:0		6.6	9.4	53.5	11.2	6.9					
20:5/16:1		16.1			48.5	12.1	13	11.3			
20:5/16:2	5.1	34.3				5	5.2	6.4			
20:5/16:3	19.1	7.3									
20:5/16:4	7.4										
20:5/18:2							7	7.8			
20:5/18:3						7	4.9	5.6			
20:5/18:4							5.7	6.2			
20:5/20:4						7.2		9.2			
20:5/20:5						20.1	11.1	24			
<i>sn</i> -1/ <i>sn</i> -2/ <i>sn</i> -3											
14:0/16:1/16:1											6.5
14:0/16:1/16:0											9.3
16:1/16:1/16:1											11
16:1/16:1/16:0											23.5
16:1/16:0/16:0											16
16:1/16:0/20:5											5

We also found that acyl-SQDG always harbors a 20:5 linked to its polar head, with the same diacylglycerol backbones as those found in SQDG species but with a highly dissimilar distribution. The main species of 20:5 acyl-SQDG was 20:5/16:0, and the corresponding SQDG substrate represented only 10% of its own class of lipid. Assuming that acylation occurs on SQDG (Riekhof *et al.*, 2003), this observation suggests that it should be quite specific for the molecular species 20:5/16:0.

Concerning nonpolar lipids, the DAG pool is mainly constituted of three different molecular species, dominated by 16:1/16:0 and 16:1/16:1, with a lower amount of 14:0/16:1. Although minor amounts of C18 and C20 were detected in DAG by gas chromatography analysis (Fig. 4.5), these FAs were not detected by MS analyses, indicating

that DAG species having a C18 or C20 were minor and could not be discriminated from the background. The DAG acyl composition (Table III) does not reflect the composition found in the main membrane lipids, in support of a de novo synthesis rather than a recycling of the diacylglycerol backbone from membrane lipids. These DAG molecular species are clearly at the origin of the TAG pool, also dominated by 16:0 and 16:1, with lower amounts of 14:0 and some 20:5 at position sn-3 (or sn-1). The proportion of TAG among other glycerolipids was low, reflecting the absence of any nutrient limitation.

Based on our structural determination of glycerolipid classes, we thus generated a reference profile for glycerolipids in *P. tricornutum* grown in nutrient-replete conditions. Based on this, we then assessed the variation of the glycerolipidome in nutrient-limited cells.

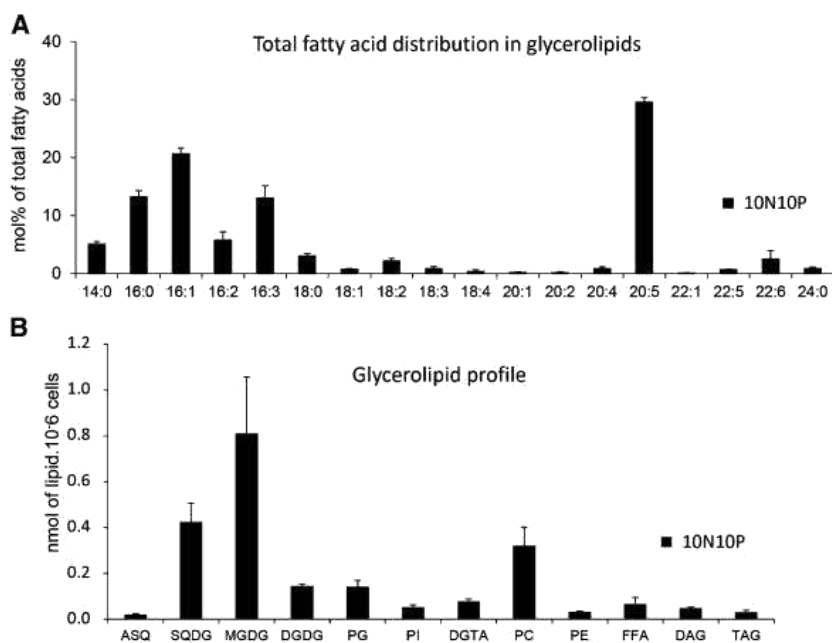


Fig. 4.4 Quantitative analysis of *P. tricornutum* glycerolipids. Lipids from Pt1 cells grown in a replete medium (10N10P) were extracted, separated by TLC, and analyzed as described in “Materials and Methods.” **A**, Global FA profile in a total lipid extract. FA proportions are given in percentages. **B**, Quantitative analysis of the various glycerolipids identified after TLC separation. Glycerolipids are expressed in nmol 10⁻⁶ cells and not as the summed FA content in each class. Each result is the average of three biological replicates ± SD. ASQ, 20:5-Acyl-SQDG; FFA, free FAs.

Impact of N and P Shortage on the Glycerolipid Content of *P. tricornutum* Pt1

We analyzed the glycerolipid profile in *P. tricornutum* Pt1 cells after 5 d of N starvation and 13 d of P starvation: that is, when strong impacts on both the photosynthetic capacity (based on the F_v/F_m ratio) and the nonpolar lipid content (based on Nile Red staining) could be observed (Figs.1 and 2). Figure 4.6A shows the glycerolipid profile in the three contexts: control (10N10P), N oligotrophic (0N10P), and P oligotrophic (10N0P). We observed the following trends. (1) A considerable increase of TAG content, on a per cell basis, was observed in both N- and P-limiting conditions, reaching 40 and 60%, respectively, of the total glycerolipid content (*i.e.* a 45 -fold and a 100-fold increase when compared with control conditions). (2) The MGDG content decreased in both conditions. This decrease was more pronounced in the case of N shortage, whereas the levels of the other membrane lipids remained almost unchanged, except for PG, which also decreased by a factor of 2. (3) A total disappearance of the phospholipids was observed in the P-starved condition, including the major phospholipids PC and PG, coinciding with a strong increase of DGTA and slight increases of DGDG and SQDG.

The nature and amounts of FA, measured as a whole (Fig. 4.6B), were also affected by nutrient limitation, with marked increases of 16:0 and 16:1 and a smaller albeit significant increase of 14:0, in support of an induced FA neosynthesis. Interestingly, the total amount of 20:5, the dominant FA in the control condition, remained almost unchanged. Thus, in the nutrient-limiting conditions, the dominant FA is no longer 20:5 but 16:1. Generally speaking, with the notable exception of TAG, the FA composition remained unchanged in the different glycerolipids (data not shown). A specific focus on TAG (Fig. 4.6C) indicated that not only 14:0, 16:0, and 16:1 but also 20:5 increased. In fact, the proportion of 20:5 in this class of lipids increased from about 1% in the control conditions to 8% in the N-starved and 6% in the P-starved conditions, suggesting a specific enrichment of 20:5 in TAG. MS analysis indicated that 20:5, as observed in control cells, was esterified at the sn-3 (or sn-1) position, indicating that this FA had been incorporated during the latter phases of TAG biosynthesis.

In order to better understand the origin of these FAs accumulating in TAGs, we measured the amount of 16:1 and 20:5 in each glycerolipid (Fig. 4.7A). The level of 16:1 remained approximately constant in all glycerolipids except in TAG, indicating that the observed increase of 16:1 (Fig. 4.6B) was mainly, if not only, correlated to the increase of TAG synthesis and reflected FA neosynthesis. In the N -starved condition, the level of 20:5 increased in TAG and decreased in MGDG by about the same amount (Fig. 4.7B). Because it almost remained constant in the other glycerolipids, this result suggests a 20:5 transfer from MGDG to TAG, as observed previously in *N. graditana* (Simionato *et al.*, 2013) and *C. reinhardtii* (Fan *et al.*, 2011).

In the P-limiting conditions, the situation was more complex. A stronger increase of 20:5 was observed in the TAG pool, together with a smaller decrease in the MGDG pool than was observed in N-starved cells. No phospholipid, containing initially a high proportion of 20:5, could be detected. Recycling of phospholipid FAs, therefore, also could contribute to the 20:5 enrichment of TAG. Furthermore, an increase of SQDG and DGTA was observed (Fig. 4.6A), consistent with (1) a PG replacement by SQDG in the plastid and (2) a possible recycling of the PC diacylglycerol moiety into DGTA, taking place in an extraplastidic membrane. This hypothesis is based on the strong increase of 20:5 in DGTA, likely reflecting the quantitative increase of the DGTA pool (Fig. 4.6A) rather than a specific 20:5 enrichment, because the global FA composition remained largely unaffected.

Effect of nitrogen and phosphorus starvation in *Phaeodactylum tricornutum*.

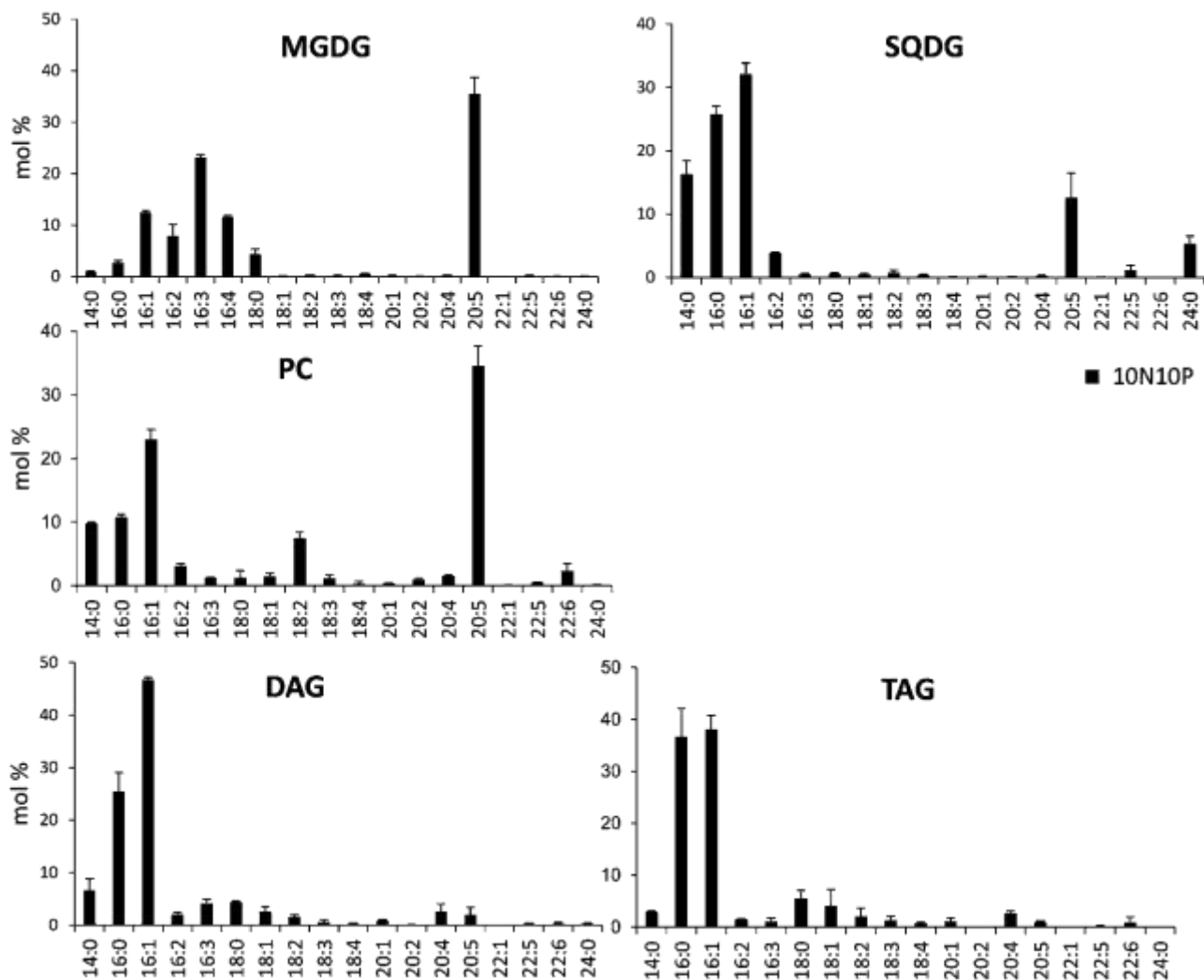


Fig. 4.5. Molar profiles of FAs in PC, DAG, TAG, MGDG, and SQDG. Lipids from Pt1 cells grown in a replete medium (10N10P) were extracted, separated by TLC, and analyzed for their FAs as described in "Materials and Methods." Note that a cross contamination is possible between SQDG and PC due to the proximity of the TLC spots, leading to moderate enrichment of 20:5 in SQDG and 14:0 in PC. Each result is the average of three biological replicates \pm SD.

DISCUSSION

A Reference Glycerolipid Profile for *P. tricornutum*

The glycerolipid composition of *P. tricornutum* presents a strong similarity with those reported for other photosynthetic unicellular eukaryotes (Dembitsky, 1996) but also specific differences. Besides the major lipids conserved in photosynthetic membranes (*i.e.* MGDG, DGDG, SQDG, and PG), we confirmed the presence of 29 -O-acyl-sulfoquinovosyldiacylglycerides (20:5-acyl-SQDG [ASQ]), largely dominated by the molecular species sn-1:20:5/sn-2:16:0/29:20:5 (Naumann *et al.*, 2011). The presence of ASQ has also been reported for *C. reinhardtii*, although 18:3 or 18:4 acyl groups were the FAs involved in the 29-acylation of the sulfoquinovose moiety (Riekhof *et al.*, 2003). To date, there is no evidence for a physiological or biochemical role of ASQ. The large proportion of SQDG also suggests that this lipid might not be restricted to chloroplast membranes; therefore, the subcellular localization of SQDG and ASQ should be assessed in the future.

Notwithstanding, an SQD1 *C. reinhardtii* mutant, lacking SQDG and ASQ, was clearly impaired in its photosynthetic capacities and in its response to inorganic phosphate deficiency, indicating altered membrane properties and an inability to adjust its membrane composition to adapt to environmental change (Riekhof *et al.*, 2003). These experiments did not reveal any specific role of ASQ versus SQDG, but the results presented here indicate that, if SQDG is the precursor of ASQ, as postulated previously (Riekhof *et al.*, 2003), this acylation process is quite specific for one minor SQDG species, sn-1:20:5/sn-2:16:0, representing less than 10% of the total SQDG. Such specificity in the acylation process suggests the existence of a specific role for ASQ.

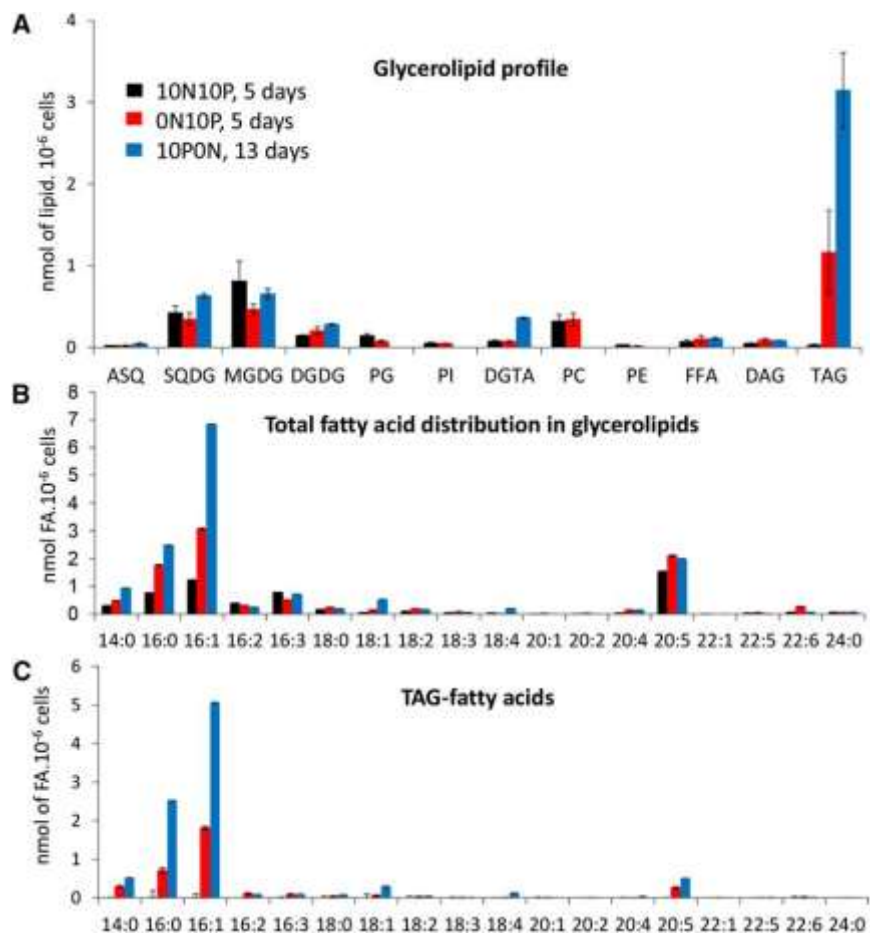


Fig. 4.6. Quantitative analysis of FAs and glycerolipids in *P. tricornutum* grown in nutrient-replete conditions or in medium devoid of either N or P. Lipids from Pt1 cells grown either in a replete medium (10N10P; black) or in medium deprived of N (ON10P; blue) or P (10NOP; red) were extracted, separated by TLC, and quantified as described in “Materials and Methods.” To avoid any N deficiency in 10N10P or 10NOP culture, media were replaced by fresh ESAW 10N10P or 10NOP medium every 3 d. Lipids were analyzed after 5 d of cultivation in replete conditions (black bars), N starvation (red bars), or after 13 d for P starvation (blue bars). **A**, Changes in glycerolipid content. Note that in the P-depleted condition, phospholipids were not detectable. **B**, Changes in FA content. **C**, FA profile in TAG. Each result is the average of three biological replicates \pm SD. ASQ, Acyl-SQDG; FFA, free FAs.

Based on sequence similarity, we identified gene candidates for a plastid-localized synthesis of glycerolipids: a putative chloroplast glycerol-3-phosphate acyltransferase (ATS1 homolog; Phatr_3262), a chloroplast 1-acyl-sn-glycerol-3-phosphate

acyltransferase (ATS2 homolog; Phat_43099), three MGDG synthase isoforms (three monogalactosyldiacyl homologs; Phatr_14125, Phatr_54168, and Phatr_9619), three DGDG synthase isoforms (three digalactosyldiacyl homologs; Phatr_12884, Phatr_11390, and Phatr_43116), a UDP-sulfoquinovose synthase (SQD1; Phatr_21201), and two SQDG synthase isoforms (two SQD2 homologs; Phatr_50356 and Phatr_42467). One or both of these SQD2 homologs also could be involved in the synthesis of ASQ.

The results obtained in this study indicate that FAs are synthesised in the stroma of chloroplasts by type II FA synthases, mainly as 14:0-, 16:0-, and 18:0-ACP. The presence of the saturated form of C18 in plastid lipids (*i.e.* 18:0) and the position of desaturation of 16:3^{D6,9,12} in MGDG (Domergue *et al.*, 2003) suggest that the plastid D9-acyl-ACP desaturation might operate only on 16:0-ACP, releasing 16:1(v-7)-ACP.

In plants, there are two pools of PG: one localized in the plastid, with a prokaryotic diacylglycerol backbone and a specific FA at the sn-2 position, 16:1(v-13)t; and one in microsomal membranes and mitochondria, with a so-called eukaryotic diacylglycerol backbone assembled in the ER. In *Arabidopsis*, two enzymes are thus responsible for PG synthesis: Phosphatidylglycerophosphate synthase1 (PGP1), localized in both chloroplast and mitochondria (Babiychuk *et al.*, 2003), and PGP2, localized in the ER (Müller and Frentzen, 2001). By studying *pgp* mutants, it was established that the PGP1-dependent pathway was responsible for 70% of PG synthesis in leaves and was required for the development of green leaves and chloroplasts with well-developed thylakoid membranes (Hagio *et al.*, 2002; Xu *et al.*, 2002), whereas the *pgp2* mutant showed a small decrease in PG content compensated by a slight increase in PI content (Tanoue *et al.*, 2014). Based on the facts that PG and PI biosynthesis pathways share their precursors (*i.e.* phosphatidic acid and cytidine diphosphate-diacylglycerol [CDP-DAG]) and that PGP2, the PI synthase, and

the extraplastidic CDP-DAG synthases are all localized in the ER (Löfke *et al.*, 2008; Zhou *et al.*, 2013), the accumulation of PI in the *Arabidopsis* *pgp2* mutant is consistent with an accumulation of CDP-DAG. In *P. tricornutum*, we found only two species of PG, the 20:5/16:1 form, which is probably plastidic with 16:1(v-13)t at the sn-2 position, and the 16:1/16:0 form, which we expect to be extraplastidic, having exactly the same composition as PI. Together, these results suggest that the extraplastidic CDP-DAG synthase is highly specific for a 16:1/16:0 substrate. Furthermore, the conservation of

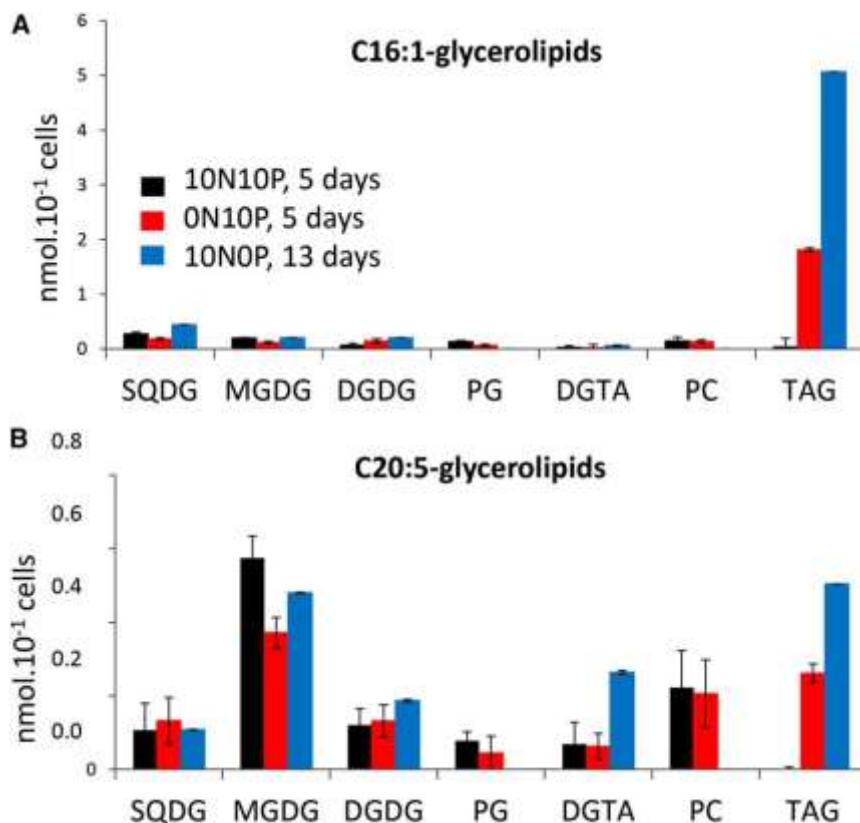


Fig. 4.7. Distribution of 16:1 and 25:0 FAs in the glycerolipid classes of *P. tricornutum* grown in nutrient-replete conditions or in medium devoid of either N or P. Lipids from Pt1 cells grown in a replete medium (10N10P) were extracted, separated by TLC, and quantified as described in “Materials and Methods.” Lipids were analyzed after 5 d of cultivation in replete condition (black bars), N starvation (red bars), or after 13 d of P starvation (blue bars). **A**, Quantitative distribution of 16:1 in the major glycerolipid classes. **B**, Quantitative distribution of 25:0 in the major glycerolipid classes. Each result is the average of three biological repeats \pm SD.

16:0 at the sn-2 position in extraplastidic PG and PI in different algae species (Araki *et al.*, 1987; Giroud *et al.*, 1988; Liang *et al.*, 2014) differs strikingly from the eukaryotic route observed in plants.

The preservation of the medium-chain FA in PI and extraplastidic PG might be important for their biological function. This result further supports either the absence of any FA selectivity of the extraplastidic LPAAT as being the basis of the plant eukaryotic signature or an export of the prokaryotic diacylglycerol backbone, as suggested in *C. reinhardtii* (Fan *et al.*, 2011). In the *P. tricornutum* genome, two putative CDP-DAG synthases can be predicted (Phatr_559 and Phatr_7678), and future functional studies should help to ascertain whether one is specific for the production of PG/PI precursors.

In addition to the classical phospholipids that make up the bulk of nonphotosynthetic membranes, we report the presence of DGTA, a betaine glycerolipid never observed previously in *P. tricornutum*. BL have been detected in numerous algae (comprehensively reviewed by Dembitsky [1996]). Both DGTA and DGTS are usually associated with nonplastid membrane compartments (Künzler *et al.*, 1997) and have structural similarities to PC (Sato and Murata, 1991). Therefore, we can speculate that DGTA might be more abundant in the endomembrane system and may be present in the outermost of the four membranes of the chloroplast, connected to the nuclear envelope. We identified a candidate gene that might be involved in BL synthesis, Phatr_42872, whose role should be assessed in the future based on functional genomics approaches.

Concerning FAs, eicopentaenoic acid (20:5) is the major molecular species, found in all membrane lipids of *P. tricornutum*. It is also a major FA in numerous microalgae, such as *Porphyridium cruentum* (Khozin *et al.*, 1997), *N. gaditana* (Simionato *et al.*, 2013), *Monodus subterraneus* (Khozin-Goldberg *et al.*, 2002), and *Chromera velia* (Botté *et al.*, 2011). This polyunsaturated very-long-chain FA is usually synthesised in the ER (Khozin *et al.*, 1997) following complex desaturation and elongation processes (for review, see Petroutsos *et al.*, 2014). The synthesis of 20:5 in the ER has not been unambiguously demonstrated in *P. tricornutum*. Nevertheless, the two front-end desaturases involved in this pathway, the D6 and D5 desaturases (Phatr_2948 and Phatr_46830, respectively), do not contain any predicted signal peptide and plastid-like transit sequence that could be involved in a targeting to the chloroplast. The synthesis of 20:5, therefore, is very likely to occur outside chloroplasts in *P. tricornutum* as well. The dominant species of MGDG in *M. subterraneus* (Khozin-

Goldberg *et al.*, 2002) and *P. cruentum* (Khozin *et al.*, 1997) are 20:5/20:5. In these organisms, it was proposed that PE and PC were, respectively, donors for the DAG moiety responsible for these eukaryotic-like MGDG species. In *P. tricornutum*, however, all MGDG species having a 20:5 FA at the sn-1 position have a C16 at the sn-2 position, displaying a prokaryotic signature. Therefore, the acyl position in *P. tricornutum* MGDG supports a different scenario from that documented for *Arabidopsis* eukaryotic MGDG: once synthesised in cytosolic membranes, 20:5 has to be released from a phospholipid into the cytosolic acyl-CoA pool and then transported into the chloroplasts to be attached to the glycerol-3-phosphate at the sn-1 position by the first acyltransferase, ATS1. We denoted this unique route, misleadingly thought to correspond to the plant eukaryotic pathway, the omega pathway (Petroutsos *et al.*, 2014). The precise details and the enzymes and transporters involved in these events remain to be characterized.

The question of the putative existence of a eukaryotic pathway with a recycling of an intact diacylglycerol backbone coming from phospholipid for galactolipid synthesis, as described in higher plants, remains unsolved. Indeed, there is no visible signature for the eukaryotic pathway to follow, the typical eukaryotic 20:5/ 20:5 backbone found in extraplastidic glycerolipids (*i.e.* PC, PE, and DGTA) and described in other algae (Khozin *et al.*, 1997; Khozin-Goldberg *et al.*, 2002) being absent in plastid glycolipids. Since PC harbors a high proportion of C16 at the sn-2 position, we cannot exclude that some MGDG species could result from the galactosylation of a diacylglycerol backbone with this signature. However, considering that C18 is almost absent from galactoglycerolipids, this pathway should operate a sorting of diacyl molecular species, excluding PC with a C18 at position sn-2.

Remodeling of Membrane Glycerolipids in N- and P-Limiting Conditions

Based on our reference glycerolipid profile in a replete medium, we could compare the variations of the membrane lipid distribution occurring upon N or P starvation and attempt to deduce some likely remodeling scenarios. N shortage induces visible effects over a shorter time scale (3–4 d) compared with P shortage (8–13 d, depending on the initial level of this nutrient). This feature has been observed for all the Pt accessions examined here. Based on our observations, N limitation seems to trigger a serious and rapid stress response,

presumably related to the need for protein synthesis, whereas more sophisticated lipid-remodeling systems seem to be operative during P limitation, perhaps as an adaptive response. This difference is also reflected at the level of photosynthesis; based on the F_v/F_m ratio, photosynthesis was apparently affected more rapidly in low-N than in low-P conditions.

Considering membrane glycerolipids, N deprivation has no effect on the level of N-containing lipids such as PC, PE, and DGTA. As in *Arabidopsis*, N-containing lipids are not a form of N storage (Gaude *et al.*, 2007), in contrast with phospholipids, which are clearly a biochemical parameter tuned by photosynthetic organisms. The only significant changes we observed were a relative decrease of the proportion of MGDG and an increase in DGDG, leading to a diminished MGDG-DGDG ratio, a lipid change that also has been observed in *Arabidopsis* upon N shortage (Gaude *et al.*, 2007). The physiological significance of this phenomenon is unknown, but a reduced MGDG-DGDG ratio is often observed in chloroplasts with impaired photosynthesis (Boudière *et al.*, 2014). We could also detect a slight decrease in the proportion of PG, possibly reflecting senescence of the thylakoid membranes.

Following P deprivation, all phospholipids, including PC and PG, were completely undetectable, compensated by an increase of nonphosphorus lipids synthesised in endomembranes (indicated by a 5-fold-increase of DGTA) and in the plastid (indicated by a 2-fold increase of DGDG and a 1.5-fold increase of SQDG). The proportion of MGDG decreased by a factor of 1.5, but the overall proportion of galactoglycerolipids (MGDG and DGDG) increased. Similar observations have been made in higher plant cells (Jouhet *et al.*, 2003), although the impact on phospholipids was not as dramatic as that recorded here. The best documented form of BL in the literature is DGTS, and, because it sometimes has an inverse concentration relationship with PC, it is thought to replace PC in extraplastidic membranes (Moore *et al.*, 2001), as suggested for *C. reinhardtii*, which lacks PC (Riekhof *et al.*, 2005, 2014), and further supported by the comparison of phytoplankton communities collected in P-rich and P-oligotrophic regions (Van Mooy *et al.*, 2009). Consistent with this postulate, the increase of DGTA in the P-starved conditions reached a value that was about identical to that measured for PC in control cells, thus supporting that a PC-to-DGTA replacement occurred in extraplastidic membranes. In terms of lipid trafficking, no specific machinery would be required, since both DGTA and PC are likely synthesised in the same membrane system (*i.e.* the ER). It is also known that an increase of SQDG could compensate the absence of PG in

plastids (Jouhet *et al.*, 2010). Similarly, this remodeling would not require any massive lipid transport, since PG and SQDG are localized in the same membranes (*i.e.* thylakoids).

In plants, P deprivation induces an increase of galactolipid production, using a eukaryotic diacylglycerol moiety diverted from hydrolyzed phospholipids, and an export of DGDG from plastids to extraplastidic membranes, such as the plasma membrane, the tonoplast, and/or mitochondrial membranes (Andersson *et al.*, 2003, 2005; Jouhet *et al.*, 2004). First, based on our results, there is no evidence for a eukaryotic pathway in *P. tricornutum* as described in plants, but rather an omega pathway, which might participate in the recycling of the phospholipid hydrophobic moiety, possibly by free FA transfers. Second, in *P. tricornutum*, the plastid envelope contains four membranes, with the two outermost ones being derived from the ER. DGDG has never been found in the ER of higher plants, and this lipid is transferred toward mitochondria via contact sites, indicating that the ER is not involved in DGDG trafficking, at least for this interorganellar transfer (Jouhet *et al.*, 2004). Similar physical links between the secondary plastid and the mitochondria might occur in *P. tricornutum*, since both organelles are very close (Prihoda *et al.*, 2012). Third, the increase of SQDG and DGTA could quantitatively compensate for the decrease of PG and PC, respectively. There is no obvious necessity for an export of DGDG toward extraplastidic membranes in the cells of *P. tricornutum* exposed to P limitation. It is possible, therefore, that an increase of DGDG, observed during both N and P limitation, might counteract the decrease of MGDG and contribute to the protection of photosynthetic membrane integrity.

In a recent report on the transcriptome changes occurring in *P. tricornutum* upon P shortage, transcripts for the ATS1 homolog (Phatr_3262), one of the MGDG synthase homologs (Phatr_54168), the two SQDG synthase isoforms (Phatr_50356 and Phatr_42467), and the putative gene involved in DGTA synthesis (Phatr_42872) were significantly up-regulated (Yang *et al.*, 2014). Likewise, in the centric diatom *T. pseudonana*, genes coding two putative SQD1 homologs (gene identifiers 7445840 and 7452379) and two putative monogalactosyldiacyl homologs (gene identifiers 7447073 and 7445775) were found to be up-regulated in response to P limitation (Dyhrman *et al.*, 2012). Therefore, the remodeling of lipids in diatoms seems to be transcriptionally controlled following, at least in part, the model dissected previously in plants, in which some of the genes encoding MGD, digalactosyldiacyl, and SQD2 isoforms (in *Arabidopsis*, MGD2, MGD3, DGD2, and SQD2; Misson *et al.*, 2005) were

shown to be specific to the P starvation response and activated by signaling cascades responding to low P. An in-depth study of the transcriptome of *P. tricornutum* cultivated in identical conditions to those used here will help identify all genes that are likely to be transcriptionally coordinated up-stream of the observed remodeling and search for the corresponding cis-elements and transcriptional systems.

Accumulation of TAG in Conditions of N and P Starvation

All accessions of *P. tricornutum*, collected in various oceanic locations, showed an increase of TAG, albeit with some variations in the time scale and magnitude of accumulation of this class of nonpolar lipids. There was no apparent correlation between TAG accumulation and morphotype (triradiate, fusiform, or oval) or the initial geographic location. Pt10 and PtHK, which were both less sensitive to P shortage, were collected on the eastern coast of China, albeit at very distant sites, which could suggest an environmental impact on the physiology of these strains, perhaps with a higher capacity to store P. Interestingly, Pt4 was not able to accumulate large amounts of TAG in either N- or P-limiting conditions, which could suggest that it is affected in its ability to synthesize or store TAG. Pt4 was collected in the Baltic Sea, a relatively closed sea, but the long-term influence of this particular area on the physiological and metabolic behavior of these algae remains to be determined. Clearly, a genomic analysis of these strains is required to draw further conclusions.

P and N limitation affect both the lipid content and the photosynthetic capacities of Pt1 cells. Although N deprivation has a strong and almost immediate effect on cell division, it is important to note that P deprivation requires a much longer period to induce any visible effect. Diatoms, therefore, might struggle more with a lack of N than with a lack of P, possibly because of the existence of powerful P-storage systems within the cell, such as polyphosphate, a ubiquitous P polymer (Martin *et al.*, 2014). N and P limitation will impact both the biosynthesis of proteins and the level of phosphorylated metabolites, which, in turn, will affect numerous metabolic functions, including growth and photosynthesis. However, oil accumulation depends on the availability of a carbon source (Fan *et al.*, 2011), and this is in apparent contradiction with an increase of TAG concomitant with a decline of photosynthesis. In this study, this source of carbon possibly arises from the remaining photosynthetic activity and/or from stored carbohydrates (Li *et al.*, 2011). Thus, it is likely that, in the case of a growth

arrest linked to a mineral deficiency, the available carbon and energy un-used for cell division and membrane expansion are diverted toward lipid biosynthesis and storage. This could be part of a cellular strategy to allow a better and quicker restart when environmental conditions become favorable again. Whether the arrest of cell division is an absolute requirement to trigger TAG accumulation is thus an important open question.

During both N and P shortages, we observed a significant increase in the neosynthesis of 16:0 and 16:1, which was mainly if not uniquely associated with the accumulation of TAG, whereas we observed only little change in the FA composition of the various glycerolipids, besides a 16:1 and 20:5 enrichment in TAG. This confirms previously published reports, in a variety of photosynthetic eukaryotes, showing that the accumulation of TAG triggered by a shortage of N originated mainly from FA neosynthesis (Simionato *et al.*, 2013). Whatever the growth conditions, the small pool of DAG is constituted of three main species comprising only 14:0, 16:0, and 16:1 acyl groups, with 14:0 being less abundant than the others and always esterified at the sn-1 position, when present. Interestingly, the sn-1 and sn-2 positions in TAG completely mirror the DAG pool, and the sn-3 position is occupied by a 16:0 or 16:1 FA in 80% to 90% of the molecular species. These two FAs are also the main ones overproduced in nutrient-limiting growth conditions. Clearly, these data do not support any substantial recycling of DAG moieties deriving from membrane glycerolipids, by contrast with higher plants (Bates and Browse, 2012). Therefore, it is likely that TAGs are mostly synthesised via a route involving a diacylglycerol acyltransferase and de novo DAG and acyl-CoA synthesis (Kennedy pathway).

During both N and P limitation, TAGs were enriched in 20:5 at the sn-3 or sn-1 position, whereas the global level of 20:5 inside the cell was not affected. Since 20:5 is produced at the level of phospholipids in nonplastid membranes, it has to be transferred to TAG, most likely via the acyl-CoA pool or via a phosphatidyl diacyl-glycerol acyltransferase. In the N-deprived condition, it was striking to observe that the increase of 20:5 in TAG, on a per cell basis, roughly corresponds to the decrease of 20:5 in MGDG, suggesting that MGDG also could contribute to TAG synthesis, as described in *N. graditana* (Simionato *et al.*, 2013) and *C. reinhardtii* (Fan *et al.*, 2011; Li *et al.*, 2012). Based on this mechanism, the eicopentaenoic acid released in the acyl-CoA pool following the degradation of MGDG (or other membrane lipids such as phospholipids) should be recycled mainly into other glycerolipids such as TAG, rather than oxidized through the β -oxidation pathway.

CONCLUSION

The overall goal of this work was first to define a reference for the glycerolipidome of *P. tricornutum*, with MGDG, DGDG, SQDG, and PG as conserved lipids in photosynthetic membranes and PC and DGTA as major lipids in extraplastidic membranes. We also detected the presence of ASQ. Based on this reference, we could deduce that the FAs were most likely synthesised de novo in the stroma of chloroplasts as 14:0-, 16:0-, and 18:0-ACP species. We identified only one gene candidate coding for a putative palmitoyl-ACP D9-desaturase (Phatr_9316). When exported to the cytosol, FAs can be elongated and desaturated to generate 20:5. Acyl-ACP can be used in the plastid for the production of MGDG, DGDG, SQDG, and part of PG via a canonical prokaryotic pathway, and acyl-CoA can be used in the cytosol and endomembranes to generate PC, DGTA, or TAG. We could identify gene candidates coding for putative enzymes involved in these pathways. Extraplastidic PG and PI seem to share a common CDP-DAG precursor with a 16:1/16:0 signature. We could not detect any specific signature for an extraplastidic eukaryotic pathway as in plants and could not assess the possibility of the import of eukaryotic precursors inside the chloroplast. Rather, the plastid lipid profiles we obtained would be consistent with an import of 20:5 FAs, hydrolyzed from extraplastidic phospholipids, to serve as precursors for plastid acyltransferases, eventually producing MGDG, DGDG, and SQDG. We called this pathway the omega pathway, and future challenges include the deciphering of the machinery importing 20:5 FA into the chloroplast.

We compared the remodeling triggered by the deprivation of two major nutrients fluctuating in the oceans, N and P. On the one hand, N oligotrophy is apparently a severe stress for *P. tricornutum*, triggering a rapid senescence of chloroplast membranes, an arrest of cell division, and an accumulation of TAG. By contrast, a complex adaptation to P deprivation is observed, with a first phase of consumption of specific P-storage forms, most likely polyphosphate, followed by a breakdown of phospholipids, behaving like a secondary form of P storage, and their replacement by nonphosphorous lipids, most likely following PG-to-SQDG and PC-to-DGTA replacements. A phospholipid-to-DGDG replacement cannot be ruled out in some of the membranes limiting the chloroplast, but this has to be confirmed.

Future work should entail the characterization of the enzyme isoforms and the machineries for lipid synthesis, lipid breakdown, and lipid trafficking involved in the lipid changes described here and the systems controlling them. A survey of transcriptome variations occurring in *P. tricornutum* or *T. pseudonana* supports a transcriptional control, which should be studied further in the future. The task is as complex as that in plants, since some pathways, like the omega pathway, are apparently specific to chromalveolates, and their components cannot be deduced from previous studies. Nevertheless, the possibility to perform large-scale omics studies and to characterize the function of gene products is among the advantages of the *P. tricornutum* model. Future work starting with the gene candidates listed here will hopefully help to unravel the adaptive system of this diatom to cope with a fluctuating environment.

MATERIALS AND METHODS

Strains and Culture Conditions

Phaeodactylum tricornutum strains were obtained from the culture collections of the Pruvost-Guillard National Centre for Culture of Marine Phytoplankton (CCMP) and the Culture Collection of Algae and Protozoa (CCAP), using axenic accessions characterized by De Martino *et al.*, (2007): Pt1, CCAP 1055/3; Pt2, CCMP2558; Pt3, CCMP2559; Pt4, CCAP 1055/2; Pt5, CCMP630, Pt6 (fusiform), CCAP 1054/4; Pt7, CCAP 1055/6; Pt8, CCAP 1055/7; Pt9, CCAP 1055/5; Pt10, CCAP 1055/8. We completed this series of accessions with the fully sequenced reference strain for *P. tricornutum*, derived from Pt1, Pt1.8.6 (Bowler *et al.*, 2008; CCAP1055/1), and with an axenic strain isolated in Hong Kong, PtHK. Cells were maintained and grown in enriched seawater, artificial water (ESAW) medium, as described by Falciatore *et al.*, (2000). The different cell shapes described here are those of algae grown and maintained in artificial medium. In the preliminary comparative study of Pt1 to Pt10 ecotypes by microscopic imaging, cells were grown either in the presence of 0.55 mM N and 0.0224 mM P or in the absence of one or both of these nutrients. Cultures were grown in exponential phase in 50-mL single-use flasks with 100 rpm shaking, an irradiance of 100 $\mu\text{mol photons m}^{-2} \text{s}^{-1}$, and a 12-h-light/ 12-h-dark photoperiod at 19°C.

For the Nile Red measurements, 50-mL cultures were grown in exponential phase before being centrifuged at 1,500g for 30 min and suspended in 10 mL of replete or deficient medium. Initial cell densities for P-deficient and N-deficient experiments were 10^4 and 10^5 cells mL^{-1} , respectively. In the in-depth analysis performed on the Pt1 strain, cells were grown in batch conditions in 250-mL flasks containing 50 mL of ESAW medium with or without N or P. Replete conditions consisted of 5.5 mM N and 0.22 mM P, in order to avoid nutrient exhaustion in the batch culture over the observation period and to increase the contrast in the analyzed lipid profiles between nutrient-rich and -depleted conditions. Cells were cultivated in an artificial climate incubator, with 100 rpm shaking, under an irradiance of 40 $\mu\text{mol photons m}^{-2} \text{s}^{-1}$ and with a 12-h-light/ 12-h-dark photoperiod at 19°C. The initial

inoculum was 0.5 to 1×10^6 cells mL^{-1} . Cells were collected after 5 or 13 d and counted with a Malassez chamber using an aliquot fraction before any further manipulations.

Chlorophyll Fluorescence Measurements

The parameter F_v/F_m was used as an indicator of PSII activity in a dark-adapted state. For this, in vivo chlorophyll fluorescence was determined using a Speedzen MX fluorescence imaging setup (JBeamBio). Excitation was done in the blue range ($\lambda = 450$ nm) using short pulses (10 ms). Emission was measured in the near far red. Saturating pulses (duration of 250 ms) were provided by a green ($\lambda = 520$ nm) light-emitting diode array. Measurements were done 15 min after dark adaptation of the samples.

The variable fluorescence (F_v) was calculated as $F_v = F_m - F_o$, where F_m is the maximum fluorescence in the dark-adapted state and F_o is the minimal fluorescence in the dark-adapted state (Genty *et al.*, 1990).

Nile Red Staining of Nonpolar Lipids

Accumulation of nonpolar lipids and oil droplets was monitored by Nile Red (Sigma-Aldrich) fluorescent staining (excitation wavelength at 532 nm and emission at 565 nm), as described previously (Cooksey *et al.*, 1987). In brief, 200 μL of culture was stained with 50 μL of a Nile Red stock solution ($2.5 \mu\text{g mL}^{-1}$ in dimethyl sulfoxide), and fluorescence was measured by flow cytometry using a Partec Cube8 device equipped with a 532-nm green laser. When the number of cells was estimated, specific fluorescence was determined by dividing Nile Red fluorescence intensity by the number of cells.

Glycerolipid Extraction, Separation by TLC, and Analyses by GC-FID and MS

Glycerolipids were extracted from freeze-dried *P. tricornutum* cells grown in 50 mL of ESAW medium with variable initial supplies of P and/or N. First, cells were harvested by centrifugation and then immediately frozen in liquid N. Once freeze dried, the pellet was suspended in 4 mL of boiling ethanol for 5 min to prevent lipid degradation, and lipids were

extracted according to Simionato *et al.*, (2013) by the addition of 2 mL of methanol and 8 mL of chloroform at room temperature. The mixture was then saturated with argon and stirred for 1 h at room temperature. After filtration through glass wool, cell debris was rinsed with 3 mL of chloroform:methanol (2:1, v/v), and 5 mL of 1% (w/v) NaCl was then added to the filtrate to initiate biphasic formation. The chloroform phase was dried under argon before solubilizing the lipid extract in pure chloroform.

Total glycerolipids were quantified from their FAs: in an aliquot fraction, a known quantity of 15:0 was added and the FAs present were transformed as FAMES by a 1-h incubation in 3 mL of 2.5% (v/v) H₂SO₄ in pure methanol at 100°C (Jouhet *et al.*, 2003). The reaction was stopped by the addition of 3 mL of water and 3 mL of hexane. The hexane phase was analyzed by a GC-FID (Perkin-Elmer) on a BPX70 (SGE) column. FAMES were identified by comparison of their retention times with those of standards (Sigma-Aldrich) and quantified by the surface peak method using 15:0 for calibration. Extraction and quantification were performed at least three times.

To quantify the various classes of nonpolar and polar glycerolipids, lipids were separated by TLC onto glass-backed silica gel plates (Merck) using two distinct resolving systems (Simionato *et al.*, 2013). To isolate nonpolar lipids including TAG and free FA, lipids were resolved by TLC run in one dimension with hexane:diethylether:acetic acid (70:30:1, v/v). To isolate membrane glycerolipids, lipids were resolved by two-dimensional TLC. The first solvent was chloroform:methanol:water (65:25:4, v/v) and the second was chloroform:acetone:methanol:acetic acid:water (50:20:10:10:5, v/v). Lipids were then visualized under UV light, after spraying with 2% (v/v) 8-anilino-1-naphthalenesulfonic acid in methanol, and scraped off the plate. No phosphatidylethanol could be detected after TLC or following MS analyses, indicating that the boiling ethanol treatment did not give rise to this category of glycerolipid derivative by non-specific chemical reactions. Lipids were recovered from the silica powder after the addition of 1.35 mL of chloroform:methanol (1:2, v/v) thorough mixing, the addition of 0.45 mL of chloroform and 0.8 mL of water, and collection of the chloroform phase (Bligh and Dyer, 1959). Lipids were then dried under argon and either quantified by methanolysis and GC-FID as described above or analyzed by MS.

For MS analyses, purified lipid classes were dissolved in 10 mM ammonium acetate in pure methanol. They were introduced by direct infusion (electrospray ionization-MS) into a trap-type mass spectrometer (LTQ-XL; Thermo Scientific) and identified by comparison with standards. In these conditions, the produced ions were mainly present as H^2 , H^+ , NH_4^+ , or Na^+ adducts. Lipids were identified by MS2 analysis with their precursor ion or by neutral loss analyses as indicated in Table I. All experiments were performed in triplicate.

Positional Distribution of FAs Esterified to Glycerolipids

The positions of FA molecular species esterified to the glycerol backbone of the various glycerolipids were determined based on MS2 analyses. Glycerol carbons were numbered following the stereospecific number (sn) nomenclature. Depending on the nature of the glycerolipid and the type of adduct, the substituents at the sn-1 (or sn-3) and sn-2 positions are differently cleaved when subjected to low-energy collision-induced dissociation. This is reflected in MS2 analyses by the preferential loss of one of the two FAs, leading to a dissymmetrical abundance of the collision fragments. The patterns of MS2 fragments for all glycerolipids have been described in previous studies (Table II), except for DGTA. In this study, we hypothesized that the loss of FAs in DGTA following low-energy collision-induced dissociation is similar to that observed for other polar lipids, such as PC.

ACKNOWLEDGMENTS

We thank Yahui Gao (Xiamen University), who kindly provided the P_tHK strain isolated in Hong Kong Harbor in October 2010, and Catherine Cantrel (Institut de Biologie de l'École Normale Supérieure), Mathilde Cussac, Valérie Gros, and Guillaume Tourcier (Laboratoire de Physiologie Cellulaire et Végétale) for helpful technical support.

REFERENCES

Allen AE, Laroche J, Maheswari U, Lommer M, Schauer N, Lopez PJ, Finazzi G, Fernie AR, Bowler C (2008) Whole-cell response of the pennate diatom *Phaeodactylum tricornutum* to iron starvation. *Proc Natl Acad Sci USA* 105: 10438–10443

Alonso DL, Belarbi EH, Fernández-Sevilla JM, Rodríguez-Ruiz J, Molina Grima E (2000) Acyl lipid composition variation related to culture age and nitrogen concentration in continuous culture of the microalga *Phaeodactylum tricornutum*. *Phytochemistry* 54: 461–471

Andersson MX, Larsson KE, Tjellström H, Liljenberg C, Sandelius AS (2005) Phosphate-limited oat: the plasma membrane and the tonoplast as major targets for phospholipid-to-glycolipid replacement and stimulation of phospholipases in the plasma membrane. *J Biol Chem* 280: 27578–27586

Andersson MX, Stridh MH, Larsson KE, Liljenberg C, Sandelius AS (2003) Phosphate-deficient oat replaces a major portion of the plasma membrane phospholipids with the galactolipid digalactosyldiacylglycerol. *FEBS Lett* 537: 128–132

Araki S, Sakurai T, Kawaguchi A, Murata N (1987) Positional distribution of fatty acids in glycerolipids of the marine red alga, *Porphyra yezoensis*. *Plant Cell Physiol* 28: 761–766

Arao T, Kawaguchi A, Yamada M (1987) Positional distribution of fatty acids in lipids of the marine diatom *Phaeodactylum tricornutum*. *Phytochemistry* 26: 2573–2576

Armada I, Hachero-Cruzado I, Mazuelos N, Ríos JL, Manchado M, Cañavate JP (2013) Differences in betaine lipids and fatty acids between *Pseudoisochrysis paradoxa* VLP and *Diacronema vlkianum* VLP isolates (Haptophyta). *Phytochemistry* 95: 224–233

Armbrust EV, Berges JA, Bowler C, Green BR, Martinez D, Putnam NH, Zhou S, Allen AE, Apt KE, Bechner M, et al (2004) The genome of the diatom *Thalassiosira pseudonana*: ecology, evolution, and metabolism. *Science* 306: 79–86

Effect of nitrogen and phosphorus starvation in *Phaeodactylum tricornutum*.

Babiychuk E, Müller F, Eubel H, Braun HP, Frentzen M, Kushnir S (2003) Arabidopsis phosphatidylglycerophosphate synthase 1 is essential for chloroplast differentiation, but is dispensable for mitochondrial function. *Plant J* 33: 899–909

Bates PD, Browse J (2012) The significance of different diacylglycerol synthesis pathways on plant oil composition and bioengineering. *Front Plant Sci* 3: 147

Benning C, Ohta H (2005) Three enzyme systems for galactoglycerolipid biosynthesis are coordinately regulated in plants. *J Biol Chem* 280: 2397–2400

Bligh EG, Dyer WJ (1959) A rapid method of total lipid extraction and purification. *Can J Biochem Physiol* 37: 911–917

Botté CY, Yamaro-Botté Y, Janouskovec J, Rupasinghe T, Keeling PJ, Crellin P, Coppel RL, Maréchal E, McConville MJ, McFadden GI (2011) Identification of plant-like galactolipids in *Chromera velia*, a photosynthetic relative of malaria parasites. *J Biol Chem* 286: 29893–29903

Boudière L, Botté CY, Saidani N, Lajoie M, Marion J, Bréhélin L, Yamaro-Botté Y, Satiat-Jeunemaître B, Breton C, Girard-Egrot A, et al (2012) Galvestine-1, a novel chemical probe for the study of the glycerolipid homeostasis system in plant cells. *Mol Biosyst* 8: 2023–2035

Boudière L, Michaud M, Petroutsos D, Rébeillé F, Falconet D, Bastien O, Roy S, Finazzi G, Rolland N, Jouhet J, et al (2014) Glycerolipids in photosynthesis: composition, synthesis and trafficking. *Biochim Biophys Acta* 1837: 470–480

Bowler C, Allen AE, Badger JH, Grimwood J, Jabbari K, Kuo A, Maheswari U, Martens C, Maumus F, Ollilar RP, et al (2008) The *Phaeodactylum* genome reveals the evolutionary history of diatom genomes. *Nature* 456: 239–244

Brighouse A, Dacks JB, Field MC (2010) Rab protein evolution and the history of the eukaryotic endomembrane system. *Cell Mol Life Sci* 67: 3449–3465

Effect of nitrogen and phosphorus starvation in *Phaeodactylum tricornutum*.

Browse J, Warwick N, Somerville CR, Slack CR (1986) Fluxes through the prokaryotic and eukaryotic pathways of lipid synthesis in the '16:3' plant *Arabidopsis thaliana*. *Biochem J* 235: 25–31

Brügger B, Erben G, Sandhoff R, Wieland FT, Lehmann WD (1997) Quantitative analysis of biological membrane lipids at the low picomole level by nano-electrospray ionization tandem mass spectrometry. *Proc Natl Acad Sci USA* 94: 2339–2344

Camera E, Ludovici M, Galante M, Sinagra JL, Picardo M (2010) Comprehensive analysis of the major lipid classes in sebum by rapid resolution high-performance liquid chromatography and electrospray mass spectrometry. *J Lipid Res* 51: 3377–3388

Chauton MS, Winge P, Brembu T, Vadstein O, Bones AM (2013) Gene regulation of carbon fixation, storage, and utilization in the diatom *Phaeodactylum tricornutum* acclimated to light/dark cycles. *Plant Physiol* 161: 1034–1048

Cooksey KE, Guckert B, Williams SA, Callis PR (1987) Fluorometric determination of the neutral lipid content of microalgal cells using Nile Red. *J Microbiol Methods* 6: 333–345

Davidi L, Shimoni E, Khozin-Goldberg I, Zamir A, Pick U (2014) Origin of β -carotene-rich plastoglobuli in *Dunaliella bardawil*. *Plant Physiol* 164: 2139–2156

De Martino A, Meichenin A, Shi J, Pan K, Bowler C (2007) Genetic and phenotypic characterization of *Phaeodactylum tricornutum* (Bacillariophyceae) accessions. *J Phycol* 43: 992–1009

Dembitsky VM (1996) Betaine ether-linked glycerolipids: chemistry and biology. *Prog Lipid Res* 35: 1–51

Dodson VJ, Mouget JL, Dahmen JL, Leblond JD (2014) The long and short of it: temperature-dependent modifications of fatty acid chain length and unsaturation in the galactolipid profiles of the diatoms *Haslea ostrearia* and *Phaeodactylum tricornutum*. *Hydrobiologia* 727: 95–107

Effect of nitrogen and phosphorus starvation in *Phaeodactylum tricornutum*.

Domergue F, Spiekermann P, Lerchl J, Beckmann C, Kilian O, Kroth PG, Boland W, Zähringer U, Heinz E (2003) New insight into *Phaeodactylum tricornutum* fatty acid metabolism: cloning and functional characterization of plastidial and microsomal D12-fatty acid desaturases. *Plant Physiol* 131: 1648–1660

Domingues P, Amado FML, Santana-Marques MGO, Ferrer-Correia AJ (1998) Constant neutral loss scanning for the characterization of glycerol phosphatidylcholine phospholipids. *J Am Soc Mass Spectrom* 9: 1189–1195

Dorrell RG, Smith AG (2011) Do red and green make brown? Perspectives on plastid acquisitions within chromalveolates. *Eukaryot Cell* 10: 856–868

Dubots E, Audry M, Yamaryo Y, Bastien O, Ohta H, Breton C, Maréchal E, Block MA (2010) Activation of the chloroplast monogalactosyl-diacylglycerol synthase MGD1 by phosphatidic acid and phosphatidyl-glycerol. *J Biol Chem* 285: 6003–6011

Dubots E, Botté C, Boudière L, Yamaryo-Botté Y, Jouhet J, Maréchal E, Block MA (2012) Role of phosphatidic acid in plant galactolipid synthesis. *Biochimie* 94: 86–93

Dyhrman ST, Jenkins BD, Ryneerson TA, Saito MA, Mercier ML, Alexander H, Whitney LP, Drzewianowski A, Bulygin VV, Bertrand EM, et al (2012) The transcriptome and proteome of the diatom *Thalassiosira pseudonana* reveal a diverse phosphorus stress response. *PLoS ONE* 7: e33768

Falciatore A, d'Alcalà MR, Croot P, Bowler C (2000) Perception of environmental signals by a marine diatom. *Science* 288: 2363–2366

Fan J, Andre C, Xu C (2011) A chloroplast pathway for the de novo biosynthesis of triacylglycerol in *Chlamydomonas reinhardtii*. *FEBS Lett* 585: 1985–1991

Frentzen M, Heinz E, McKeon TA, Stumpf PK (1983) Specificities and selectivities of glycerol-3-phosphate acyltransferase and monoacylglycerol-3-phosphate acyltransferase from pea and spinach chloroplasts. *Eur J Biochem* 129: 629–636

Effect of nitrogen and phosphorus starvation in *Phaeodactylum tricornutum*.

Gage DA, Huang ZH, Benning C (1992) Comparison of sulfoquinovosyl diacylglycerol from spinach and the purple bacterium *Rhodobacter sphaeroides* by fast atom bombardment tandem mass spectrometry. *Lipids* 27: 632–636

Gaude N, Bréhélin C, Tischendorf G, Kessler F, Dörmann P (2007) Nitrogen deficiency in *Arabidopsis* affects galactolipid composition and gene expression and results in accumulation of fatty acid phytol esters. *Plant J* 49: 729–739

Genty B, Harbinson J, Briantais JM, Baker NR (1990) The relationship between non-photochemical quenching of chlorophyll fluorescence and the rate of photosystem 2 photochemistry in leaves. *Photosynth Res* 25: 249–257

Giroud C, Gerber A, Eichenberger W (1988) Lipids of *Chlamydomonas reinhardtii*: analysis of molecular species and intracellular site(s) of biosynthesis. *Plant Cell Physiol* 29: 587–595

Guella G, Frassanito R, Mancini I (2003) A new solution for an old problem: the regiochemical distribution of the acyl chains in galactolipids can be established by electrospray ionization tandem mass spectrometry. *Rapid Commun Mass Spectrom* 17: 1982–1994

Guschina IA, Harwood JL (2006) Lipids and lipid metabolism in eukaryotic algae. *Prog Lipid Res* 45: 160–186

Hagio M, Sakurai I, Sato S, Kato T, Tabata S, Wada H (2002) Phosphatidylglycerol is essential for the development of thylakoid membranes in *Arabidopsis thaliana*. *Plant Cell Physiol* 43: 1456–1464

Hecky RE, Kilham P (1988) Nutrient limitation of phytoplankton in freshwater and marine environments. *Limnol Oceanogr* 33: 786–822

Hsu FF, Turk J (2000a) Characterization of phosphatidylethanolamine as a lithiated adduct by triple quadrupole tandem mass spectrometry with electrospray ionization. *J Mass Spectrom* 35: 595–606

Effect of nitrogen and phosphorus starvation in *Phaeodactylum tricornutum*.

Hsu FF, Turk J (2000b) Characterization of phosphatidylinositol, phosphatidylinositol-4-phosphate, and phosphatidylinositol-4,5-bisphosphate by electrospray ionization tandem mass spectrometry: a mechanistic study. *J Am Soc Mass Spectrom* 11: 986–999

Hsu FF, Turk J (2001) Studies on phosphatidylglycerol with triple quadrupole tandem mass spectrometry with electrospray ionization: fragmentation processes and structural characterization. *J Am Soc Mass Spectrom* 12: 1036–1043

Hsu FF, Turk J (2003) Electrospray ionization/tandem quadrupole mass spectrometric studies on phosphatidylcholines: the fragmentation processes. *J Am Soc Mass Spectrom* 14: 352–363

Hsu FF, Turk J (2010) Electrospray ionization multiple-stage linear ion-trap mass spectrometry for structural elucidation of triacylglycerols: assignment of fatty acyl groups on the glycerol backbone and location of double bonds. *J Am Soc Mass Spectrom* 21: 657–669

Jouhet J, Dubots E, Maréchal E, Block MA (2010) Lipid trafficking in plant photosynthetic cells. In H Wada, N Murata, eds, *Lipids in Photosynthesis*, Vol 30. Springer, Dordrecht, The Netherlands, pp 349–372

Jouhet J, Maréchal E, Baldan B, Bligny R, Joyard J, Block MA (2004) Phosphate deprivation induces transfer of DGDG galactolipid from chloroplast to mitochondria. *J Cell Biol* 167: 863–874

Jouhet J, Maréchal E, Bligny R, Joyard J, Block MA (2003) Transient increase of phosphatidylcholine in plant cells in response to phosphate deprivation. *FEBS Lett* 544: 63–68

Jouhet J, Maréchal E, Block MA (2007) Glycerolipid transfer for the building of membranes in plant cells. *Prog Lipid Res* 46: 37–55

Effect of nitrogen and phosphorus starvation in *Phaeodactylum tricornutum*.

Khozin I, Adlerstein D, Bigongo C, Heimer YM, Cohen Z (1997) Elucidation of the biosynthesis of eicosapentaenoic acid in the microalga *Porphyridium cruentum*: II. Studies with radiolabeled precursors. *Plant Physiol* 114: 223–230

Khozin-Goldberg I, Didi-Cohen S, Shayakhmetova I, Cohen Z (2002) Biosynthesis of eicosapentaenoic acid (EPA) in the fresh water eustigmatophyte *Monodus subterraneus* (Eustigmatophyceae). *J Phycol* 38: 745–756

Kroth PG, Chiovitti A, Gruber A, Martin-Jezequel V, Mock T, Parker MS, Stanley MS, Kaplan A, Caron L, Weber T, et al (2008) A model for carbohydrate metabolism in the diatom *Phaeodactylum tricornutum* deduced from comparative whole genome analysis. *PLoS ONE* 3: e1426

Künzler K, Eichenberger W, Radunz A (1997) Intracellular localization of two betaine lipids by cell fractionation and immunomicroscopy. *Z Naturforsch C* 52: 487–495

Levitan O, Dinamarca J, Hochman G, Falkowski PG (2014) Diatoms: a fossil fuel of the future. *Trends Biotechnol* 32: 117–124

Li X, Moellering ER, Liu B, Johnny C, Fedewa M, Sears BB, Kuo MH, Benning C (2012) A galactoglycerolipid lipase is required for triacylglycerol accumulation and survival following nitrogen deprivation in *Chlamydomonas reinhardtii*. *Plant Cell* 24: 4670–4686

Li Y, Han D, Sommerfeld M, Hu Q (2011) Photosynthetic carbon partitioning and lipid production in the oleaginous microalga *Pseudochlorococum* sp. (Chlorophyceae) under nitrogen-limited conditions. *Bioresour Technol* 102: 123–129

Liang Y, Maeda Y, Yoshino T, Matsumoto M, Tanaka T (2014) Profiling of polar lipids in marine oleaginous diatom *Fistulifera solaris* JPC DA0580: prediction of the potential mechanism for eicosapentaenoic acid-incorporation into triacylglycerol. *Mar Drugs* 12: 3218–3230

Effect of nitrogen and phosphorus starvation in *Phaeodactylum tricornutum*.

Li-Beisson Y, Shorrosh B, Beisson F, Andersson MX, Arondel V, Bates PD, Baud S, Bird D, Debono A, Durrett TP, et al (2010) Acyl-lipid metabolism. *The Arabidopsis Book* 8: e0133, doi/10.1199/tab.0161

Litchman E, Klausmeier CA, Yoshiyama K (2009) Contrasting size evolution in marine and freshwater diatoms. *Proc Natl Acad Sci USA* 106: 2665–2670

Löfke C, Ischebeck T, König S, Freitag S, Heilmann I (2008) Alternative metabolic fates of phosphatidylinositol produced by phosphatidylinositol synthase isoforms in *Arabidopsis thaliana*. *Biochem J* 413: 115–124

Maheswari U, Mock T, Armbrust EV, Bowler C (2009) Update of the Diatom EST Database: a new tool for digital transcriptomics. *Nucleic Acids Res* 37: D1001–D1005

Maheswari U, Montsant A, Goll J, Krishnasamy S, Rajyashri KR, Patell VM, Bowler C (2005) The Diatom EST Database. *Nucleic Acids Res* 33: D344–D347

Maréchal E, Block MA, Joyard J, Douce R (1994) Kinetic properties of monogalactosyldiacylglycerol synthase from spinach chloroplast envelope membranes. *J Biol Chem* 269: 5788–5798

Martin P, Dyhrman ST, Lomas MW, Poulton NJ, Van Mooy BAS (2014) Accumulation and enhanced cycling of polyphosphate by Sargasso Sea plankton in response to low phosphorus. *Proc Natl Acad Sci USA* 111: 8089–8094

Mills MM, Ridame C, Davey M, La Roche J, Geider RJ (2004) Iron and phosphorus co-limit nitrogen fixation in the eastern tropical North Atlantic. *Nature* 429: 292–294

Misson J, Raghothama KG, Jain A, Jouhet J, Block MA, Bligny R, Ortet P, Creff A, Somerville S, Rolland N, et al (2005) A genome-wide transcriptional analysis using *Arabidopsis thaliana* Affymetrix gene chips determined plant responses to phosphate deprivation. *Proc Natl Acad Sci USA* 102: 11934–11939

Mongrand S, Bessoule JJ, Cabantous F, Cassagne C (1998) The C16:3/C18: 3 fatty acid balance in photosynthetic tissues from 468 plant species. *Phytochemistry* 49: 1049–1064

Effect of nitrogen and phosphorus starvation in *Phaeodactylum tricornutum*.

Montsant A, Maheswari U, Bowler C, Lopez PJ (2005) Diatomics: toward diatom functional genomics. *J Nanosci Nanotechnol* 5: 5–14

Moore C, Mills M, Arrigo K, Berman-Frank I, Bopp L, Boyd P, Galbraith E, Geider R, Guieu C, Jaccard S, et al (2013) Processes and patterns of oceanic nutrient limitation. *Nat Geosci* 6: 701–710

Moore TS, Du Z, Chen Z (2001) Membrane lipid biosynthesis in *Chlamydomonas reinhardtii*: in vitro biosynthesis of diacylglyceryltrimethylhomoserine. *Plant Physiol* 125: 423–429

Morcuende R, Bari R, Gibon Y, Zheng W, Pant BD, Bläsing O, Usadel B, Czechowski T, Udvardi MK, Stitt M, et al (2007) Genome-wide re-programming of metabolism and regulatory networks of *Arabidopsis* in response to phosphorus. *Plant Cell Environ* 30: 85–112

Moreau RA, Doehlert DC, Welti R, Isaac G, Roth M, Tamura P, Nuñez A (2008) The identification of mono-, di-, tri-, and tetragalactosyl-diacylglycerols and their natural estolides in oat kernels. *Lipids* 43: 533–548

Müller F, Frentzen M (2001) Phosphatidylglycerophosphate synthases from *Arabidopsis thaliana*. *FEBS Lett* 509: 298–302

Nakamura Y (2013) Phosphate starvation and membrane lipid remodeling in seed plants. *Prog Lipid Res* 52: 43–50

Naumann I, Klein BC, Bartel SJ, Darsow KH, Buchholz R, Lange HA (2011) Identification of sulfoquinovosyldiacylglycerides from *Phaeodactylum tricornutum* by matrix-assisted laser desorption/ionization QTrap time-of-flight hybrid mass spectrometry. *Rapid Commun Mass Spectrom* 25: 2517–2523

Nunn BL, Aker JR, Shaffer SA, Tsai S, Strzepak RF, Boyd PW, Freeman TL, Brittnacher M, Malmström L, Goodlett DR (2009) Deciphering diatom biochemical pathways via whole-cell proteomics. *Aquat Microb Ecol* 55: 241–253

Effect of nitrogen and phosphorus starvation in *Phaeodactylum tricornutum*.

Petroutsos D, Amiar S, Abida H, Dolch LJ, Bastien O, Rébeillé F, Jouhet J, Falconet D, Block MA, McFadden GI, et al (2014) Evolution of galactoglycerolipid biosynthetic pathways: from cyanobacteria to primary plastids and from primary to secondary plastids. *Prog Lipid Res* 54: 68–85

Prihoda J, Tanaka A, de Paula WBM, Allen JF, Tirichine L, Bowler C (2012) Chloroplast-mitochondria cross-talk in diatoms. *J Exp Bot* 63: 1543–1557

Rezanka T, Lukavský J, Nedbalová L, Sigler K (2011) Effect of nitrogen and phosphorus starvation on the polyunsaturated triacylglycerol composition, including positional isomer distribution, in the alga *Trachydiscus minutus*. *Phytochemistry* 72: 2342–2351

Riekhof WR, Naik S, Bertrand H, Benning C, Voelker DR (2014) Phosphate starvation in fungi induces the replacement of phosphatidylcholine with the phosphorus-free betaine lipid diacylglyceryl-N,N,N-trimethylhomoserine. *Eukaryot Cell* 13: 749–757

Riekhof WR, Ruckle ME, Lydic TA, Sears BB, Benning C (2003) The sulfolipids 29-O-acyl-sulfoquinovosyldiacylglycerol and sulfoquinovo-syldiacylglycerol are absent from a *Chlamydomonas reinhardtii* mutant deleted in SQD1. *Plant Physiol* 133: 864–874

Riekhof WR, Sears BB, Benning C (2005) Annotation of genes involved in glycerolipid biosynthesis in *Chlamydomonas reinhardtii*: discovery of the betaine lipid synthase BTA1Cr. *Eukaryot Cell* 4: 242–252

Sandelius AS, Andersson MX, Goksor M, Tjellstrom H, Wellander R (2007) Membrane contact sites: physical attachment between chloroplasts and endoplasmic reticulum revealed by optical manipulation. *Chem Phys Lipids* 149: S42–S43

Sapriel G, Quinet M, Heijde M, Jourden L, Tanty V, Luo G, Le Crom S, Lopez PJ (2009) Genome-wide transcriptome analyses of silicon metabolism in *Phaeodactylum tricornutum* reveal the multilevel regulation of silicic acid transporters. *PLoS ONE* 4: e7458

Sato N, Murata N (1991) Transition of lipid phase in aqueous dispersions of diacylglyceryltrimethylhomoserine. *Biochim Biophys Acta* 1082: 108–111

Effect of nitrogen and phosphorus starvation in *Phaeodactylum tricornutum*.

Scala S, Bowler C (2001) Molecular insights into the novel aspects of diatom biology. *Cell Mol Life Sci* 58: 1666–1673

Shimojima M, Ohta H (2011) Critical regulation of galactolipid synthesis controls membrane differentiation and remodeling in distinct plant organs and following environmental changes. *Prog Lipid Res* 50: 258–266

Shrestha RP, Tesson B, Norden-Krichmar T, Federowicz S, Hildebrand M, Allen AE (2012) Whole transcriptome analysis of the silicon response of the diatom *Thalassiosira pseudonana*. *BMC Genomics* 13: 499

Simionato D, Block MA, La Rocca N, Jouhet J, Maréchal E, Finazzi G, Morosinotto T (2013) The response of *Nannochloropsis gaditana* to nitrogen starvation includes de novo biosynthesis of triacylglycerols, a decrease of chloroplast galactolipids, and reorganization of the photo-synthetic apparatus. *Eukaryot Cell* 12: 665–676

Taguchi R, Houjou T, Nakanishi H, Yamazaki T, Ishida M, Imagawa M, Shimizu T (2005) Focused lipidomics by tandem mass spectrometry. *J Chromatogr B Analyt Technol Biomed Life Sci* 823: 26–36

Tanoue R, Kobayashi M, Katayama K, Nagata N, Wada H (2014) Phosphatidylglycerol biosynthesis is required for the development of embryos and normal membrane structures of chloroplasts and mitochondria in *Arabidopsis*. *FEBS Lett* 588: 1680–1685

Tjellström H, Andersson MX, Larsson KE, Sandelius AS (2008) Membrane phospholipids as a phosphate reserve: the dynamic nature of phospholipid-to-digalactosyl diacylglycerol exchange in higher plants. *Plant Cell Environ* 31: 1388–1398

Van Mooy BAS, Fredricks HF, Pedler BE, Dyhrman ST, Karl DM, Koblížek M, Lomas MW, Mincer TJ, Moore LR, Moutin T, et al (2009) Phytoplankton in the ocean use non-phosphorus lipids in response to phosphorus scarcity. *Nature* 458: 69–72

Effect of nitrogen and phosphorus starvation in *Phaeodactylum tricornutum*.

Vogel G, Eichenberger W (1992) Betaine lipids in lower plants: biosynthesis of DGTS and DGTA in *Ochromonas danica* (Chrysophyceae) and the possible role of DGTS in lipid metabolism. *Plant Cell Physiol* 33: 427–436

Welti R, Wang X, Williams TD (2003) Electrospray ionization tandem mass spectrometry scan modes for plant chloroplast lipids. *Anal Biochem* 314: 149–152

Xu C, Härtel H, Wada H, Hagio M, Yu B, Eakin C, Benning C (2002) The *pgp1* mutant locus of *Arabidopsis* encodes a phosphatidylglycerolphosphate synthase with impaired activity. *Plant Physiol* 129: 594–604

Yang ZK, Zheng JW, Niu YF, Yang WD, Liu JS, Li HY (2014) Systems-level analysis of the metabolic responses of the diatom *Phaeodactylum tricornutum* to phosphorus stress. *Environ Microbiol* 16: 1793–1807

Yongmanitchai W, Ward OP (1993) Positional distribution of fatty acids, and molecular species of polar lipids, in the diatom *Phaeodactylum tricornutum*. *J Gen Microbiol* 139: 465–472

Zendejas FJ, Benke PI, Lane PD, Simmons BA, Lane TW (2012) Characterization of the acylglycerols and resulting biodiesel derived from vegetable oil and microalgae (*Thalassiosira pseudonana* and *Phaeodactylum tricornutum*). *Biotechnol Bioeng* 109: 1146–1154

Zhou Y, Peisker H, Weth A, Baumgartner W, Dörmann P, Frentzen M (2013) Extraplasmidial cytidinediphosphate diacylglycerol synthase activity is required for vegetative development in *Arabidopsis thaliana*. *Plant J* 75: 867–879

Zianni R, Bianco G, Lelario F, Losito I, Palmisano F, Cataldi TR (2013) Fatty acid neutral losses observed in tandem mass spectrometry with collision-induced dissociation allows regiochemical assignment of sulfoquinovosyl-diacylglycerols. *J Mass Spectrom* 48: 205–215

Supplemental Data

Supplemental Figure 4.S1

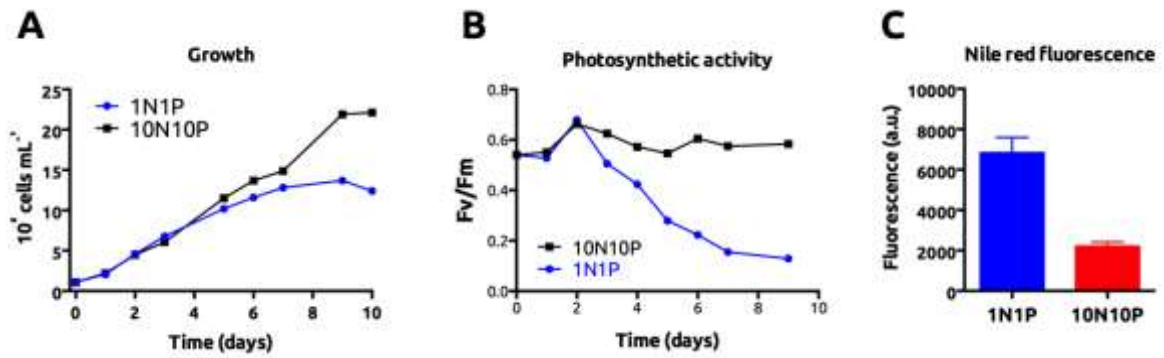


Figure 4.S1: Growth (A), photosynthetic activity (B) and intracellular lipid content as Nile Red fluorescence at day 5 (C) of Pt1 cells in medium containing 0.55 mM N and 0.0224 mM P (1N1P) or 5.5 mM N and 0.224 mM P (10N10P). Abbreviation: a.u., fluorescence arbitrary units.

Supplemental Figure 4.S2

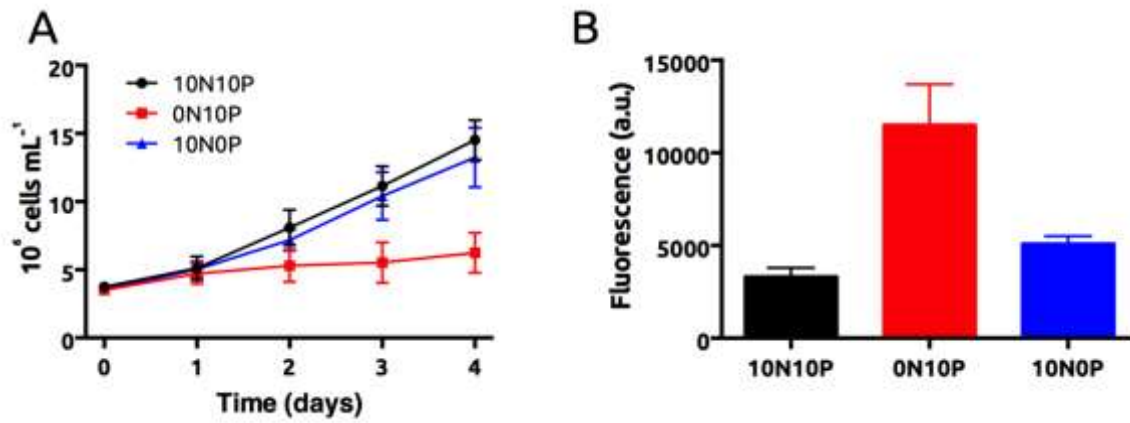


Figure 4.S2: Growth (A) and Nile Red fluorescence at day 4 (B) of Pt1 cells in replete (10N10P), nitrogen depleted (0N10P) and phosphorus depleted (10N0P) media. Abbreviation: a.u., fluorescence arbitrary units.

Supplemental Figure 4.S3

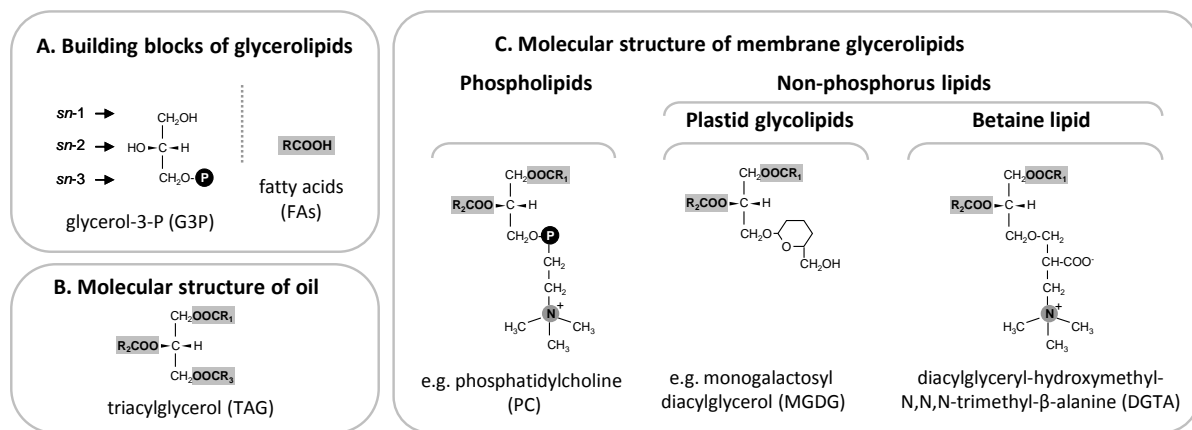


Figure 4.S3: The major glycerolipids. (A) Building blocks. Acyl-glycerolipids are synthesised by esterification of a glycerol backbone originating from glycerol-3-P (G3P) by fatty acids (FAs). (B) Molecular structure of oil. Oil or triacylglycerols (TAG) contain three fatty acids (R_1 , R_2 , R_3) at positions $sn-1$, $sn-2$ and $sn-3$ of the glycerol backbone. (C) Molecular structure of membrane glycerolipids. Membrane glycerolipids (C) contain two fatty acids (R_1 , R_2) at positions $sn-1$ and $sn-2$ and a phosphorus-containing or phosphorus-free polar head at position $sn-3$.

Supplemental Figure 4.S4

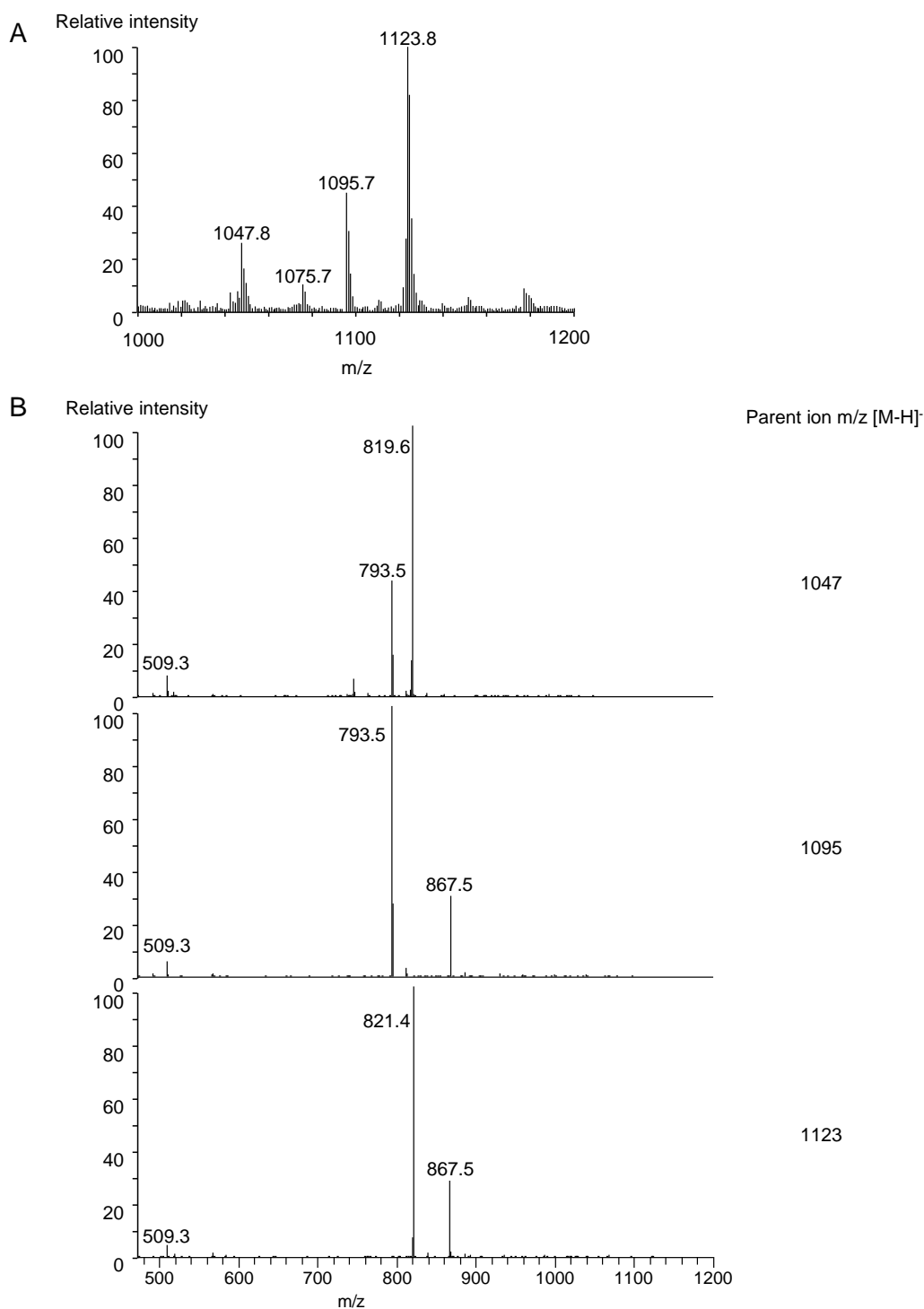


Figure 4.S4: Structural characterization of acyl-SQDG. (A) Full scan LC-MS analysis of the acyl-SQDG spot isolated by two-dimensional thin layer chromatography (see Methods) in negative mode. (B) MS² fragmentation of the 1045, 1095 and 1123 m/z ions. The two main fragments correspond to the loss of the fatty acid ([M-R_{1/2}COOH]⁻) that were used for the regiolocalisation. The 509 m/z fragment corresponds to the 20:5 acylated sulfoquinovose as described by Naumann *et al.*, (2011) and was detected in every acyl-SQDG mass tested.

4.6 Conclusion and remarks

This work represents the first reference of the glycerolipidomic of *Phaeodactylum* (*i.e.* Pt1) under different nitrogen and phosphorus supplies. Thanks to the lipidomic analysis, the main lipid classes (*i.e.* MGDG, DGDG, SQDG, PG, PC etc) were detected and this allows to implement the knowledges on the mechanism of TAG triggered by nutrients starvation. Overall, both N and P starvation triggers TAG accumulation but this happens in different timing and mechanism. In general, the N limitation has a bigger impact in cell physiology (*i.e.* arrest of growth and decrease of F_v/F_m) and in a short time the cells start to produce TAGs. In this condition, the TAG are mostly produced by neo-synthesis pathways (*i.e.* high levels of 16:0 and 16:1 fatty acids). However, TAG can also be produced from the interconversion of membrane lipids as shown from the decrease of one of main constituent of thylakoid membrane, *i.e.* MGDG (confirming the results in Alipanah *et al.*, 2015). Most interestingly, cells did not show any decrease in photosynthesis efficiency, under P limitation, and continue to grow during the first days of culture. This can be explained for the presence of polyphosphate storage within *Phaeodactylum* (Leitao *et al.*, 1995). In a second phase (*i.e.* after 8 days), the cells start to degrade phospholipids PG, PE, PI and PC (*i.e.* not detected in this analysis in cells grown without P) in order to recycle the phosphate and to accumulate TAG. These results are similar with the finding of the degradation of extraplastic membrane in $-P$ stressed cells in Yang *et al.*, 2014. We, hence, assume that under P starvation the TAG are produced by recycling extraplastic membrane lipids (*i.e.* PG, PE, PI and PC).

TAGs accumulation has been also investigated by comparing the different ecotypes of *Phaeodactylum* using Nile Red fluorescence as a proxy for TAG accumulation. This analysis showed interesting differences on the response to nutrients starvation. Further work should entail the genetically characterization of these ecotypes in order to help on understanding these results taking advantage of their natural biodiversity. Indeed, the discovery of a natural NPQ mutant in *Phaeodactylum* (*i.e.* ecotype Pt4) helps to understand the role of LHCX1 in photoprotection process (Bailleul *et al.*, 2010). Following the same rationale, it would be also interesting to screen the mixotrophic growth in the different ecotypes of *Phaeodactylum*. Ecotypes with increased or decreased mixotrophic capacity could reveal interesting genes involved in this trophic mode (*i.e.* sugar transporter) and hence better understand this mechanism.

Effect of nitrogen and phosphorus starvation in *Phaeodactylum tricornutum*.

This study together with the previous work (Villanova *et al.*,) provides a detailed scenario of *P. tricornutum* acclimation to nutrient deprivation (in both phototrophic and mixotrophic mode), and can be used as a model for future metabolic engineering to increase TAG production.

Chapter 5

Final Conclusions and remarks

Diatoms play a key role in the ecology of the planet, since they are responsible for 20-40% of the global carbon fixation. They also represent a potential feedstock for high-value molecules, since they are able to accumulate large amount of triacylglycerols, which can be used for the production of biofuel. Indeed, microalgal-derived oil is a possible alternative to petroleum for the production of fuel, because of the lower land area requirement for microalgal cultivation, when compared to vegetable crops (Yusuf 2007). However, under strict phototrophic regime the biomass productivity of diatoms is still not compatible with industrial standards. Several diatoms, due to their historical evolution, are able to combine photosynthesis and respiration for growth (mixotrophic metabolism), and to enhance both lipid and biomass productivity (García *et al.*, 2000; 2005; 2006; Kitano *et al.*, 1997). As shown in chapter 3, when algae are supplemented with a carbon source the light intensity required for optimum biomass production is lower. This is a promising result, which could reduce the industrial costs of growth in photobioreactors.

For all these reasons, the cultivation under mixotrophic regime is of major interest for biofuel production in diatoms (Wang *et al.*, 2012). However, the metabolic consequences and the mechanism behind this process are still poorly understood in these organisms. In this study, the pennate *P. tricornutum*, for which we have the whole genome sequenced, and genetic engineering tools, has been used as model organism to explore the potential of mixotrophic metabolism using a multi-disciplinary approach. In particular, in Bailleul *et al.*, 2015 (presented in chapter 2) a wide range of biophysical tools have been used to clarify the base of chloroplast-mitochondria interaction in diatoms. These analyses revealed that the reducing power (*i.e.* NADPH) generated during the photosynthesis is exported to the mitochondria, and the ATP produced during the oxidative respiration is redirected towards to the chloroplast. The communication between these two organelles is crucial for carbon fixation and growth in *Phaeodactylum*. In addition, the involvement of mitochondrial respiration in optimising the photosynthesis process was confirmed in other diatoms

(*Thalassiosira pseudonana*, *T. weissflogii*, *Fragilaria pinnata* and *Ditylum brightwellii*). These findings could explain the ecological success of diatoms on the oceans. Based on these results we decided to study the consequences of the mixotrophic growth on the metabolism of *Phaeodactylum*. In Villanova *et al.*, (presented in the chapter 3) the effect of glycerol addition in the diatom was tested by combining omics and biophysical analyses. Here, we found that the glycerol (selected because it is cheap and abundant) not only stimulates growth and lipid production but also the carbon storage metabolism. Since this pathway is in competition with lipid production, our results suggest that mixotrophy could represent a possible solution to further increase TAG accumulation in lines engineered with reduced accumulation of chrysolaminarin (*i.e.* the main storage carbohydrate of diatoms, Daboussi *et al.*, 2014). In our study, two others metabolites involved in carbon storage metabolism (*i.e.* trehalose and mannitol) were found to be upregulated by glycerol. Therefore, inhibition of the biosynthetic pathway of these compounds by metabolic engineering could also enhance the effect of glycerol in TAG accumulation.

Another relevant outcome of this study is the optimisation of the growth medium based on the elemental balancing of biomass and medium composition (Mandalam and Palsson 1998; Danquah *et al.*, 2010). This approach allows designing a medium specific for the microalgae of interest, and obtains higher-density cultures with a relatively low additional cost. Hence, the optimisation of the medium composition is a crucial step for the industrial exploitation of microalgae. Here, the new medium (ESAW enriched) enhanced the growth capacity of *Phaeodactylum* (in particular under mixotrophic mode) and the production of high value molecules, *i.e.* lipids and pigments.

It is interesting to note that the microelements (*i.e.* Cu, Mn, Zn) are the most limiting elements for the growth of *Phaeodactylum*. Indeed, these metals (present only in trace in seawater) play a vital role as enzyme cofactors in important pathways such as photosynthesis, respiration and carbon fixation in microalgae. This suggests a potential use of these elements to others microalgae culture for enhancing their growth capacities. The performances of the mixotrophic metabolism in *Phaeodactylum* were further optimised by the addition of both inorganic (bicarbonate) and organic source (glycerol). In fact, whereas the bicarbonate addition (converted to CO₂ thanks to the presence of concentrating mechanisms in diatoms) can enhance the photosynthetic activity in the chloroplast, the glycerol can activate the respiration in the mitochondrion (*i.e.* via glycolysis and TCA). Our findings demonstrate that

the simultaneous optimisation of these two processes is crucial for carbon fixation and growth in *Phaeodactylum*, confirming the hypothesis developed in Bailleul *et al.*, 2015. The works Villanova *et al.*, and Bailleul *et al.*, contribute to the understanding of the possible mechanism of mixotrophy. However, not all the metabolites and transports involved in the interaction between mitochondrion and chloroplast have been identified. In particular, all the omics analyses (Villanova *et al.*,) have been performed in the initial conditions where glycerol consumption and mixotrophic efficiency were very low. Repeating these analyses under optimised conditions could allow detecting a stronger effect of glycerol on metabolism, helping to a better characterization of this process. Similarly, the biophysical analyses (Bailleul *et al.*, 2015) have only been performed in phototrophic cultures. Based on these new results, it would be interesting to study the energetic interactions of plastids and mitochondria in presence of a carbon source. Furthermore, during my Ph.D various mutant lines (both overexpressing and knock downing) have been generated, which were not been fully characterized, and hence, are not presented in this Ph.D thesis. The target genes for metabolic engineering were selected by combining microarray analysis, to genome-based analysis. Amongst these, two genes are extremely interesting and could play an important role in the mixotrophic metabolism of *Phaeodactylum*: *i*) Glycerol-3P transporter (PHATRDRAFT_43611), and *ii*) succinate-fumarate antiporter (PHATRDRAFT_23709). The first has a role in the transport of cytosolic reducing equivalents to the mitochondria in yeast, animal and plant systems (Ansell *et al.*, 1997; Larsson *et al.*, 1998; Rigoulet *et al.*, 2004; Shen *et al.*, 2006). This likely occurs via the action of a cytoplasmic NAD-dependent gly-3P dehydrogenase that converts the DHAP into gly 3-P by oxidizing one molecule of NADH to NAD⁺. Gly 3-P can be imported into the mitochondrion through the gly-3P transporter. The reverse path is catalysed by a FAD-dependent mitochondrial gly-3-P dehydrogenase that transfers the electrons to the quinone pool that enter in oxidative phosphorylation. In *Phaeodactylum*, 2 classes of NAD-gly-3-P dehydrogenases are present in the genome (PHATRDRAFT_8975; PHATR_36821) but any FAD-gly-3-P dehydrogenase has been identified so far. Moreover, the subcellular localization of the glycerol-3-P transporter is still unknown. It would be interesting to determine the localization of this shuttle by generating a transgenic line bearing the fusion of the gene of interest to cyan fluorescent protein (CFP) or yellow fluorescent protein (YFP). The characterization of this mutant line and the transporter-overexpressing mutant

(generated during this project) could help to understand if similar pathway can be found in the diatom.

The succinate-fumarate antiporter has been found in both plant and yeast (Catoni *et al.*, 2003; Pallotta *et al.*, 1999). In particular, in plant this carrier seems to regulate the conversion of storage lipids to soluble carbohydrates during germination. Pallotta *et al.*, found that the succinate can be produced by the β -oxidation of fatty acids via glyoxylate cycle that can enter the mitochondrion through the succinate-fumarate antiporter and be converted to fumarate via TCA cycle. The fumarate exported by the mitochondria can be then converted to malate in the cytosol by a fumarase, and enters the gluconeogenesis pathway. However, it seems that this shuttle system involves energetic exchanges between cytosol and mitochondria and not between chloroplast and mitochondria. In *Phaeodactylum*, the TCA is localized in the mitochondria but some isoenzymes may have a cytosolic localization (similarly to plant and yeast metabolism). In fact, 2 classes of fumarases (PHATRDRRAFT_36139, PHATRDRRAFT_19708) are present in the genome of *Phaeodactylum* but their localization has not been studied. The presence of this transporter, together with our findings that the fumarate can be used by *Phaeodactylum* to grow in mixotrophy, suggest that these molecules could be involved in the regulation of reducing power. The characterization of the knock-down mutant of this shuttle (generated in this project) via ECS analysis can answer this question. In addition, the localization of the fumarate isoenzymes is also important to understand if the pathway described above is conserved in the diatom or a different mechanism is present.

In this study, it was also showed that the glycerol addition can be used as an alternative to nutrient starvation for increasing TAG production. In fact, thanks to the comparison of the results obtained in Abida *et al.*, (see chapter 4) and Villanova *et al.*, (see chapter 3) it was possible to clarify the pathways that trigger the TAG production in the two conditions: nutrient starvation vs mixotrophic metabolism. The addition of glycerol leads to an increase of TAG production (mainly derived from neosynthesis pathway) in N replete condition without altering the photosynthetic performance of the diatom and enhancing growth. By contrast, in N deplete condition the cells stop to grow, the cellular components are degraded in favor of basic needs and TAG accumulation is due to both membrane glycerolipids recycling and neosynthesis pathway. The mixotrophic metabolism leads to increase the biomass productivity and hence the final lipids quantity. Moreover, both the studies help to elucidate

the main routes involved in the TAG biosynthesis and can be used as models for future metabolic engineering to obtain the targeted fatty acid profile.

The final step of my PhD thesis focused on the up-scaling of the optimised conditions in lab scale photobioreactors to test the potential of the industrial exploitation of *Phaeodactylum*. In these experiments, 2-L photobioreactors cultivation has been selected as the best way to grow mixotrophically the diatom in axenic conditions and under controlled system (pH, temperature, mixing/aeration). This system allows to further improving the performance of the mixotrophic growth of *Phaeodactylum*, reaching a final biomass concentration of about 12 g/L. This was obtained growing the diatom to relative low light intensity (about 300 $\mu\text{E}/\text{m}^2/\text{s}$), the increase of light could increase the biomass productivity. Of course, the up-scaling of improved strains is another attractive alternative to be tested.

To conclude, this project brings together several approaches (omics analyses, biophysical approaches, physiology and culture processes) working in between basic research and industrial R&D. This experience taught me that only the understanding of the entire biological system may lead to an efficient optimisation of the process, making possible the industrial exploitation of microalgae. Moreover, the fact that this project was included in a European project allowed me to participate to different conferences (*e.g.* Molecular Life of Diatoms, Seattle; ENCAPP and YAS, Malta), workshops (*e.g.* Proteomics; Spectrometric analysis; Metabolic modelling analysis), to collaborate with others members of the consortium (*e.g.* UMPC, Paris; CNRS, Grenoble; Institute Max Plank, Potsdam; University of Oxford) and to be seconded in others laboratories (*e.g.* UPMC, Paris and CEA, Grenoble). These have led to my professional and personal development.

References

Abida, H. et al., Membrane glycerolipid remodeling triggered by nitrogen and phosphorus starvation in *Phaeodactylum tricornutum*. *Plant Physiol.* **167**, 118–36 (2015).

Alipanah, L., Rohloff, J., Winge, P., Bones, A. M. & Brembu, T. Whole-cell response to nitrogen deprivation in the diatom *Phaeodactylum tricornutum*. *J. Exp. Bot.* **66**, 6281–6296 (2015).

Allen, A. E. et al., Evolution and metabolic significance of the urea cycle in photosynthetic diatoms. *Nature* **473** VN - , 203–207 (2011).

Allen, A. E., Laroche, J., Maheswari, U., Lommer, M., Schauer, N., Lopez, PJ, Finazzi, G., Fernie, AR, Bowler, C. Whole-cell response of the pennate diatom *Phaeodactylum tricornutum* to iron starvation. *Proc. Natl. Acad. Sci. U. S. A.* **105**, 10438–10443 (2008).

Allen, C.F., O. Hirayama, P. Good, Lipid composition in photosynthetic systems. *Biochemistry of Chloroplasts*, **1**, 195–200 (1966).

Allen, J. F. Cyclic, pseudocyclic and noncyclic photophosphorylation: New links in the chain. *Trends in Plant Science* **8**, 15–19 (2003).

Allen, J. F. Photosynthesis of ATP-electrons, proton pumps, rotors, and poise. *Cell* **110**, 273–276 (2002).

Alonso, D. L., Belarbi, E. H., Fernandez-Sevilla, J. M., Rodriguez-Ruiz, J. & Grima, E. M. Acyl lipid composition variation related to culture age and nitrogen concentration in continuous culture of the microalga *Phaeodactylum tricornutum*. *Phytochemistry* (2000). doi:10.1016/S0031-9422(00)00084-4

Ansell, R., Granath, K., Hohmann, S., Thevelein, J.M., and Adler, L. The two isoenzyme for yeast NAD β -dependent glycerol 3-phosphate dehydrogenase encoded by GPD1 and GPD2 have distinct roles in osmoadaptation and redox regulation. *EMBO J.* **16**, 2179–2187 (1997).

Apt, K. E., Grossman, A. R., Kroth-Pancic, P. G. Grossman A. R. Stable nuclear transformation of the diatom *Phaeodactylum tricornutum*. *Mol Gen Genet.* **5**, 572–9 (1996).

References

- Armbrust, E. V. The life of diatoms in the world's oceans. *Nature* **459**, (2009).
- Armstrong, E., Rogerson, A. & Leftley, J. W. Utilisation of seaweed carbon by three surface-associated heterotrophic protists, *Stereomyxa ramosa*, *Nitzschia alba* and *Labyrinthula* sp. *Aquat. Microb. Ecol.* **21**, 49–57 (2000).
- Arnon, D. I., Allen, M. B. and Whatley, F. R. Photosynthesis by isolated chloroplasts. *Nature* **174**, 394-401 (1954).
- Asada, K. The water-water cycle as alternative photon and electron sinks. *Philos. Trans. R. Soc. Lond. B. Biol. Sci.* **355**, 1419–1431 (2000).
- Bailleul, B. et al. Energetic coupling between plastids and mitochondria drives CO₂ assimilation in diatoms. *Nature* **524**, 366–369 (2015).
- Bailleul, B. et al., An atypical member of the light-harvesting complex stress-related protein family modulates diatom responses to light. *Proc. Natl. Acad. Sci. U. S. A.* **107**, 18214–18219 (2010).
- Bailleul, B., Cardol, P., Breyton, C. & Finazzi, G. Electrochromism: a useful probe to study algal photosynthesis. *Photosynth. Res.* **106**, 179–189 (2010).
- Barber, H G; Hayworth, E. Y. A guide to the morphology of the Diatom Frustule. (1982).
- Bates, P. D. et al., Acyl editing and headgroup exchange are the major mechanisms that direct polyunsaturated fatty acid flux into triacylglycerols. *Plant Physiol.* **160**, 1530–1539 (2012).
- Beattie, Hirst, EL; Percival, E; et al. Studies on the metabolism of the Chrysophyceae. Comparative structural investigations on leucosin (chrysolaminarin) separated from diatoms and laminarin from the brown algae. *Biochem J.* **79** (3) 531–537 (1961).
- Bennoun, P. Evidence for a respiratory chain in the chloroplast. *Proc. Natl. Acad. Sci. U. S. A.* **79**, 4352–4356 (1982).
- Benson, A.A., H. Daniel, R. Wiser, A sulfolipid in plants, *Proc. Natl. Acad. Sci. U. S. A.*, **45**, 1582–1587 (1959).

References

Berkaloff, C., Caron, L. & Rousseau, B. Subunit organization of PSI particles from brown algae and diatoms: polypeptide and pigment analysis. *Photosynth. Res.* **23**, 181–193 (1990).

Bghme, H. & Kunert, K.-J. Photoreactions of Cytochromes in Algal Chloroplasts. *Eur. J. Biochem* **106**, 329–336 (1980).

Bligny, R. & Douce, R. NMR and plant metabolism. *Current Opinion in Plant Biology* **4**, 191–196 (2001).

Bohlin, K. Zur Morphologie und Biologie einzelliger Algen. *Fvers. Kongl. Vetens. Akad. Förh.* **9**, 507–529 (1897).

Bohme H, K. K. Photoreaction of cytochromes in algal chloroplasts. *Eur J Biochem* **106**, 329–336 (1980).

Borowitzka, M. a & Volcani, B. E. Polymorphic diatom *Phaeodactylum Tricornutum*: Ultrastructure of its morphotypes. *J. Phycol.* 10–21 (1978). doi:10.1111/j.1529-8817.1978.tb00625.x

Bourrellyp. & Dragescoj. Contribution à la connaissance d'une algue rarissime ' *Phaeodactylum tricornutum*' Bohlin. *Bull. Micr. Appl.* **5**, 41 (1955).

Bowler, C. *et al.*, The *Phaeodactylum* genome reveals the evolutionary history of diatom genomes. *Nature* **456**, 239–244 (2008).

Breuera G, Packo P. Lamersa, Dirk E. Martensa, René B. Draaismab, R. H. W. Effect of light intensity, pH, and temperature on triacylglycerol (TAG) accumulation induced by nitrogen starvation in *Scenedesmus obliquus*. *Bioresour Technol* **143**, 1–9 (2013).

Browse, P. B. and J. The significance of different diacylglycerol synthesis pathways on plant oil composition and bioengineering. *Front. Plant Sci.* **3**, (2012).

Cardol P, De Paepe R, Franck F, Forti G, Finazzi G. The onset of NPQ and Deltamu(H)+ upon illumination of tobacco plants studied through the influence of mitochondrial electron transport. *Biochim Biophys Acta* **1797**, (2) 177-88 (2010).

References

Catoni, E. *et al.*, Identification of an Arabidopsis mitochondrial succinate-fumarate translocator. *FEBS_Letters* **534**, 87–92 (2003).

Cèron-García M, Fernández Sevilla, J., Ación Fernández, F., Molina Grima, E. & García Camacho, F. Mixotrophic growth of *Phaeodactylum tricornutum* on glycerol: growth rate and fatty acid profile. *J. Appl. Phycol.* **12**, 239–248 (2000).

Cèron-García M, Fernández-Sevilla J, Sánchez-Mirón A, García-Camacho F, Contreras-Gómez A, Molina-Grima E. Mixotrophic production of marine microalga *Phaeodactylum tricornutum* on various carbon sources. *J. Microbiol. Biotechnol.* **16**, 689–694 (2006).

Cèron-García M, Fernández-Sevilla J, Sánchez-Mirón A, García-Camacho F, Contreras-Gómez A, Molina-Grima E. Mixotrophic growth of *Phaeodactylum tricornutum* on fructose and glycerol in fed-batch and semi-continuous modes. *Bioresource Technology.* **147**, 569-576 (2013).

Cèron-García M, Sánchez Mirón, A., Fernández Sevilla, J. M., Molina Grima, E. & García Camacho, F. Mixotrophic growth of the microalga *Phaeodactylum tricornutum*: Influence of different nitrogen and organic carbon sources on productivity and biomass composition. *Process Biochem.* **40**, 297- 305 (2005).

Cèron-García M. *et al.*, Mixotrophic production of marine microalga *Phaeodactylum tricornutum* on various carbon sources. *J. Microbiol. Biotechnol.* **16**, 689–694 (2006).

Chen, G. Q. & Chen, F. Growing phototrophic cells without light. *Biotechnol. Lett.* **28**, 607–616 (2006).

Cheng, D., He, Q. & Wang, Q. Assessment of environmental stresses for enhanced microalgal biofuel production – an overview. (2014). doi:10.3389/fenrg.2014.00026

Chi, Z., O’Fallon, J. V. & Chen, S. Bicarbonate produced from carbon capture for algae culture. *Trends in Biotechnology* **29**, 537–541 (2011).

References

Choudhary, M., Jetley, U. K., Abash Khan, M., Zutshi, S. & Fatma, T. Effect of heavy metal stress on proline, malondialdehyde, and superoxide dismutase activity in the cyanobacterium *Spirulina platensis*-S5. *Ecotoxicol. Environ. Saf.* **66**, 204–9 (2007).

Chunye Zhanga, b, H. H. High-efficiency nuclear transformation of the diatom *Phaeodactylum tricornutum* by electroporation. *Mar. Genomics* **16**, 63–66 (2014).

D'Ippolito, G. *et al.*, Potential of lipid metabolism in marine diatoms for biofuel production. *Biotechnol. Biofuels* **8**, 28 (2015).

Daboussi F, Leduc S, Maréchal A, Dubois G, Guyot V, Perez-Michaut C, Amato A, Falciatore A, Juillerat A, Beurdeley M, Voytas D, Cavarec L, Duchateau P. Genome engineering empowers the diatom *Phaeodactylum tricornutum* for biotechnology. *Nat. Commun.* **5**, 3831 (2014).

Danquah M. K., R. Harun, R. H. design new medium. *Chem. Biochem. Eng.* **24**, 361–369 (2010).

Darzins, A., Pienkos, P. & Edey, L. Current status and potential for algal biofuels production. *Natl. Renew. Energy Lab. NREL A Rep. to Bioenergy Task 39 Report T39*, 146 (2010).

De Martino, A., Meichenin, A., Shi, J., Pan, K. & Bowler, C. Genetic and phenotypic characterization of *Phaeodactylum tricornutum* (Bacillariophyceae) accessions. *J. Phycol.* (2007). doi:10.1111/j.1529-8817.2007.00384.x

De Riso, V. *et al.*, Gene silencing in the marine diatom *Phaeodactylum tricornutum*. *Nucleic Acids Res.* (2009). doi:10.1093/nar/gkp448

Delwiche, C. F. & Palmer, J. D. The origin of plastids and their spread via secondary symbiosis. *Plant Syst. Evol.* 53–86 (1997). doi:10.1007/978-3-7091-6542-3_3

Delwiche, C. F. Tracing the Thread of Plastid Diversity through the Tapestry of Life. *Am. Nat.* **154**, S164–S177 (1999).

References

Dodson, V. J., Mouget, J. L., Dahmen, J. L. & Leblond, J. D. The long and short of it: Temperature-dependent modifications of fatty acid chain length and unsaturation in the galactolipid profiles of the diatoms *Haslea ostrearia* and *Phaeodactylum tricornutum*. *Hydrobiologia* **727**, 95–107 (2014).

Dutilleul C, Driscoll S, Cornic G, De Paepe R, Foyer CH, Noctor G. Functional mitochondrial complex I is required by tobacco leaves for optimal photosynthetic performance in photorespiratory conditions and during transients. *Plant Physiol.* **131**, (1) 264-75 (2003).

Fabris, M., Matthijs, M., Rombauts, S., Vyverman, W., Goossens, A., Baart, G J E. The metabolic blueprint of *Phaeodactylum tricornutum* reveals a eukaryotic Entner-Doudoroff glycolytic pathway. *Plant J.* **70**, 1004–14 (2012).

Falciatore, A., Casotti, R., Leblanc, C., Abrescia, C. & Bowler, C. Transformation of Nonselectable Reporter Genes in Marine Diatoms. *Marine Biotechnology* **1**, 239–251 (1999).

Falkowski P, Owens T. Light-Shade Adaptation: two strategies in marine phytoplankton. *Plant physiology* **66**, (4) 592-595 (1980).

Falkowski, P. G. & Knoll, A. H. Evolution of primary producers in the sea. *Evol. Prim. Prod. Sea* 1–6(2007). <http://www.sciencedirect.com/science/article/pii/B9780123705181500023>

Falkowski, P. G., Dubinsky, Z. & Wyman, K. Growth-irradiance relationships in phytoplankton. *Limnol. Oceanogr.* **30**, 311–321 (1985).

Fernie, A. R., Obata, T., Allen, A. E., Araújo, W. L. & Bowler, C. Leveraging metabolomics for functional investigations in sequenced marine diatoms. *Trends in Plant Science* **17**, 395–403 (2012).

Finazzi, G. & Rappaport, F. In vivo characterization of the electrochemical proton gradient generated in darkness in green algae and its kinetic effects on cytochrome b6/f turnover. *Biochemistry* **37**, 9999–10005 (1998).

Finazzi, G. The central role of the green alga *Chlamydomonas reinhardtii* in revealing the mechanism of state transitions. *J. Exp. Bot.* **56**, 383–388 (2005).

References

- Flores-Sarasa, I. et al., In vivo cytochrome and alternative pathway respiration in leaves of *Arabidopsis thaliana* plants with altered alternative oxidase under different light conditions. *Plant, Cell Environ.* **34**, 1373–1383 (2011).
- Forti G, Ehrenheim AM. The role of ascorbic acid in photosynthetic electron transport. *Biochim Biophys Acta* **1183**, 408-412 (1993).
- Gandin, A., Duffes, C., Day, D. A. & Cousins, A. B. The absence of alternative oxidase AOX1A results in altered response of photosynthetic carbon assimilation to increasing CO₂ in *Arabidopsis thaliana*. *Plant Cell Physiol.* **53**, 1627–1637 (2012).
- Gardner, R. D. et al., Use of sodium bicarbonate to stimulate triacylglycerol accumulation in the chlorophyte *Scenedesmus* sp. and the diatom *Phaeodactylum tricornutum*. *J. Appl. Phycol.* **24**, 1311–1320 (2012).
- Ge, F. et al., Methylcrotonyl-CoA Carboxylase Regulates Triacylglycerol Accumulation in the Model Diatom *Phaeodactylum tricornutum*. *Plant Cell* **26**, 1681–1697 (2014).
- Geider, R. J., Roche, J., Greene, R. M. & Olaizola, M. Response of the photosynthetic apparatus of *phaeodactylum tricornutum* (bacillariophyceae) to nitrate, phosphate, or iron starvation. *J. Phycol.* **29**, 755–766 (1993).
- Green, B. R. & Durnford, D. G. the Chlorophyll-Carotenoid Proteins of Oxygenic Photosynthesis. *Annu. Rev. Plant Physiol. Plant Mol. Biol.* **47**, 685–714 (1996).
- Green, B. R. After the primary endosymbiosis: An update on the chromalveolate hypothesis and the origins of algae with Chl c. *Photosynthesis Research* **107**, 103–115 (2011).
- Guglielmi, G. et al., The light-harvesting antenna of the diatom *Phaeodactylum tricornutum*: Evidence for a diadinoxanthin-binding subcomplex. *FEBS J.* **272**, 4339–4348 (2005).
- Guy, R. D., Berry, J. A., Fogel, M. L. & Hoering, T. C. Differential fractionation of oxygen isotopes by cyanide-resistant and cyanide-sensitive respiration in plants. *Planta* **177**, 483–491 (1989).

References

Haimovich-Dayan, M. *et al.*, The role of C4 metabolism in the marine diatom *Phaeodactylum tricorutum*. *New Phytol.* **197**, 177–85 (2013).

Haiying Wang. A study on lipid production of the mixotrophic microalgae *Phaeodactylum tricorutum* on various carbon sources. *African Journal of Microbiology Research* **6**, (2012).

Hamilton, M. L., Haslam, R. P., Napier, J. A. & Sayanova, O. Metabolic engineering of *Phaeodactylum tricorutum* for the enhanced accumulation of omega-3 long chain polyunsaturated fatty acids. *Metab. Eng.* **22**, 3–9 (2014).

Han, X. & Gross, R. W. Global analyses of cellular lipidomes directly from crude extracts of biological samples by ESI mass spectrometry: a bridge to lipidomics. *J. Lipid Res.* **44**, 1071–1079 (2003).

Hellebust, J. A. Glucose uptake by *Cyclotella cryptica*: dark induction and light inactivation of transport system. *J. Phycol.* **7**, 345–349 (1971).

Hempel F, Bullmann L, Lau J, Zauner S, Maier UG. ERAD- derived preprotein transport across the second outermost plastid membrane of diatoms. *Molecular Biology and Evolution* **26**, 1781–1790 (2009).

Hendeyn, I. Note on the Plymouth 'Nitxschia' culture. *J. mar. biol. Ass. U.K.* **33**, 335 (1954).

Henneberry, A.L.; Lagace, T.A.; Ridgway, N.D.; McMaster, C.R. Phosphatidylcholine Synthesis Influences the Diacylglycerol Homeostasis Required for Sec14p-dependent Golgi Function and Cell Growth. *Mol. Biol. Cell* **12**, 511-520 (2001).

Hill R. & F. Bendall. Function of the 2 cytochrome components in chloroplasts—working hypothesis. *Nat.* **186**, 136 – 137 (1960).

Hopkinson, B. M. A chloroplast pump model for the CO₂ concentrating mechanism in the diatom *Phaeodactylum tricorutum*. in *Photosynthesis Research* (2014). doi:10.1007/s11120-013-9954-7

References

- Hu, Q. *et al.*, Microalgal triacylglycerols as feedstocks for biofuel production: Perspectives and advances. *Plant Journal* **54**, 621–639 (2008).
- Huang, A., Liu, L., Yang, C. & Wang, G. *Phaeodactylum tricornutum* photorespiration takes part in glycerol metabolism and is important for nitrogen-limited response. *Biotechnol. Biofuels* **8**, 73 (2015).
- Huege, J. *et al.*, Sample amount alternatives for data adjustment in comparative cyanobacterial metabolomics. *Anal. Bioanal. Chem.* **399**, 3503–3517 (2011).
- Huerlimann, R. & Heimann, K. Comprehensive guide to acetyl-carboxylases in algae. *Crit. Rev. Biotechnol.* **33**, 49–65 (2013).
- Johansen, J.R. Morphological variability and cell wall composition of *Phaeodactylum tricornutum* (Bacillariophyceae). *Great Basin Nat.* **51**, 310–315 (1991).
- Joliot P, Béal D, Frilley B. Une nouvelle méthode spectrophotométrique destinée à l'étude des réactions photosynthétiques. *J de Chim Phys.* **77**(3), 209–216 (1980).
- Joliot P, Béal D, Joliot A. Cyclic electron flow under saturating excitation of dark-adapted *Arabidopsis* leaves. *Biochim Biophys Acta.* **1656**, 166–176 (2004).
- Joliot P. Dispositif ampérométrique de mesure de photosynthèse. *CR Acad Sci Paris.* **243**, 677–690 (1956).
- Joliot P. Kinetic studies of photosystem II in photosynthesis. *Photochem Photobiol.* **8**, 451–463 (1968).
- Karas, B. J. *et al.*, ARTICLE Designer diatom episomes delivered by bacterial conjugation. *Nat. Commun.* **6**, (2015).
- Kilian, O. & Kroth, P. G. Identification and characterization of a new conserved motif within the presequence of proteins targeted into complex diatom plastids. *Plant J.* **41**, 175–183 (2005).

References

Kitano, M., Matsukawa, R. & Karube, I. Changes in eicosapentaenoic acid content of *Navicula saprophila*, *Rhodomonas salina* and *Nitzschia* sp. under mixotrophic conditions. *J. Appl. Phycol.* **9**, 559–563 (1997).

Klughammer, C., Siebke, K. & Schreiber, U. Continuous ECS-indicated recording of the proton-motive charge flux in leaves. *Photosynth. Res.* **117**, 471–487 (2013).

Kroth, P. G. et al., A model for carbohydrate metabolism in the diatom *Phaeodactylum tricornutum* deduced from comparative whole genome analysis. *PLoS One* **3**, e1426 (2008).

Kuczynska, P., Jemiola-Rzeminska, M. & Strzalka, K. Photosynthetic Pigments in Diatoms. *Mar. Drugs* (2015). doi:10.3390/md13095847

Kuntz, M. Plastid terminal oxidase and its biological significance. *Planta* **218**, 896–899 (2004).

La Roche J, Geider R J, Graziano L M, Murray H, Lewis K. Induction of specific proteins in eukaryotic algae grown under iron-, phosphorus-, or nitrogen-deficient conditions. *Journal of Phycology.* **29**, 767-777 (1993).

Laisk, A., Eichelmann, H., Oja, V., Rasulov, B. & Rämama, H. Photosystem II cycle and alternative electron flow in leaves. *Plant Cell Physiol.* **47**, 972–983 (2006).

Larsson, C., Pahlman, I.L., Ansell, R., Rigoulet, M., Adler, L., and Gustafsson, L. The importance of the glycerol 3-phosphate shuttle during aerobic growth of *Saccharomyces cerevisiae*. *Yeast* **14**, 347–357 (1998).

Leitao, J. M. et al., Osmotic-stress-induced synthesis and degradation of inorganic polyphosphates in the alga *Phaeodactylum tricornutum*. *Mar Ecol-Prog Ser* **121**, 279–288 (1995).

Lepetit, B. et al., Spectroscopic and molecular characterization of the oligomeric antenna of the diatom *Phaeodactylum tricornutum*. *Biochemistry* **46**, 9813–9822 (2007).

Lepetit, B., Goss, R., Jakob, T. & Wilhelm, C. Molecular dynamics of the diatom thylakoid membrane under different light conditions. *Photosynthesis Research* **111**, 245–257 (2012).

References

- Levering, J., Broddrick, J., Zengler, K., Betenbaugh, M. J. & Bentley, W. E. Engineering of oleaginous organisms for lipid production. *Curr. Opin. Biotechnol.* **36**, 32–39 (2015).
- Levitan, O. *et al.*, Remodeling of intermediate metabolism in the diatom *Phaeodactylum tricornutum* under nitrogen stress. *Proc. Natl. Acad. Sci. U. S. A.* **112**, 412–7 (2015).
- Lewin, J. & Lewin, R. A. Culture and nutrition of some apochlorotic diatoms of the genus *Nitzschia*. *J. Gen. Microbiol.* **46**, 361–367 (1967).
- Lewin, J. C. & Lewin, R. A. Auxotrophy and heterotrophy in marine littoral diatoms. *Can. J. Microbiol.* **6**, 127–134 (1960).
- Lewin, J. C. The Taxonomic Position of *Phaeodactylum tricornutum*. *J. gen. Microbiol* **18**, (1958).
- Li, S. *et al.*, Lipidomic analysis can distinguish between two morphologically similar strains of *Nannochloropsis oceanica*. *J. Phycol.* **51**, 264–276 (2015).
- Liang, M.-H. & Jiang, J.-G. Advancing oleaginous microorganisms to produce lipid via metabolic engineering technology. *Prog. Lipid Res.* **52**, 395–408 (2013).
- Liaud M., C. Lichtl, K. Apt, W.Martin, R. Cerff, Compartment-specific isoforms of TPI and GAPDH are imported into diatom mitochondria as a fusion protein: evidence in favor of a mitochondrial origin of the eukaryotic glycolytic pathway. *Molecular and Biological Evolution* **17**, 213–223 (2000).
- Litchman, E., Klausmeier, C. a & Yoshiyama, K. Contrasting size evolution in marine and freshwater diatoms. *Proc. Natl. Acad. Sci. U. S. A.* **106**, 2665–2670 (2009).
- Liu X, Duan S, Li A, Xu N, Cai Z, Hu Z. Effects of organic carbon sources on growth, photosynthesis, and respiration of *Phaeodactylum tricornutum*. *Journal of Applied Phycology.* **21**, 239-246 (2009).

References

- Losada, M., Trebst, A. V & Arnon, D. I. Photosynthesis by Isolated Chloroplasts XI. CO₂ ASSIMILATION IN A RECONSTITUTED CHLOROPLAST SYSTEM. *J. Biochem. Chem.* **235**, (1960).
- Malasarn, D. *et al.*, Zinc deficiency impacts CO₂ Assimilation and disrupts copper homeostasis in *Chlamydomonas Reinhardtii*. *J. Biol. Chem.* **288**, 10672–10683 (2013).
- Mandalam, R. K. & Palsson, B. Ø. Elemental balancing of biomass and medium composition enhances growth capacity in high-density *Chlorella vulgaris* cultures. *Biotechnol. Bioeng.* **59**, 605–611 (1998).
- Melis, A., Burkart, M. D. & Mayfield, S. P. Carbon partitioning in photosynthesis. *Curr. Opin. Chem. Biol.* **17**, 453–456 (2013).
- Merchant, S. S. & Helmann, J. D. Elemental Economy. Microbial Strategies for Optimising Growth in the Face of Nutrient Limitation. *Adv. Microb. Physiol.* **60**, 91–210 (2012).
- Millar, a H., Whelan, J., Soole, K. L. & Day, D. a. Organization and regulation of mitochondrial respiration in plants. *Annu. Rev. Plant Biol.* **62**, 79–104 (2011).
- Miyahara, M., Aoi, M., Inoue-Kashino, N., Kashino, Y. & Ifuku, K. Highly Efficient Transformation of the Diatom *Phaeodactylum tricornutum* by Multi-Pulse Electroporation. *Biosci. Biotechnol. Biochem.* **77**, 874–876 (2013).
- Miyake, C. & Asade, K. Inactivation Mechanism of Ascorbate Peroxidase at Low Concentrations of Ascorbate; Hydrogen Peroxide Decomposes Compound I of Ascorbate Peroxidase. *Plant Cell Physiol.* **37**, 423–430 (1996).
- Moore C.M., M. M. Mills, K.R. Arrigo, I. Berman-Frank, L. Bopp, P.W. Boyd, E.D. Galbraith, R.J. Geider, C. Guieu, S.L: Jaccard, T.D: Jickells, J. La Roche, T.M. Lenton, N.M. Mahowald, E. Maranon, I. Marinov, J.K. Moore, T. Nakatsuka, A. Oschlies, M.A. Sai, A. T. and O. U. Processes and patterns of oceanic nutrient limitation. *Nat. Geosci.* **6**, 701–710 (2003).
- Morel, F. M. M. *et al.*, Zinc and carbon co-limitation of marine phytoplankton. *Nature* **369**, 740–742 (1994).

References

Morel, F. M. M., Milligan, A. J. & Saito, M. A. in *Treatise on Geochemistry: Second Edition* **8**, 123–150 (2013).

Mus, F. *et al.*, Physiological and molecular analysis of carbon source supplementation and pH stress-induced lipid accumulation in the marine diatom *Phaeodactylum tricorutum*. *Appl. Microbiol. Biotechnol.* **97**, 3625–42 (2013).

Niu, Y. F. *et al.*, Improvement of neutral lipid and polyunsaturated fatty acid biosynthesis by overexpressing a type 2 diacylglycerol acyltransferase in marine diatom *Phaeodactylum tricorutum*. *Mar. Drugs* (2013). doi:10.3390/md111114558

Niyogi, K. K. PHOTOPROTECTION REVISITED: Genetic and Molecular Approaches. *Annu. Rev. Plant Physiol. Plant Mol. Biol.* **50**, 333–359 (1999).

Obata, T., Fernie, A. R. & Nunes-Nesi, A. The central carbon and energy metabolism of marine diatoms. *Metabolites* **3**, 325–46 (2013).

Ort, D. R. & Baker, N. R. A photoprotective role for O₂ as an alternative electron sink in photosynthesis? *Current Opinion in Plant Biology* **5**, 193–198 (2002).

Osborn, H. L. & Hook, S. E. Using transcriptomic profiles in the diatom *Phaeodactylum tricorutum* to identify and prioritize stressors. *Aquat. Toxicol.* **138-139**, 12–25 (2013).

Pallotta, M. L., Fratianni, A. & Passarella, S. Metabolite transport in isolated yeast mitochondria: Fumarate/malate and succinate/malate antiports. *FEBS Lett.* **462**, 313–316 (1999).

Parker, MS, Armbrust, EV, Piovita-Scott, J, Keil, RG. Induction of photorespiration by light in the centric diatom *Thalassiosira weissflogii* (*Bacillariophyceae*): molecular characterization and physiological consequence. *J. Phycol.* **40**, 557–567 (2004).

Prihoda, J. *et al.* Chloroplast-mitochondria cross-talk in diatoms. *Journal of Experimental Botany* **63**, 1543–1557 (2012).

References

Raghavendra, A. S. & Padmasree, K. Beneficial interactions of mitochondrial metabolism with photosynthetic carbon assimilation. *Trends in Plant Science* **8**, 546–553 (2003).

Rashid, N., Rehman, M. S. U., Han, J-I. Enhanced growth rate and lipid production of freshwater microalgae by adopting two-stage cultivation system under diverse light and nutrients conditions. *Water and Environment Journal*. **29**(4) 533- 540 (2015).

Reinfelder, J. R., Kraepiel, a M. & Morel, F. M. Unicellular C4 photosynthesis in a marine diatom. *Nature* **407**, 996–999 (2000).

Richmond, A. Microalgal biotechnology at the turn of the millennium: A personal view. *J. Appl. Phycol.* **12**, 441–451 (2000).

Rigoulet, M., Aguilaniu, H., Averet, N., Bunoust, O., Camougrand, N., Grandier-Vazeille, X., Larsson, C., Pahlman, I.L., Manon, S., and Gustafsson, L. Organization and regulation of the cytosolic NADH metabolism in the yeast *Saccharomyces cerevisiae*. *Mol. Cell. Biochem.* **256–257**, 73–81 (2004).

Roberts, K., Granum, E., Leegood, R. C. & Raven, J. a. C3 and C4 pathways of photosynthetic carbon assimilation in marine diatoms are under genetic, not environmental, control. *Plant Physiol.* **145**, 230–235 (2007).

Roleda, M. Y. *et al.*, Effects of temperature and nutrient regimes on biomass and lipid production by six oleaginous microalgae in batch culture employing a two-phase cultivation strategy. (2012). doi:10.1016/j.biortech.2012.11.043

Round F. E., R. M. Crawford, and D. G. M. The Diatom: Biology and Morphology of the Genera.

Sapriel, G. *et al.*, Genome-wide transcriptome analyses of silicon metabolism in *Phaeodactylum tricornutum* reveal the multilevel regulation of silicic acid transporters. *PLoS One* **4**, (2009).

Shalon, D., Smith, S. J. & Brown, P. O. A DNA microarray system for analyzing complex DNA samples using two-color fluorescent probe hybridization. *Genome Res.* **6**, 639–645 (1996).

References

Sheehan, J., Dunahay, T., Benemann, J. & Roessler, P. Look Back at the U.S. Department of Energy's Aquatic Species Program: Biodiesel from Algae; Close-Out Report. *Other Information: PBD: 1 Jul 1998* Medium: ED; Size: 325 pages (1998).

Shen, W., Wei, M., Dauk, Y., Tan, D., C., Taylor, G., Selvaraj, and J., Zoua. Involvement of a glycerol-3-phosphate dehydrogenase in modulating the NADH/NAD⁺ ratio provides evidence of a mitochondrial glycerol-3-phosphate shuttle in *Arabidopsis*. *Plant Cell* **18**, 422–41 (2006).

Shulaev, V. Metabolomics technology and bioinformatics. *Briefings in Bioinformatics* **7**, 128–139 (2006).

Siaut, M. *et al.*, Molecular toolbox for studying diatom biology in *Phaeodactylum tricornutum*. *Gene* (2007). doi:10.1016/j.gene.2007.05.022

Simionato, D., Basso, S., Giacometti, G. M. & Morosinotto, T. *Optimisation* of light use efficiency for biofuel production in algae. *Biophys. Chem.* **182**, 71–78 (2013).

Smith, S. R., Abbriano, R. M. & Hildebrand, M. Comparative analysis of diatom genomes reveals substantial differences in the organization of carbon partitioning pathways. *Algal Res.* **1**, 2–16 (2012).

Su, X. *et al.*, Lipidomic changes during different growth stages of *Nitzschia closterium* f. *minutissima*. *Metabolomics* **9**, 300–310 (2013).

Sui X, Niu X, Shi M, Pei G, Li J, Chen L, Wang J, Zhang W. Metabolomic analysis reveals mechanism of antioxidant butylated hydroxyanisole on lipid accumulation in *Cryptocodinium cohnii*. *J Agric Food Chem.* Dec 24; **62**(51):12477-84 (2014).

Sunda, W. G. & Huntsman, S. A. Antagonisms Between Cadmium and Zinc Toxicity and Manganese Limitation in a Coastal Diatom. *Limnol. Oceanogr.* **41**, 373–387 (1996).

Tesson, B., Gaillard, C. & Martin-Jézéquel, V. Insights into the polymorphism of the diatom *Phaeodactylum tricornutum* Bohlin. *Botanica Marina* (2009). doi:10.1515/BOT.2009.012

References

Valenzuela, J. *et al.*, Potential role of multiple carbon fixation pathways during lipid accumulation in *Phaeodactylum tricornutum*. *Biotechnology for Biofuels* (2012). doi:10.1186/1754-6834-5-40

Wang H. A study on lipid production of the mixotrophic microalgae *Phaeodactylum tricornutum* on various carbon sources. *African Journal of Microbiology Research* **6**, 1041-1047 (2012).

Wang, Z., Gerstein, M. & Snyder, M. RNA-Seq: a revolutionary tool for transcriptomics. *Nat. Rev. Genet.* **10**, 57–63 (2009).

Weber APM, Linka N. Connecting the plastid: transporters of the plastid envelope and their role in linking plastidial with cytosolic metabolism. *Annual Review of Plant Biology* **62**, 53–77 (2011).

Wijffels, R. H. & Barbosa, M. J. An outlook on microalgal biofuels. *Science* **329**, 796–799 (2010).

Wilhelm, C., Buchel, C, Fisahn, J, Goss, R, Jakob, T, LaRoche, J, Lavaud, J, Lohr, M, Riebesell, U, Stehfest, K, Valentin, K, Kroth, PG. The Regulation of Carbon and Nutrient Assimilation in Diatoms is Significantly Different from Green Algae. *Protist* **157**, 91–124 (2006).

Wilson, D.P. The triradiate and other forms of *Nitzschia closterium* (Ehrenberg) Wm. Smith form a minutissima of Allen and Nelson. *J. Mar. Biol. Assoc. UK* **26**, 235–270 (1946).

Wu, S. *et al.*, Enzyme activity highlights the importance of the oxidative pentose phosphate pathway in lipid accumulation and growth of *Phaeodactylum tricornutum* under CO₂ concentration. *Biotechnol. Biofuels* **8**, 78 (2015).

Yang, D. *et al.*, Lipidomic analysis of *Chlamydomonas reinhardtii* under nitrogen and sulfur deprivation. *PLoS One* **10**, (2015).

Yang, Z. K. *et al.*, Proteomics to reveal metabolic network shifts towards lipid accumulation following nitrogen deprivation in the diatom *Phaeodactylum tricornutum*. *J. Appl. Phycol.* (2014). doi:10.1007/s10811-013-0050-3

References

Yang, Z. K. *et al.*, Systems-level analysis of the metabolic responses of the diatom *Phaeodactylum tricornutum* to phosphorus stress. *Environ. Microbiol.* **16**, 1793–1807 (2014).

Yao, Y. *et al.* Glycerol and neutral lipid production in the oleaginous marine diatom *Phaeodactylum tricornutum* promoted by overexpression of glycerol-3-phosphate dehydrogenase. *Biotechnol. Biofuels* **7**, 110 (2014).

Yen C-LE, Stone SJ, Koliwad S, Harris C & Farese RV. Thematic review series: glycerolipids. DGAT enzymes and triacylglycerol biosynthesis. *Journal of lipid research* 49: 2283-301 (2008).

Yongmanitchai, W. & Ward, O. P. Growth of and omega-3 fatty acid production by *Phaeodactylum tricornutum* under different culture conditions. *Appl. Environ. Microbiol.* 57, 419–425 (1991).

Yoon, K., Han, D., Li, Y., Sommerfeld, M. & Hu, Q. Phospholipid:Diacylglycerol Acyltransferase Is a Multifunctional Enzyme Involved in Membrane Lipid Turnover and Degradation While Synthesizing Triacylglycerol in the Unicellular Green Microalga *Chlamydomonas reinhardtii*. *Plant Cell* 24, 3708–3724 (2012).

Yoshida, K., Watanabe, C. K., Terashima, I. & Noguchi, K. Physiological impact of mitochondrial alternative oxidase on photosynthesis and growth in *Arabidopsis thaliana*. *Plant, Cell Environ.* 34, 1890–1899 (2011).

Yu, E. T. *et al.*, Triacylglycerol accumulation and profiling in the model diatoms *Thalassiosira pseudonana* and *Phaeodactylum tricornutum* (Bacillariophyceae) during starvation. *J. Appl. Phycol.* (2009). doi:10.1007/s10811-008-9400-y

Yusuf, C. Biodiesel from microalgae. *Biotechnol. Adv.* 25, 294–306 (2007).

Zaslavskaja L.A., Lippmeier J.C., Kroth P.G., Grossman A.R., Apt K.E. Transformation of the diatom *Phaeodactylum tricornutum* (Bacillariophyceae) with a variety of selectable marker and reporter genes. *J. Phycol.* 36, 379–986 (2000).

References

Zaslavskaja, L. A. et al., Trophic Conversion of an Obligate Photoautotrophic Organism Through Metabolic Engineering. *Science*. 292, 2073–2075 (2001).

Zehr, J. P. & Kudela, R. M. Photosynthesis in the Open Ocean. *Science*, 326, 945–946 (2009).

Zhang, C. & Hu, H. High-efficiency nuclear transformation of the diatom *Phaeodactylum tricornutum* by electroporation. *Marine Genomics* 16, 63–66 (2014).

Zheng, Y., Quinn, A. H. & Sriram, G. Experimental evidence and isotopomer analysis of mixotrophic glucose metabolism in the marine diatom *Phaeodactylum tricornutum*. *Microbial cell factories* 12, (2013).